University of Modena and Reggio Emilia

PhD Programme in MATHEMATICS

in convention with
the University of Ferrara and
the University of Parma

XXXIII Cycle

Some Challenging Control Problems in Mathematical and Behavioral Epidemiology

Scientific Disciplinary Sector: MAT/07

Candidate:
DELLA MARCA ROSSELLA

Tutor:
Prof. GROPPI MARIA

PhD Programme Coordinator:
Prof. GIARDINÀ CRISTIAN

Acknowledgements

I feel very honored to have met and worked with so many wonderful people during these years.

My PhD tutor Prof. Maria Groppi was a maternal guide, always generous with good advice coming from her great and eclectic experience. She has done its utmost to ensure the best for me and cared about my well–being in every facet of life.

A mentor since the time of the master's degree was Prof. Bruno Buonomo. He instilled in me the fascination for mathematical epidemiology and has never stopped to feed my research interests. I owe most of what I know to him.

A very fruitful collaboration was that with Dr. Luca Bolzoni. He opened my eyes to a different way of conceiving and interpreting mathematics, that captures its essentiality for meeting the real–world needs.

A special mention goes to my advisors during the research periods at iPRI (International Prevention Research Institute) in Lyon (France) and at University of Minho in Guimarães (Portugal). In Lyon, I was hosted by Dr. Alberto d'Onofrio (later appointed my *scientific uncle*), he is a whirlwind of genius and humor, and stimulated me with many challenging questions. In Guimarães, I was hearty welcomed by Prof. Ana Jacinta Soares while the pandemic of COVID–19 was emerging in Europe, in those hard times she treated me like family.

I would like to acknowledge University of Parma and GNFM (Gruppo Nazionale per la Fisica Matematica) of INdAM (Istituto Nazionale di Alta Matematica), whose financial support allowed me to attend conferences, workshops and schools. They constituted precious opportunities of meeting, learning and sharing ideas.

I am also thankful to LIS LYSM AMU–CNRS–ECM–INdAM, who financed my two months scientific visit at iPRI during the second PhD year, and to University of Modena and Reggio Emilia, who financed my a month and a half scientific visit at University of Minho during the third (last) PhD year.

And last but not least, I am indebted to Prof. Ezio Venturino and Prof. Delfim Torres for the time they spent in reviewing this thesis and the appreciation of the overall work.

Abstract (english version)

Despite major achievements in the elimination of long–established infections (or even eradication, as in the very well known case of smallpox), recent decades have seen the continual emergence or re–emergence of infectious diseases (last but not least COVID–19). They are not only threats to global health, but direct and indirect costs generated by human and animal epidemics are responsible for major economic losses worldwide.

Mathematical models of infectious diseases spreading have played a significant role in infection control. On the one hand, they have given an important contribution to the biological and epidemiological understanding of disease outbreak patterns; on the other hand, they have helped to determine how and when to apply control measures in order to quickly and most effectively contain epidemics. Nonetheless, in order to shape local and global public health policies, it is essential to gain a better and more comprehensive understanding of effective actions to control diseases, by finding ways to employ new complexity layers. This was the main focus of the research I have carried out during my PhD. Here, the products of this research are collected and connected. However, because out of context, other problems I interested in have been excluded from this collection: they rely in the fields of autoimmune diseases and landscape ecology.

We start with an Introduction chapter, which traces the history of epidemiological models, the rationales and the breathtaking incremental advances. We focus on two critical aspects: i) the qualitative and quantitative assessment of control strategies specific to the problem at hand (via e.g. *optimal control* or *threshold policies*); ii) the incorporation into the model of the *human behavioral changes* in response to disease dynamics. In this framework, our studies are inserted and contextualized. Hereafter, to each of them a specific chapter is devoted.

The techniques used include the construction of appropriate deterministic models given by non–linear ordinary differential equations, their qualitative analysis (via e.g. stability and bifurcation theory), the parameterization and validation with available data. Numerical tests are performed with advanced simulation methods of dynamical systems. As far as optimal control problems are concerned, the formulation follows the classical approach by Pontryagin, while both direct and indirect optimization methods are adopted for the numerical resolution.

In Chapter 1, within a basic Susceptible–Infected–Removed model framework, we address the problem of minimizing simultaneously the epidemic size and the elimination time via optimal vaccination or isolation strategies.

A two–patches metapopulation epidemic model, describing the dynamics of Susceptibles and Infected in wildlife diseases, is formulated and analyzed in Chapter 2. Here, two types of localized culling strategies are considered and compared: proactive and reactive.

Chapter 3 concerns a model for vaccine–preventable childhood diseases transmission, where newborns vaccination follows an imitation game dynamics and is affected by awareness campaigns by the public health system.

Vaccination is also incorporated in the model of Chapter 4. Here, it addresses susceptible individuals of any age and depends on the information and rumors about the disease. Further, the vaccine effectiveness is assumed to be partial and waning over time.

The last Chapter 5 is devoted to the ongoing pandemic of COVID–19. We build an epidemic model with information–dependent contact and quarantine rates. The model is applied to the first epidemic wave in Italy and incorporates the progressive lockdown restrictions.

Each of these contributions has a double aim. The first one is being interesting *per se* from the theoretical point of view: the modeling process and the analytical techniques support this aspect. The second aim is giving directions to shape health policies suited to the situation: recourse to numerical tools is essential to that end.

I hope this thesis will incite further research in the fields of mathematical and behavioral epidemiology of infectious diseases.

Abstract (versione italiana)

Nonostante gli ingenti progressi nell'eliminazione di infezioni da lungo in circolazione (o addirittura nell'eradicazione, come nel celeberrimo caso del vaiolo), gli ultimi decenni hanno visto la continua comparsa o ricomparsa di malattie infettive (ultimo ma non da meno il COVID–19). Esse non solo minacciano la salute globale, ma i costi diretti e indiretti generati da epidemie nell'uomo e negli animali sono responsabili di considerevoli perdite economiche a livello mondiale.

I modelli matematici della diffusione di malattie infettive hanno svolto un ruolo significativo nel controllo delle infezioni. Da un lato, hanno fornito un importante contributo alla comprensione biologica ed epidemiologica degli andamenti di scoppi epidemici; d'altro canto, hanno concorso a determinare come e quando applicare le misure di controllo al fine di contenere rapidamente ed efficacemente le epidemie. Ciononostante, per dare forma alle politiche di sanità pubblica locali e globali, è essenziale acquisire una migliore e più completa comprensione delle azioni efficaci per controllare il diffondersi di malattie, impiegando nuovi livelli di complessità. Questo è stato l'obiettivo fondamentale della ricerca che ho svolto durante il dottorato; in questa tesi i prodotti di questa ricerca sono raccolti e interconnessi. Tuttavia, poiché fuori contesto, altri problemi a cui mi sono interessata sono stati qui esclusi: essi riguardano le malattie autoimmuni e l'ecologia del paesaggio.

Si inizia con un capitolo di Introduzione, che ripercorre la storia dei modelli epidemici, le motivazioni e gli incredibili progressi. Sono due gli aspetti su cui ci concentriamo: i) la valutazione qualitativa e quantitativa di strategie di controllo specifiche per il problema in questione (attraverso, ad esempio, il *controllo ottimo* o le *politiche a soglia*); ii) l'incorporazione nel modello dei *cambiamenti nel comportamento umano* in risposta alla dinamica della malattia. In questo quadro si inseriscono e contestualizzano i nostri studi. Di seguito, a ciascuno di essi è dedicato un capitolo specifico.

Le tecniche matematiche utilizzate includono la costruzione di opportuni modelli deterministici descritti da equazioni differenziali ordinarie non lineari, la loro analisi qualitativa (tramite, ad esempio, la teoria della stabilità e delle biforcazioni), la parametrizzazione e la validazione con i dati disponibili. I test numerici sono eseguiti con avanzati metodi di simulazione di sistemi dinamici. Per i problemi di controllo ottimo, la formulazione segue l'approccio classico di Pontryagin, mentre la risoluzione numerica è svolta mediante metodi di ottimizzazione sia diretta che indiretta.

Nel Capitolo 1, utilizzando come base di partenza un modello Suscettibili–Infetti–Rimossi, affrontiamo il problema di minimizzare al contempo la portata e il tempo di eliminazione di un'epidemia tramite strategie di vaccinazione o isolamento.

Un modello epidemico tra due sottopopolazioni, che descrive la dinamica di Suscettibili e Infetti in malattie della fauna selvatica, è formulato e analizzato nel Capitolo 2. Qui, vengono considerati e confrontati due tipi di strategie di abbattimento localizzato: proattivo

e reattivo.

Il Capitolo 3 tratta di un modello per la trasmissione di malattie pediatriche prevenibili con vaccino, dove la vaccinazione dei neonati segue la dinamica di un gioco imitativo ed è influenzata da campagne di sensibilizzazione da parte del sistema sanitario.

La vaccinazione è anche incorporata nel modello del Capitolo 4. In questo caso è rivolta a individui suscettibili di ogni età ed è funzione dell'informazione e delle voci circolanti sulla malattia. Inoltre, si assume che l'efficacia del vaccino sia parziale ed evanescente col passare del tempo.

L'ultimo Capitolo 5 è dedicato all'attuale pandemia di COVID–19. Si costruisce un modello epidemico con tassi di contatto e di quarantena dipendenti dall'informazione circolante. Il modello è applicato alla prima ondata epidemica in Italia e incorpora le progressive restrizioni imposte durante il lockdown.

Ciascuno di questi contributi ha un duplice scopo. Il primo è essere interessante di per sè dal punto di vista teorico: il processo di modellizzazione e le tecniche analitiche supportano questo aspetto. Il secondo è dare indicazioni utili a pianificare politiche sanitarie adatte alla situazione in esame: il ricorso a strumenti numerici è essenziale a tal fine.

Mi auguro che questa tesi possa stimolare ulteriori ricerche nel campo dell'epidemiologia matematica e comportamentale delle malattie infettive.

Contents

List of abbreviations

BCM behavioral change model. 22, 26

BRN basic reproduction number. 99

CSF classical swine fever. 30, 38

DE differential evolution. 88, 89, 90, 91, 96, 97

DFE disease–free equilibrium. 80, 99, 111

DP dynamic programming. 16, 17

EE endemic equilibrium/equilibria. 104, 105, 107, 109, 110, 112, 113, 115, 116

ERID emerging and re–emerging infectious disease. 54

FBS forward–backward sweep. 7, 85, 86, 87, 88, 89, 91, 93, 94, 96

FMD foot and mouth disease. 29, 30, 31, 32, 37, 38, 51

FoI force of infection. 123

Grad gradient descent. 7, 85, 86, 87, 88, 89, 91, 96

HJB Hamilton–Jacobi–Bellman. 16

HOA heuristic optimization algorithm. 87, 88, 91, 96, 97

HPAI highly–pathogenic avian influenza. 30, 37, 38

ICU intensive care unit. 120, 129, 137

IDEM information–dependent epidemic model. 24, 25, 26

LAS locally asymptotically stable. 108, 109

MMR measles–mumps–rubella. 22, 23, 24, 100

MOOC multi–objective optimal control. 34, 36, 37, 38, 40, 41, 42, 43, 44, 45, 46, 47, 49, 50

MP Pontryagin maximum principle. 16, 17, 82, 86

OC optimal control. 77, 85, 86, 87, 88, 89, 90, 91, 92, 97

ODE ordinary differential equation. 25, 55, 72, 81

PH public health. 76, 77, 80, 88, 90

PHS public health system. 76, 77, 78, 81, 88, 96, 97

PSO particle swarm optimization. 87, 88, 89, 90, 91, 92, 93, 94, 95, 96, 97

QSSA quasi–steady–state approximation. 95, 96

SEIR Susceptible–Exposed–Infectious–Removed. 100, 120, 128, 136

SI Susceptible–Infected. 21, 55

SIR Susceptible–Infected–Removed. 12, 13, 18, 20, 23, 30, 31, 51, 76, 78, 80, 96, 97, 100, 103, 138

SIRV Susceptible–Infected–Removed–Vaccinated. 101

SIS Susceptible–Infected–Susceptible. 102

SISV Susceptible–Infected–Susceptible–Vaccinated. 26, 101, 117

TOC time optimal control. 46, 47, 48, 49, 51

VAC vaccine awareness campaign. 23, 24, 76, 77, 80, 81, 89, 95

VSE vaccine–related side effect. 23, 25, 78

WHO World Health Organization. 129

Chapter I

Introduction

I.1 Epidemics and epidemiological models: a brief history

The first significant epidemic described by historians was the Plague of Athens, a devastating infectious disease that struck the city–state of ancient Greece in 430–426 B.C. The most precise description of that plague was provided by the historian Thucydides (460–400 B.C.) in his *History of the Peloponnesian War*, and probably influenced by the Hippocratic medical writings. In his treatise *Epidemics*, the physician Hippocrates (459–337 B.C.) delineated the factors that affected the spread of diseases at that time [176]. Hippocrates is often considered the father of 'epidemiology' (from Greek *epi*, 'upon, among', *demos*, 'people', and *logos*, 'study'): the study of the distribution and determinants of health–related states and events in specified populations. He is the first known person to have examined the relationships between the occurrence of diseases and environmental influences.

After the plague of Athens, recorded history continuously documents the invasion of populations by infectious agents, some causing many deaths before disappearing, others reappearing in invasions some years later in populations that have acquired some degree of immunity, due to prior exposure to related infectious pathogens. Many of these diseases – measles, pertussis, influenza, and many others – have been burdening us for centuries, while new infectious diseases – such as Ebola, Zika virus, and the currently spreading COVID–19 – continue to emerge from animal populations and make the jump to human populations, or spreading to new human populations due to climate change or other anthropogenic disturbances [222]. One of the most well documented epidemics that devastated Europe was the Black Death. The Black Death spread throughout the Mediterranean and Europe and is estimated to have killed one–third of the population of Europe between 1346 and 1350 [8]. The disease reappeared regularly in various regions of Europe for more than 300 years, a notable outbreak being that of the Great Plague of London of 1665–1666. It gradually withdrew from Europe afterwards [46].

Although epidemiology itself has a long history, the mathematical study of diseases and their spread is only about 350 years old. The first statistical study of infectious diseases is attributed to John Graunt (1620–1674), whose 1663 book *Natural and Political Observations Made upon the Bills of Mortality* was concerned with methods of public health statistics. A century later, Daniel Bernoulli (1700–1782) used mathematical methods to estimate the impact of inoculation against smallpox. In 1766, he published what is now considered the first epidemiological model [27] (reviewed in [16,147]). Bernoulli argued that inoculation with live virus obtained from a mild strain of smallpox would reduce the death rate and thereby increase the life expectancy, even if the inoculation itself might occasionally be fatal.

In the late 1800s, science could finally explain the mechanism of how one becomes ill: the concept of passing a bacterial disease through contact between an infected individual and a healthy one became known. This paved the way for the mathematical modeling of infectious diseases. Significant strides were made with the work of William Hamer (1862–1936), in the early twentieth century. He was looking for an explanation of the recurrence of measles. Hamer was the first to suggest a mass action law for the rate of new infections [153], an idea that has been basic in *compartmental models* since that time. But it is Sir Ronald Ross (1857–1932) who is considered the father of modern *mathematical epidemiology*. He did pioneering work on malaria and discovered that it is transmitted between humans and mosquitoes. For his work on malaria, Ross received the Nobel Prize in 1902. In the second edition of his book *The Prevention of Malaria* (1911), he developed mathematical models of

Figure I.1: Forerunners of mathematical epidemiology: Sir Ronald Ross (left), William Ogilvy Kermack (centre), Anderson Gray McKendrick (right).

malaria transmission and derived a threshold quantity [260], marking the first introduction of the concept of the *basic reproduction number*.

Susceptible–Infected–Removed

Mathematical epidemiology was raised to a new level by the model of the spread of infectious diseases, published by Kermack (1898–1970) and McKendrick (1876–1943) in 1927. In their joint article *A contribution to the mathematical theory of epidemics* [185], Kermack and McKendrick published for the first time a deterministic epidemic model that included three *compartments*: susceptible, infected and removed individuals. Compartments are a convenient way to describe the individual life–course of infection by a sequence of transitions between a few epidemiological classes, triggered by specific processes and parameters.

They imported from statistical physics the mass–action law of chemical reaction kinetics to describe infection transmission as the outcome of the social contact process between infected and susceptible individuals. They made the counter–factual hypothesis that the population behaves as a collection of 'particles' of different types randomly moving in the environment, where each encounter ('collision') between a particle of susceptible–type and one of infected–type has a uniform probability that the susceptible–type particle switches into infected–type.

The original formulation of the Susceptible–Infected–Removed (SIR) epidemic model given in [185] was

$$\begin{aligned} v(t) &= -\dot{x}(t) \\ \dot{x}(t) &= -x(t)\left[\int_0^t A(s)v(t-s)ds + A(t)y(0)\right] \\ \dot{z}(t) &= \int_0^t C(s)v(t-s)ds + C(t)y(0) \\ y(t) &= \int_0^t B(s)v(t-s)ds + B(t)y(0), \end{aligned} \tag{I.1}$$

where $x(t)$, $y(t)$, $z(t)$ are the number of susceptible, infected (and infectious) and removed individuals at time t, respectively. Also

$$B(s) = e^{-\int_0^s \psi(t)dt}, \;\; A(s) = \phi(s)B(s), \;\; C(s) = \psi(s)B(s),$$

where $\phi(s)$ is the infectivity rate when the age of infection is s, $\psi(s)$ is the removal rate at infection age s (that is the sum of the recovery and disease–induced death rates). It is assumed that there are no disease deaths, so that the total population size remains constant: $x(t) + y(t) + z(t) \equiv N$. If we define $S(t) = x(t)$, $I(t) = y(t)$, $R(t) = z(t)$ and assume that the infectivity and removal rates are constant: $\phi(s) \equiv \beta$, $\psi(s) \equiv \gamma$, then the model (I.1) can be reduced to the system

$$\begin{aligned} \dot{S} &= -\beta SI \\ \dot{I} &= \beta SI - \gamma I \\ \dot{R} &= \gamma I. \end{aligned} \tag{I.2}$$

For many years, the model (I.2) was known as the Kermack–McKendrick epidemic model, overlooking the fact that it is a very special case of the actual Kermack–McKendrick model (I.1). The general model includes dependence on age of infection, that is the time since becoming infected, and can be used to provide a unified approach to compartmental epidemic models.

The original SIR model does not include natural birth and death rates and, consequently, models only disease outbreaks. To capture epidemic modeling of diseases that can become established in a population and persist, Kermack and McKendrick published part. II and part. III of their *Contributions to the mathematical theory of epidemics* in 1932 and 1933, respectively [186, 187].

In the work of Kermack and McKendrick, as in that of Ross, there is a threshold quantity, a critical level below which the disease would be eliminated. It is now almost universally denoted by $\mathcal{R}_0$. Neither Ross nor Kermack and McKendrick identified this threshold quantity or gave it a name. It appears that the first person to name it explicitly was MacDonald in 1957 in his work on malaria [206].

The explicit definition of the basic reproduction number is that it is *the expected number of disease cases produced by a typical infected individual in a wholly susceptible population over the full course of the infectious period*. In an epidemic situation, in which the time period is short enough to neglect demographic effects and all infected individuals recover with full immunity against re–infection, the threshold $\mathcal{R}_0 = 1$ is the dividing line between the infection dying out and the onset of an epidemic. In a situation that includes a flow of new susceptibles, either through demographic effects or recovery without full immunity against re–infection, the threshold $\mathcal{R}_0 = 1$ is the dividing line between approach to a disease–free equilibrium and approach to an endemic equilibrium, in which the disease is always present. For the simple Kermack–McKendrick model (I.2) it is easy to verify that

$$\mathcal{R}_0 = \frac{\beta}{\gamma},$$

namely the ratio between the infectivity rate and the removal rate.

What happens next

The momentum impressed by Kermack and McKendrick work yielded, with a certain delay, an explosion of biomathematical studies, mostly devoted to the investigation of a number of variants of the key models introduced by the forerunners. Since 1933 there has been a great deal of work on compartmental disease transmission models, with generalizations in many directions.

There is a second major shift however, dating 1975–1980, when another group of innovators [11, 160] started the systematically use of mathematical models to interpret epidemiological data and trends aiming to deep the perspectives for infection control. In this phase, dramatically accelerated first by the HIV/AIDS epidemics in the 1980s, and in the 2000s by the emergence of influenza pandemic threats, mathematical models of infectious diseases definitely left the boundary of biomathematics and became a central supporting tools for public health decisions. They determined the duration of travel restrictions or of school closure during a pandemic event, or the fraction of newborns to be immunized for a vaccine–preventable infection, as measles.

Some of the adopted mathematical approaches are presented in the next sections.

I.2 Optimal control

The successful elimination of infectious diseases does not depend only on the availability of medical infrastructures but also on the ability to understand the transmission dynamics, the application of control strategies and the implementation of logistic policies. Mathematical models have been used in planning, evaluating, comparing and optimizing various detection, prevention, therapy and control programs. To this aim, optimal control theory proved to be a powerful tool in serving the cause.

A controversial date of birth

The conventional wisdom holds that optimal control theory was born about 60 years ago in the former Soviet Union with the work on the *Pontryagin maximum principle* by L. S. Pontryagin and his group [240]. Some mathematicians believed that this new theory was no more than a minor addition to classical calculus of variations, essentially involving the incorporation of inequality constraints. In addition, other factors may have also contributed to the cold reception: first of all Pontryagin's personality and, in particular, his notorious anti–Semitism, and second, the feeling that many held that the result was primarily intended for military applications [277].

Actually, it is widely recognized that optimal control is significantly richer and broader than the calculus of variations, from which it differs in some fundamental ways. The calculus of variations deals mainly with optimization of the following 'standard' form:

$$\begin{aligned} \text{minimize } & J = \int_0^T g(x(t), \dot{x}(t), t)dt \\ \text{subject to } & x(0) = x_0,\ x(T) = x_T, \end{aligned}$$

or, equivalently, of the form

$$\begin{aligned} \text{minimize } & J = \int_0^T g(x(t), u(t), t)dt \\ \text{subject to } & x(0) = x_0,\ x(T) = x_T \\ \text{and } & \dot{x}(t) = u(t) \text{ for } t \in [0, T]. \end{aligned} \tag{I.3}$$

The minimization takes place in the space of 'all' curves, so nothing interesting happens on the level of the set of curves under consideration, and all the nontrivial features of the problem arise because of the integrand g.

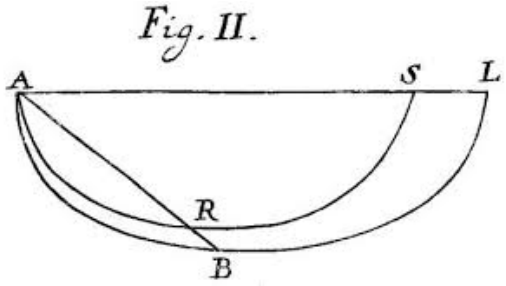

Figure I.2: Johann Bernoulli's solution to the brachystochrone problem: the cycloid (*Acta Eruditorum*, 1697).

Optimal control problems, by contrast, involve a minimization over a set $\mathcal{C}$ of curves which is itself determined by some dynamical constraints. For example, $\mathcal{C}$ might be the set of all curves $t \to x(t)$ that satisty a differential equation (the *state equation*)

$$\dot{x}(t) = f(x(t), u(t), t) \text{ for } t \in [0, T] \tag{I.4}$$

for some choice of the *control function* $t \to u(t)$. Even more precisely, since it may happen that a member of $\mathcal{C}$ does not uniquely determine the control $u(\cdot)$ that generates it, it should be talking about trajectory *control pairs* $(x(\cdot), u(\cdot))$. So, in an optimal control problem there are at least two objectives that give the situation an interesting structure, namely the dynamics f and the *objective functional* J to be minimized.

Within this framework, the birth of optimal control should be dated more than 250 years before: in 1697. In that year, in Groningen, a university town in the north of The Netherlands, Johann Bernoulli (1654–1705), the father of the above–mentioned Daniel and professor of mathematics at the local university, published his solution of the *brachystochrone* problem (from Greek *brachistos*, 'shortest', and *chronos*, 'time'). The year before he had challenged his contemporaries to solve this problem: 'If in a vertical plane two points A and B are given, then it is required to specify the orbit AMB of the movable point M, along which it, starting from A, and under the influence of its own weight, arrives at B in the shortest possible time'.

Bernoulli's problem, as posed in the *Acta Eruditorum*, is a true *minimum time problem* of the kind that is studied in optimal control theory. Namely, a problem in which it is desired to minimize time – i.e. the integral J of (I.3) with $g \equiv 1$ – among all curves $t \to x(t)$ that satisfy endpoint constraints as in (I.3) and are solutions of suitable differential equations (I.4) for some control $t \to u(t)$. Moreover, the brachystochrone problem is the first one ever to deal with a dynamical behavior and explicitly ask for the optimal selection of a path.

Bellman vs Pontryagin

The Pontryagin's principle and the contemporary development of *dynamic programming* by Bellman and his colleagues [24] paved the way for the applications of the methods of optimization in all fields: from physics to economy, from aerospace to medicine.

In its most common form, an optimal control problem (say, CP) reads:

$$\begin{aligned} \text{minimize } & J = \int_s^T g(x(t), u(t), t)dt + h(x(T)) \\ \text{subject to } & \dot{x} = f(x(t), u(t), t) \text{ for } t \in [s, T] \qquad \text{(I.5a)} \\ \text{and } & x(s) = x_s \qquad \text{(I.5b)} \end{aligned}$$

with $(x_s, s) \in \mathbb{R}^n \times [0, T]$, among all the admissible controls

$$u \in \Omega = \{u(\cdot) |\, u \text{ is a Lebesgue measurable function from } [s, T] \text{ to } U\}, \qquad \text{(I.6)}$$

where U is a prescribed arbitrary set in $\mathbb{R}^m$. The *value function* is defined as

$$V(x_s, s) = \inf\{J : u \in \Omega\}.$$

The pair $(x^*(\cdot), u^*(\cdot))$ is called *optimal* if x^* is the corresponding solution of (I.5) for $u^* \in \Omega$ and $J\big|_{(x^*, u^*)} = V(x_s, s)$.

The Pontryagin maximum principle (MP) says that, if $(x^*(\cdot), u^*(\cdot))$ is optimal for the problem CP, then it minimizes the so–called *Hamiltonian* function, namely

$$H(x^*(t), u^*(t), \lambda(t), t) = \min_{u \in U} H(x^*(t), u(t), \lambda(t), t) \text{ for } t \in [s, T],$$

where H is defined by

$$H(x, u, p, t) = p \cdot f(x, u, t) + g(x, u, t)$$

for $(x, u, p, t) \in \mathbb{R}^n \times U \times \mathbb{R}^n \times [s, T]$, and $\lambda(\cdot)$ is a function from $[s, T]$ to $\mathbb{R}^n$ satisfying the *adjoint equation*

$$\begin{aligned} \dot{\lambda}(t) &= -\partial_x H(x^*(t), u^*(t), \lambda(t), t) \text{ for } t \in [s, T] \\ \lambda(T) &= \partial_x h(x^*(T)). \end{aligned}$$

Instead, dynamic programming (DP) asserts that, if the value function $V(\cdot, \cdot)$ happens to be continuously differentiable, then it satisfies the so–called *Hamilton–Jacobi–Bellman* (HJB) equation

$$\begin{aligned} &\partial_t V(x, t) + \inf_{u \in U} H(x, u, \partial_x V(x, t), t) = 0 \text{ for } (x, t) \in \mathbb{R}^n \times [s, T] \\ &V(x, T) = h(x). \end{aligned}$$

It seems, however, that the DP fails to have a solid ground from its very beginning, since it requires the value function to be smooth, which is not true even in simple cases. As for connection between MP and DP, the known result is

$$\lambda(t) = \partial_x V(x^*(t), t) \text{ for } t \in [s, T],$$

which also lacks generality, due to the same reason above. This is an important gap, that was partially bridged by introducing new concept of solutions of nonlinear partial differential equations, including the HJB equation, e.g. *viscosity solutions* [92], *minimax solutions* [274].

Controlling infectious diseases spreading

In epidemiological problems control policies usually affect the *rates* at which population components are transferred from one compartment (e.g. susceptible) to another (e.g. immunised). A survey of the works on the optimal or other control of pests and infectious

diseases published until 1977 was provided by Wickwire [297]. In these first applications the control function appears linearly in both the state system and the objective functional, leading to *bang–bang* or *singular* optimal control cases. Bang–bang means that the optimal control takes values only on the boundary of its set of allowable values and switches (with a bang!) from one extreme to another during the course of operation. Singular control happens when the optimal control value can be obtained neither by MP nor by DP approach and other methods must be used.

For example, Wickwire investigated the optimal control of a Kermack–McKendrick model and determined the isolation strategy that minimizes the total infected burden over an outbreak plus a cost for using the control [296]. Starting from (I.2), he supposed that control affects only the rate $h(S,I)u$ at which infected are isolated, where $h(\cdot,\cdot) \geq 0$ is measurable and $u = u(t)$ is a measurable control function with values in $[0,1]$. The dynamics is therefore

$$\begin{aligned} \dot{S} &= -\beta SI \\ \dot{I} &= \beta SI - \gamma I - h(S,I)u \\ \dot{R} &= \gamma I + h(S,I)u, \end{aligned}$$

and it is desired to choose for given h a measurable control u which minimizes

$$J = \int_0^T [I(t) + ch(S(t), I(t))u(t)]\, dt,$$

where $c = const. > 0$ and $T = \inf\{t : I(t) = 0\}$ is the control–dependent duration of the epidemic. By means of DP approach, he found that the optimal isolation strategy is to use either maximal control for the entire epidemic ($u \equiv 1$) or to use no control at all ($u \equiv 0$). The same objective, but via immunization strategy and $h(S,I) \equiv 1$, had been investigated by Morton and Wickwire in [224], employing if necessary both MP and DP. They pointed out that the optimal immunization policy must be of bang–bang type and that at most one switch from $u \equiv 1$ to $u \equiv 0$ may occur under such a policy.

Since then, the theory, the application areas and the corresponding numerical algorithms have steadily progressed. The technical questions of whether the optimal solution exists and is uniquely determined have been handled under general assumptions, mainly based on the Lipschitz properties of the solutions of the involved differential equations [6, 127].

Optimal control theory has been applied to the mathematical models of HIV [146, 177], vector–borne diseases [58, 225, 247], tuberculosis [83, 180, 258], childhood diseases [28, 61, 65] (including *behavioral* vaccination models, which we will deal with in Section I.4), wildlife and livestock diseases [14, 39, 179, 318] and others [227, 249]. Since bang–bang or singular controls are more difficult to handle or sometimes considered unsuitable for the particular application, a quadratic dependence on the control in the objective functional was widely adopted [14, 39, 58, 61, 65, 83, 177, 179, 180, 225, 227, 247, 249, 258, 318].

As far as the numerical methods, we can discriminate two major classes: i) *indirect methods*, that convert the optimal control problem into a boundary–value problem; ii) *direct methods*, that transcribe an infinite–dimensional optimization problem to a finite–dimensional one. For specific details and differences between such methods, see the surveys [251, 257].

Minimum time From the epidemiological point of view, the main indicators generally used to describe the severity of infection events are: i) the total number of infected individuals

(humans or animals) during an epidemic, and ii) the duration of the epidemic. The rationale behind these indicators is based on the evidence that epidemic surveillance and control costs are directly related to spatial and temporal extension of the epidemic events. Furthermore, the effect of the epidemic duration is responsible for significant socio–economic costs. This is due to the sanitary restrictions imposed in infected areas until a disease–free status is regained, such as travel and trade restrictions.

Optimal control theory has been widely applied to solve the problem of minimizing the total number of infected individuals (or the total infected burden) by means of different control policies. However, few attempts have been made to address the problem of minimizing the epidemic duration from a theoretical point of view (to our knowledge, just [33, 96, 317]).

In order to fill this gap, we investigated the problem of minimizing both the epidemic size and duration through the implementation of emergency prophylactic vaccination plans or the isolation of infected individuals [32]. Namely, starting from a basic SIR model (I.2), we searched for the time–profile of these controls that minimizes

$$J = \int_0^T (A_0 + A_1 \beta S(t) I(t)) dt = A_0 T + A_1 \int_0^T \beta S(t) I(t) dt,$$

where A_0, A_1 are the costs per unit of time of epidemic duration and of a single new infection, respectively, and T is the control–dependent elimination time (i.e. the first time that I drops below 1). Furthermore, we expanded the model applicability, by realistically imposing a possible limitation on the total amount of resources available for the control during the whole epidemic (e.g. limited vaccine supply or limited isolation places and funding), yielding a *limited resources* problem. Detailed motivations, analytical findings and numerical simulations are given in Chapter 1.

I.3 Threshold policies

In mathematical epidemiology, optimal control constitutes the most traditional approach for comparing, implementing and evaluating various detection, prevention and control programs with a view to balance benefits and costs.

However, due to a number of social, economic and political reasons, the optimal solution (especially if time–continuous) could hardly be implemented in practice for health organizations and institutions, whose plannings are usually not so flexible. Thus, the real management of infectious diseases spreading is often performed by fixing quotas, lengths of control seasons, costs of incentives and subsidies, or similar variables. In other words, the structure of the controller is fixed and only a few parameters are selected by the control agency.

In many cases, implementation of intervention measures depends on the *current* status of the disease in the community, for example control is active as long as the number of susceptible individuals exceeds a given threshold or only when the infections number reaches a critical level. It follows that the compartment sizes are used as an index for the authorities to implement control strategies. Also, several analyses have suggested that individuals reactively reduce their contact rates, in response to high levels of mortality or the presence of many infected individuals, during an epidemic [280, 315].

From a mathematical point of view, such kinds of interventions are modeled and represented by using a piecewise–continuous function which is dependent on the model

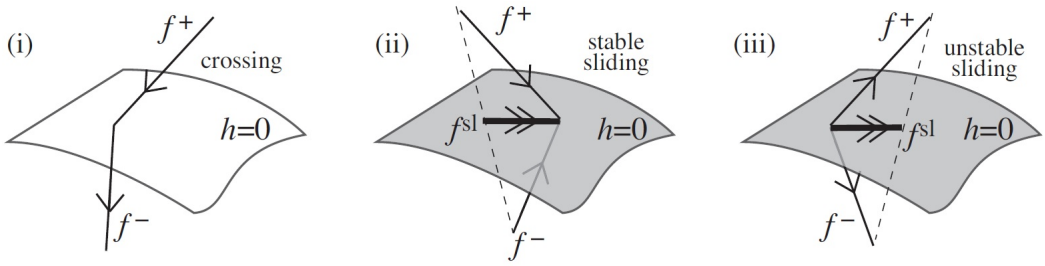

Figure I.3: (from [174]) Piecewise–smooth vector fields in regions of (i) crossing, (ii) stable sliding, and (iii) unstable sliding. This formalism is due to Filippov [125] and Utkin [286] and is said to define a Filippov system.

state variables. This type of control strategies is a so–called *threshold policy*, also referred as an *on–off* control or as a special and simple case of variable structure control in the control literature [125, 286]. The threshold introduces a discontinuity, so that the controlled system is, in the end, a discontinuous system.

Why discontinuous?

Many dynamical systems that naturally occur in the description of physical phenomena are discontinuous. That is, their motion is characterized by periods of smooth evolutions interrupted by instantaneous events. Traditional analysis of dynamical systems restricted its attention to smooth problems, thus preventing the investigation of non–smooth processes such as impact, switching, sliding and other discrete state transitions. These phenomena arise in any application involving processes with switching components or intermittently constrained systems. Plankton blooms in shallow lakes, recurrent invasions of insect pests in forests, children epidemics, pulsed chemotherapy, populations with selective switching between alternative habitats are important examples.

Earlier studies of non–smooth dynamics appeared in the Eastern European literature: for instance the pioneering work of Andronov *et al.* on non–smooth equilibrium bifurcations [12], Feigin on C–bifurcations [101, 123], Peterka and Babitskii on impact oscillators [15, 238] and Filippov on sliding motion [125].

There are various classes of discontinuous systems which have their own special features and require different methods for their analysis [26]. A first class is that of *impact* models originally used in mechanics to describe the dynamics of mechanical systems characterized by impacts among various masses (see [52] and references therein). Impact models represent the most naïve approach to the description of systems characterized by dynamic phenomena occurring at very diversified time scales. An apparently similar but substantially different class of models is that of *periodically pulsed* systems where the discontinuity in state space is generated by a periodic exogenous shock on the system.

A third class of discontinuous system, which is the one related to threshold policies in epidemic models, is that of piecewise–smooth system, often called *Filippov system*. Filippov systems are expressible in the form

$$\dot{x} = f(x(t), t),$$

where $x \in \mathbb{R}^n$ and f is piecewise–smooth, with discontinuities occurring across a hypersurface

through the phase space, called *switching manifold*. A local form for such system is

$$\dot{x} = f(x) = \begin{cases} f^+(x) & \text{if } h(x) > 0 \\ f^-(x) & \text{if } h(x) < 0 \end{cases}$$

where $h(x) = 0$ implicitly defines the switching manifold and each of the vector fields f^+ and f^- is smooth and defined for all x. At $h = 0$, trajectories either cross through the switching manifold or slide along it (see Fig. I.3). Sliding trajectories are solutions of $\dot{x} = f^{sl}$, where f^{sl} is a convex combination of f^+ and f^-:

$$\dot{x} = f^{sl} = (1 - \lambda)f^+ + \lambda f^-, \tag{I.7}$$

with

$$\lambda = \frac{\nabla h \cdot f^+}{\nabla h \cdot (f^+ - f^-)}$$

such that f^{sl} is always tangent to the switching manifold.

The analysis of this class of systems is not trivial since the onset of sliding motion can lead to intricate dynamics [26, 125, 174, 286], and often a numerical approach is required [98, 99, 239]. There are also distinctive phenomena unique to piecewise–smooth systems, which can be analyzed mathematically but fall outside the usual methodology for smooth dynamical systems.

Filippov systems in epidemiology

Although some attempts were made to introduce threshold policies into epidemic models since the early 2000s [154, 280], the first formal example (to the best of our knowledge) of a Filippov system in epidemiology can be found in [315] where a basic SIR–like model is extended by including a piecewise–constant transmission rate to represent control or precautionary measures being triggered once the number of infected individuals exceeds a threshold level. Starting from (I.2), the following system is considered

$$\begin{aligned} \dot{S} &= \Lambda - \beta(1 - c)SI - \mu S \\ \dot{I} &= \beta(1 - c)SI - \gamma I - \mu I \\ \dot{R} &= \gamma I - \mu R \end{aligned}$$

with

$$c = \begin{cases} 0 & \text{if } I - \theta < 0 \\ \bar{c} & \text{if } I - \theta > 0 \end{cases}$$

where $\Lambda \geq 0$ is the (constant) recruitment rate and $\mu \geq 0$ the natural mortality rate of the population. θ is the critical level of infected individuals at which people are sufficiently aware of the infection to change their behavior and some control measures are implemented, resulting in the reduction ($\bar{c}$) in transmission. The authors investigated the long–term dynamic behavior of the model, by studying the stability properties of both equilibria and *pseudo–equilibria* (i.e. stationary sliding solutions of (I.7)), and pointed out that choosing a proper combination of threshold level and control intensities is crucial in order to preclude the outbreak or to stabilize the infection at a desired level.

Reactive culling Since the work of Xiao *et al.* [315], theoretical investigations of sliding control in epidemiology have been developed and applications for different infections were provided, such as West Nile Virus [316] and avian influenza [85, 86]. We followed this approach to investigate the effectiveness of culling strategies to control infectious diseases in wildlife.

The majority of emerging and re–emerging diseases have originated from or are still maintained in wildlife hosts [175]. The common intervention strategy to control wildlife diseases is non–selective culling, i.e. the slaughtering of both infected and healthy individuals. The appeal of culling relies on two main reasons: i) vaccination and drug treatments, typically implemented for humans and livestock diseases, are often not available or unpractical in the case of wildlife diseases; ii) culling is relatively easy to implement, for instance through game hunting or traps.

As intensive culling rates can be enforced only for a limited amount of time for economic and logistic reasons, a variety of intermittent culling strategies has been historically implemented by health authorities in order to fight wildlife diseases. In particular, intensified hunting campaigns at the onset of the epidemics (the so–called *reactive culling*) were performed to control bovine tuberculosis in British badger [108], rabies in European fox [298] and Canadian raccoon [259], in the effort to drive population density below the threshold for disease elimination. However, there is an increasing amount of theoretical [34, 35, 84] and empirical [107, 197, 223, 298] evidences that culling may be ineffective in eliminating pathogens from wild populations, even increase the severity of epidemics.

Motivated by these counter–intuitive findings, we investigated the effectiveness of localized culling using the following two–patches metapopulation Susceptible–Infected (SI) model

$$\begin{aligned}\dot{S}_i &= \nu S_i - \beta S_i I_i - (\mu + \eta N_i + c_i) S_i - D(S_i - S_j)\\ \dot{I}_i &= \beta S_i I_i - (\mu + \alpha + \eta N_i + c_i) I_1 - D(I_i - I_j)\end{aligned}$$

with $N_i = S_i + I_i$ and $i, j \in \{1, 2\}$, $i \neq j$. All the parameters are positive constants: ν is the fertility rate; β is the transmission rate; μ, η and α are the natural, density–dependent and disease–induced mortality rates, respectively; D is the per–capita dispersal rate from a patch to the other.

Culling activities (at a rate c_i) are performed in only one patch ($c_2 = 0$). In the controlled patch we compared the use of *proactive culling*, namely constant control

$$c_1 = \bar{c} = const.$$

with that of reactive culling, namely the prevalence–dependent threshold policy

$$c_1 = \begin{cases} 0 & \text{if } I_1 - \theta < 0 \\ \bar{c} & \text{if } I_1 - \theta > 0 \end{cases}$$

leading to a Filippov system. In Chapter 2, we faced the problem both analytically and numerically. Our results confirm that localized culling may be ineffective in controlling diseases in wild populations, even leading to unexpected increases in the number of infected individuals in the nearby areas.

I.4 Behavioral change models

In the last decades, mathematical models of infectious diseases have become more and more sophisticated tools for assisting public health decisions and policies, and are used in a growing number of countries worldwide. Despite these advancements, there is an increasing awareness that this sophisticated modeling neglects a 'layer' of complexity, which is critical to understand the mechanisms underlying infection transmission and control. This missing layer is *human behavior*.

For instance, unfounded vaccine scares such as the ongoing measles–mumps–rubella (MMR) vaccine autism scare which started in 1997, or the oral polio vaccine scare in northern Nigeria in 2003–2004 which arguably delayed global polio eradication by a decade, can enable a resurgence of the disease in a population [199]. Similarly, traditional infection control methods such as isolation, quarantine, and contact tracing require adequate levels of support from the public. When this is lacking, sometimes due to mismanagement of the situation by authorities or inadequate response of the international community, then infection control can fail, as was observed in the early stages of the 2014 West African Ebola outbreaks and in many other situations [100].

We refer to models incorporating behavioral aspects as *behavioral change models* (BCMs), which typically complement models for disease transmission in an attempt to mimic real life dynamics. In essence, a BCM is a model in which individuals are responsive to external information about the disease and, as a result, decide whether to take one or more preventive measures to reduce the chance of contracting the infection. The external information to which individuals respond can be global (equally available and relevant to all individuals) or local (individual availability and relevance determined by physical or social proximity to the information source). Furthermore, this information can be specified in terms of actual risks ('prevalence–based') or of perceptions of these risks ('belief–based'), as well as a mixture of all the above [130].

A widely used theoretical foundation for the formation and dynamic nature of individuals' behavior comes from game theory [130, 289]. Game theory has a rich history in social sciences with the Prisoner's Dilemma [138] being a frequently used illustration*. Game theory assumes individuals take rational decisions based on a trade–off that embodies the anticipated rational decisions of all other individuals in society.

Another foundation for behavior change is found in the fields of network science and individual–based modeling, where there are opportunities to develop more realistic models by introducing (more) heterogeneity [217, 255]. The challenge here is to find a balance between model complexity and computational boundaries.

The vaccination game

The vaccination policies of a large number of countries are based on voluntary compliance, and drops in vaccination coverage have led to increased interest in so–called rational vaccination decisions and their effects on the epidemiology of vaccine–preventable infectious diseases.

By making a rational choice of whether to vaccinate themselves or their children, individuals weigh up the costs and risks associated with vaccination with its benefit of

*So called because it was originally explained as a decision process made by two prisoners being interrogated in separate jail cells who must decide whether to confess their crime, or stick to their story of being innocent.

removing or reducing the risk of infection. Game theory provides a tool to study simple conflicts of individuals choosing between actions of different costs and benefits while acting perfectly rationally to maximize their own gain.

A powerful approach to modeling behavior by setting ideas from game theory into a population dynamics framework is the *imitation game dynamics* [293]. *Imitation* represents a main avenue through which the different strategies enacted by players can spread within a population, through mutual learning between individuals. The first application of imitation game dynamics to investigate vaccinating behavior and its feedback on infection dynamics and control was developed in a seminal paper by Bauch [21]. He considered an SIR–like model describing the dynamics of a vaccine–preventable childhood disease:

$$\begin{aligned} \dot{S} &= \mu(1-p(t)) - \beta SI - \mu S \\ \dot{I} &= \beta SI - \gamma I - \mu I \\ \dot{R} &= \mu p(t) + \gamma I - \mu R. \end{aligned} \tag{I.8}$$

Here the state variables S, I, R are *fractions* w.r.t. the total (constant) population; μ is the natural birth and mortality rate, β the transmission rate and γ the recovery rate.

Vaccination is administered at birth alone, hence $p(t)$ represents the 'propensity to vaccinate' among parents. The dynamics of p follows an imitation game dynamics that could be inferred by employing the concept of pay–offs, even if at its core there is again a mass–action diffusion process based on statistical physics [293]. The basic idea is that the population of parents is proportional to the total population and is divided into two subgroups: 'pro–vaccine' (p) and 'anti–vaccine' ($1-p$). The dynamics of the two involved groups is ruled by a 'double contagion' of ideas yielding

$$\dot{p} = kp(1-p)(\theta(I) - \alpha), \tag{I.9}$$

where $\theta(\cdot)$ is the perceived risk of infection, assumed prevalence–dependent, α is the perceived risk of vaccine–related side effects (VSEs) and k is a time scale tuning parameter modeling the *imitation speed*. The ensuing model predicts the possibility of vaccine uptake oscillations, that are more likely if individuals imitate others more readily (higher k) or exhibit a stronger response to increases in prevalence (higher $\theta'(I)$). Oscillations are also more likely when the perceived risk of VSEs (α) is high.

The Bauch model (I.8)–(I.9) was then extended by considering that the perceived risk of vaccination is not constant, but depending on the available information or rumors on VSEs ($\alpha = \alpha(p)$) [111], and accounting for vaccine awareness campaigns (VACs) enacted by the public health system at a rate $u(\cdot)$ (either constant [112] or time–dependent [57, 65]), finally yielding

$$\dot{p} = kp(1-p)(\theta(I) - \alpha(p)) + ku(t)(1-p). \tag{I.10}$$

Under these assumptions, it was shown that VACs (including information, education, availability of vaccination infrastructures, etc) have a stabilising role which may eliminate the disease and, in any case, reduce the strength of imitation–induced oscillations [57, 65, 112]. This is a rather realistic scenario: for example, in England and Wales public campaigns allowed to achieve a large MMR vaccine uptake although under the elimination threshold (see Fig. I.4).

Rapid opinion switching In [21, 57, 65, 111, 112] the analytical and numerical investigation was focused on scenarios where individuals slowly change their opinion

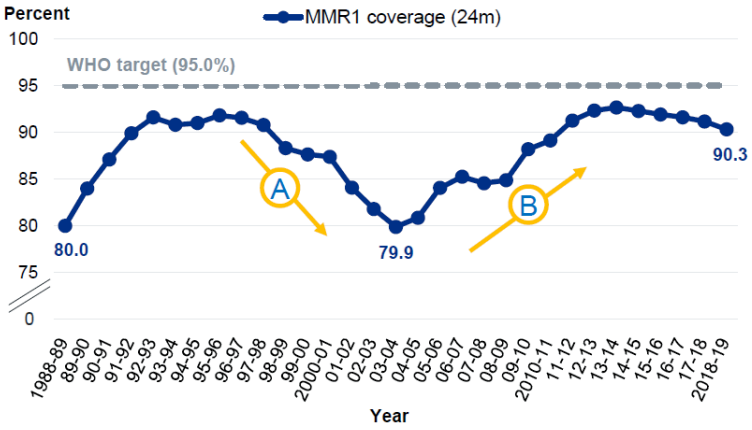

Figure I.4: England national coverage of MMR first dose (MMR1) at 24 months from birth. Arrow A: impact on coverage of a since discredited potential link between the MMR vaccine and autism and Crohn's disease. Arrow B: subsequent recovery of coverage rates as a result of national campaigns and local initiatives [229].

($k \not\gg 1$ in (I.10)). This assumption, however, in the age of social media is increasingly questionable. Nowadays, the opinion formation is based on information and noises collected and exchanged via Internet–based communication channels. This makes the opinion of population much more volatile than in the past on many sensitive subjects, including politics [7] and vaccines [53, 215].

From these considerations, it seemed appropriate to us to assume that the time–scale of imitation speed is nowadays very short: $k \gg 1$, so allowing to apply a quasi–steady–state approximation to the imitation game dynamics equation for p (I.10), that passes from being differential to algebraic:

$$p(1-p)(\theta(I) - \alpha(p)) + u(t)(1-p) = 0.$$

In Chapter 3 this problem was thoroughly motivated and faced. In particular, the control function $u(\cdot)$ was assumed to be 'optimal' (in the sense of Section I.2) and an optimal control problem was set by searching for the control time–profile that jointly minimizes the disease–burden, the vaccination costs and the economic burden to enact VACs. Since for the problem at hand the existence of the optimal solution turned out to be not guaranteed, the recourse to direct optimization methods was required.

A phenomenological approach

A *behavior–implicit* or phenomenological approach to mathematically modeling behavior is represented by *information–dependent* epidemic models (IDEMs), first introduced in [113] for vaccine–preventable childhood diseases.

It is known that individuals follow possibly complex behavioral rules when deciding whether to use or not use a disease–protective tool. The underlying rationale is that these rules will often translate into simple relationships between the individual probability to adopt the tool and the gathered information (or rumors) on infection spread. Therefore, these models postulate relatively simple feedback mechanisms whereby trends of infection can affect the current protection level, eventually feeding–back on infection dynamics.

According to the idea of IDEMs, the rate of adoption of the protective tool (e.g. the newborns vaccine uptake p in model (I.8)) is a function of an *information index* $M(t)$. This

index is defined in terms of a delay τ, a memory kernel K and a function g which describes the information that is relevant to the public in determining its final choice to adopt or not to adopt the protective measure (the *message* function). Therefore, $M(t)$ is given by the following distributed delay

$$M(t) = \int_{-\infty}^{t} g\left(x_1(\tau), \ldots, x_k(\tau)\right) \, K(t-\tau) d\tau, \tag{I.11}$$

where the message function g depends on one or more model state variables, say x_1, ..., x_k, $k \in \mathbb{N}$ (usually on prevalence [113, 114], incidence [64] or other relevant quantities like VSEs [115]). It is usually assumed that $g(x_1, \ldots, x_k) = 0$ if $t < 0$. The delaying kernel $K(\cdot)$ is a probability density function representing the weight given to past history of the disease. Besides the relatively simple case $K(t) = \delta(t)$, the literature has focused on kernels allowing reduction to ordinary differential equations (ODEs) [55, 113–115]. In particular, when an n–order Erlang memory kernel is used, namely

$$K(t) = Erl_{n,a}(t) = \frac{a^n}{(n-1)!} t^{n-1} e^{-at}, \;\; t, a \in \mathbb{R}_+, \, n \in \mathbb{N}, \tag{I.12}$$

the so called 'linear chain trick' can be applied [207]: it allows to pass from (I.11) to a system of n ODEs.

IDEMs are described as phenomenological because, although motivated by psychological factors, the equations only describe the impact of such psychological factors on the transmission rate without actually modeling specific psychological processes such as individual cognition or social learning.

Actually the class of imitation–based models and that of the phenomenological models are strictly linked [111]. For vaccination models, also IDEMs may trigger the onset of steady oscillations [64, 113, 114] and other new dynamical phenomena compared with the corresponding non–behavioral models. Thus, human behavior might be a critical factor in explaining the presence of oscillations in time–series of some vaccine–preventable infectious diseases.

Besides the case of newborns vaccination, the method of IDEMs was adopted for modeling vaccination also to later ages [55, 113], social distancing measures [109] and others, and is currently under development.

Imperfect waning vaccines Below the voluntariness of immunization programs, the degree of protection against vaccine–preventable diseases is also affected by the effectiveness of vaccination. Indeed, some vaccines, especially those for new or constantly evolving viruses, reduce the infection risk, but do not prevent a vaccinated individual from acquiring and transmitting the disease (the so–called *leaky* vaccines [152, 195]). Further, the vaccine–acquired immunity may wane over time. For instance, there is evidence that US influenza vaccine effectiveness declined up to 11% about per month from the 2011–2012 trough 2014–2015 influenza seasons [124]. At the moment[†], there is a heated debate about candidate COVID–19 vaccines, whose efficacy assessment seems very challenging [162, 203].

These two critical aspects (behavioral change and partially effective immunity), taken individually, have been deeply investigated through epidemiological models and, generally speaking, the relative studies have enlightened the dangerous implications on the public

[†]December 2020.

health. However, only recently attempts to incorporate both aspects into the same model are arising [82, 110, 194].

The interest in further investigating the interplay between human behavior, vaccine imperfection and disease dynamics led us to develop a new BCM. Specifically, we considered the following Susceptible–Infected–Susceptible–Vaccinated (SISV) model describing the dynamic of vaccine–preventable diseases not conferring any long–lasting immunity

$$\begin{aligned}\dot{S} &= \mu + \gamma I + \vartheta V - \beta SI - \varphi(t)\, S - \mu S\\ \dot{I} &= \beta SI + \sigma\beta VI - \gamma I - \mu I\\ \dot{V} &= \varphi(t)\, S - \sigma\beta VI - \vartheta V - \mu V.\end{aligned}$$

Here, at variance with (I.8), vaccination is administered at all ages (with time–dependent rate $\varphi(t)$). Individuals of the vaccinated class (V) may still acquire the disease at the reduced rate $\sigma\beta$ ($0 < \sigma < 1$) and lose their immunity with rate ϑ.

Following the idea of IDEMs, we assumed that $\varphi(t)$ is a positive increasing function of the present and past information concerning the disease: $\varphi(t) = \varphi(M(t))$, with $M(t)$ as in (I.11) by choosing $K = Erl_{1,a}$ and a prevalence–dependent message function $g = g(I)$.

As shown in Chapter 4, model qualitative analysis reveals a large spectrum of possible dynamical patterns, which appears much more diversified compared with that of models including behavioral aspects but not the imperfect vaccine or vice versa.

The COVID–19 pandemic At time of writing this thesis, the world is facing a pandemic of a novel coronavirus (SARS–CoV–2), which started as an outbreak of pneumonia of unknown cause in Wuhan city of China in December 2019 [70, 288]. In the absence of pharmaceutical interventions (such as a safe and effective vaccine and a COVID–19 anti–viral), efforts aimed at containing the disease spreading have been focused on the implementation of non–pharmaceutical interventions, such as social distance, use of face–masks, quarantine of suspected cases, isolation and hospitalization of confirmed cases, contact–tracing, mass testing, etc. Each government enacted a series of restrictions, including recommendation of restricted movements for some or all of their citizens, and localized or national *lockdown* with the partial or full closing–off of non–essential companies and manufacturing plants [50].

Although most people have followed the rules, there were many reports of people breaching restrictions or even protest against lockdown [48]. This behavior might be related to costs that individuals affected by epidemic control measures paid in terms of both health and economic conditions, including interruption of work activities, psychological pressure and loss of relationships, resulting in a substantial damage to population well–being [51].

In order to qualitatively investigate the impact on disease spreading and control of human behavior responses to social alarm, we adopted the method of IDEMs. In particular, we considered an epidemic model with seven compartments: susceptible (S), exposed (E), post–latent (I_p), asymptomatic/mildly symptomatic (I_m), severely symptomatic/hospitalized (I_s), quarantined (Q) and recovered (R) individuals; and assumed that the choice to respect the lockdown restrictions, specifically the social distance and the quarantine, is partially determined on voluntary basis and depends on the information index. It follows that the transmission [resp. quarantine] rate is a positive decreasing [resp. increasing] function w.r.t. M, with M as in (I.11) by choosing $K = Erl_{1,a}$ and $g = g(I_s, Q)$.

Detailed model derivation and numerical investigations are given in Chapter 5. We focused on the case of the first COVID–19 epidemic wave in Italy during the period that begins on February 24, 2020, when the first bulletin by the Italian Civil Protection was reported [171], includes the partial and full lockdown restrictions, and ends on May 18, 2020, when the lockdown restrictions were mostly (but just temporally) removed.

Chapter 1

Minimizing epidemic size and duration with limited resources

The total number of infections (epidemic size) and the time needed for the infection to go extinct (epidemic duration) represent two of the main indicators for the severity of infectious disease epidemics in humans and livestocks. However, few attempts have been made to address the problem of minimizing at the same time the epidemic size and duration from a theoretical point of view by using optimal control theory. In this chapter, we investigate the multi–objective optimal control problem aiming to minimize, through either vaccination or isolation, a suitable combination of epidemic size and duration when both maximum control effort and total amount of resources available during the entire epidemic period are limited.

Application of Pontryagin's maximum principle to a Susceptible–Infected–Removed epidemic model, shows that, when the resources are not sufficient to maintain the maximum control effort for the entire duration of the epidemic, the optimal vaccination control admits only bang–bang solutions with one or two switches, while the optimal isolation control admits only bang–bang solutions with one switch. We also find that, especially when the maximum control effort is low, there may exist a trade–off between the minimization of the two objectives. Consideration of this conflict among objectives can be crucial in successfully tackling real–world problems, where different stakeholders with potentially different objectives are involved.

Finally, the particular case of the minimum time optimal control problem with limited resources is discussed. The results of this study have been published in [32].

1.1 Background

Direct and indirect costs generated by human and livestock epidemics are responsible for significant economic losses worldwide [245]. Direct costs of epidemics are strictly related to the epidemic size, i.e. the total number of infected individuals or farms. In humans, direct costs are associated to the number of medications and hospitalizations, while, in livestock, they are associated to the number of vaccinated/slaughtered animals and/or the number of farms where surveillance and control operations are conducted. Although direct costs of epidemics are usually not negligible, they are often overtaken by the indirect costs generated by production losses due to morbidity, mortality, and sanitary restrictions [233, 265].

Indirect costs can depend on the epidemic size, such as production losses due to worker illnesses or animal slaughtering, but also on other factors, such as the epidemic duration (i.e. the time passed between the first infection and the extinction of the epidemic). The latter involves the cases of restrictions on travels and trades, which are imposed until a disease–free status is regained. Some kinds of travel restrictions have been implemented for SARS, H1N1 influenza pandemic, and Ebola, causing severe economic burdens in the countries affected by these actions [78, 157, 252]. Similarly, trade restrictions have been enforced in the past during livestock outbreaks – such as bovine spongiform encephalopathy, foot and mouth disease (FMD), and avian influenza – resulting in devastating economic losses in countries with export–focused livestock industries [188, 191].

As anticipated in Section I.2, optimal control models have been widely used to identify effective strategies for minimizing the economic impacts of infectious diseases through vaccination, isolation and culling [22, 39, 155, 224, 296]. The aim of these models has been to minimize the costs of the epidemic, which have been usually assumed proportional to the total number of infected individuals (or the total infected burden). Conversely, the costs associated to the epidemic duration have been often overlooked in these analyses (but see [33, 96, 317]). Although we would expect a large level of correlation between the size of

epidemics and their duration, simulation models developed to evaluate the effectiveness of control policies for infections in livestock showed that the recommended interventions may differ when considering different objectives to pursue, such as minimizing the epidemic size or duration [246].

Resources available for public health programs are often constrained, limiting the admissible disease control actions. Limitations on the availability of personnel, material, and logistical resources can affect the implementation of disease control measures in different ways. Shortages in workforce generally limit the maximum effort available per unit time for given activities. For instance, an insufficient number of medical doctors and other healthcare workers will limit the number of patients that can be examined, treated, or vaccinated daily. Such shortages in healthcare workers have been experienced during past epidemic events, as Western Africa Ebola epidemic [144], and are expected in the case of influenza pandemics [19] or bioterrorist attacks [295]. Similarly, in livestock diseases, constraints in the availability of veterinaries and other personnel can limit the number of farms where the activities of surveillance, vaccination, disinfection or slaughtering are implemented each day. In recent classical swine fever (CSF) and FMD outbreaks, the operations of disposal of slaughtered animals and decontamination of infected farms underwent serious delays due to the insufficient number of veterinarians and haulers involved, with severe consequences on disease spread [41, 211, 230].

Furthermore, shortages in drugs supply or logistic resources can also affect the total amount of activities implemented during the outbreak. For instance, limitations in the vaccine stockpile available impose a bound on the total number of administered vaccinations during the entire epidemic period. There are different examples of shortages in vaccine stockpile negatively affecting the control of human – such as yellow fever [226] and seasonal influenza [71] – as well as livestock epidemics – such as avian influenza [212] and FMD [242]. Analogously, limitations in logistical resources, such as the number of hospital beds in the case of human diseases or the capacity of burial sites in the case of livestock diseases, bind the total amount of hospitalized patients [141, 279] or slaughtered animals [41, 230] during the entire epidemic period, respectively.

Here, by using the optimal control theory on simple SIR models, we investigate the problem of minimizing both the epidemic size and duration through isolation or vaccination, by taking into account limitations in the maximum control effort available per unit time and in the total amount of resources allocated for the epidemic (limited resources problem, [155]).

The theoretical framework of disease control with limited resources, as the one proposed here, represents a common scenario faced by decision–makers in real–world applications. For several highly contagious diseases (in both human and livestock), the sanitary and economic costs due to the infection are orders of magnitude higher than the costs of control. Paradigmatic examples of these cases are Ebola and meningococcal meningitis (in human) and highly–pathogenic avian influenza (HPAI) and FMD (in livestock). In addition, the response to terrorist attacks committed with biological agents (e.g. anthrax) could also be included in these scenarios.

For these infections, contingency plans and preparedness programmes are commonly in place in disease–free countries considered at risk of introduction. These programs can dictate the amount of vaccine doses stockpiled for emergency vaccination campaigns, the personnel, equipment, and facilities required to manage emergencies, etc. Then, it follows that the resources for disease control are already available at the beginning of epidemics, implying that several costs associated to control implementation have been already borne before the first infection event occurs. For instance, both the European Union (Council

Decision 91/666/EEC) and the USA (Agriculture Improvement Act of 2018) have established, and mandatory funded, the vaccine banks for FMD. Moreover, the World Organization for Animal Health has established global vaccine banks funded by the member states for different animal diseases, such as avian influenza, FMD, rabies, and Peste des Petits Ruminants [313]. In a similar way, global stockpiles have been established by the World Health Organization for human infections, such as cholera, meningococcal meningitis, and yellow fever [301]. However, there exist different examples where the number of stockpiled doses in vaccine banks were insufficient to face large outbreaks. During the 2015 outbreak of meningococcal meningitis (serogroup C) in Niger, the reserves of polysaccharide and conjugate vaccines used for emergency vaccinations were quickly deprived and the additional doses urgently produced by the pharmaceutical industries were dispatched to Niger only five months after the beginning of the epidemic [302]. Analogously, the emergency vaccination activities implemented during an outbreak of FMD in South Korea livestock in 2010 depleted the FMD vaccine banks from all around the world [91]. Thus, in these contexts, the role of the health authorities appointed to epidemic control consists of allocating in space and time the (limited) resources already available instead of evaluating the financial costs and benefits associated to different control policies.

The chapter is organized as follows. Firstly, we will present the model equations (Section 1.2) and will investigate the optimal control problem of minimizing epidemic size and duration (multi–objective problem) via vaccination or isolation under the constraints of limited resources (Section 1.3). Then, in the limited resources framework, we will provide the solutions for the optimal vaccination and isolation problems to minimize the epidemic duration only, where (conversely to the minimization of the epidemic size, see [155]) the shape of optimal control solutions has not yet been investigated, to our knowledge (Section 1.4). In addition to the analytical solutions, we will provide numerical simulations in order to understand how the profiles of the optimal control solutions change as functions of: (*i*) the maximum effort; (*ii*) the total amount of available resources; and, (*iii*) for the multi–objective problem, different assumptions on the weight of the size and the duration on the epidemic costs. Finally, the presented results are discussed in Section 1.5.

1.2 Model formulation

We consider an infectious disease spreading in a host population (human or animal), whose time–evolution is ruled by the basic SIR model:

$$\begin{aligned} \dot{S} &= f_1(S,I) = -\beta SI \\ \dot{I} &= f_2(S,I) = \beta SI - \gamma I, \end{aligned} \tag{1.1}$$

where S and I are functions of time denoting the number of susceptible and infected units at time t, respectively. The units of observation in model (1.1) may represent either individuals (in the case of human diseases) or farms (in the case of livestock diseases). The upper dot denotes the time–derivative. The parameters are positive constants: β represents the transmission rate and γ represents the sum of the recovery rate and the disease–induced mortality rate.

We look for optimal time profiles of two alternative control policies: vaccination of susceptible units and isolation of infected units. Let us denote by $u(t)$ the generic per–capita control rate and assume that $u(t) \in U = [0, u_{max}]$, with $u_{max} \in \mathbb{R}_+$. The

assumption of upper boundedness for $u(t)$ reflects the realistic scenario of practical limitations on the maximum rate at which the control strategy may be employed. Such a restriction is due to several factors, including the limited number of health officers, the time necessary for detecting the target individuals, the reduced capacity of infrastructures and so on. Specifically, by setting an upper bound on $u(t)$, we are assuming a limit on the maximum control effort relative to the target population instead on the overall control activities performed per unit time (which are represented by $u(t)S(t)$ [resp. $u(t)I(t)$] in the case of vaccination [resp. isolation]). While the bound on the overall activities represents the most suitable assumption in the case of planned operations (such as vaccination for childhood diseases in developed countries), the bound on the control effort seems more suitable in the case of emergency operations where the procedures of vaccination and/or isolation are forerun by surveillance and testing activities aimed at detecting the target populations. Typical examples in this sense are represented by the test–and–vaccinate [264], test–and–isolate [250], and test–and–cull [235] control strategies. Our assumption is consistent with those made in simulation–based models developed for FMD control in livestock where the resources for control are considered as 'consumed' regardless of whether surveillance visits to farms lead to positive assessment or not [44].

Let us now introduce a further state variable, z. It denotes the total number of units adopting the control strategy up to time t, i.e. the number of vaccinated individuals or farms

$$z = z_v = \int_0^t u(\tau)S(\tau)d\tau$$

or, alternately, the number of isolated units

$$z = z_i = \int_0^t u(\tau)I(\tau)d\tau.$$

Then, the general controlled system with limited resources in compact form reads:

$$\dot{x} = f(x) + u(t)g(x), \tag{1.2}$$

where $x = (S, I, z)^T$ is the state–variables vector, $f = (f_1, f_2, 0)^T$ with f_1 and f_2 defined by the right–hand side of (1.1) and g depends on the chosen control policy. In detail,

$$g = g_v = \begin{pmatrix} -S \\ 0 \\ S \end{pmatrix} \quad \text{for vaccination control} \tag{1.3}$$

$$g = g_i = \begin{pmatrix} 0 \\ -I \\ I \end{pmatrix} \quad \text{for isolation control.} \tag{1.4}$$

As in [33, 155], we choose the *elimination time* T as the terminal time of planning (i.e. time horizon). Formally, let ε be a positive constant such that $\varepsilon < 1$, then

$$T = \inf\{t \in \mathbb{R}_+ | I(t) = \varepsilon\}. \tag{1.5}$$

To make the definition (1.5) meaningful, we choose the initial number of infected units $I(0)$ strictly greater than ε. As a consequence, T is the first time at which the state variable I drops to ε. Using this approach, we avoid the undesirable possibility of subsequent peaks

of infection caused by a fractional number of infectives [155]. From a biological point of view, by setting $\varepsilon < 1$ as the condition to identify the elimination time means assuming the infection goes extinct when there is less than one infected individual in the population.

As far as the terminal constraints are concerned, we follow the approach developed in [155]. Namely, we realistically impose a limitation on the total amount of resources available for the control during the whole epidemic (e.g. limited vaccine supply or limited isolation places and funding), yielding:

$$z(T) \leq z_{max}, \tag{1.6}$$

with $z_{max} \in \mathbb{R}_+$. In details,

$$z_v(T) = \int_0^T u(\tau)S(\tau)d\tau \leq z_{max} \quad \text{for vaccination control} \tag{1.7}$$

$$z_i(T) = \int_0^T u(\tau)I(\tau)d\tau \leq z_{max} \quad \text{for isolation control.} \tag{1.8}$$

From an epidemiological point of view, we can interpret $z_{max}/S(0)$ as the maximum fraction of the original population before the introduction of the infection that can be vaccinated or isolated.

It is important to stress that the assumption of finite control resources is different from that of upper bound on the control rate $u(t)$. Indeed, the former reflects constraints on the total number of individuals or farms that can be recruited (for vaccination or isolation), whereas the latter on the rate at which we can recruit them.

For convenience and clarity, we label as *limited* those resources not sufficient to maintain a maximum control rate for the entire duration of the outbreak, i.e. such that $z_{max} < z(T)\big|_{u\equiv u_{max}}$. Otherwise, if $z_{max} \geq z(T)\big|_{u\equiv u_{max}}$, then we say that the resources are *not limited*.

To model equations (1.2), we associate the following epidemiologically well–posed initial conditions:

$$S(0) = S_0 > 0,\ I(0) = I_0 > \varepsilon,\ z(0) = 0. \tag{1.9}$$

Note that, by simply adding the equations in (1.2), one gets that the set

$$\mathfrak{D} = \left\{x \in \mathbb{R}^3_+ |\, S + I + z \leq S_0 + I_0\right\} \tag{1.10}$$

is positively invariant, i.e. solutions of (1.2) starting in $\mathfrak{D}$ remain in $\mathfrak{D}$ for all $t \geq 0$. Therefore, it is not restrictive to limit our analyses to region $\mathfrak{D}$.

In the following sections we will complete the definition of the optimal control problem, by specifying two possible different targets. For each policy theoretical results are given and illustrated by means of numerical simulations.

1.3 Multi–objective control problem

As discussed in the Background section 1.1, in presence of a disease outbreak it may be of interest for public health authorities to minimize both the elimination time and the total epidemic size. To this aim, this section is devoted to the study of the control problem involving two different and coexisting goals, namely minimization of:

- costs due to the time period needed for outbreak elimination:

$$\int_0^T A_0 dt;$$

- costs due to the number of individuals or farms that were infected during the whole outbreak:

$$\int_0^T A_1 \beta SI dt; \tag{1.11}$$

where A_0, $A_1 \in \mathbb{R}^+$ are the balancing weight factors, representing the costs per unit time of epidemic duration and the costs of a single new infection, respectively.

Since the particular case $A_0 = 0$ was already studied in [155] and that with $A_1 = 0$ will be investigated in Section 1.4, it is not restrictive to set $A = A_0/A_1 > 0$, with A representing the relative cost per unit time of epidemic duration over the cost of a single new infection. Then, we consider the following multi–objective optimal control (MOOC) problem, aiming at minimizing simultaneously epidemic size and duration:

(MOOC) *Find an optimal control function $u^*(t)$ that minimizes the objective functional*

$$J = \int_0^T (A + \beta SI) dt, \tag{1.12}$$

with T given by (1.5), on the admissible set

$$\Omega = \left\{ u(\cdot) \in L^1(0,T) \mid u(t) \in U = [0, u_{max}] \right\},$$

subject to (1.2) with initial conditions (1.9) and terminal constraint (1.6).

The existence of the solution for the MOOC problem is guaranteed since the requirements of classical existence theorems are satisfied. More precisely, we refer to the formulation of Filippov theorem and its corresponding corollary given in [6] for proving the following theorem:

Theorem 1.1. *There exists an optimal control solution $u^*(t)$ to the MOOC problem.*

Proof. We list the requirements of the corollary of Filippov existence theorem in [6]:

1. the control set $U = [0, u_{max}]$ is compact;
2. the sets $A_U(x) = \{f(x) + u(t)g(x) | \, u(t) \in U\}$, $x \in \mathfrak{D}$ (with $\mathfrak{D}$ as in (1.10)), are convex;
3. there exists a constant C such that:

$$|f(x) + u(t)g(x)| \leq C(1 + |x|),$$

with $x \in \mathfrak{D}$ and $u(t) \in U$.

Condition 1 is trivial. Since $x \in \mathfrak{D}$ and $u(t) \in U$ the state and the control variables are *a priori* bounded and also Condition 3 is verified.

To check that Condition 2 holds, firstly we fix $x \in \mathfrak{D}$ and prove that the line connecting two points of $A_U(x)$ entirely lies in $A_U(x)$.

Let us take y_1, $y_2 \in A_U(x)$, then there exist $u_1(t)$, $u_2(t) \in U$ such that $y_j = f(x) + u_j(t)g(x)$, $j = 1, 2$. One easily gets:

$$\alpha y_1 + (1 - \alpha) y_2 = f(x) + (\alpha u_1(t) + (1 - \alpha) u_2(t)) g(x).$$

Since U is convex, $\alpha u_1(t) + (1 - \alpha) u_2(t) \in U$, $\forall \alpha \in [0, 1]$, and then

$$\alpha y_1 + (1 - \alpha) y_2 \in A_U(x), \, \forall \alpha \in [0, 1].$$

□

As regard the characterization of the optimal control, according to Pontryagin's maximum principle [77, 240], the problem of finding the time–dependent control variable $u^*(t)$ that minimizes the objective functional (1.12) is equivalent to the problem of minimizing the Hamiltonian:

$$H(x, u(t), \lambda) = A + \beta SI + \lambda^T \left(f(x) + u(t)g(x)\right), \tag{1.13}$$

given by the sum of the integrand of (1.12) and the scalar product of λ and the right–hand side of the state system (1.2). Here $\lambda = (\lambda_S, \lambda_I, \lambda_z)^T$ denotes as usual the *adjoint* variables vector at time t, which is the solution of the adjoint system

$$\dot{\lambda} = -\partial_x H(x^*, u^*(t), \lambda), \tag{1.14}$$

with the *transversality conditions*

$$\lambda_S(T) = 0, \;\; \lambda_I(T) \;\text{ free }, \;\; \lambda_z(T) \geq 0,$$

and $\lambda_z(T)$ such that

$$\lambda_z(T)\left(z(T) - z_{max}\right) = 0. \tag{1.15}$$

The notation with superscript * is used to denote the solution to the state system (1.2) corresponding to the optimal control $u^*(t)$.

The above transversality conditions are consequence of the equality terminal constraint on the state variable I (given by (1.5)) and of the inequality terminal constraint on the state variable z (given by (1.6)). For analytical details see [77, 240, 263]. Actually, as H does not depend on z, we can simplify right now:

$$\lambda_z(T) = \lambda_z = const. \geq 0. \tag{1.16}$$

Further, H is constantly equal to zero along the optimal solution:

$$H(x^*, u^*(t), \lambda) \equiv 0.$$

In sum, the optimal control $u^*(t)$ that solves the control problem is the time–dependent function that minimizes the Hamiltonian:

$$H(x^*, u^*(t), \lambda) = \min_{u \in U} H(x^*, u(t), \lambda),$$

with H given by (1.13), where $(x^*, u^*(t), \lambda)$ must satisfy

$$\begin{aligned}
\dot{x} &= f(x) + u(t)g(x) \\
x(0) &= (S_0, I_0, 0)^T, \;\; I(T) = \varepsilon, \;\; z(T) \leq z_{max} \\
\dot{\lambda} &= -\partial_x H(x, u(t), \lambda) \\
\lambda_S(T) &= 0, \;\; \lambda_z \geq 0, \;\; \lambda_z(z(T) - z_{max}) = 0 \\
0 &= H(x, u(t), \lambda),
\end{aligned}$$

and the control horizon T is defined by (1.5).

Since H is linear respect to $u(t)$, the value of $u^*(t)$ is determined by the sign of the so–called *switching function*:

$$\psi(x, \lambda) = \partial_u H = \lambda^T g(x).$$

In particular,

$$u^*(t) = \begin{cases} 0 & \text{if } \psi(x^*, \lambda) > 0 \\ u_s(t) & \text{if } \psi(x^*, \lambda) = 0 \\ u_{max} & \text{if } \psi(x^*, \lambda) < 0 \end{cases} \tag{1.17}$$

with $u_s(t) \in U$.

If $\psi(x^*, \lambda)$ vanishes on a set of isolated points, the corresponding control function is a *bang–bang* control, as well known, and its value at these points is not defined. However, for convenience of numerical simulations, we consider it equal to u_{max}. The isolated time instants, internal to $[0, T]$, in which ψ vanishes are called *switching times*.

Unless otherwise specified, we restrict the use of the superscript * only to the optimal control function $u^*(t)$, in order to simplify the notation.

Admissible optimal controls and numerical method

The results that we will prove in the next sections can be summarized in the following theorem.

Theorem 1.2. *For each considered control policy, the optimal solution to the MOOC problem is a bang–bang control. In the most general form it reads:*

$$u^*(t) = \begin{cases} 0 & t \in [0, \tau_1) \\ u_{max} & t \in [\tau_1, \tau_2] \\ 0 & t \in (\tau_2, T] \end{cases} \tag{1.18}$$

with $\tau_1, \tau_2 \in [0, T]$*, and* $\tau_1 < \tau_2$.

The time instants $\tau_1 \in [0, T]$ and $\tau_2 \in (\tau_1, T]$ are introduced to extend the concept of switching time. Specifically, τ_1 [resp. τ_2] is the *starting* [resp. *ending*] *intervention time*, i.e. the first [resp. last] time instant at which the control $u^*(t)$ assumes the value u_{max}. The knowledge of such time instants allows to immediately obtain the control time–profile.

From Theorem 1.2 it follows that for each control policy at most four possible control profiles are allowed (sketched in Fig. 1.1):

(a) $\tau_1 = 0$ and $\tau_2 = T$, i.e. $u^*(t) \equiv u_{max}$ (namely, constant control),

(b) $\tau_1 > 0$ and $\tau_2 = T$, i.e. τ_1 is the only switching time and $u^*(t)$ changes its value from 0 to u_{max} ($0 \to u_{max}$, delayed control),

(c) $\tau_1 = 0$ and $\tau_2 < T$, i.e. τ_2 is the only switching time and $u^*(t)$ changes its value from u_{max} to 0 ($u_{max} \to 0$, reactive control),

(d) τ_1, $\tau_2 \in (0, T)$ are two switching times and $u^*(t)$ changes its value from 0 to u_{max} and again back to 0 ($0 \to u_{max} \to 0$, two–switches control).

As far as the numerical simulations are concerned, the shape of admissible optimal controls allows us to adopt a simple *ad hoc* numerical scheme, which generalizes that one implemented in Bolzoni *et al.* [33]. Such a scheme is based on the idea of identifying each bang–bang solution $u^*(t)$ with two real parameters: the starting and ending intervention times. Therefore, the functional $J(u)$ to be minimized, given by (1.12), can be seen as the

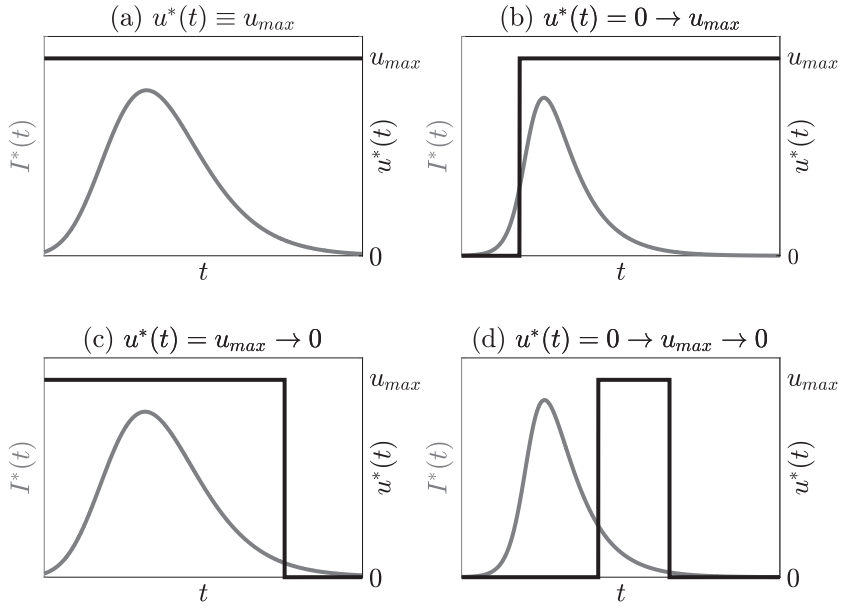

Figure 1.1: Schematisation of the four possible types of admissible controls. Namely, constant (a), delayed (b), reactive (c), and two–switches (d) controls. The time location of the switches with respect to the peak of infection is purely indicative.

function $J : (\tau_1, \tau_2) \to T$ that links the couple of characteristic intervention times to the elimination time T of the MOOC problem. An optimal control $u^*(t)$ will be identified by the pair (τ_1, τ_2) such that (τ_1, τ_2)=argmin$J$. The numerical solution will be computed by evaluating the function $J(\tau_1, \tau_2)$ over a suitable interval and looking for its minimum value. For the numerical integrations of the Cauchy problem (1.2)–(1.6)–(1.9) the Crank–Nicholson scheme with uniform time steps is used. For a detailed discussion of the implemented numerical method see [33]. Of course, if, for a certain policy, the MOOC admits only optimal control profiles with $\tau_1 = 0$ [resp. $\tau_2 = T$], then J can be seen as a function of one parameter only, being the starting [resp. ending] intervention time fixed.

Epidemiological parameters and initial conditions

Since the economic effects of epidemic duration (alongside with epidemic size) are larger in livestock diseases with respect to human ones, we focus on the applications of our study to livestock diseases and we set the epidemiological parameters and the initial conditions in the numerical simulations to investigate the between–farm dynamics of a domestic animals infection. In the simulations, we assume the farm as the unit of observation. We opt for a farm–based model (instead of an animal–based one) since the spread of infections in livestock is more suitably described by between–farm than between–animal transmission. In addition, the disease control measures (which are the main focus of our investigations) are generally implemented at farm level [246, 256]. The initial conditions for model (1.1) variables are set to a single infected unit ($I_0 = 1$) in a totally susceptible population of farms ($S_0 = 2000$).

We set the farm infectious period (corresponding to the average time a farm stays infected before recovering) to 6 days, which is consistent with the estimates obtained for highly contagious livestock diseases, such as FMD in cattle, range $2 - 14$ days [41, 156, 261, 283], and HPAI, range $1.5 - 7.4$ days [30, 266]. To keep our numerical results comparable with respect to those obtained by Bolzoni *et al.* [33], which provided numerical solutions of the

time–optimal control problems without resource limitations, we express our parameters as monthly rates. Then, the removal rate (γ) in model (1.1) is set to $\gamma = 5$ month^{-1}.

The basic reproduction number, $\mathcal{R}_0$, represents the average number of secondary infections produced by a single infected individual in a completely susceptible population in the absence of control (see Section I.1). Following Hethcote [159], we write $\mathcal{R}_0$ in model (1.1) as $\mathcal{R}_0 = \beta S_0/\gamma$. In our simulations, we set $\mathcal{R}_0 = 4$, which is consistent with the estimates of between–farm basic reproduction number obtained for FMD ($3 - 4$, [41, 156, 299]) and HPAI ($3 - 6.5$, [266, 270]).

We set our simulations to reproduce control scenarios where the available efforts for vaccination and isolation are limited. This is especially true in the early stages after the introduction of a new infection in a farm system. For instance, in the case of FMD in Australia, the human resource capacity for vaccination, based on the availability of teams with time to complete vaccination, has been estimated to be initially sufficient to vaccinate about $10 - 50$ farms per day [134, 253]. This means that, in a population of about 2000 farms (as set in our simulations), at most $0.15 - 0.75$ of the farms can be vaccinated per unit time (i.e. month). These data are consistent with those estimated in the case of CSF in Germany, where a maximum of 30 pig farms are expected to be vaccinated per day [54].

Following the argument in Coyne *et al.* [90], in model (1.2) with vaccination (1.3) the fraction of farms that can be treated per unit time can be approximated to $1 - \exp(-u_{max})$. Then, for vaccination, we set $u_{max} = 1$, meaning that about $1 - \exp(-1) = 0.63$ of the farms can be potentially vaccinated in a month, which is consistent with the data available on the field. Furthermore, Garner *et al.* [134] showed that in Australia the available effort for emergency vaccination in the case of FMD outbreaks, both in terms of available teams and time required to conduct visits on each farm, is similar to that for surveillance and infected premises operations (such as isolation and slaughtering). Then, in the simulations on the optimal control through isolation (i.e. model (1.2) given (1.4)), we set also the maximum isolation effort to $u_{max} = 1$.

In the numerical simulations, we set $\varepsilon = 0.5$ as in [33, 155]. However, as pointed out by Hansen and Day [155], any value smaller than one would work just as well for this purpose. Then, to test the sensitivity of the optimal solutions to ε, we perform numerical simulations using different parameter conditions (specifically, $\varepsilon = 0.1, 0.999$). In addition, we test the sensitivity of the optimal control solutions to different combinations of the other control parameters z_{max} and A. Finally, we explore in our simulations the impact of the maximum available efforts for vaccination and isolation on the shape of the optimal control functions by assuming less strict resource capacities for control (i.e. larger values of u_{max}), such as those available in later stages of epidemics [134, 253].

Vaccination policy

Let us first consider the problem of minimizing the epidemic size and duration through vaccination. The main result is that the admissible optimal controls are bang–bang with at most two switching times (see Fig. 1.1).

Theorem 1.3. *The optimal solution $u^*(t)$ to the MOOC problem, with $g = g_v$ given by (1.3) and terminal constraint (1.7), is a bang–bang control of the form (1.18) with at most two switches at $\tau_1, \tau_2 \in [0, T]$, and $\tau_1 < \tau_2$.*

In particular, if $\lambda_z = 0$, then τ_1 precedes the time–occurrence of the peak of infection, $\tau_2 = T$ and $z_v(T) \leq z_{max}$. Otherwise, if $\lambda_z > 0$, then $\tau_2 < T$ and $z_v(T) = z_{max}$ (namely, the resources are not limited).

Furthermore, if $u_{max} \gg \gamma$, *then* $\tau_1 = 0$.

Proof. Throughout the proof we omit the superscript * for the optimal quantities, in order to simplify the notation.

First we compute the Hamiltonian (1.13) along the optimal solution:

$$H = A + \beta SI - \lambda_S \left(\beta SI + u(t)S\right) + \lambda_I \left(\beta SI - \gamma I\right) + \lambda_z u(t) S \equiv 0, \tag{1.19}$$

and explicitly write the adjoint system (1.14):

$$\begin{aligned} \dot{\lambda}_S &= \left(\lambda_S - \lambda_I - 1\right)\beta I + \left(\lambda_S - \lambda_z\right) u(t) \\ \dot{\lambda}_I &= \left(\lambda_S - \lambda_I - 1\right)\beta S + \gamma \lambda_I \\ \dot{\lambda}_z &= 0. \end{aligned} \tag{1.20}$$

Since $\lambda_z = const.$, we denote indifferently with λ_z both the function and its constant value.

The switching function with its first and second time derivatives read, respectively:

$$\psi = \left(\lambda_z - \lambda_S\right) S \tag{1.21}$$

$$\dot{\psi} = \left(\lambda_I + 1 - \lambda_z\right) \beta SI \tag{1.22}$$

$$\ddot{\psi} = \beta SI \left((\lambda_z - 1)\gamma + \left(\lambda_S - \lambda_z\right)\beta S - \left(\beta I + u(t)\right)\left(\lambda_I + 1 - \lambda_z\right)\right). \tag{1.23}$$

By handling the (1.19) and (1.21), it is possible to rewrite the second equation in (1.20) as:

$$\dot{\lambda}_I = \frac{A + u(t)\psi}{I}. \tag{1.24}$$

Let us prove that ψ vanishes only in isolated points. Suppose that ψ vanishes in an open interval $\mathcal{I}$, then also all its time derivatives vanish there. In particular, $\psi = \dot{\psi} = \ddot{\psi} = 0$ in $\mathcal{I}$ yields:

$$\lambda_S = \lambda_z = 1, \;\; \lambda_I = 0,$$

and

$$H = A > 0$$

in $\mathcal{I}$, which contradicts the (1.19). As a consequence, $u(t)$ is a bang–bang control, i.e. a piecewise–continuous function that can assume only the extreme values of U: 0 and u_{max}. We denote by τ_s the generic switching time, namely $\tau_s \in (0, T)$ and $\psi(\tau_s) = 0$.

Two cases must be considered (see (1.15)–(1.16)):

- $\lambda_z = 0$ From (1.15) it immediately follows that $z_v(T) \leq z_{max}$.

  At the elimination time T, $\psi(T) = 0$ and $\dot{\psi}(T) = \left(\lambda_I(T) + 1\right)\beta S(T) I(T)$. The latter is positive, because:

  $$\lambda_I(T) + 1 = -\frac{A + \gamma I(T)}{\dot{I}(T)} > 0,$$

  as one can easily obtain by substituting the transversality condition $\lambda_S(T) = 0$ in the Hamiltonian (1.19). As a consequence,

  $$u(T) = u_{max} \tag{1.25}$$

  and, if multiple switching times are admissible, at the last one $\dot{\psi}(\tau_s) < 0$ (see (1.17)). Moreover, by setting $\lambda_z = 0$ in (1.21) and (1.22), we obtain that $\lambda_S(\tau_s) = 0$ and the

sign of $\dot{\psi}(\tau_s)$ coincides with that of $\lambda_I(\tau_s)+1$, namely, analogously to what happens at the elimination time T:

$$sign\left(\dot{\psi}(\tau_s)\right) = sign\left(-\frac{A+\gamma I(\tau_s)}{\dot{I}(\tau_s)}\right) = -sign\left(\beta S(\tau_s)-\gamma\right).$$

Since S is, by construction, a decreasing function and at the last switching time $\dot{\psi}$ is negative, the presence of two or more switching times must be excluded. Further, from the above considerations, it easily follows that the switch of $u(t)$ from 0 to u_{max} necessarily occurs before the time of the peak of infection, at which $S=\gamma/\beta$.

- $\lambda_z > 0$ From (1.15) it immediately follows that $z_v(T) = z_{max}$.

  Since at the elimination time T, $\psi(T) = \lambda_z S(T) > 0$, then $u(T) = 0$ and, if multiple switching times are admissible, at the last one $\dot{\psi}(\tau_s) > 0$ (see (1.17)). From (1.24) it follows that $\psi \geq 0$ implies $\dot{\lambda}_I > 0$. Thus, in virtue of (1.22), between two subsequent switching times the sign of ψ is necessarily negative. This definitely excludes the presence of three or more switching times. In synthesis, the optimal control $u(t)$ can change its value at most two times, in any case being null at the end.

In addition, we have to check that $u \equiv 0$ is not optimal for the MOOC problem. In fact, $u \equiv 0$ means that none of the available vaccination resources are used, hence $\lambda_z = 0$ (see (1.15)). This contradicts the (1.25). The first part of the statement is then proved.

To conclude the proof, we consider the particular case where $u_{max} \gg \gamma$ and verify that the optimal control $u(t)$ is constantly equal to u_{max} or switches from u_{max} to 0.

Suppose that $\tau_1 > 0$ is a switching time for $u(t)$ from no control to the maximum control rate; and let τ_2 be the second time at which ψ vanishes. From the above considerations, if $\lambda_z = 0$, then τ_2 is the elimination time T; otherwise, if $\lambda_z > 0$, then $\tau_2 < T$ is a switching time from u_{max} to 0. Further, taking into account the sign of (1.21) and (1.22), the following chain of inequalities holds:

$$\lambda_I(\tau_1)+1 < \lambda_S(\tau_1) = \lambda_z = \lambda_S(\tau_2) < \lambda_I(\tau_2)+1, \tag{1.26}$$

with $\tau_2 = T$ [resp. $\tau_2 < T$], if $\lambda_z = 0$ [resp. $\lambda_z > 0$].

Let us prove that

$$\dot{\lambda}_I > 0 \text{ in } [\tau_1, \tau_2]. \tag{1.27}$$

From (1.24) one obtains $\dot{\lambda}_I(\tau_j) = A/I(\tau_j) > 0$ for $j = 1, 2$. Let us suppose that there exists a time instant $\bar{t} \in (\tau_1, \tau_2)$ at which $\dot{\lambda}_I$ vanishes. Computing the second derivative of λ_I and evaluating it at $\bar{t}$, we obtain:

$$\ddot{\lambda}_I(\bar{t}) = (\lambda_I(\bar{t})+1-\lambda_z)\beta S(\bar{t})u_{max},$$

whose sign implies that $\dot{\lambda}_I$ vanishes at most one time in (τ_1, τ_2). Since $\dot{\lambda}_I$ is positive at τ_j, $j = 1, 2$, then it is necessarily positive in the whole interval (τ_1, τ_2).

From (1.26) and (1.27), it follows that $\lambda_I + 1$ intersects λ_S from below at least once in (τ_1, τ_2). Then, there exists a time instant $\tilde{t} \in (\tau_1, \tau_2)$ such that $\lambda_I(\tilde{t}) + 1 = \lambda_S(\tilde{t})$ and $\dot{\lambda}_I(\tilde{t}) > \dot{\lambda}_S(\tilde{t})$. If $u_{max} > \gamma$ the last inequality is equivalent to

$$\lambda_S(\tilde{t}) < \frac{u_{max}\lambda_z - \gamma}{u_{max} - \gamma}, \tag{1.28}$$

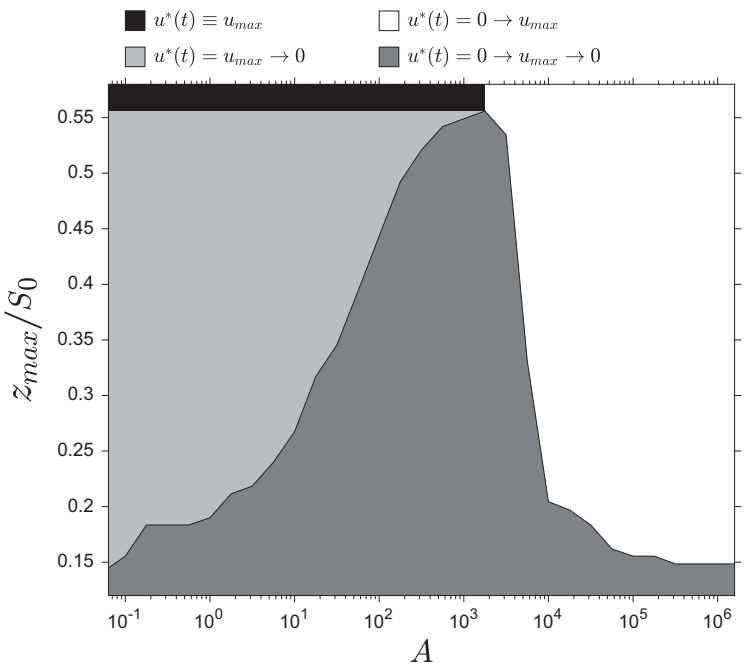

Figure 1.2: Numerical simulations of MOOC problem implementing vaccination strategy. The colors of each area in the parameter space $[A,\ z_{max}/S_0]$ (in semi–logarithmic scale) represents the corresponding type of optimal control solution. Color meaning is specified in the figure legend and refers to the four types of admissible vaccination control sketched in Fig. 1.1. Fixed parameters: $S_0 = 2000$, $I_0 = 1$, $\gamma = 5$ month^{-1}, $\mathcal{R}_0 = \beta S_0/\gamma = 4$, $\varepsilon = 0.5$, $u_{max} = 1$ month^{-1}.

where we substituted the equations (1.20). In particular, if $u_{max} \gg \gamma$, then the (1.28) reduces to $\lambda_S(\tilde{t}) < \lambda_z - \gamma/u_{max}$. Moreover, $u(t) = u_{max}$ in (τ_1, τ_2), hence it must be $\lambda_S(\tilde{t}) > \lambda_z$ (see (1.17) and (1.21)). Since we found a contradiction, it is necessarily $u(0) = u_{max}$. Namely, the MOOC problem selects for constant or reactive vaccination when $u_{max} \gg \gamma$. □

If we consider the limit case $u_{max} \gg \gamma$, then the possibilities reduce to two: constant control (Fig. 1.1a) or reactive control (Fig. 1.1c), as stated by Theorem 1.3.

Moreover, if the optimal vaccination problem selects for reactive or two–switches control (Fig. 1.1c and Fig. 1.1d, respectively), then all the available resources are used, i.e. $z_v(T) = z_{max}$. Otherwise, if the optimal vaccination control is constant or delayed (Fig. 1.1a and Fig. 1.1b, respectively), then it is feasible that not all resources are used. This is what happens, for example, if the available resources are not limited.

The numerical analyses of the optimal vaccination problem aimed at minimizing epidemic size and duration with limited resources are illustrated in Figs. 1.2 and 1.3. In Fig. 1.2, we show the results of the simulations performed in the parameter space $[A,\ z_{max}/S_0]$, where z_{max}/S_0 represents the maximum fraction of the original population before the introduction of the infection that can be vaccinated. The black, white, light gray and dark gray areas in Fig. 1.2 represent the combinations of parameters $[A,\ z_{max}/S_0]$ for which the optimal vaccination problem selects for constant (u_{max}, Fig. 1.1a), delayed ($0 \to u_{max}$, Fig. 1.1b), reactive ($u_{max} \to 0$, Fig. 1.1c), and two–switches control ($0 \to u_{max} \to 0$, Fig. 1.1d), respectively. We notice that, when the amount of available resources is sufficient to maintain a maximum control effort for the entire duration of the epidemic (large values of z_{max}/S_0), the optimal vaccination problem selects for constant control (when A is small) and for delayed

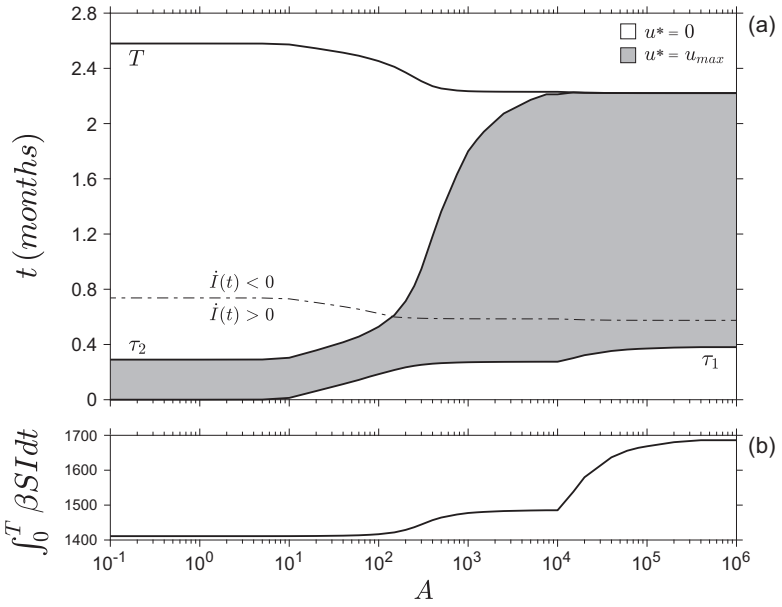

Figure 1.3: Numerical simulations of MOOC problem implementing vaccination strategy. (a) Starting intervention time τ_1, ending intervention time τ_2 and elimination time T as functions of A in semi–logarithmic scale. The dot-dashed curve represents the time instants in which $\dot{I}(t) = 0$. Control region color is gray [resp. white] where $u^*(t) = u_{max}$ [resp. $u^*(t) = 0$]. (b) Total number of infected units $\int_0^T \beta SIdt$ as function of A in semi–logarithmic scale. Fixed parameters: $S_0 = 2000$, $I_0 = 1$, $\gamma = 5$ month^{-1}, $\mathcal{R}_0 = \beta S_0/\gamma = 4$, $\varepsilon = 0.5$, $u_{max} = 1$ month^{-1} and $z_{max}/S_0 = 0.25$.

control (when A is larger). This is in agreement with the results obtained by Hansen and Day [155] and Bolzoni *et al.* [33] for the unconstrained problems of minimizing epidemic size and duration, respectively. For smaller values of z_{max}/S_0, the total amount of resources are not sufficient to maintain a maximum control effort for the entire epidemic (limited resources), then the constant control is unfeasible and the optimal vaccination problem always selects for control strategies with at least one switch.

The details on the shape of the optimal control solution when the resources for vaccination are limited are shown in Fig. 1.3. Fig. 1.3a shows the optimal starting (τ_1) and ending (τ_2) intervention times and the final time (T) for the optimal vaccination strategy as functions of the relative cost per unit time of epidemic duration over the cost of a single new infection (A). From Fig. 1.3a, we notice that the optimal vaccination strategy is reactive ($\tau_1 = 0$ and $\tau_2 < T$) for small values of A, admits two–switches ($\tau_1, \tau_2 \in (0, T)$) for intermediate values of A, and is delayed ($\tau_1 > 0$ and $\tau_2 = T$) for large values of A. From Fig. 1.3a, we also notice that for small values of A the control actions end before the peak of infection, while for larger A the control actions continue far beyond the peak (see dot–dashed line).

Fig. 1.3b displays the number of infected units over the entire epidemic period ($\int_0^T \beta SIdt$) under the optimal vaccination strategy as a function of A. By comparing the performance along the two competing objectives of the control displayed in the Fig. 1.3 (i.e. the epidemic duration, T, and the epidemic size, $\int_0^T \beta SIdt$), we notice that both slightly change for increasing values of A as long as the optimal control is reactive, while they show a *step–like* change with respect to A when the optimal control displays two switches. Finally, when the control is delayed, the epidemic duration does not show significant changes, while the epidemic size largely increases with respect to A (see Fig. 1.3b).

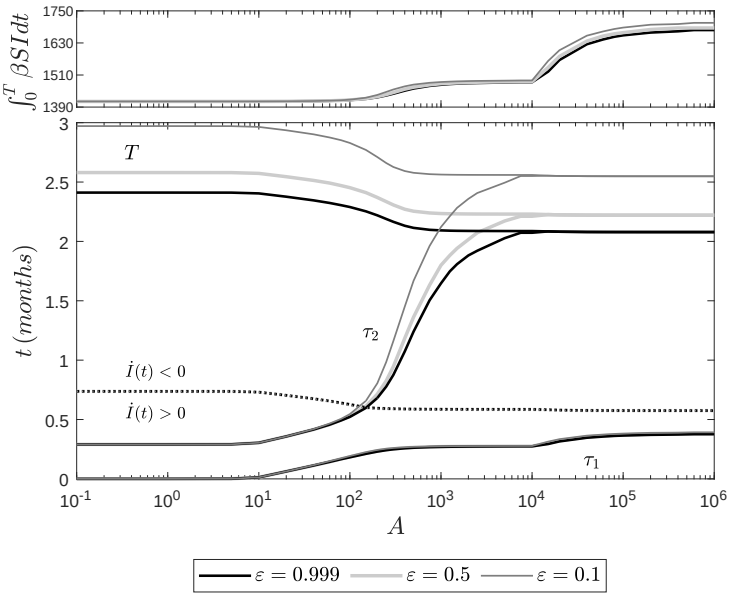

Figure 1.4: Numerical simulations of MOOC problem implementing vaccination strategy. Top panel: total number of infected units $\int_0^T \beta SIdt$ as function of A in semi–logarithmic scale. Bottom panel: starting intervention time τ_1, ending intervention time τ_2 and elimination time T as functions of A in semi–logarithmic scale. The dotted curves represent the time instants in which $\dot{I}(t) = 0$. Line color meaning is specified in the figure legend and refers to three possible choices of parameter ε ($\varepsilon = I(T)$). Fixed parameters: $S_0 = 2000$, $I_0 = 1$, $\gamma = 5$ month^{-1}, $\mathcal{R}_0 = \beta S_0/\gamma = 4$, $u_{max} = 1$ month^{-1} and $z_{max}/S_0 = 0.25$.

The sensitivity analysis performed on the threshold for disease elimination highlights that the shape of the optimal vaccination control observed in the case of $\varepsilon = 0.5$ qualitatively and quantitatively holds also considering different values of ε. Specifically, the values of A where the optimal vaccination control problem selects for reactive, two-switches, or delayed control do not significantly depend on the chosen value of ε (see Fig. 1.4).

Isolation policy

Let us now consider the problem of minimizing the epidemic size and duration through isolation. The following theorem prescribes that the optimal control solution is bang–bang with at most one switching time (constant or delayed control).

Theorem 1.4. *The optimal solution $u^*(t)$ to the MOOC problem, with $g = g_i$ given by (1.4) and terminal constraint (1.8), is a bang–bang control of the form:*

$$u^*(t) = \begin{cases} 0 & t \in [0, \tau) \\ u_{max} & t \in [\tau, T] \end{cases} \tag{1.29}$$

with $\tau \in [0, T]$.

Proof. Throughout the proof we omit the superscript * for the optimal quantities, in order to simplify the notation.

Let us start by making the expression of Hamiltonian (1.13) explicit along the optimal solution:

$$H = A + \beta SI - \lambda_S \beta SI + \lambda_I \left(\beta SI - (\gamma + u(t))\, I\right) + \lambda_z u(t) I \equiv 0. \tag{1.30}$$

where λ_z is constant and non–negative (see (1.16)).

The switching function and its first time derivative read, respectively:

$$\psi = (\lambda_z - \lambda_I)\, I \tag{1.31}$$

$$\dot{\psi} = (\lambda_z + 1 - \lambda_S)\, \beta SI - \lambda_z \gamma I. \tag{1.32}$$

We verify that the optimal control cannot be singular, namely that ψ vanishes only in isolated points. Suppose that ψ vanishes in an open interval $\mathcal{I}$, then also all its time derivatives vanish there. In particular, $\psi = \dot{\psi} = 0$ in $\mathcal{I}$ yields:

$$\lambda_I = \lambda_z, \;\; \lambda_S = \lambda_z + 1 - \frac{\lambda_z \gamma}{\beta S}$$

and

$$H = A > 0$$

in $\mathcal{I}$, which contradicts the (1.30). As a consequence, $u(t)$ is a bang–bang control, i.e. a piecewise–continuous function that can assume only the extreme values of U: 0 and u_{max}.

Now we prove that $u(t) \equiv u_{max}$ or there is at most a switching time from no control to the maximum control rate.

As first step, we check that $u \equiv 0$ is not optimal for the MOOC problem. In fact, $u \equiv 0$ means that none of the available resources for isolation are used, hence $\lambda_z = 0$ (see (1.15)). Equation (1.31) would imply that $\lambda_I \leq 0$ in $[0, T]$. However, at the elimination time T, λ_I assumes a positive value:

$$\lambda_I(T) = -\frac{A + \beta S(T) I(T)}{\dot{I}(T)} > 0,$$

as one can easily obtain by substituting the transversality condition $\lambda_S(T) = 0$ in the Hamiltonian (1.30).

Let now τ_s be a generic switching time, namely $\psi(\tau_s) = 0$. Then, $\lambda_I(\tau_s) = \lambda_z$ and, by substituting in (1.30), one obtains $\dot{\psi}(\tau_s) = -A < 0$. From (1.17) the assert follows. □

Then, there are two alternatives for the optimal control function (see Fig. 1.1a and Fig. 1.1b):

(a) $\tau = 0$, i.e. $u^*(t) \equiv u_{max}$,

(b) $\tau \in (0, T]$ is the only switching time and $u^*(t)$ changes its value from 0 to u_{max} (say, $0 \to u_{max}$).

Thus, for isolation policy $\tau \in [0, T]$ is the starting intervention time (as defined in Section 1.3), whereas the ending intervention time is equal to T anyway.

The numerical analyses of the optimal isolation problem aimed at minimizing epidemic size and duration with limited resources are illustrated in Fig. 1.5. Fig. 1.5a displays the optimal starting intervention time (dashed curves, τ) and the final time (solid curves, T) for the optimal isolation strategies as functions of the relative cost per unit time of epidemic duration over the cost of a single new infection (A) for two levels of total resources (represented as the maximum fraction of the original population that can be

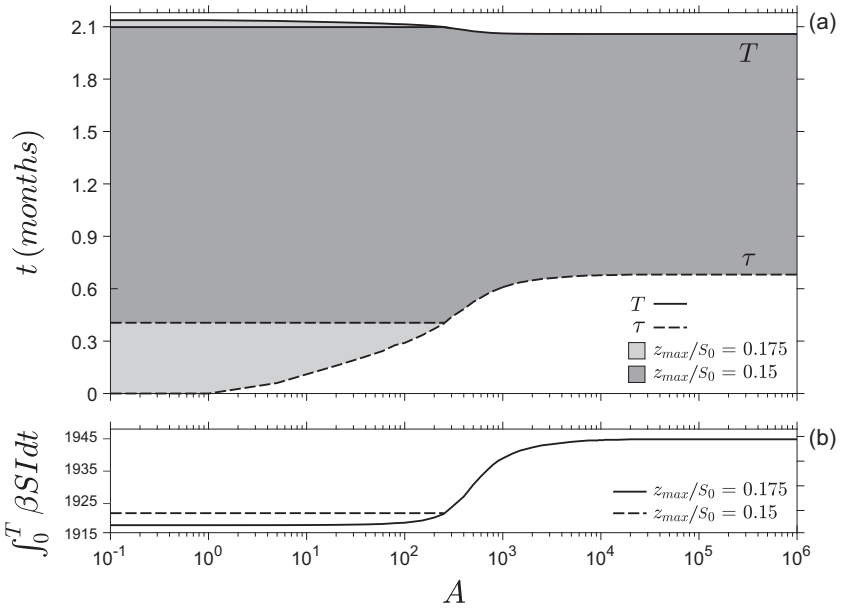

Figure 1.5: Numerical simulations of MOOC problem implementing isolation strategy. (a) Starting intervention time τ (dotted lines) and elimination time T (solid lines) as functions of A in semi–logarithmic scale, by assuming $z_{max}/S_0 = 0.15$ and $z_{max}/S_0 = 0.175$. Control region color is gray [resp. white] where $u^*(t) = u_{max}$ [resp. $u^*(t) = 0$]. Color meaning for the two levels of total resources z_{max} is specified in the figure legend. (b) Total number of infected units $\int_0^T \beta SIdt$ as function of A in semi–logarithmic scale, by assuming $z_{max}/S_0 = 0.15$ (dotted line) and $z_{max}/S_0 = 0.175$ (solid line). Fixed parameters: $S_0 = 2000$, $I_0 = 1$, $\gamma = 5$ month^{-1}, $\mathcal{R}_0 = \beta S_0/\gamma = 4$, $\varepsilon = 0.5$, $u_{max} = 1$ month^{-1}.

isolated z_{max}/S_0). Specifically, $z_{max}/S_0 = 0.175$ [resp. $z_{max}/S_0 = 0.15$], which represents an amount of resources sufficient [resp. not sufficient] to maintain a maximum control effort for the entire duration of the epidemic (corresponding to $u \equiv u_{max}$). From Fig. 1.5a, we notice that the optimal isolation control is always delayed ($\tau > 0$) for large values of A, while, for small values of A, the optimal isolation control can be constant when the resources are not a limiting factor, i.e. larger z_{max}/S_0 (light gray area), or delayed in any case where they are a limiting factor, i.e. smaller z_{max}/S_0 (dark gray area). Fig. 1.5a shows that, when the resources are not sufficient to maintain a maximum control effort for the entire epidemic (as it is for $z_{max}/S_0 = 0.15$), the optimal starting intervention time (τ) does not change with respect to A as far as the use of all the available resources remains optimal (i.e. $A \approx 2 \cdot 10^2$). Conversely, for larger values of A, Fig. 1.5a shows that the optimal delayed control does not use all the available resources, i.e. $z_i(T) < z_{max}$. This conclusion can be deduced by noticing that, for large A, the optimal controls are the same for different levels of resources available, z_{max} (see the dashed curves in Fig. 1.5a).

Fig. 1.5b displays the number of infected units over the entire epidemic period ($\int_0^T \beta SIdt$) under the optimal isolation strategies as a function of A for two levels of z_{max}/S_0. By comparing the performance along the two competing objectives of the control displayed in the Fig. 1.5 (i.e. the epidemic duration, T, and the epidemic size, $\int_0^T \beta SIdt$), we notice that both slightly change for increasing values of A as long as the optimal control is constant, while they show a *step–like* change with respect to A when the optimal control is delayed.

The sensitivity analysis performed on the threshold for disease elimination highlights that the shape of the optimal isolation control observed in the case of $\varepsilon = 0.5$ qualitatively

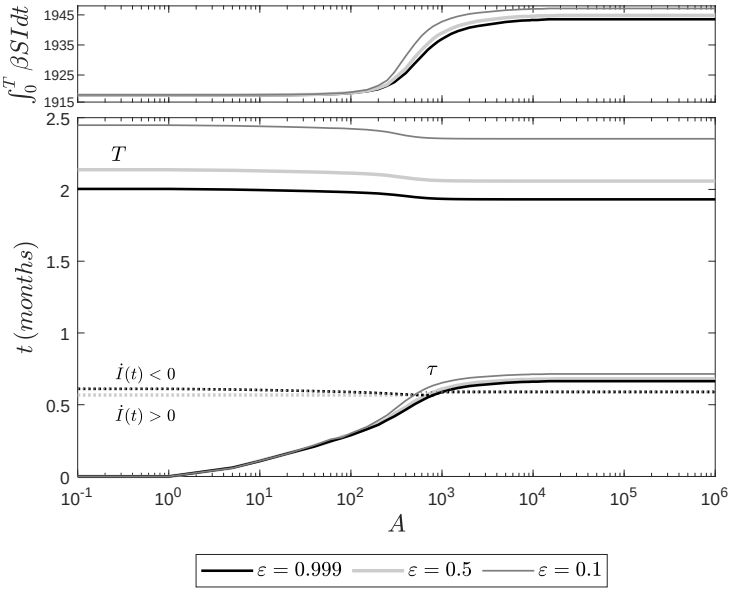

Figure 1.6: Numerical simulations of MOOC problem implementing isolation strategy. Top panel: total number of infected units $\int_0^T \beta SIdt$ as function of A in semi–logarithmic scale. Bottom panel: starting intervention time τ and elimination time T as functions of A in semi–logarithmic scale. The dotted curves represent the time instants in which $\dot{I}(t) = 0$. Line color meaning is specified in the figure legend and refers to three possible choices of parameter ε ($\varepsilon = I(T)$). Fixed parameters: $S_0 = 2000$, $I_0 = 1$, $\gamma = 5$ month^{-1}, $\mathcal{R}_0 = \beta S_0/\gamma = 4$, $u_{max} = 1$ month^{-1} and $z_{max}/S_0 = 0.175$.

and quantitatively holds also considering different values of ε. Specifically, the values of A where the optimal isolation control problem selects for constant or delayed control do not significantly depend on the chosen value of ε (see Fig. 1.6).

1.4 Time–optimal control problem

In this section, we investigate the control problem having as unique goal the minimization of the elimination time of the infection T, given by (1.5). Unlike the problem studied in [33], here the amount of usable control resources is subject to constraints.

The time optimal control (TOC) problem can be formalized as follows:

(TOC) *Find an optimal control function $u^*(t)$ that minimizes the objective functional*

$$J = \int_0^T 1dt, \tag{1.33}$$

with T given by (1.5), on the admissible set

$$\Omega = \left\{ u(\cdot) \in L^1(0,T) \mid u(t) \in U = [0, u_{max}] \right\},$$

subject to (1.2) with initial conditions (1.9) and terminal constraint (1.6).

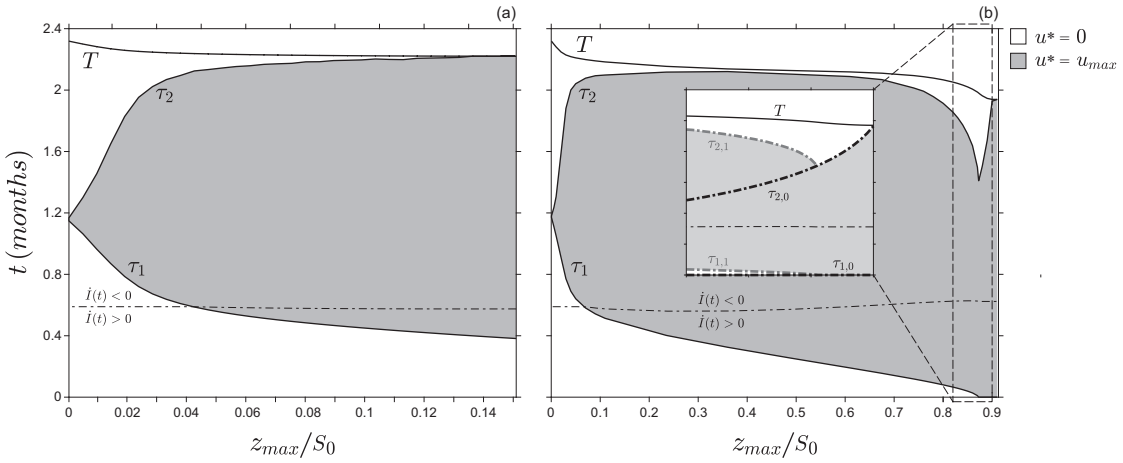

Figure 1.7: Numerical simulations of TOC problem implementing vaccination strategy. Starting intervention time τ_1, ending intervention time τ_2 and elimination time T as functions of z_{max} in semi–logarithmic scale. Control region color is gray [resp. white] where $u^*(t) = u_{max}$ [resp. $u^*(t) = 0$]. (a) Simulations by assuming $u_{max} = 1$ month^{-1}. (b) Simulations by assuming $u_{max} = 2$ month^{-1}; in–box: starting and ending intervention times associated to reactive controls (dot–dashed black lines, $\tau_{j,0}$ with $j = 1, 2$) and to two–switches optimal controls (dot–dashed gray lines, $\tau_{j,1}$ with $j = 1, 2$). Fixed parameters: $S_0 = 2000$, $I_0 = 1$, $\gamma = 5$ month^{-1}, $\mathcal{R}_0 = \beta S_0/\gamma = 4$, $\varepsilon = 0.5$.

The existence of the optimal solution can be proved with the same arguments employed for the MOOC problem, as it is independent from the formulation of the objective functional (see Theorem 1.1).

The characterization differs for the expression of the Hamiltonian function, which now reads:

$$H(x, u(t), \lambda) = 1 + \lambda^T \left(f(x) + u(t)g(x)\right).$$

Anyway, the TOC problem can be formally accounted for by taking $A_1 = 0$ in (1.11), that corresponds to letting $A \to +\infty$ in the objective functional (1.12) which defines the MOOC problem. Hence, the spectrum of admissible optimal control functions is not affected by the change made in the objective functional with respect to the MOOC problem (see Theorem 1.2).

For numerical simulations we adopt the same numerical scheme and the same parameter values discussed in Section 1.3.

Vaccination policy

Here, we consider the problem of minimizing the epidemic duration only through vaccination. Being Theorem 1.3 still valid in the limit case $A \to +\infty$, the optimal solution $u^*(t)$ to the TOC problem, with $g = g_v$ given by (1.3) and terminal constraint (1.7), is a bang–bang control of the form (1.18) with at most two switches at $\tau_1, \tau_2 \in [0, T]$, and $\tau_1 < \tau_2$.

The numerical analyses are illustrated in Fig. 1.7. Such figure displays the optimal starting (τ_1) and ending (τ_2) intervention times and the final time (T) for the optimal vaccination strategy as functions of the total amount of resources available for vaccination (represented as the maximum fraction of the original population that can be vaccinated, z_{max}/S_0) for two values of maximum per–capita control rate (u_{max}). Specifically, $u_{max} = 1$

month^{-1} (Fig. 1.7a) [resp. $u_{max} = 2$ month^{-1} (Fig. 1.7b)], which represents a parameter setting where delayed [resp. constant] control is selected in the corresponding unconstrained time–optimal control problem (i.e. with $z_{max} \to +\infty$) [33]. The range of z_{max}/S_0 values in Fig. 1.7 is restricted to the interval in which the resources act as a limiting factor with respect to the unconstrained problem [33]. Namely, the last value of z_{max}/S_0 is close to the optimal value of resources used if they are not limited.

From Fig. 1.7a, we notice that the optimal vaccination strategy displays two switches ($\tau_1, \tau_2 \in (0, T)$) for small values of z_{max}/S_0 and is delayed ($\tau_1 > 0$ and $\tau_2 = T$) for large values of z_{max}/S_0. In addition, conversely to the unconstrained problem, where the starting intervention time (τ_1) always occurs before the peak of infection ($\dot{I}(t) > 0$), for small values of z_{max}/S_0 the starting intervention time may occur when $\dot{I}(t) < 0$.

Fig. 1.7b shows that, when the resources are limited (i.e. $z_{max}/S_0 < 0.9$), the vaccination control displays two switches for small values of z_{max}/S_0 and is reactive ($\tau_1 = 0$ and $\tau_2 < T$) for large values of z_{max}/S_0. In addition, Fig. 1.7b shows that, at the value of z_{max}/S_0 corresponding to the control change from a two–switches function to a one switch function, the ending intervention time (τ_2) displays a *cusp–like* shape, with an abrupt change in its derivative (both in modulus and sign) with respect to z_{max}/S_0. This is due to the transition between two different local *minima* in the objective function, one associated to reactive controls (the bold dot–dashed black curves in the in–box in Fig. 1.7b, $\tau_{j,0}$ with $j = 1, 2$) and one associated to two–switching controls (the bold dot–dashed gray curves in the in–box in Fig. 1.7b, $\tau_{j,1}$ with $j = 1, 2$).

Isolation policy

Let us finally consider the problem of minimizing the epidemic duration only through isolation. Theorem 1.4 still holds by letting $A \to +\infty$, namely the optimal solution $u^*(t)$ to the TOC problem, with $g = g_i$ given by (1.4) and terminal constraint (1.8), consists either in a constant control ($\tau = 0$ in (1.29)) or in a delayed control with a single switching time ($\tau \in (0, T]$ in (1.29)).

The numerical analyses are illustrated in Fig. 1.8. Such figure shows the optimal starting intervention time (τ) and the final time (T) for the optimal isolation strategy as functions of the total amount of resources available for isolation (represented as the maximum fraction of the original population that can be isolated, z_{max}/S_0) for two values of maximum per–capita control rate (u_{max}). Specifically, $u_{max} = 1$ month^{-1} [resp. $u_{max} = 16$ month^{-1}], which represents a parameter setting where delayed [resp. constant] control is selected in the corresponding unconstrained time–optimal control problem (i.e. with $z_{max} \to +\infty$) [33]. In Fig. 1.8, the values of z_{max}/S_0 range in the interval in which the resources act as a limiting factor with respect to the unconstrained problem when we assume $u_{max} = 1$ month^{-1} [33]. For $u_{max} = 16$ month^{-1} such interval is much smaller: it ends at the point when τ and T have a step change and after which they remain constant.

Fig. 1.8 shows that, when the unconstrained isolation problem selects for delayed control, the isolation is always delayed in the presence of limited resources (light gray area). Conversely, when the unconstrained isolation problem selects for a constant control, by decreasing the available resources, we observe at $z_i(T)\big|_{u \equiv u_{max}} = z_{max}$ an abrupt transition from constant to delayed control (see the dark gray areas in Fig. 1.8). This transition is characterized by a discontinuity both in the starting intervention (τ) and the final time (T), suggesting that small differences in the amount of resources allocated to isolation may cause dramatic changes in the effectiveness of the implemented optimal

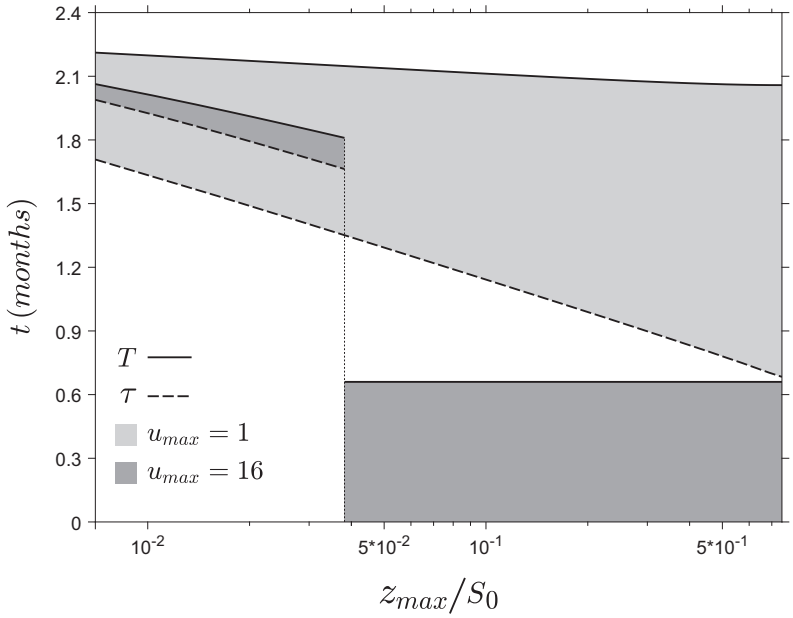

Figure 1.8: Numerical simulations of TOC problem implementing isolation strategy. Starting intervention time τ (dotted lines) and elimination time T (solid lines) as functions of z_{max}/S_0 in semi–logarithmic scale, by assuming $u_{max} = 1$ month^{-1} and $u_{max} = 16$ month^{-1}. Control region color is gray [resp. white] where $u^*(t) = u_{max}$ [resp. $u^*(t) = 0$]. Color meaning for the two values of maximum control rate u_{max} is specified in the figure legend. Fixed parameters: $S_0 = 2000$, $I_0 = 1$, $\gamma = 5$ month^{-1}, $\mathcal{R}_0 = \beta S_0/\gamma = 4$, $\varepsilon = 0.5$.

strategy. In addition, the transition in the optimal control leads to very different epidemiological dynamics. When in Fig. 1.8 the control is constant, the number of infected units is always decreasing (i.e. $\dot{I}(0) < 0$). Conversely, when in Fig. 1.8 the control is delayed, the number of infected units follows a classic epidemic dynamics reaching a peak of infection before starting to decrease (i.e. $\dot{I}(0) > 0$).

1.5 Discussion and conclusions

In this chapter, we investigated the multi–objective optimal control (MOOC) problem aiming at simultaneously minimizing, through vaccination or isolation policies, epidemic size and duration when the total amount of resources available for control during the entire epidemic period is limited.

Working within an optimal control framework [240], we proved that, when the resources for disease control are limited (i.e. the maximum control effort can not be sustained for the entire epidemic period), the MOOC problem implementing vaccination admits only bang–bang solutions with one or two switches. When only one switch is admitted, the MOOC problem can select both for reactive vaccination (characterized by $u^*(0) = u_{max}$ and $u^*(T) = 0$, see Fig. 1.1c) and delayed vaccination (characterized by $u^*(0) = 0$ and $u^*(T) = u_{max}$, see Fig. 1.1b). When the optimal solution admits two switches, then the MOOC problem selects for controls where vaccination is implemented within a temporal window between times τ_1 and τ_2 (with $\tau_1 < \tau_2$ and $\tau_1, \tau_2 \in (0, T)$). In addition, when resources are limited, we proved that, for very large allowed values of the maximum vaccination effort with respect to the rate of removal of infected units (i.e. $u_{max} \gg \gamma$), the optimal vaccination in the

MOOC problem is always reactive and uses all the resources available (i.e. $z_v(T) = z_{max}$). From the last result, together with the results obtained by [155] and in Section 1.4 here, it follows that, when $u_{max} \gg \gamma$, minimizing the epidemic size is equivalent to minimize the epidemic duration. However, this conclusion does not hold in general. We found that, when the maximum rate at which vaccine can be administered in the unit time is relatively low, it may exist a trade–off between the minimization of the two objectives.

By analyzing the MOOC problem implementing isolation, we proved that, when the resources for disease control are limited, the optimal solution is bang–bang and admits only one switch. Specifically, the MOOC problem always selects for delayed isolation control. In addition, we showed that the optimal delayed isolation strategy may not use all of the available resources (meaning $z_i(T) < z_{max}$, see Fig. 1.5). Last finding is in contrast with the results obtained by Hansen and Day [155] on the optimal isolation problem aimed at minimizing the epidemic size with limited resources. They proved that, when the resources are limited, the optimal isolation policy is any control that uses all the resources available [155]. From the two findings, it follows that, in a optimal isolation problem with limited resources, minimizing the epidemic size is not always equivalent to minimize the epidemic duration and *vice versa*.

Our analysis has been performed through linear scalarization of the multi–objective problem. This means formulating a single–objective optimization such that its solutions are Pareto–optimal in the corresponding multi–objective problem [117]. Specifically, in our framework, the different Pareto–optimal solutions (namely, Pareto–front) can be reached by varying the parameter A, which represents the relative cost per unit time of epidemic duration over the cost of a single new infection (see Figs. 1.3 and 1.5). While it seems unrealistic to expect that stakeholders and policy–makers can express their preferences on specific values of parameter A, the outputs of the optimization problem can identify the regions in the Pareto–front where the two objectives are more conflicting, thus helping stakeholders and policy–makers to explicit their preferences on the control goals. Fig. 1.3a and Fig. 1.3b provide a good example of this tension in the case of vaccination control. For instance, Fig. 1.3a shows that applying an optimal two–switches control characterized by a temporal window for vaccine administration across the peak of infection would reduce by about 10% the epidemic duration, with respect to a reactive optimal control (see changes in T for $10^1 < A < 10^3$ in Fig. 1.3a). Conversely, the same change in the optimal policy would increase by about 5% the epidemic size (see the range $10^1 < A < 10^3$ in Fig. 1.3b). In this way, given the constraints on the available resources, policy–makers can knowingly choose between the different outcomes.

The simple epidemic model proposed here does not provide immediate solutions to real–world cases of disease control. However, our study serves as a proof–of–principle verification of the conflicting nature of different control goals, such as epidemic size and duration, in the presence of constraints on the control actions. These theoretical findings can be used to inform more complex simulation models developed for specific epidemiological scenarios where multiple management objectives are involved. (For instance by testing how different objectives perform under the assumption of a delayed beginning of the control actions.)

The MOOC problem as defined in this study assumes that the costs of the epidemic vary linearly with both size and duration. The assumption of linearity of the costs of infection has been widely used both in theoretical optimal control studies [22,39,224,296] as well as in cost–benefit analyses based on simulation models [31, 242]. However, complex feedbacks due to variations in individual behaviors and market dynamics following human/livestock outbreaks may add nonlinear components to the epidemic costs (as described in [128, 190, 200]), that

are not taken into account in our analysis.

While multi–objective approaches have been frequently used in studies on optimal disease control, they do not generally account for the effect of epidemic duration on the cost of infection. A multi–objective approach including the costs associated to the epidemic duration has been recently implemented by de Pinho *et al.* [96]. They investigated the multi–objective problem of minimizing the epidemic duration and the social costs associated to the infection (defined as a linear combination of the number of infections and the costs of control) through both vaccination and treatment. Despite the different framework used with respect to our study (both in the cost function and in the applied policies), analogously to our results, they found through numerical simulations that there exists a trade–off between minimizing the epidemic duration and other social costs associated to the disease (which included the epidemic size) [96].

Hansen and Day [155] thoroughly investigated the optimal control problem of reducing epidemic size with limited resources. However, similar investigations have not been performed focusing on the single–objective problem of reducing epidemic duration so far. In Section 1.4, we provided solutions of the optimal vaccination and isolation controls, respectively, aiming at minimizing the epidemic duration when the control resources are limited.

We found that the time optimal control (TOC) implementing vaccination qualitatively changes with respect to the problem with unlimited resources investigated in Bolzoni *et al.* [33]. In the case of unlimited resources, the TOC problem selects for solutions characterized by constant or delayed controls [33]. Conversely, we proved here that, when the resources are a limiting factor (i.e. $z_{max} < z_v(T)\big|_{u\equiv u_{max}}$), the TOC vaccination problem selects for solutions characterized by reactive or two–switches controls. Furthermore, we showed that, in the TOC problem with limited vaccination resources, two local minima, corresponding to either reactive or two–switches solutions, can coexist in the objective function (see Fig. 1.7b).

By investigating the TOC isolation problem, we proved that, when the resources are a limiting factor, the optimal control is always delayed. We also found that there may exist an abrupt transition in the shape and outcome of the optimal isolation control at the interface between non–limited and limited resources scenarios (i.e. at $z_{max} = z_i(T)\big|_{u\equiv u_{max}}$). We provided such an example in Fig. 1.8 (for $u_{max} = 16$ month^{-1}), where a small reduction in the total amount of resources available leads to a transition of the optimal solution from a constant to a delayed isolation control, with a corresponding abrupt change in the starting intervention (τ) and elimination (T) times. An analogous jump in the value of the objective function at the limited/non–limited resources interface was also observed by Hansen and Day [155] while investigating the optimal control problem of reducing the epidemic size through isolation. This suggests that, independently on the objective of the control (whether is to minimize the epidemic size or duration), shortages in the total amount of resources available for isolation can be more critical for the success of the interventions with respect to shortages in resources for vaccination (where smoother changes in the objective functions occurred). This conclusion is in accordance with the results obtained by Roche *et al.* [256] with a data–driven stochastic model simulating FMD outbreaks in Australia. They found that, when the resources available for the control are adequate, a policy implementing the stamping–out of infected farms (which corresponds to the isolation policy in an SIR framework) can effectively control the outbreaks. However, when resources become constrained, vaccination was more likely to achieve disease elimination faster than the stamping–out [256].

The results obtained here on the critical role of available resources on the effectiveness

of disease control confirm the conclusions obtained in other works, which observed strongly nonlinear (and sometimes non–monotonic) relationships between the effort applied in the control and the resulting reduction in disease costs (see [35, 38, 84, 209]).

Chapter 2

Localized culling strategies in a metapopulation epidemic model

A two–patches metapopulation mathematical model, describing the dynamics of Susceptibles and Infected in wildlife diseases, is presented in this chapter. The two patches are identical in absence of control, and culling activities are performed in only one of them.

Firstly, the dynamics of the system in absence of control is investigated. Then, two types of localized culling strategies (proactive end reactive) are considered. The proactive control is modeled by a constant culling effort, and for the ensuing model the disease free equilibrium is characterized and existence of the endemic equilibrium is discussed in terms of a suitable control reproduction number. The localized reactive control is modeled by a piecewise–constant culling effort function, that introduces an extra–mortality when the number of infected individuals in the patch overcomes a given threshold. The reactive control is then analytically and numerically investigated in the frame of *Filippov systems* [125].

We find that localized culling may be ineffective in controlling diseases in wild populations when the infection affects host fecundity in addition to host mortality, even leading to unexpected increases in the number of infected individuals in the nearby areas. The results of this study have been published in [37].

2.1 Background

In the last decades, emerging and re–emerging infectious diseases (ERIDs) have been responsible for significant economic and social impacts in both developed [106] and developing countries [193]. Jones *et al.* [175] showed that zoonotic infections originated in wildlife have accounted for the majority of ERID events since the 1940s and are representing a growing threat to global health. As a consequence, actions aiming at controlling diseases in wild populations can provide benefits on wildlife protection and conservation as well as on the sustainability of agriculture and public health.

However, disease control through vaccination and drug treatments, which represent common intervention measures in human and livestock infections, is often not feasible, or practical, in wildlife because of the lack of resources or the unavailability of suitable diagnostic tools [87]. In these circumstances, non–selective culling, which consists in the slaughtering of both infected and healthy individuals, represents the only available disease control strategy.

The effectiveness of culling relies on the assumption that, under a given threshold of host density, the population becomes too sparse, then, the number of potentially infectious contacts between infected and susceptible individuals become too low to allow the disease to spread and persist in the population [10]. Yet there are empirical evidences suggesting that culling has been ineffective in reducing disease burden in wildlife populations for different infections, such as rabies in canids [223, 298], facial tumor disease in Tasmanian devil [197], and bovine tuberculosis in European badger [108].

The main causes for the failure of culling in the elimination of diseases in wild populations have been ascribed to compensatory mechanisms, such as the density–dependent positive feedbacks on recruitment and dispersal triggered by the excess of mortality due to culling [42, 285]. Specifically, by reducing the host population abundance, culling can reduce the density–dependent constrains on host birth rate, thereby producing a flush in new susceptible individuals in the population [129, 298]. These new susceptibles represent a reservoir for new infections, which nullifies the expected benefits of disease control campaigns or, in some cases, even increases the disease burden in the population [35, 38, 84] or the duration of the epidemic [32, 33].

Furthermore, different studies showed that culling may disrupt the host social structure increasing the animal home range and prompting long–distance movement and dispersal (perturbation hypothesis), thus increasing the probability of potentially infectious contacts between neighboring groups [67,241,284]. In particular, studies carried in the British Isles on the effectiveness of localized proactive and reactive culling as measures for bovine tuberculosis (*Mycobacterium bovis*) control in European badger showed that culling led to a decrease in disease burden in the controlled lands, while caused an increase in the infections in the nearby areas [29,107,291]. As expected from the perturbation hypothesis, the increase of *M. bovis* prevalence was associated with expanded home ranges and more frequent migration events in badger [29].

In this chapter, we will consider a metapopulation epidemic mathematical model, described by a system of ODEs for Susceptibles and Infected, with two patches which are identical in absence of control and localized culling control which is performed in only one of them. We will show by means of qualitative analysis and numerical simulations that, also in the absence of the density–dependent compensatory effects on recruitment and dispersal, localized culling may be ineffective in controlling diseases in wild populations and it may even lead to unexpected increases in the number of infected individuals in the nearby areas.

Here, we investigate the effectiveness of localized culling using a metapopulation Susceptible–Infected (SI) model with density–dependent mortality of the host and disease–induced host sterilization. Disease–induced fecundity reduction (or sterilization) of the host has been frequently observed in host–pathogen interactions. Mathematical models describing the dynamics of fecundity–reducing infections have been developed for rabies – where the fecundity reduction is generated by the severely debilitating nature of the infection and the frenzied behavior induced – in different mammal species [36], cowpox in wild rodents [269], and several infections of invertebrate hosts, such as crustaceans and mollusks [40]. Moreover, we will show that the counter–intuitive effects of culling hold also relaxing the hypotheses of disease–induced host sterility and density–dependent host mortality in the infection model.

2.2 The metapopulation mathematical model

We expand a traditional SI epidemic framework developed for host–sterilizing infections in wild animals to describe the effect of localized proactive and reactive culling on the control of wildlife diseases in a two–patches metapopulation model (see e.g. [10, 35, 90]). From an epidemiological point of view, hosts can be subdivided into compartments with respect to the infection: the susceptible compartments $S_j(t)$ – i.e., healthy individuals that can be infected by the pathogen – and the infected compartments $I_j(t)$ – i.e., diseased individuals that can infect other individuals; subscript $j(= 1, 2)$ defines the patch in the metapopulation to which the epidemiological compartment belongs.

In order to describe localized culling control in the model we assume that culling activities can be performed in one of the two patches only (specifically patch 1), while the other one (patch 2) is uncontrolled. We also assume the two patches are identical in the absence of control, namely the demographic and epidemiological parameters are the same.

Then, the metapopulation model can be represented by the following set of four ordinary

differential equations

$$\dot{S}_1 = rS_1 - \eta S_1 N_1 - \beta S_1 I_1 - cS_1 - DS_1 + DS_2 \tag{2.1a}$$

$$\dot{I}_1 = \beta S_1 I_1 - (\mu + \alpha + c + \eta N_1) I_1 - DI_1 + DI_2 \tag{2.1b}$$

$$\dot{S}_2 = rS_2 - \eta S_2 N_2 - \beta S_2 I_2 - DS_2 + DS_1 \tag{2.1c}$$

$$\dot{I}_2 = \beta S_2 I_2 - (\mu + \alpha + \eta N_2) I_2 - DI_2 + DI_1, \tag{2.1d}$$

where the upper dot is used to denote the time derivative. $N_j = S_j + I_j$ represents the total host population in patch j. All the parameters are positive constants: $r = \nu - \mu$ represents the intrinsic growth rate, being ν the fertility rate and μ the natural mortality rate; η and α represent the density–dependent mortality rate of a disease–free host population and the additional mortality rate caused by the infection, respectively; and β represents the transmission rate between infected and susceptible individuals. Moreover, we define D to be the per–capita dispersal rate from a patch to the other; and c to be the culling effort.

In order to analyze the effects of both localized proactive and reactive culling strategies in model (2.1), we implement two different control functions. Thus, the localized proactive culling strategy in model (2.1) is obtained by imposing culling effort c to be a constant function

$$c = \bar{c} = const, \tag{2.2}$$

and the localized reactive culling strategy by imposing culling effort c to be a piecewise–constant function as in [98]

$$c = \frac{\bar{c}}{2}[1 + sgn(I_1 - \theta)], \tag{2.3}$$

where $\bar{c}$ represents the maximum effort enforceable, and θ represents the threshold for the detection of the infection. Expression (2.3) implies that population N_1 in patch 1 undergoes an extra–mortality $\bar{c}$ due to culling when the number of infected individuals in the patch is higher than threshold θ, while no culling activities are performed when the infection is under the threshold of detection. Therefore, threshold θ introduces a discontinuity, so that model (2.1) with (2.3) becomes a piecewise–smooth system (also called *Filippov system*) in which sliding motions are possible on the manifold separating the region (in state space) where control is allowed from that where it is not [125]. An introduction to Filippov systems is given in Section I.3.

More precisely, by introducing the so–called *switching manifold*

$$\Sigma = \{(S_1, I_1, S_2, I_2) \in \mathbb{R}^4 : I_1 - \theta = 0\},$$

and denoting with $f^{(1)}$ [resp. $f^{(2)}$] the r.h.s. of model (2.1) with $c = 0$ [resp. $c = \bar{c}$], then sliding occurs on the *sliding set*

$$\Sigma_s = \{(S_1, I_1, S_2, I_2) \in \Sigma : f_2^{(2)} \leq 0 \leq f_2^{(1)}\}, \tag{2.4}$$

namely, where the components of two vector fields $f^{(i)}$, $i = 1, 2$, transversal to Σ are 'pushing' in opposite directions, forcing the state of the system to remain on the switching manifold and slide on it. Σ_s terminates in Σ when a *tangency* occurs, i.e. when $f_2^{(1)}$ or $f_2^{(2)}$ vanish, implying that $f^{(1)}$ or $f^{(2)}$ are tangent to the switching manifold. Tangencies are strategically important for bifurcation analysis.

As first pointed out by Filippov, sliding motions obey the ODE system having as r.h.s. the unique convex combination of $f^{(1)}$ and $f^{(2)}$ parallel to Σ_s [125], i.e.,

$$(\dot{S}_1, \dot{I}_1, \dot{S}_2, \dot{I}_2)^T \Big|_{\Sigma_s} = \lambda f^{(1)} + (1 - \lambda) f^{(2)} \tag{2.5}$$

with

$$\lambda = \frac{(\nabla(I_1 - \theta))^T \cdot f^{(2)}}{(\nabla(I_1 - \theta))^T \cdot (f^{(2)} - f^{(1)})}.$$

Equilibrium points of system (2.5) are called *pseudo–equilibria* for model (2.1)–(2.3) and correspond to a stationary sliding solution.

The analysis of planar piecewise–smooth autonomous systems has been widely developed in recent years, see e.g. [163, 196]. However, there is still no obvious classification of the dynamics of higher dimensional piecewise–smooth systems [143]. Then, the behaviors exhibited by model (2.1) with localized reactive culling (2.3), which represents a four–dimension piecewise–smooth system, are too complex to be fully investigated analytically. As a consequence, we numerically investigate system (2.1)–(2.3) through simulations performed with the event–driven method developed by Piiroinen and Kuznetsov [239] for sliding systems to find model attractors. A bifurcation analysis in the parameter space identified by the reactive control parameters, $\bar{c}$ and θ, has been also performed with SLIDECONT [99], which is a software based on the package AUTO [105] to continue solutions to nonlinear boundary–value problems via orthogonal collocation.

2.3 Results

It can be shown that model (2.1) is consistent, namely its state variables remain positive for any trajectory starting from positive conditions, as stated by the following theorem:

Theorem 2.1. *If we consider positive initial conditions $S_1(0)$, $I_1(0)$, $S_2(0)$ and $I_2(0)$, then the solutions of the differential system (2.1) are positive at each time $t > 0$.*

Proof. We shall prove the statement by contradiction.

Let us start by considering the state variables $S_1(t)$ and $S_2(t)$ and let $t_1 > 0$ be the first time instant when $S_1(t)S_2(t) = 0$. Since the initial conditions are positive, the variables S_1 and S_2 (and hence their product) are positive in $[0, t_1)$.

If we assume that $S_1(t_1) = 0$ and $S_2(t_1) \geq 0$, then, by denoting with

$$m = \min_{[0,t_1]}\{r - c - D - \beta I_1(t) - \eta S_1(t)\},$$

one yields $\dot{S}_1(t) \geq mS_1(t)$ for $t \in [0, t_1]$. Therefore, $S_1(t_1) \geq S_1(0)e^{mt_1} > 0$, that contradicts our assumption. Then, it must be $S_1(t_1) > 0$ and $S_2(t_1) = 0$, which, however, implies that $\dot{S}_2(t_1) > 0$, namely $S_2(t)$ must be negative just before t_1. Thus, the existence of t_1 is definitely excluded.

With the same arguments one can prove the positivity of the infected state variables $I_1(t)$ and $I_2(t)$. □

Metapopulation model without control

Before exploring the effects of localized proactive and reactive culling on the infection dynamics, we analyze the main features of model (2.1), deriving the equilibria in the absence of control ($c = 0$) and the expression for the basic reproduction number, $\mathcal{R}_0$ (see the epidemiological definition in Section I.1).

In the absence of control ($c = 0$), model (2.1) assumes a symmetric form, which allows us to prove that:

Theorem 2.2. *If $c = 0$ in model (2.1), then at any equilibrium point the size of the susceptible [resp. infected] compartment in patch 1 is equal to the size of the susceptible [resp. infected] compartment in patch 2.*

Proof. Let us consider the algebraic system obtained by setting the r.h.s. of model (2.1), with $c = 0$, equal to zero, namely:

$$rS_1 - \eta S_1 N_1 - \beta S_1 I_1 - DS_1 + DS_2 = 0 \tag{2.6a}$$
$$\beta S_1 I_1 - (\mu + \alpha + \eta N_1) I_1 - DI_1 + DI_2 = 0 \tag{2.6b}$$
$$rS_2 - \eta S_2 N_2 - \beta S_2 I_2 - DS_2 + DS_1 = 0 \tag{2.6c}$$
$$\beta S_2 I_2 - (\mu + \alpha + \eta N_2) I_2 - DI_2 + DI_1 = 0. \tag{2.6d}$$

By contradiction, we assume that there exists a positive solution to system (2.6), say $(\bar{S}_1, \bar{I}_1, \bar{S}_2, \bar{I}_2)$, such that $\bar{S}_1 \neq \bar{S}_2$ or $\bar{I}_1 \neq \bar{I}_2$, possibly being both valid. Denote with $\bar{N}_i = \bar{S}_i + \bar{I}_i$, $i = 1, 2$. Then, two cases must be considered:

- $\bar{I}_1 = \bar{I}_2$ If $\bar{S}_1 > \bar{S}_2$, then from (2.6a) and (2.6c) it follows that

  $$r - \eta \bar{N}_1 - \beta \bar{I}_1 > 0 > r - \eta \bar{N}_2 - \beta \bar{I}_2, \tag{2.7}$$

  which reduce to $\bar{N}_1 < \bar{N}_2$ and a contradiction arises.

  A similar argument applies if $\bar{S}_2 > \bar{S}_1$.

- $\bar{I}_1 \neq \bar{I}_2$ In order to fix the ideas, let us assume $\bar{I}_1 > \bar{I}_2$ (the opposite case follows in analogous way).

  If $\bar{S}_1 > \bar{S}_2$, then, analogously to what happens if $\bar{I}_1 = \bar{I}_2$, the inequalities (2.7) reduce to $\eta \bar{N}_1 + \beta \bar{I}_1 < \eta \bar{N}_2 + \beta \bar{I}_2$, which is in contrast with the assumptions $\bar{S}_1 > \bar{S}_2$, $\bar{I}_1 > \bar{I}_2$.

  Otherwise, if $0 < \bar{S}_1 \leq \bar{S}_2$, then, the inequalities (2.7) must be reversed, namely

  $$r - \eta \bar{N}_2 - \beta \bar{I}_2 \geq 0 \geq r - \eta \bar{N}_1 - \beta \bar{I}_1, \tag{2.8}$$

  yielding:

  $$\eta \bar{N}_2 + \beta \bar{I}_2 \leq \eta \bar{N}_1 + \beta \bar{I}_1. \tag{2.9}$$

  Moreover, by handling the (2.6b) and (2.6d), one obtains

  $$(\beta \bar{S}_1 - (\mu + \alpha + \eta \bar{N}_1)) \bar{I}_1 > 0 > (\beta \bar{S}_2 - (\mu + \alpha + \eta \bar{N}_2)) \bar{I}_2, \tag{2.10}$$

  which, for the positivity of the $\bar{I}_i$, $i = 1, 2$, reduce to

  $$\eta(\bar{N}_1 - \bar{N}_2) < \beta(\bar{S}_1 - \bar{S}_2). \tag{2.11}$$

  Being $\bar{S}_1 \leq \bar{S}_2$, the last inequality implies that $\bar{N}_1 < \bar{N}_2$. However, adding the (2.9) and (2.11) leads to a contradiction: $\bar{N}_1 > \bar{N}_2$.

  In conclusion, if $\bar{S}_1 = \bar{S}_2 = 0$, then the (2.10) are still valid and reduce to $\bar{I}_1 < \bar{I}_2$, which is again in contrast with the initial assumption.

□

In other words, in searching model equilibria, it is not restrictive to assume the two patches are identical. In particular, model (2.1) with $c = 0$ has always a trivial equilibrium, $E_0 = (0, 0, 0, 0)$, and a disease–free equilibrium, $E_1 = (K, 0, K, 0)$, where

$$K = \frac{r}{\eta} \tag{2.12}$$

represents the carrying capacity for a disease–free host population. It is easy to prove that E_0 is always unstable if $r > 0$, while E_1 is asymptotically stable if and only if the basic reproduction number of model (2.1), $\mathcal{R}_0$, is lower than 1 [11].

The basic reproduction number can be calculated as the spectral radius of the *next generation* matrix, $\mathcal{R}_0 = \rho(FV^{-1})$, where F and V are defined as Jacobian matrices of the new infections appearance and the other rates of transfer, respectively, calculated for infected compartments at model (2.1) disease–free equilibrium [103, 287]. Then, model (2.1) basic reproduction number can be defined as

$$\mathcal{R}_0 = \frac{\beta K}{\mu + \alpha + r}, \tag{2.13}$$

with K given in (2.12) and coincides with that for the corresponding homogeneous mixing model. When $\mathcal{R}_0 > 1$ in equation (2.13), the disease–free equilibrium is unstable and there exists a unique asymptotically stable positive endemic equilibrium, called $E_2 = (\bar{S}, \bar{I}, \bar{S}, \bar{I})$, where

$$\bar{S} = \frac{\mu + \alpha + \eta\bar{N}}{\beta} \tag{2.14a}$$

$$\bar{I} = \frac{r - \eta\bar{N}}{\beta} \tag{2.14b}$$

with

$$\bar{N} = \frac{r + \mu + \alpha}{\beta}. \tag{2.15}$$

We notice that expressions (2.14), defining the endemic equilibrium in (2.1) for $c = 0$, correspond to the endemic equilibrium for the associated homogeneous mixing model (see [10], under the assumption of negligible incubation period) and stability properties follow straightforwardly.

Note also that necessary condition for being $\bar{I}$ positive is that

$$\beta > \eta,$$

hence we assume it always fulfilled in the following.

The effect of localized proactive culling

Analyzing metapopulation model (2.1)–(2.2) – i.e., with localized proactive culling strategy –, we find that there always exists a trivial equilibrium, $E_0^{\bar{c}} = (0, 0, 0, 0)$. Conversely than the case with $c = 0$, the trivial equilibrium $E_0^{\bar{c}}$ is not always unstable when $r > 0$. Indeed, linearization of system (2.1)–(2.2) around $E_0^{\bar{c}}$ leads to $E_0^{\bar{c}}$ locally asymptotically stable if and only if

$$D > r \text{ and } \bar{c} > \hat{c} = \frac{r(2D - r)}{D - r}, \tag{2.16}$$

as can be proved by Sylvester criterion [164], being the Jacobian matrix of system (2.1)–(2.2) evaluated at $E_0^{\bar{c}}$ a symmetric matrix.

Expression (2.16) suggests that, for frequent dispersers (i.e., species with $D > r$, as defined in [68]), sufficiently high levels of constant culling efforts ($\bar{c} > \hat{c}$) in one of the patches can lead to the extinction of the entire population.

When expression (2.16) is not satisfied, the trivial equilibrium is unstable and there exists a positive disease–free equilibrium, $E_1^{\bar{c}}$, as stated by the following theorem:

Theorem 2.3. *If condition (2.16) is not verified, then model (2.1)–(2.2) admits an unique positive disease–free equilibrium* $E_1^{\bar{c}} = (\hat{K}_1, 0, \hat{K}_2, 0)$ *and* $0 < \hat{K}_1 \leq \hat{K}_2$.

Proof. Denote the generic disease–free equilibrium of model (2.1)–(2.2) by $E_1^{\bar{c}} = (\hat{K}_1, 0, \hat{K}_2, 0)$, where $\hat{K}_1$, $\hat{K}_2 > 0$. The components $\hat{K}_1$, $\hat{K}_2$ are the solutions of the algebraic system obtained by setting the r.h.s. of equations (2.1a) and (2.1c), with $c = \bar{c}$, equal to zero, namely:

$$\begin{aligned}(r - \bar{c} - D)\hat{K}_1 - \eta\hat{K}_1^2 + D\hat{K}_2 = 0 \\ (r - D)\hat{K}_2 - \eta\hat{K}_2^2 + D\hat{K}_1 = 0,\end{aligned} \tag{2.17}$$

yielding the admissibility condition:

$$\hat{K}_1 = \frac{D - r + \eta\hat{K}_2}{D}\hat{K}_2 > 0 \iff \hat{K}_2 > \frac{r - D}{\eta}. \tag{2.18}$$

Substituting the expression of $\hat{K}_1$ into (2.17), one obtains $\hat{K}_2 \neq 0$ as solution of

$$f(\hat{K}_2) = 0, \tag{2.19}$$

with

$$f(\hat{K}_2) = a_0 + a_1\hat{K}_2 + a_2\hat{K}_2^2 + a_3\hat{K}_2^3,$$

and

$$\begin{aligned}a_0 &= D(\bar{c}(D - r) - r(2D - r)) \\ a_1 &= \eta(\bar{c}D + (D - r)(2D - r)) \\ a_2 &= 2\eta^2(D - r) \\ a_3 &= \eta^3 > 0.\end{aligned}$$

Let us differentiate the equation (2.19), yielding:

$$f'(\hat{K}_2) = a_1 + 2a_2\hat{K}_2 + 3a_3\hat{K}_2^2 = 0,$$

whose discriminant is $\Delta = a_2^2 - 3a_1a_3 = -3\bar{c}D - 2D^2 + Dr + r^2$. If $\Delta \leq 0$, then f is an increasing function. Otherwise, if $\Delta > 0$, then (2.3) admits two real solutions:

$$\hat{K}_{2\pm} = \frac{2(r - D) \pm \sqrt{\Delta}}{3\eta},$$

that are relative minimum/maximum points for f and it is straightforward to check that

$$\hat{K}_{2-} < \frac{r - D}{\eta}.$$

In any case, we have

$$f\left(\frac{r-D}{\eta}\right) = -D^3 \leq 0.$$

Thus, exactly one root of (2.19) satisfies the admissibility condition (2.18). If $D > r$, it is not obvious that such a root is positive: one can easily check that $a_0 = f(0)$ is [resp. is not] positive if expression (2.16) is [resp. is not] fulfilled. Hence, in summary, system (2.1)–(2.2) admits an unique disease–free equilibrium $E_1^{\bar{c}}$ if condition (2.16) is not satisfied; there are none if (2.16) is verified.

To conclude the proof, we have to prove that, when the disease–free equilibrium $E_1^{\bar{c}}$ exists, $\hat{K}_1 \leq \hat{K}_2$ or, equivalently, $\hat{K}_2 \leq r/\eta$ (from (2.18)). Being $f(r/\eta) = cD^2 \geq 0$, the last inequality always holds. □

Thus, in the presence of localized proactive culling the disease–free equilibrium becomes $E_1^{\bar{c}} = (\hat{K}_1, 0, \hat{K}_2, 0)$, where $\hat{K}_1$ and $\hat{K}_2$ can not be easily written explicitly, since they come from solutions of the third–order equation (2.19).

When proactive culling as in (2.2) is implemented in model (2.1), we can compute through the *next generation* matrix method the control reproduction number, $\mathcal{R}_C$, similarly to $\mathcal{R}_0$. The control reproduction number is defined as the average number of secondary infections produced by a single infected individual in a susceptible population at its disease–free equilibrium experiencing culling effort $\bar{c}$. Its expression is given in the following theorem:

Theorem 2.4. *The control reproduction number of model (2.1)–(2.2) is*

$$\mathcal{R}_C = \frac{1}{2}\beta \frac{\hat{K}_1\,(\mu+\alpha+D) + \hat{K}_2(\mu+\alpha+\bar{c}+D) + 2\eta\hat{K}_1\hat{K}_2 + \sqrt{\Delta_C}}{\Big(\mu+\alpha+\bar{c}+\eta\hat{K}_1+D\Big)\Big(\mu+\alpha+\eta\hat{K}_2+D\Big) - D^2}, \tag{2.20}$$

with

$$\begin{aligned}\Delta_C =& \hat{K}_1^2(\mu+\alpha+D)^2 + \hat{K}_2^2(\mu+\alpha+\bar{c}+D)^2 + \\ &+ 2\hat{K}_1\hat{K}_2\left[2D^2 - (\mu+\alpha+\bar{c}+D)(\mu+\alpha+D)\right].\end{aligned} \tag{2.21}$$

Proof. Following the procedure and the notations in [103, 287], let us consider the r.h.s. of equations (2.1b) and (2.1d), with $c = \bar{c}$, and distinguish the new infections appearance from the other rates of transfer, by defining the vectors

$$\mathcal{F} = \begin{pmatrix} \beta S_1 I_1 \\ \beta S_2 I_2 \end{pmatrix} \text{ and } \mathcal{V} = \begin{pmatrix} (\mu+\alpha+\bar{c}+\eta N_1)I_1 + DI_1 - DI_2 \\ (\mu+\alpha+\eta N_2)I_2 + DI_2 - DI_1 \end{pmatrix}.$$

The Jacobian matrices of $\mathcal{F}$ and $\mathcal{V}$ evaluated at model (2.1)–(2.2) disease–free equilibrium $E_1^{\bar{c}} = (\hat{K}_1, 0, \hat{K}_2, 0)$ read, respectively,

$$F = \begin{pmatrix} \beta\hat{K}_1 & 0 \\ 0 & \beta\hat{K}_2 \end{pmatrix} \text{ and } V = \begin{pmatrix} \mu+\alpha+\bar{c}+\eta\hat{K}_1+D & -D \\ -D & \mu+\alpha+\eta\hat{K}_2+D \end{pmatrix}.$$

As proved in [103, 287], the control reproduction number is given by the spectral radius of

the *next generation* matrix FV^{-1}. Simple algebra yields

$$(FV^{-1})_{11} = \frac{\beta\hat{K}_1\left(\mu+\alpha+\eta\hat{K}_2+D\right)}{\left(\mu+\alpha+\bar{c}+\eta\hat{K}_1+D\right)\left(\mu+\alpha+\eta\hat{K}_2+D\right)-D^2}$$

$$(FV^{-1})_{12} = \frac{\beta\hat{K}_1 D}{\left(\mu+\alpha+\bar{c}+\eta\hat{K}_1+D\right)\left(\mu+\alpha+\eta\hat{K}_2+D\right)-D^2}$$

$$(FV^{-1})_{21} = \frac{\beta\hat{K}_2 D}{\left(\mu+\alpha+\bar{c}+\eta\hat{K}_1+D\right)\left(\mu+\alpha+\eta\hat{K}_2+D\right)-D^2}$$

$$(FV^{-1})_{22} = \frac{\beta\hat{K}_2\left(\mu+\alpha+\bar{c}+\eta\hat{K}_1+D\right)}{\left(\mu+\alpha+\bar{c}+\eta\hat{K}_1+D\right)\left(\mu+\alpha+\eta\hat{K}_2+D\right)-D^2},$$

and, being the eigenvalues $\lambda_\pm$ of FV^{-1} given by

$$\lambda_\pm = \frac{1}{2}\beta\frac{\hat{K}_1\left(\mu+\alpha+D\right)+\hat{K}_2(\mu+\alpha+\bar{c}+D)+2\eta\hat{K}_1\hat{K}_2 \pm \sqrt{\Delta_C}}{\left(\mu+\alpha+\bar{c}+\eta\hat{K}_1+D\right)\left(\mu+\alpha+\eta\hat{K}_2+D\right)-D^2},$$

with Δ_C as in (2.21), we get (2.20). □

When it exists, disease–free equilibrium $E_1^{\bar{c}}$ is asymptotically stable if and only if the control reproduction number $\mathcal{R}_C$ in (2.20) is lower than 1; on the contrary, if $\mathcal{R}_C > 1$ the disease–free equilibrium is unstable [103, 287].

As far as the existence and the number of model endemic equilibria, an analytical investigation is very hard to perform. Therefore, numerical analyses are carried out to understand the effect of localized proactive culling on the disease dynamics. Extensive numerical tests suggest that there are no endemic equilibria when $\mathcal{R}_C < 1$; otherwise, when $\mathcal{R}_C > 1$, there exists an unique asymptotically stable endemic equilibrium, say $E_2^{\bar{c}} = (\hat{S}_1, \hat{I}_1, \hat{S}_2, \hat{I}_2)$.

In Fig. 2.1 we show the effect of the host dispersal rate (D) and the localized proactive culling effort ($\bar{c}$) on the existence and stability of model (2.1)–(2.2) equilibria through bifurcation analysis [273]. The curve TC_0 defines a transcritical bifurcation representing the threshold for host extinction (in (2.16)) that separates the region in which the total host population goes extinct from the region in which model (2.1)–(2.2) converges toward a disease–free equilibrium. The curve TC_1 defines a transcritical bifurcation representing the threshold for infection establishment ($\mathcal{R}_C = 1$) that separates the region in which the pathogen fails to establish itself (disease–free equilibrium) from the region in which the pathogen is able to invade the host population and model (2.1)–(2.2) converges toward an endemic equilibrium.

We investigate the effectiveness of localized proactive culling (2.2) in successfully control infectious diseases in wildlife by analysing the variation of susceptible and infected individuals as a function of $\bar{c}$ at endemic equilibrium $E_2^{\bar{c}}$ in model (2.1)–(2.2). Most of all, we are interested in understanding whether localized proactive culling, $\bar{c}$, can reduce the number of infected individuals both in the culling area ($\hat{I}_1$ in patch 1) and in the neighboring areas ($\hat{I}_2$ in patch 2). Firstly, we provide analytical results on the variation of $\hat{S}_j$ and $\hat{I}_j$ (with $j = 1, 2$) with respect to $\bar{c}$. In particular, we show that $\partial_{\bar{c}}\hat{I}_2|_{\bar{c}=0}$ can be positive for suitable ecological

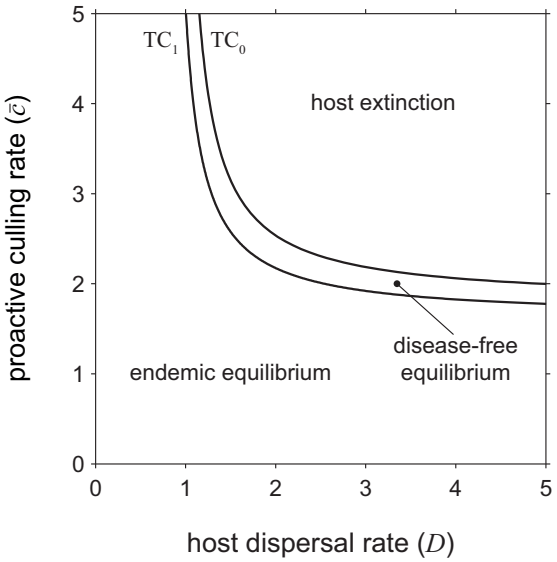

Figure 2.1: The effects of variation in host dispersal rate (D) and localized proactive culling effort ($\bar{c}$) on model (2.1)–(2.2) behaviors. The curves TC_0 (i.e., $\bar{c} = \hat{c}$ in (2.16)) and TC_1 (i.e., $\mathcal{R}_C = 1$), which represent transcritical bifurcations, delimit three different regions in the parameter space $[D, \bar{c}]$ where system (2.1), in the presence of localized proactive culling (2.2), converges to host extinction, disease–free equilibrium, or endemic equilibrium. Parameter values for model (2.1)–(2.2) have been fixed to: $r = 0.9$; $\mu = 0.2$; $K = 600$; $\alpha = 0$; $\mathcal{R}_0 = 10$ (or rather $\beta = 0.01833$, see (2.13)).

and epidemiological conditions (see Theorem 2.5). Secondly, since endemic equilibrium $E_2^{\bar{c}}$ is too complex to be computed analytically for strictly positive values of $\bar{c}$, we simulate numerically the number of infected individuals at endemic equilibrium $E_2^{\bar{c}}$ for different values of localized proactive culling, $\bar{c}$.

Theorem 2.5. *The number of infected individuals in patch 1 (I_1) at endemic equilibrium of model (2.1)–(2.2), as function of $\bar{c}$, is maximum in $\bar{c} = 0$; namely, $\hat{I}_1(\bar{c}) < \hat{I}_1(0) = \bar{I}$, $\forall \bar{c} > 0$.*

Proof. By considering equations (2.1) evaluated at equilibrium $E_2^{\bar{c}} = (\hat{S}_1, \hat{I}_1, \hat{S}_2, \hat{I}_2)$ and at equilibrium $E_2 = (\bar{S}, \bar{I}, \bar{S}, \bar{I})$, as given in (2.14), and subtracting side by side, one obtains:

$$(\beta + \eta)\left(\hat{I}_1(\bar{c}) - \bar{I}\right) + \bar{c} = -\eta\left(\hat{S}_1(\bar{c}) - \bar{S}\right) + D\left[\frac{\hat{S}_2(\bar{c})}{\hat{S}_1(\bar{c})} - 1\right] \tag{2.22a}$$

$$(\beta - \eta)\left(\hat{S}_1(\bar{c}) - \bar{S}\right) = \bar{c} + \eta\left(\hat{I}_1(\bar{c}) - \bar{I}\right) - D\left[\frac{\hat{I}_2(\bar{c})}{\hat{I}_1(\bar{c})} - 1\right] \tag{2.22b}$$

$$(\beta + \eta)\left(\hat{I}_2(\bar{c}) - \bar{I}\right) = -\eta\left(\hat{S}_2(\bar{c}) - \bar{S}\right) + D\left[\frac{\hat{S}_1(\bar{c})}{\hat{S}_2(\bar{c})} - 1\right] \tag{2.22c}$$

$$(\beta - \eta)\left(\hat{S}_2(\bar{c}) - \bar{S}\right) = \eta\left(\hat{I}_2(\bar{c}) - \bar{I}\right) - D\left[\frac{\hat{I}_1(\bar{c})}{\hat{I}_2(\bar{c})} - 1\right]. \tag{2.22d}$$

By contradiction, we assume that there exists a $\bar{c}_0 > 0$ such that $\hat{I}_1(\bar{c}_0) \geq \bar{I}$. Then, signs in (2.22b) impose that at least one of the following inequalities holds:

- $\hat{I}_2(\bar{c}_0) > \hat{I}_1(\bar{c}_0)$. Then, $\hat{I}_2(\bar{c}_0) > \bar{I}$ and addenda signs in (2.22c) and (2.22d) impose that $\hat{S}_1(\bar{c}_0) > \hat{S}_2(\bar{c}_0) > \bar{S}$. However, a contradiction in (2.22a) arises.
- $\hat{S}_1(\bar{c}_0) > \bar{S}$. From sign of equations (2.22a) and (2.22c) one yields $\hat{S}_2(\bar{c}_0) > \hat{S}_1(\bar{c}_0) > \bar{S}$ and $\hat{I}_1(\bar{c}_0) \geq \bar{I} > \hat{I}_2(\bar{c}_0)$, respectively. This leads to a contradiction in (2.22d).

Thus, it must be $\hat{I}_1(\bar{c}) < \bar{I}$, $\forall \bar{c} > 0$. □

Theorem 2.6. *$\forall \bar{c} > 0$, the number of infected individuals in patch 1 at endemic equilibrium $E_2^{\bar{c}}$ of model (2.1)–(2.2) is smaller than the corresponding number of infected individuals in patch 2 (I_2); namely, $\hat{I}_1(\bar{c}) < \hat{I}_2(\bar{c})$, $\forall \bar{c} > 0$.*

Proof. By contradiction, we assume that there exists a $\bar{c}_0 > 0$ such that $\hat{I}_1(\bar{c}_0) \geq \hat{I}_2(\bar{c}_0)$. Then, from (2.22c) and (2.22d) and in virtue of Theorem 2.5, one yields $\hat{S}_1(\bar{c}_0) < \hat{S}_2(\bar{c}_0) < \bar{S}$. Moreover, by handling equations (2.1b)–(2.1d) at endemic equilibrium $E_2^{\bar{c}_0}$ and subtracting side by side, we obtain

$$(\beta - \eta)(\hat{S}_1 - \hat{S}_2) - \bar{c}_0 - \eta(\hat{I}_1 - \hat{I}_2) + D\left(\frac{\hat{I}_2}{\hat{I}_1} - \frac{\hat{I}_1}{\hat{I}_2}\right) = 0,$$

which is in contradiction with addenda signs. Hence, it must be $\hat{I}_1(\bar{c}) < \hat{I}_2(\bar{c})$, $\forall \bar{c} > 0$. □

Theorem 2.7. *The derivative of the number of susceptible individuals in patch 2 (S_2) with respect to $\bar{c}$, at endemic equilibrium of model (2.1)–(2.2), is always positive when $\bar{c} = 0$. Instead, the derivative of the number of infected individuals in patch 2 is positive when $\bar{c} = 0$ if and only if the following condition holds:*

$$\partial_{\bar{c}} \hat{I}_2\Big|_{\bar{c}=0} > 0 \iff \frac{2D}{r} < \frac{\mathcal{R}_0 - 2}{\mathcal{R}_0}, \tag{2.23}$$

with $\mathcal{R}_0$ defined in (2.13).

Proof. By differentiating with respect to $\bar{c}$ the r.h.s. of equations (2.1) at endemic equilibrium $E_2^{\bar{c}}$, we obtain

$$\beta \hat{I}_1'(\bar{c}) = -1 - \eta \hat{S}_1'(\bar{c}) - \eta \hat{I}_1'(\bar{c}) + \frac{D}{\hat{S}_1^2(\bar{c})}[\hat{S}_2'(\bar{c})\hat{S}_1(\bar{c}) - \hat{S}_1'(\bar{c})\hat{S}_2(\bar{c})] \tag{2.24a}$$

$$\beta \hat{S}_1'(\bar{c}) = 1 + \eta \hat{S}_1'(\bar{c}) + \eta \hat{I}_1'(\bar{c}) - \frac{D}{\hat{I}_1^2(\bar{c})}[\hat{I}_2'(\bar{c})\hat{I}_1(\bar{c}) - \hat{I}_1'(\bar{c})\hat{I}_2(\bar{c})] \tag{2.24b}$$

$$\beta \hat{I}_2'(\bar{c}) = -\eta \hat{S}_2'(\bar{c}) - \eta \hat{I}_2'(\bar{c}) + \frac{D}{\hat{S}_2^2(\bar{c})}[\hat{S}_1'(\bar{c})\hat{S}_2(\bar{c}) - \hat{S}_2'(\bar{c})\hat{S}_1(\bar{c})] \tag{2.24c}$$

$$\beta \hat{S}_2'(\bar{c}) = \eta \hat{S}_2'(\bar{c}) + \eta \hat{I}_2'(\bar{c}) - \frac{D}{\hat{I}_2^2(\bar{c})}[\hat{I}_1'(\bar{c})\hat{I}_2(\bar{c}) - \hat{I}_2'(\bar{c})\hat{I}_1(\bar{c})]. \tag{2.24d}$$

When $\bar{c} = 0$, $\hat{S}_j(0) = \bar{S}$ and $\hat{I}_j(0) = \bar{I}$, with $\bar{S}$ and $\bar{I}$ defined as in (2.14). Then – by substituting the expressions for $\hat{I}_1'(0)$ and $\hat{I}_2'(0)$ (derived in (2.24a) and (2.24c), respectively) as functions of $\hat{S}_1'(0)$ and $\hat{S}_2'(0)$ –, we can re–write (2.24b) and (2.24d) as follows:

$$A(\bar{S}, \bar{I})\hat{S}_1'(0) = \beta - \frac{D}{\bar{I}} + B(\bar{S}, \bar{I})\hat{S}_2'(0) \tag{2.25a}$$

$$A(\bar{S}, \bar{I})\hat{S}_2'(0) = \frac{D}{\bar{I}} + B(\bar{S}, \bar{I})\hat{S}_1'(0), \tag{2.25b}$$

where

$$A(\bar{S},\bar{I}) = \beta^2 + B(\bar{S},\bar{I}), \tag{2.26}$$

and

$$B(\bar{S},\bar{I}) = \eta\frac{D}{\bar{I}} + \eta\frac{D}{\bar{S}} + 2\frac{D^2}{\bar{S}\bar{I}}. \tag{2.27}$$

By substituting (2.25a) in (2.25b) and rearranging, we find the equation

$$\frac{A^2 - B^2}{A}\hat{S}_2'(0) = \beta\frac{B}{A} + \left(1 - \frac{B}{A}\right)\frac{D}{\bar{I}}.$$

Being $A(\bar{S},\bar{I}) > B(\bar{S},\bar{I})$, condition $\hat{S}_2'(0) > 0$ is always satisfied.

In a similar way, we prove the second part of the statement. By substituting the expressions for $\hat{S}_1'(0)$ and $\hat{S}_2'(0)$ (derived in (2.24b) and (2.24d), respectively) as functions of $\hat{I}_1'(0)$ and $\hat{I}_2'(0)$, we can re–write (2.24a) and (2.24c) as follows:

$$A(\bar{S},\bar{I})\hat{I}_1'(0) = -\beta - \frac{D}{\bar{S}} + B(\bar{S},\bar{I})\hat{I}_2'(0) \tag{2.28a}$$

$$A(\bar{S},\bar{I})\hat{I}_2'(0) = \frac{D}{\bar{S}} + B(\bar{S},\bar{I})\hat{I}_1'(0), \tag{2.28b}$$

where functions A and B are given in (2.26) and (2.27), respectively. By substituting (2.28a) in (2.28b) and rearranging, we find the equation

$$\frac{A^2 - B^2}{A}\hat{I}_2'(0) = -\beta\frac{B}{A} + \left(1 - \frac{B}{A}\right)\frac{D}{\bar{S}}. \tag{2.29}$$

Hence, condition $\hat{I}_2'(0) > 0$ is fulfilled if and only if the r.h.s. of (2.29) is positive (i.e., if $\beta D - B(\bar{S},\bar{I})\bar{S} > 0$). With simple algebraic manipulations – and remembering equalities (2.13) and (2.14) – then yields to

$$\frac{2D}{r} < \frac{\mathcal{R}_0 - 2}{\mathcal{R}_0}.$$

□

Proposition 2.8. *In the limit case $D \to 0$, the derivative of the number of susceptible individuals in patch 1 (S_1) with respect to $\bar{c}$, at endemic equilibrium $E_2^{\bar{c}}$ of model (2.1)–(2.2), converges to $1/\beta$.*

Proof. It is an immediate consequence of equations (2.24a) and (2.24b). □

From expression (2.23), we notice that necessary conditions for localized proactive culling to increase (instead of decrease) the number of infected individuals in patch 2 are: $2D < r$ (i.e., hosts are very infrequent dispersers) and $\mathcal{R}_0 > 2$ (i.e., in the corresponding uncontrolled model the first infected individual can, on average, infect more than two individuals).

Remark 2.9. *In the case the total host population at endemic equilibrium for $c = 0$ (2.15) is much lower than the carrying capacity K, the effect of the density–dependent mortality rate at the endemic equilibrium is negligible, which corresponds to assume $\eta \to 0$. In this scenario, it is straightforward to check that condition (2.23) for being $\hat{I}_2'(0) > 0$ reduces to: $2D < r$.*

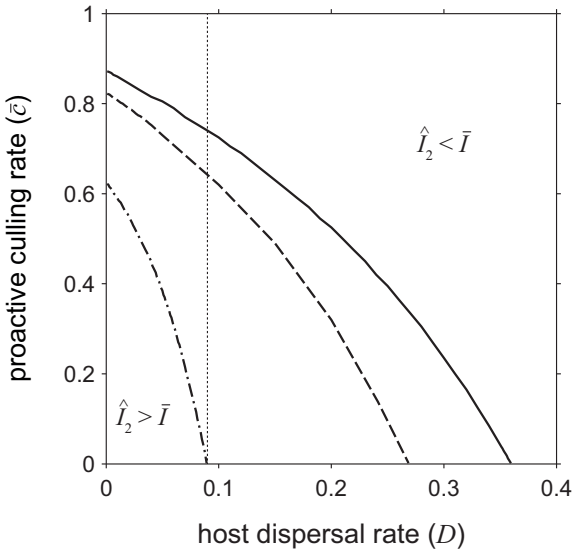

Figure 2.2: Curves in the parameter space $[D, \bar{c}]$ separating the regions in which condition $\hat{I}_2(\bar{c}) > \bar{I}$ or condition $\hat{I}_2(\bar{c}) < \bar{I}$ are satisfied for different values of the basic reproduction number of model (2.1) with $c = 0$ ($\mathcal{R}_0$, given by (2.13)). Solid thick curve: $\mathcal{R}_0 = 10$; dashed thick curve: $\mathcal{R}_0 = 5$; dot–dashed thick curve: $\mathcal{R}_0 = 2.5$. The dynamics of infected individuals in patch 2 ($\hat{I}_2$) corresponding to the parameter space along the thin dotted line ($D = 0.1r$) is illustrated in Fig. 2.3. Unspecified parameters as in Fig. 2.1.

Instead, if, in addition to setting $\eta \to 0$, we also relax the hypothesis of disease–induced sterility (see the next subsection), then such a condition becomes slightly more complex:

$$(\alpha - r)\left(1 - \frac{2D}{r}\right) - (\mu + r) - \frac{\mu + r}{\mu + \alpha}\left(r\frac{\mu + r}{\alpha - r} + 2D\right) > 0, \tag{2.30}$$

where $\alpha > r$ (which represents the necessary condition for the existence of the endemic equilibrium in the absence of control, see the next subsection). However, once again, formula (2.30) indicates that having $2D < r$ is necessary for proactive culling to increase the endemic value of infected in the uncontrolled patch.

To investigate more deeply the counter–intuitive result obtained in Theorem 2.7, we numerically compute the parameter conditions for which the number of infected individuals in patch 2 at the endemic equilibrium is higher in the presence of localized proactive control than with the do–nothing alternative (i.e., $\hat{I}_2(\bar{c}) > \bar{I}$). The numerical analyses presented here are performed by exploring the effects of different values of host dispersal (D), proactive culling effort ($\bar{c}$), and disease basic reproduction number of model (2.1) with $c = 0$ ($\mathcal{R}_0$, given by (2.13)) on control effectiveness and by keeping the host demographic parameters constant in the simulations. Specifically, we set the host demographic parameters as in [35].

In Fig. 2.2 we show the parametric regions where condition $\hat{I}_2(\bar{c}) > \bar{I}$ is satisfied for different values of basic reproduction number of the corresponding uncontrolled model ($\mathcal{R}_0$) in the parameter space $[D, \bar{c}]$. Fig. 2.2 highlights that for low values of host dispersal rates (D), localized culling is ineffective in reducing the infection outside the control zone (i.e., $\hat{I}_2(\bar{c}) > \bar{I}$) for a wide range of culling rate values, also when the basic reproduction number is relatively low.

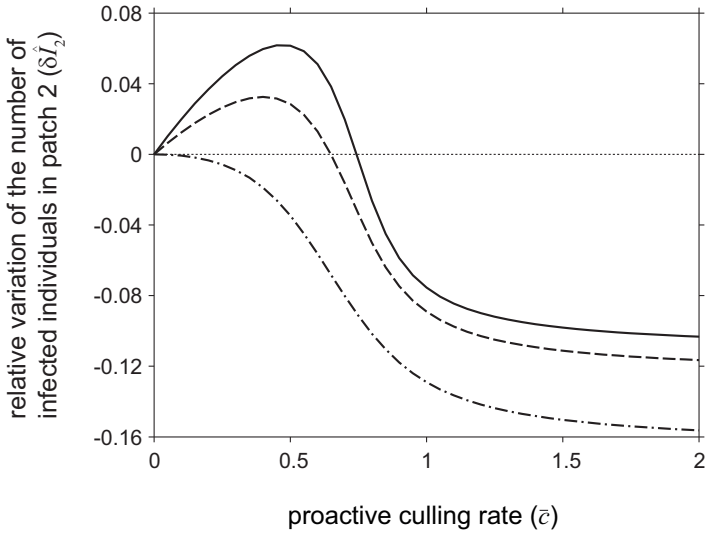

Figure 2.3: Relative variation of the number of infected individuals in patch 2 at endemic equilibrium $E_2^{\bar{c}}$ with respect to the number of infected in the absence of control (i.e., $\delta\hat{I}_2 = (\hat{I}_2 - \bar{I})/\bar{I}$) as a function of the localized proactive culling rate ($\bar{c}$) for a very infrequent disperser host species ($D/r = 0.1$). Solid thick curve: $\mathcal{R}_0 = 10$; dashed thick curve: $\mathcal{R}_0 = 5$; dot–dashed thick curve: $\mathcal{R}_0 = 2.5$. The thin dotted line represents the condition $\hat{I}_2 = \bar{I}$. Unspecified parameters as in Fig. 2.1.

The dynamics of infected individuals in patch 2 corresponding to the parameter space along the thin dotted line in Fig. 2.2 is illustrated in Fig. 2.3. In particular, in Fig. 2.3 we show the relative variation of the number of infected individuals in patch 2 at endemic equilibrium $E_2^{\bar{c}}$ with respect to the number of infected in the absence of control (i.e., $\delta\hat{I}_2 = (\hat{I}_2 - \bar{I})/\bar{I}$) as a function of the localized proactive culling rate ($\bar{c}$) for an infrequent disperser host ($D/r = 0.1$) and for different values of $\mathcal{R}_0$.

Ineffectiveness of proactive culling by relaxing some hypotheses

Let us consider the following metapopulation epidemic model

$$\dot{S}_1 = \nu N_1 - \beta S_1 I_1 - (\mu + c) S_1 - D S_1 + D S_2 \tag{2.31a}$$

$$\dot{I}_1 = \beta S_1 I_1 - (\mu + \alpha + c) I_1 - D I_1 + D I_2 \tag{2.31b}$$

$$\dot{S}_2 = \nu N_2 - \beta S_2 I_2 - \mu S_2 - D S_2 + D S_1 \tag{2.31c}$$

$$\dot{I}_2 = \beta S_2 I_2 - (\mu + \alpha) I_2 - D I_2 + D I_1, \tag{2.31d}$$

that differs from model (2.1) in the absence of both pathogen–induced sterility (also infected individuals reproduce) and density–dependent host mortality ($\eta = 0$). Remember that we called $r = \nu - \mu$ the intrinsic growth rate.

Firstly, one can easily check that, in the absence of control ($c = 0$), an endemic equilibrium (say, E_2) exists only if $\alpha > r$ and has components equal in pairs [104]: $E_2 = (\bar{S}, \bar{I}, \bar{S}, \bar{I})$, where

$$\bar{S} = \frac{\mu + \alpha}{\beta} \tag{2.32a}$$

$$\bar{I} = \frac{r(\mu + \alpha)}{\beta(\alpha - r)}. \tag{2.32b}$$

For E_2 stability properties, see [104].

Then, let us denote with $E_2^{\bar{c}} = (\hat{S}_1(\bar{c}), \hat{I}_1(\bar{c}), \hat{S}_2(\bar{c}), \hat{I}_2(\bar{c}))$ the generic endemic equilibrium of model (2.31) with $c = \bar{c}$. By differentiating with respect to $\bar{c}$ the r.h.s. side of equations (2.31) at $E_2^{\bar{c}}$, we obtain

$$\beta \hat{I}_1'(\bar{c}) = -1 + \frac{\nu}{\hat{S}_1^2(\bar{c})}[\hat{I}_1'(\bar{c})\hat{S}_1(\bar{c}) - \hat{S}_1'(\bar{c})\hat{I}_1(\bar{c})] + \frac{D}{\hat{S}_1^2(\bar{c})}[\hat{S}_2'(\bar{c})\hat{S}_1(\bar{c}) - \hat{S}_1'(\bar{c})\hat{S}_2(\bar{c})] \tag{2.33a}$$

$$\beta \hat{S}_1'(\bar{c}) = 1 - \frac{D}{\hat{I}_1^2(\bar{c})}[\hat{I}_2'(\bar{c})\hat{I}_1(\bar{c}) - \hat{I}_1'(\bar{c})\hat{I}_2(\bar{c})] \tag{2.33b}$$

$$\beta \hat{I}_2'(\bar{c}) = \frac{\nu}{\hat{S}_2^2(\bar{c})}[\hat{I}_2'(\bar{c})\hat{S}_2(\bar{c}) - \hat{S}_2'(\bar{c})\hat{I}_2(\bar{c})] + \frac{D}{\hat{S}_2^2(\bar{c})}[\hat{S}_1'(\bar{c})\hat{S}_2(\bar{c}) - \hat{S}_2'(\bar{c})\hat{S}_1(\bar{c})] \tag{2.33c}$$

$$\beta \hat{S}_2'(\bar{c}) = -\frac{D}{\hat{I}_2^2(\bar{c})}[\hat{I}_1'(\bar{c})\hat{I}_2(\bar{c}) - \hat{I}_2'(\bar{c})\hat{I}_1(\bar{c})]. \tag{2.33d}$$

Of course, when $\bar{c} = 0$, $\hat{S}_j(0) = \bar{S}$ and $\hat{I}_j(0) = \bar{I}$, as given in (2.32). Then – by substituting the expressions for $\hat{S}_1'(0)$ and $\hat{S}_2'(0)$ (derived in (2.33b) and (2.33d), respectively) as functions of $\hat{I}_1'(0)$ and $\hat{I}_2'(0)$ –, we can re–write (2.33a) and (2.33c) as follows:

$$A(\bar{S}, \bar{I})\hat{I}_1'(0) = -\beta - \frac{D}{\bar{S}} - \frac{\nu \bar{I}}{\bar{S}^2} + B(\bar{S}, \bar{I})\hat{I}_2'(0) \tag{2.34a}$$

$$A(\bar{S}, \bar{I})\hat{I}_2'(0) = \frac{D}{\bar{S}} + B(\bar{S}, \bar{I})\hat{I}_1'(0), \tag{2.34b}$$

where

$$A(\bar{S}, \bar{I}) = \beta\left(\beta - \frac{\nu}{\bar{S}}\right) + B(\bar{S}, \bar{I}),$$

and

$$B(\bar{S}, \bar{I}) = \frac{D\nu}{\bar{S}^2} + 2\frac{D^2}{\bar{S}\bar{I}}.$$

By substituting (2.34a) in (2.34b) and rearranging, we find the equation

$$\frac{A^2 - B^2}{A}\hat{I}_2'(0) = -\left(\beta + \frac{\nu \bar{I}}{\bar{S}^2}\right)\frac{B}{A} + \left(1 - \frac{B}{A}\right)\frac{D}{\bar{S}}. \tag{2.35}$$

Since $A(\bar{S}, \bar{I}) > B(\bar{S}, \bar{I})$, condition $\hat{I}_2'(0) > 0$ is fulfilled if and only if the r.h.s. of (2.35) is positive. With simple algebraic manipulations – and remembering equalities (2.32) – one yields

$$(\alpha - r)\left(1 - \frac{2D}{r}\right) - \nu - \frac{\nu}{\mu + \alpha}\left(\frac{r\nu}{\alpha - r} + 2D\right) > 0.$$

The effect of localized reactive culling

Let us consider model (2.1) with the piecewise–constant function (2.3) representing the culling effort in the localized reactive control strategy. We are interested in investigating the long term dynamics of model solutions and, in particular, of sliding motions, occurring on the sliding set (2.4). To this aim, the following results concerning the existence and stability of stationary sliding solutions (also called pseudo–equilibria) can be proved:

Theorem 2.10. *Necessary condition for the existence of pseudo–equilibria for model (2.1)–(2.3) is that*

$$\hat{I}_1 \leq \theta \leq \bar{I}, \tag{2.36}$$

where $\hat{I}_1$ [resp. $\bar{I}$] is the number of infected individuals in patch 1 at endemic equilibrium $E_2^{\bar{c}}$ [resp. E_2] of model (2.1) with $c = \bar{c}$ [resp. $c = 0$].

Proof. Firstly note that Theorem 2.5 ensures that $\hat{I}_1 \leq \bar{I}$.

By definition, a pseudo–equilibrium of model (2.1)–(2.3) is an equilibrium for system (2.5) belonging to the sliding set Σ_s (given in (2.4)), i.e. such that $I_1 = \theta$, and S_1, S_2, I_2 satisfy

$$(r + \mu + \alpha)S_1 - \beta S_1^2 - \beta\theta S_1 - D\frac{I_2}{\theta}S_1 + DS_2 = 0 \tag{2.37a}$$

$$rS_2 - \eta S_2 N_2 - \beta S_2 I_2 - DS_2 + DS_1 = 0 \tag{2.37b}$$

$$\beta S_2 I_2 - (\mu + \alpha + \eta N_2)I_2 - DI_2 + D\theta = 0, \tag{2.37c}$$

with

$$(\beta - \eta)S_1 \geq \mu + \alpha + \eta\theta + D - D\frac{I_2}{\theta} \tag{2.38a}$$

$$(\beta - \eta)S_1 \leq \mu + \alpha + \eta\theta + \bar{c} + D - D\frac{I_2}{\theta}. \tag{2.38b}$$

By contradiction, we assume that one of the following inequalities holds:

- $\theta < \hat{I}_1$. Then – by handling the inequality (2.38b) and equation (2.1b) at equilibrium $E_2^{\bar{c}}$ –, one yields

$$(\beta - \eta)(S_1 - \hat{S}_1) - \eta(\theta - \hat{I}_1) + D\left(\frac{I_2}{\theta} - \frac{\hat{I}_2}{\hat{I}_1}\right) \leq 0,$$

  implying that two mutually–exclusive conditions must be considered:

  - $S_1 < \hat{S}_1$. Then, $N_1 = S_1 + \theta < \hat{S}_1 + \hat{I}_1 = \hat{N}_1$ and by substituting the expression for $\mu + \alpha - DI_2/\theta$ derived from (2.37a) in (2.38b) and rearranging, we obtain

$$r - \beta\theta - \eta N_1 - \bar{c} - D\left(1 - \frac{S_2}{S_1}\right) \leq 0.$$

    Subtracting the latter inequality and equation (2.1a) at equilibrium $E_2^{\bar{c}}$ side by side yields

$$\beta(\theta - \hat{I}_1) + \eta(N_1 - \hat{N}_1) + D\left(\frac{\hat{S}_2}{\hat{S}_1} - \frac{S_2}{S_1}\right) \geq 0,$$

    implying $\hat{S}_2/\hat{S}_1 > S_2/S_1$ and, in particular, $\hat{S}_2 > S_2$.
    Let us consider now equations (2.37b)–(2.37c) and (2.1c)–(2.1d) at equilibrium $E_2^{\bar{c}}$ and subtract side by side, yielding:

$$(\beta + \eta)\left(I_2 - \hat{I}_2\right) = -\eta\left(S_2 - \hat{S}_2\right) + D\left(\frac{S_1}{S_2} - \frac{\hat{S}_1}{\hat{S}_2}\right) \tag{2.39a}$$

$$(\beta - \eta)\left(S_2 - \hat{S}_2\right) = \eta\left(I_2 - \hat{I}_2\right) - D\left(\frac{\theta}{I_2} - \frac{\hat{I}_1}{\hat{I}_2}\right). \tag{2.39b}$$

Sign of (2.39a) r.h.s. imposes that $I_2 > \hat{I}_2$, which, however, is in contrast with (2.39b).

– $S_1 \geq \hat{S}_1$, $I_2/\theta < \hat{I}_2/\hat{I}_1$. Then, $I_2 < \hat{I}_2$ and sign of (2.39b) r.h.s. implies that $S_2 > \hat{S}_2$, which is in contradiction with (2.39a).

- $\theta > \bar{I}$. Then – by remembering inequality (2.38a) and equation (2.1b) at equilibrium E_2 –, one yields

$$(\beta - \eta)(S_1 - \bar{S}) - \eta(\theta - \bar{I}) + D\left(\frac{I_2}{\theta} - 1\right) \geq 0,$$

hence at least one between the first and the last addendum must be positive; namely, we consider two alternative cases:

– $S_1 > \bar{S}$. Then, $N_1 > \bar{S} + \bar{I} = \bar{N}$ and by substituting the expression for $\mu + \alpha - DI_2/\theta$ derived from (2.37a) in (2.38a) and rearranging, one obtains

$$r - \eta N_1 - D\left(1 - \frac{S_2}{S_1}\right) \geq \beta\theta.$$

Being $\theta > \bar{I}$, with $\bar{I}$ given in (2.14b), then $S_2 > S_1 > \bar{S}$.

Accounting now for equations (2.37b)–(2.37c) and (2.1c)–(2.1d) at equilibrium E_2 and subtracting side by side, yields:

$$(\beta + \eta)\left(I_2 - \bar{I}\right) = -\eta\left(S_2 - \bar{S}\right) + D\left(\frac{S_1}{S_2} - 1\right) \tag{2.40a}$$

$$(\beta - \eta)\left(S_2 - \bar{S}\right) = \eta\left(I_2 - \bar{I}\right) - D\left(\frac{\theta}{I_2} - 1\right). \tag{2.40b}$$

Addenda signs in (2.40a)–(2.40b) impose that $\bar{I} > I_2 > \theta$, which contradicts the initial assumption.

– $S_1 \leq \bar{S}$, $I_2 > \theta$. Then, sign of (2.40b) r.h.s. implies that $S_2 > \bar{S} \geq S_1$, which, however, is in contrast with (2.40a).

Since in any case we find a contradiction, θ must belong to the interval (2.36). □

Remark 2.11. *Note that when θ belongs to the interval (2.36), pseudo–equilibria are the unique possible attractors of model (2.1)–(2.3). Indeed, from (2.3), neither E_2 nor $E_2^{\bar{c}}$ can exist.*

Theorem 2.12. *A pseudo–equilibrium of model (2.1)–(2.3) is locally asymptotically stable if, and only if,*

$$\begin{aligned}(d_1 + d_2)\left[d_3(d_1 + d_2 + d_3) + \eta D\frac{S_2^2}{S_1} + \beta S_1 d_2\right] + \\ + (\beta^2 - \eta^2)S_2 I_2(d_2 + d_3) - \frac{D^2}{\theta}(\beta - \eta)S_1 I_2 > 0,\end{aligned} \tag{2.41}$$

with

$$d_1 = \beta S_1 + D\frac{S_2}{S_1}, \;\; d_2 = \eta S_2 + D\frac{S_1}{S_2}, \;\; d_3 = \eta I_2 + D\frac{\theta}{I_2}. \tag{2.42}$$

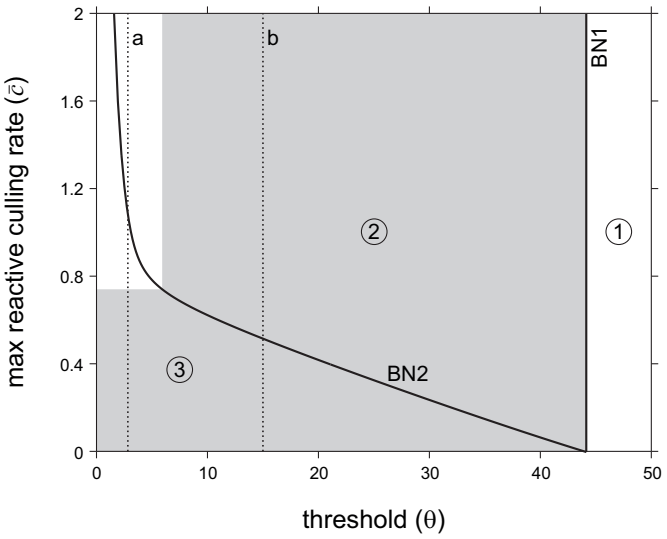

Figure 2.4: Bifurcation diagram of epidemic model (2.1)–(2.3) in the parameter space $[\theta, \bar{c}]$. The curves BN1 and BN2 represent boundary–node bifurcations. A stable equilibrium is the only attractor in regions 1 and 3. A pseudo–equilibrium is the only attractor in region 2. The shaded area represents the parameter combinations for which model (2.1)–(2.3) displays $I_2^{\theta,\bar{c}} > I_2^{0,0} = \bar{I}$. The relative variations of the number of infected individuals at model (2.1)–(2.3) steady–state with respect to the number of infected in the absence of control ($\delta I_j^{\theta,\bar{c}}$) as a function of parameter $\bar{c}$, corresponding to the dotted lines a and b, are illustrated in Figs. 2.5 and 2.6. Other parameters are: $r = 0.9$; $\mu = 0.2$; $K = 600$; $\mathcal{R}_0 = 10$; $\alpha = 0$, $D = 0.1r$.

Proof. From (2.37), the Jacobian matrix of system (2.5) at a pseudo–equilibrium reads

$$J = \begin{pmatrix} -d_1 & D & -\dfrac{D}{\theta}S_1 \\ D & -d_2 & -(\beta+\eta)S_2 \\ 0 & (\beta-\eta)I_2 & -d_3 \end{pmatrix},$$

with d_1, d_2 and d_3 given in (2.42). With simple algebraic calculations, we derive the characteristic polynomial of J (say, $P(\lambda)$):

$$P(\lambda) = l_0 + l_1\lambda + l_2\lambda^2 + \lambda^3,$$

where

$$\begin{aligned} l_0 =& (\beta^2-\eta^2)S_2I_2d_1 + \left(\eta D\frac{S_2^2}{S_1} + \beta S_1 d_2\right)d_3 + \frac{D^2}{\theta}(\beta-\eta)S_1I_2 \\ l_1 =& (d_1+d_2)d_3 + (\beta^2-\eta^2)S_2I_2 + \eta D\frac{S_2^2}{S_1} + \beta S_1 d_2 \\ l_2 =& d_1+d_2+d_3. \end{aligned}$$

Being $l_i > 0$, $\forall i = 0, \ldots, 2$, the presence of positive real roots for $P(\lambda)$ is excluded in virtue of Descartes' rule of sign. According to Routh–Hurwitz theorem, also complex roots with positive real part are not admissible if, and only if, $l_1l_2 - l_0 > 0$, which corresponds to (2.41). □

The analytical condition (2.41) provided in Theorem 2.12 depends in a complicated manner on unknown pseudo–equilibrium values as well as on crucial parameters, like β,

η, D, θ; hence, it is difficult to give easier sufficient conditions for its positivity. However, in the specific case the hosts are very infrequent dispersers (i.e. $D \to 0$), which corresponds to the scenario where culling leads to an increase of infected individuals in the uncontrolled patch, expression (2.41) is always verified. In this case, a pseudo–equilibrium of model (2.1)–(2.3) is locally asymptotically stable.

Since the analytical results provided in Theorems 2.10 and 2.12 are not exhaustive, we perform different sets of numerical simulations on a wide range of parameters combinations for θ and $\bar{c}$ (as in Fig. 2.4) and for different initial conditions of model (2.1) variables. For each pair of parameters θ and $\bar{c}$, we find a unique attractor regardless of the initial conditions chosen for the simulations. Specifically, we find that the only suitable attractors for model (2.1)–(2.3) are either stable equilibria or pseudo–equilibria (which represent points of the sliding set (2.4)).

The bifurcation analysis of epidemic model (2.1)–(2.3) in the parameter space $[\theta, \bar{c}]$, derived from the continuation of stable equilibria and pseudo–equilibria found in the numerical simulations, is illustrated in Fig. 2.4.

Fig. 2.4 shows that, for large values of culling threshold (θ), model (2.1)–(2.3) equilibrium is unique, namely a stable equilibrium (independent from the values assumed by $\bar{c}$) corresponding to endemic equilibrium (2.14) as defined in continuous model (2.1) in the absence of control, namely E_2 (see region 1 in Fig. 2.4). By decreasing threshold θ, equilibrium E_2 found in region 1 undergoes a boundary–node bifurcation for $\theta = I_1^{0,0} = I_2^{0,0} = \bar{I}$ (line BN1 in Fig. 2.4), where $I_j^{\theta,\bar{c}}$ denotes the steady–state value of infected individuals in patches j for localized reactive control (2.3) with parameters θ, $\bar{c}$. By crossing BN1 and entering region 2 the original E_2 equilibrium disappears and a pseudo–equilibrium characterized by $I_1^{\theta,\bar{c}} = \theta$ appears (see region 2 in Fig. 2.4). Curve BN2 represents a boundary–node bifurcation: by crossing it and entering region 3, the pseudo–equilibrium characterized by $I_1^{\theta,\bar{c}} = \theta$ disappears and a stable equilibrium characterized by $I_1^{\theta,\bar{c}} > \theta$ appears. Boundary–node bifurcations BN1 and BN2 correspond to the vanishing of the vector fields components $f_2^{(1)}$ and $f_2^{(2)}$, respectively, as defined in (2.4). The grey area in Fig. 2.4 represents the conditions in the parameter space $[\theta, \bar{c}]$ where $I_2^{\theta,\bar{c}} > I_2^{0,0} = \bar{I}$, i.e., where localized reactive culling is ineffective in reducing the infection burden in both areas.

Specifically, Fig. 2.4 shows that, in the case of low levels of culling threshold θ, sufficiently high efforts of culling, $\bar{c}$, are able to reduce the infection burden in both areas, as in the case of localized proactive culling (see solid line in Fig. 2.3). On the contrary, in the case of intermediate values of θ, localized reactive culling is ineffective in reducing the infection burden in both areas regardless of the culling effort applied in disease control. These findings are highlighted in Figs. 2.5 and 2.6, where the effects of localized reactive control on the relative variation of the number of infected individuals in patches 1 (panels A) and 2 (panels B) at model (2.1)–(2.3) steady–state with respect to the number of infected in the absence of control ($\delta I_j^{\theta,\bar{c}} = (I_j^{\theta,\bar{c}} - \bar{I})/\bar{I}$, with $j = 1, 2$) are shown for two different levels of culling threshold ($\theta = 2.5$ in Fig. 2.5, $\theta = 15$ in Fig. 2.6).

2.4 Discussion and conclusions

In this chapter, we analyzed the effect of localized proactive and reactive culling on the disease dynamics in a metapopulation model with two patches (one with control and the other one without control). Proactive culling is described through a classical ODE continuous

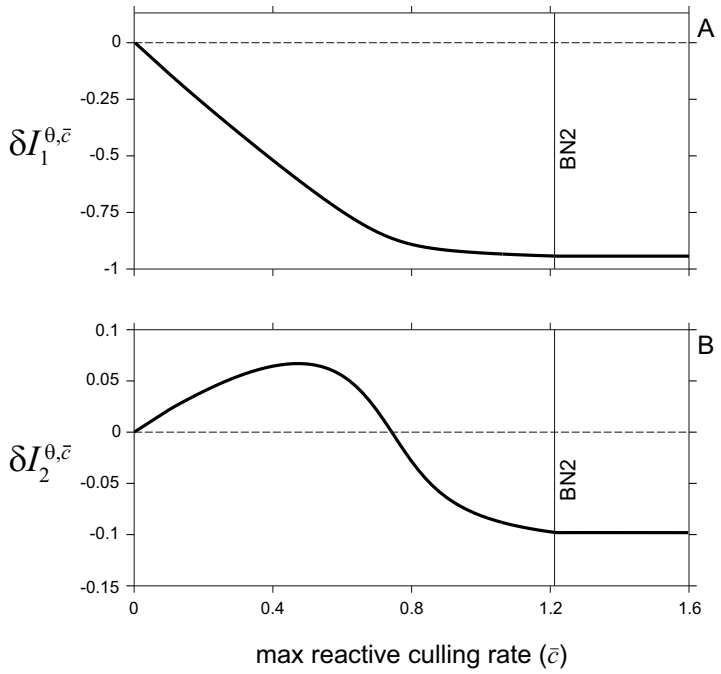

Figure 2.5: Relative variation of the number of infected individuals in patches 1 (panel A) and 2 (panel B) at model (2.1)–(2.3) steady–state with respect to the number of infected in the absence of control ($\delta I_j^{\theta,\bar{c}}$, with $j = 1, 2$) as a function of parameter $\bar{c}$. BN2 represents a boundary–node bifurcation point as in Fig. 2.4. The dashed line represents the condition $I_j^{\theta,\bar{c}} = \bar{I}$. Parameter $\theta = 2.5$, unspecified parameters as in Fig. 2.4.

system, while reactive culling is described through a piecewise–smooth system where the control activities are implemented when the number of infected individuals exceeds a given threshold.

Models implementing sliding control have been already developed in recent years for different infections, such as West Nile Virus [316], avian influenza [85, 86], and SARS [315]. Here, we found that localized culling implemented in one of the patches may lead to an unexpected increase in the number of infected individuals in the other patch. In the case of continuous model (2.1)–(2.2), we provided the necessary conditions for this counter–intuitive outcome to occur (see Theorem 2.7). In details, the equilibrium value of infected individuals $\hat{I}_2$ in presence of proactive culling can increase only if $2D < r$ (hosts are very infrequent dispersers) and $\mathcal{R}_0 > 2$, namely if the basic reproduction number of the corresponding uncontrolled model is at least twice the endemicity threshold. In addition, we numerically found that the number of infected individuals in the uncontrolled patch eventually peaks for intermediate values of culling and then decreases only for high level of culling effort (see Fig. 2.3). Conversely, in sliding model (2.1)–(2.3), we numerically found that, for intermediate levels of disease detection, localized reactive culling increases the infection burden in the uncontrolled patch regardless of the culling effort applied in the disease control (see Figs. 2.4 and 2.6B).

The biological explanation for this unexpected effect relies on the remark that, when the dispersal rate (D) is low, the introduction of culling induces an increase in the number of susceptible individuals in both the controlled and uncontrolled patches (see Theorem 2.7 and Proposition 2.8). This leads to a flush of new susceptibles entering the uncontrolled

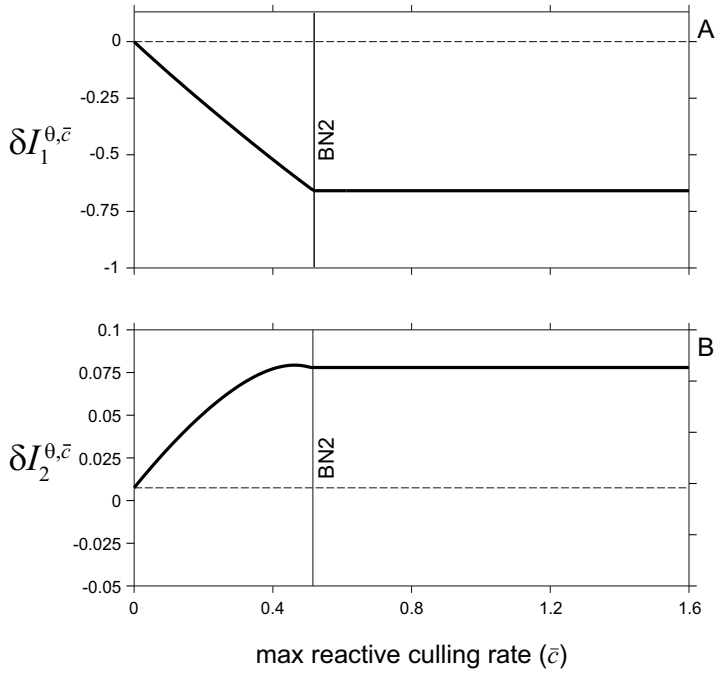

Figure 2.6: Relative variation of the number of infected individuals in patches 1 (panel A) and 2 (panel B) at model (2.1)–(2.3) steady–state with respect to the number of infected in the absence of control ($\delta I_j^{\theta,\bar{c}}$, with $j = 1, 2$) as a function of parameter $\bar{c}$. BN2 represents a boundary–node bifurcation point as in Fig. 2.4. The dashed line represents the condition $I_j^{\theta,\bar{c}} = \bar{I}$. Parameter $\theta = 15$, unspecified parameters as in Fig. 2.4.

patch, then providing a bust to the infection transmission. We have proved the generality of this result by showing that it does not depend on the specific assumptions made in model (2.1), but it holds also relaxing the hypotheses of disease–induced host sterility and density–dependent mortality in the infection model (see Remark 2.9).

The epidemiological and economic conditions leading to the ineffectiveness of disease control through culling have also been investigated in optimal control frameworks. Bolzoni *et al.* [39] showed that reactive culling implemented around the peak of infection represents an optimal control strategy only when the basic reproduction number of the infection is low and the costs of control are high.

In conclusion, this study shows that also in the absence of the density–dependent compensatory effects – which were previously associated to disease control failure –, localized culling may represent an ineffective strategy in limiting infectious diseases in wildlife.

Chapter 3

Optimal vaccine awareness campaigns in presence of volatile opinions

In the remaining part of the thesis we focus on infectious diseases in human populations, and we add to classical epidemic models and relevant control problems a key factor: the modelling of opinions of individuals and their effects on the propensity to adopt protective measures.

In modern societies the main sources of information are Internet–based social networks. Thus, the opinion of citizens on key topics, such as vaccines, is very volatile. In this chapter, we explore the impact of volatility on the modeling of public response to vaccine awareness campaigns (VACs) for favouring vaccine uptake. We apply a quasi–steady–state approximation to the model of the spread and control via VACs of SIR diseases proposed in [112]. This allows us to infer and analyze a new behavioral epidemiology model that is nonlinear in the control. Then, we investigate the efficient design of VACs by adopting optimal control theory.

The resulting problem has important issues: 1) the integrand of its objective functional is non–convex; 2) the application of *forward–backward sweep* [201] and *gradient descent* [13] algorithms in some key cases does not work; 3) analytical approaches provide continuous solutions that cannot rigorously be implemented since public health interventions cannot be fully flexible. Thus, we resort to direct optimization of the objective functional via heuristic stochastic optimization, in particular via *particle swarm optimization* [184] and *differential evolution* [271] algorithms.

Finally, since the optimization algorithms are stochastic, we provide a statistical assessment of the obtained solutions.

This study was conceived and carried out during a two months scientific visit in 2019 at the International Prevention Research Institute in Lyon (France), under the supervision of Dr. A. d'Onofrio. The results have been published in [97].

3.1 Background

A major challenge for global public health (PH) is the spread of hesitancy and refusal of vaccines to prevent childhood diseases. This is due to the phenomenon of 'pseudo–rational' exemption to vaccination: parents overweight real and imaginary side effects of vaccines and underweight real risks due to the target infectious diseases. To mitigate the impact of this challenge, the public health systems (PHSs) may counteract by means of public campaigns to favor vaccine uptake.

These scenarios make it increasingly important a new approach to modeling the spread and control of infectious diseases, by including in the modeling the description of human decision making. In particular, the complex dynamics of vaccine decision has been modeled as an *imitation game* [21, 111] or, equivalently, as an infection of ideas process [293] (see also Section I.4). The approach introduced in [21, 111] was suitably modified by d'Onofrio *et al.* [112] in order to take into the account the actions enacted by PHS to favor vaccination. In papers [21, 111, 112] the analytical and numerical investigations were focused on scenarios where citizens slowly change their opinion. This assumption, however, in the age of social media is increasingly questionable. Nowadays, the opinion form is based on information and rumors collected and exchanged on Internet–based social media such as Facebook, Twitter, Instagram, etc, and, at the micro–scale of small chat groups, WhatsApp, Snapchat and Facebook Messenger. This impressive *exponential growth in public opinion channels* [181] makes the opinion of population much more volatile than in

the past on many sensitive subjects [7], including politics [7, 178] and vaccines [53, 231]. Such a radical change of scenario must be taken into the account in the models of behavioral epidemiology of infectious diseases.

We are here particularly interested in the optimal design of vaccine awareness campaigns (VACs) in the current context of extremely volatile opinion among the population targeted by these campaigns by applying optimal control (OC) theory. As already seen in previous chapters, OC theory [127, 240] is a classical tool applied in mathematical epidemiology of infectious diseases (see Section I.2). However, the adoption of an optimal control strategy, given an health economy objective and appropriate constraints, posits some remarkable problems. The first one is common to a number of other problems in numerical analysis: the chosen numerical algorithms could lack convergence due to stiffness of the mathematical model or to complex chaotic behaviors induced by the recursive nature of the adopted algorithms. Sensitivity to initial conditions could make impossible to numerically solve a problem. The second one is that the solution of the optimal control problem via the maximum principle by Pontryagin is a continuous function of time which requires a continuous adaptation of the PH intervention. Unfortunately, in most case a PHS is not endowed for practical reasons such a large degree of flexibility. The third problem is that, once obtained the optimal solution for the control (say, $u(t)$), one has no indication of the degree of robustness of this solution. Due to the above–mentioned low degree of flexibility of the PHS action, it would be desirable to have an idea of how much a given OC solution is flexible to deviations. The fourth problem is also extremely relevant: it may happen that for the OC problem in study the requirements of classical existence theorems are not satisfied. One cannot say to PH officers that the problem cannot be investigated for lack of appropriate theorems.

The first problem was first faced in behavioral epidemiology by Buonomo *et al.* [65], whose solution led to consider, in part, the second one. On the contrary, the other two are specific to this study. Namely, in [65] the lack of convergence of some well known OC algorithms aimed at the solution of the Pontryagin differential–algebraic constrained system [240], led the authors to consider the application of a direct optimization strategy. It was adopted the oldest algorithm of stochastic heuristic optimization, the *simulated annealing* [43]. This led to consider OC strategies that are piecewise–constant. This was needed for numerical analysis but was at the same time a first contribute to finding realistic OC strategies more adapt to the reality of not so flexible PH interventions.

We propose here some important novelties with respect to the paper [65]. We adopt two more recent and robust heuristic optimization algorithms [43]: the particle swarm optimization [43, 184] and the differential evolution [43, 244, 272]. We select these two great popular methods not for comparing their efficiency or performances, but just to have a double check of the results. The direct optimization results allow us to better evaluate the robustness of the OC solution to temporary perturbations of large amplitude. As far as the degree of flexibility of the VACs is concerned, we propose a more advanced analysis with respect to [65]. Indeed, we consider three strategies of intervention: with 3–months changes, with annual changes and with biennial changes. Concerning the last problem, the OC problem in study is characterized by an objective functional whose integrand is non–convex w.r.t. $u(t)$. Moreover, at variance with many studies, in the proposed model the dependence on the control is nonlinear.

3.2 Model formulation

The starting framework

Let us consider the SIR–like model describing the dynamics of a vaccine–preventable childhood disease under voluntary vaccination choices introduced in [111, 112]:

$$\begin{aligned} \dot{S} &= \mu(1 - p(t)) - \beta SI - \mu S \\ \dot{I} &= \beta SI - (\gamma + \mu)I, \end{aligned} \tag{3.1}$$

where S and I denote the fraction of susceptible and infected individuals w.r.t. the total population at time t, respectively; the time–dependent variable p models the vaccine uptake of newborns. The other parameters are positive constants: i) birth and mortality rates are equal to a value μ (implying a stationary population); ii) β is the transmission rate; iii) γ is the recovery rate.

To model the impact of human responses to both the spread of the disease and vaccine adverse events on the dynamics of vaccine propensity p, we follow [21, 111, 112] and assume that there exist two interacting vaccine–related strategies among the (interacting) individuals: 'pro–vaccine' and 'anti–vaccine'. We denote by p and $A = 1 - p$ the fractions of the two above groups at time t. As anticipated in Section I.4, the basic idea is that the dynamics of p and A are ruled by a 'double contagion' of ideas between the two involved groups. This approach yields the following family of models:

$$\begin{aligned} \dot{p} &= k\theta(I)pA - k\alpha(M_{se})Ap \\ \dot{A} &= -k\theta(I)pA + k\alpha(M_{se})Ap, \end{aligned}$$

where: i) the 'force of infection' concerning the switch from the strategy 'no–vaccinator' to the strategy 'vaccinator' is $k\theta(I)p$, where $\theta(I)$ is an increasing function of prevalence of the disease; ii) the 'force of infection' concerning the switch from the strategy 'vaccinator' to the strategy 'no–vaccinator' is $k\alpha(M_{se})A$ where $M_{se}(t)$ is an information variable on the extent of vaccine–related side effects (VSEs); iii) the parameter k, although not strictly necessary, is a time scale tuning parameter. Its role here is similar to the role of the parameter k in the Glauber model of the mean–field kinetic of phase transitions of the Ising model [142]: it characterizes the time scale of the velocity of opinion switching for the parents population.

The action of the PHS to favor the vaccine uptake is simply modeled as an additional switch from the strategy 'no vaccine' to the strategy 'vaccine'. This yields the model [293]

$$\begin{aligned} \dot{p} &= k\theta(I)pA - k\alpha(M_{se})Ap + ku(t)A \\ \dot{A} &= -k\theta(I)pA + k\alpha(M_{se})Ap - ku(t)A. \end{aligned}$$

The function $ku(t)$ represents the rate of switching from the strategy 'no vaccine' to the strategy 'vaccine' induced by the campaigns enacted by the public health system to increase the vaccine propensity. Taking into the account that $A = 1 - p$ yields the following model:

$$\dot{p} = kp(1 - p)(\theta(I) - \alpha(M_{se})) + ku(t)(1 - p),$$

originally proposed in [112] by an economy–oriented game–theoretic approach. In the following we will focus on the case of linear $\alpha(M_{se})$, with M_{se} proportional to the vaccine

uptake of newborns p, yielding (with slight abuse of notation) $\alpha(M_{se}) = \alpha p$. Hence, the equation for p reads

$$\dot{p} = kp(1-p)(\theta(I) - \alpha p) + ku(t)(1-p). \tag{3.2}$$

In case of constant $u(t) = u = const.$ studied in [112], it was shown that public intervention has a stabilising role to reduce the strength of imitation–induced oscillations, and if $u > \alpha p_c^2$ (with p_c given in (3.7)), it allows disease elimination by making the disease–free equilibrium where everyone is vaccinated globally attractive. The cases of periodic $u(t)$ (corresponding to the alternate work–holidays terms) and of periodic contact rate were investigated, respectively, in [57] and in [56].

The current scenario

To model the current scenario of volatile opinion switching, we assume that the imitation speed, tuned by the parameter k, is very rapid: $k \gg 1$. Thus, a *quasi–steady–state approximation* [202] for p can be used in (3.2), which yields:

$$p(1-p)(\theta(I) - \alpha p) + u(t)(1-p) = \frac{\dot{p}}{k} \approx 0.$$

As a consequence, in the limit $k \to +\infty$, p is the solution of the following algebraic equation:

$$0 = (1-p)(u(t) + \theta(I)p - \alpha p^2) \tag{3.3}$$

to be solved under the constraint:

$$0 \leq p \leq 1. \tag{3.4}$$

Equation (3.3) with condition (3.4) has two solutions: $p = 1$; and the unique positive solution of

$$u(t) + \theta(I)p - \alpha p^2 = 0.$$

Summarizing:

$$p = \zeta(I, u(t)) = \min\left(1, \frac{\theta(I) + \sqrt{\theta^2(I) + 4\alpha u(t)}}{2\alpha}\right). \tag{3.5}$$

Thus, model (3.1)–(3.2) reduces to the following bidimensional model:

$$\dot{S} = \mu(1 - \zeta(I, u(t))) - \beta SI - \mu S \tag{3.6a}$$

$$\dot{I} = \beta SI - (\gamma + \mu)I, \tag{3.6b}$$

with ζ given in (3.5). Model (3.6), from the control theory viewpoint [88, 213], is a nonlinear controlled model

$$\dot{x}(t) = F(x(t), u(t))$$

where $x = (S, I)$ and F nonlinearly depends on the enacted control:

$$F(x, u(t)) \neq a(x)u(t) + b(x),$$

for given $a(\cdot)$, $b(\cdot)$, i.e. $F(x, u(t))$ is not a linear–affine function of $u(t)$. Note that the original system proposed in [56, 57, 112, 293] was, instead, linearly dependent on $u(t)$.

More precisely, we may say that in this section we will deal with open–loop control of (3.6). Later on we will focus on one of the most important, especially for the health economy viewpoint, form of feedback control, i.e. optimal control [240].

In the important case of constant control $u(t) = u = const.$, model (3.6) belongs to the class of models proposed and investigated in [113], where the equation for S reads as follows

$$\dot{S} = \mu(1 - p_0 - p_1(I)) - \beta SI - \mu S.$$

Here, the baseline vaccination rate p_0, which is independent on the information received concerning the disease and the side effects of the vaccine, has a fundamental role. Indeed, in [113] it was shown that, by denoting with $\mathcal{R}_0 = \beta/(\gamma + \mu)$ the SIR basic reproduction number (see Section I.1), if

$$p_0 > p_c = 1 - \frac{1}{\mathcal{R}_0}, \tag{3.7}$$

then the disease elimination is possible; if $p_0 < p_c$, instead, the disease–free equilibrium is unstable and an endemic equilibrium onsets. Note that p_c is the May Anderson elimination threshold in presence of mandatory vaccination (see [47, 214]). It is clear that in absence of a PH intervention a typical target population is unlikely to be characterized by a p_0 larger than the elimination threshold in presence of mandatory vaccine.

Here the baseline behavior–independent vaccination rate p_0 introduced in [113] is better explained. Indeed, it is equal to

$$p_0 = \zeta(0, u),$$

i.e. $p_0 = p_0(u)$ is an increasing function of u. Thus, an appropriately intense VACs might induce the disease elimination provided that

$$p_0(u) > 1 - \frac{1}{\mathcal{R}_0},$$

i.e.

$$u > p_0^{-1}(p_c). \tag{3.8}$$

From the control theory viewpoint, we may say that if (3.8) holds, then the open–loop constant control globally stabilizes the disease–free equilibrium (DFE).

In the case where the open–loop control $u(t)$ is not constant, but $u_{min} \leq u(t) \leq u_{max}$, with $u_{min} < u_{max} < +\infty$, we get straightforwardly that: i) if

$$p_0(u_{min}) > 1 - \frac{1}{\mathcal{R}_0},$$

then the DFE is globally attractive; ii) if

$$p_0(u_{max}) < 1 - \frac{1}{\mathcal{R}_0},$$

then the DFE is unstable.

An interesting special case is when $u(t)$ is periodic, which mimics the alternance of the work and holidays terms in the PH interventions. Namely, it is easy to show that, denoting as $Y_\infty(t)$ the periodic solution of

$$\dot{Y} = \mu(1 - \zeta(0, u(t)) - Y),$$

it holds that if

$$\mathcal{R}_0 \frac{1}{T} \int_0^T Y_\infty(t)dt < 1,$$

i.e. if

$$SC = \mathcal{R}_0 \left(1 - \frac{1}{T}\int_0^T \zeta(0, u(t))dt\right) < 1, \tag{3.9}$$

then the disease–free solution is globally attractive, whereas if $SC > 1$, with SC given in (3.9), then it is unstable.

Let us consider the case where $u(t)$ assumes periodically only two values in $[0, T]$:

$$u(t) = \begin{cases} u_1 & \text{if } 0 \leq t \leq T_1 \\ u_2 & \text{if } T_1 < t \leq T \end{cases}$$

This scenario mimics in the most schematic case a lower pressure of PHS during, for example, a single period of holidays. In such a case the elimination condition becomes

$$\zeta(0, u_1)\frac{T_1}{T} + \zeta(0, u_2)\left(1 - \frac{T_1}{T}\right) > 1 - \frac{1}{\mathcal{R}_0}. \tag{3.10}$$

It is easy to show that constraint (3.10) holds also in case of a more complex pattern of alternance between the two values u_1 and u_2, for example due to multiple holidays terms.

3.3 The optimal control problem

In the previous sections, we illustrated as the proposed ODEs model (3.6) can be seen, in its general case, as an 'open–loop' controlled system. As it is well known, whenever possible, it is preferable to control a system by means of feedback–based strategy [88, 213]. In health economy, probably the most important form of feedback–based control is optimal control, which is aimed at minimizing the economic and human burden of some health related phenomena [137].

As a consequence, in this section we start investigating which are the implications of the current age of fast opinion switching on the determination of the optimal time profile for the VACs, summarized in the control variable $u(t)$, so that the overall costs are minimized. These costs include the following three components [61, 65]: i) the costs due to the disease

$$J_d = K_d \int_0^T N\beta SIdt;$$

ii) the costs due to the vaccination and its (although rare) side effects

$$J_v = K_v \int_0^T N\mu\zeta(I, u(t))dt;$$

and iii) the costs of enacting VACs, J_u.

As far as the last cost is concerned, reminding that the flux of subjects switching from the strategy 'no vaccine' to the strategy 'vaccine' is $ku(t)A$, we may express it as

$$J_u = \int_0^T \frac{C_u}{k}\rho(u(t), A)ku(t)Adt.$$

Here the critical assumption is that, since the opinion switching rate is very fast, then the cost to make a person switches from 'NO' to 'YES' is accordingly low and of order $1/k$. The

inverse proportionality w.r.t. k implies that the population–wide global cost is neither null nor infinite. Finally, as in [65], we assume $\rho = u(t)/A$ leading to

$$J_u = \int_0^T C_u u^2(t) dt.$$

It is of interest to stress that the quadratic dependence of this cost component w.r.t. the control $u(t)$ is not decided *a priori*, i.e. based on mathematical convenience, but based on reasoning on the phenomenon in study.

In sum, we are looking for the optimal control function $u^*(t)$ that minimizes the objective functional

$$J\left(u(t)\right) = \int_0^T \left(C_d SI + C_v \zeta(I, u(t)) + C_u u^2(t)\right) dt, \tag{3.11}$$

where $C_d = K_d \beta N$, $C_v = K_v \mu N$, on the admissible set for the control $u(t)$

$$\Omega = \left\{ u(t) \in L^1\left(0, T\right),\, u_{min} \leq u(t) \leq u_{max} \right\}.$$

Candidate optimal controls

According to Pontryagin maximum principle (MP), if an optimal solution exists, then the optimal control $u^*(t)$ minimizes the *Hamiltonian* function pointwise w.r.t. the control [240]. Here, the Hamiltonian H reads:

$$\begin{aligned} H = \;& C_d SI + C_v \zeta(I, u(t)) + C_u u^2(t) + \\ & + \lambda_1 \left[\mu \left(1 - \zeta(I, u(t))\right) - \mu S - \beta SI\right] + \\ & + \lambda_2 \left[\beta SI - (\mu + \gamma) I\right] \end{aligned} \tag{3.12}$$

where $\lambda = (\lambda_1, \lambda_2)$ is the solution vector of the adjoint system

$$\dot{\lambda}_1 = -C_d I + (\lambda_1 - \lambda_2)\beta I + \mu \lambda_1$$

$$\dot{\lambda}_2 = \begin{cases} -C_d S + (\lambda_1 - \lambda_2)\beta S + \lambda_2 (\mu + \gamma) + W & \text{if } f(I, u(t)) < 1 \\ -C_d S + (\lambda_1 - \lambda_2)\beta S + \lambda_2 (\mu + \gamma) & \text{if } f(I, u(t)) \geq 1 \end{cases}$$

with

$$W = \frac{\lambda_1 \mu - C_v}{2\alpha} \partial_I \theta(I) \left(1 + \frac{\theta(I)}{\sqrt{\theta^2(I) + 4\alpha u(t)}}\right),$$

and transversality conditions

$$\lambda(T) = 0.$$

The existence of the solution for our OC problem is not provided by classical existence theorems [6, 127, 189, 201, 262], whose requirements are not satisfied here. In particular, it is not guaranteed that the velocity sets

$$F_u(S, I) = \{F(S, I, u(t)) |\, u(t) \in [u_{min}, u_{max}]\},$$

where F is the r.h.s. of (3.6), are convex for every (S, I). Hence, there is no analytical evidence (to the best of our knowledge) that the derivation of the constrained minimum point of H at each time instant t can provide us the 'true' minimizing control. Nonetheless, the $u(t)$ obtained by applying the interpolation procedure can be considered at least a useful starting point for numerical computations. In other words, we can call it a *candidate* optimal control.

In order to derive the minimum point of H at each time instant t, we must distinguish the following three cases:

- If $\theta(I) \geq \alpha$, then $f(I, u(t)) \geq 1$ and H is increasing w.r.t. $u(t)$. Hence,

$$u^*(t) = u_{min}. \tag{3.13}$$

- If $\theta(I) < \alpha$ and $C_v - \lambda_1 \mu \geq 0$, then

$$\partial_u H = \begin{cases} 2C_u u(t) + (C_v - \lambda_1 \mu) \dfrac{1}{\sqrt{\theta^2(I) + 4\alpha u(t)}} & \text{if } u(t) < \alpha - \theta(I) \\ 2C_u u(t) & \text{if } u(t) \geq \alpha - \theta(I) \end{cases} \tag{3.14}$$

  namely, H is increasing w.r.t. $u(t)$ and also for such instants the (3.13) holds.

- If $\theta(I) < \alpha$ and $C_v - \lambda_1 \mu < 0$, then from (3.14) it follows that H is an increasing function of $u(t)$ in the time interval when $u(t) \geq \alpha - \theta(I)$. Otherwise, if $u(t) < \alpha - \theta(I)$, H can still be increasing or have a minimum point, that is the unique solution of:

$$2C_u u(t) \sqrt{\theta^2(I) + 4\alpha u(t)} = \lambda_1 \mu - C_v \tag{3.15}$$

  namely, the intersection point of an increasing function of $u(t)$ (the l.h.s. of (3.15)) and a constant function (the r.h.s. of (3.15)). Note that the (3.15) is equivalent to the cubic equation:

$$4\alpha u^3(t) + \theta^2(I) u^2(t) - \left(\frac{\lambda_1 \mu - C_v}{2C_u} \right)^2 = 0.$$

  Denote with $\tilde{u}(t)$ the solution of (3.15), then

$$u^*(t) = \begin{cases} \min\left(\max\left(u_{min}, \tilde{u}(t)\right), u_{max}\right) & \text{if } \tilde{u}(t) < \alpha - \theta(I) \\ \min\left(\max\left(u_{min}, \alpha - \theta(I)\right), u_{max}\right) & \text{if } \tilde{u}(t) \geq \alpha - \theta(I) \end{cases}$$

Summarizing, we may say that the above procedure provides us with the following candidate optimal control:

$$u^*(t) = \begin{cases} u_{min} & \text{if } \theta(I) \geq \alpha \text{ or } (\theta(I) < \alpha \text{ and } C_v - \lambda_1 \mu \geq 0) \\ \min\left(\max\left(u_{min}, \tilde{u}(t)\right), u_{max}\right) & \text{if } \theta(I) < \alpha \text{ and } C_v - \lambda_1 \mu < 0 \text{ and } \tilde{u}(t) < \alpha - \theta(I) \\ \min\left(\max\left(u_{min}, \alpha - \theta(I)\right), u_{max}\right) & \text{if } \theta(I) < \alpha \text{ and } C_v - \lambda_1 \mu < 0 \text{ and } \tilde{u}(t) \geq \alpha - \theta(I) \end{cases}$$

For convenience of notation, in the following we will omit the use of superscript * for the optimal control function.

3.4 Parameterization and simulation scenarios

In order to make comparisons with the 'slower' imitation speed model, studied in [65], we choose the same parameter values, that are listed and described in Table 3.1, and assume

$$\theta(I) = \theta_0 + \theta_1 I,$$

with θ_0 and θ_1 non–negative constants. In particular, we consider five possible simulation scenarios that differ for the combination of the rate of perceived risk of infection θ_1 and the maximum intervention level u_{max} and should capture all the relevant situations:

Parameter	Description	Baseline value
μ	Natural birth/death rate	$1/50$ years^{-1}
γ	Recovery rate	$1/10$ days^{-1}
$\mathcal{R}_0$	Basic reproduction number	10
β	Transmission rate	$\mathcal{R}_0(\gamma+\mu)$
p_c	Critical immunization threshold	$1-1/\mathcal{R}_0$
ε	Emigration/immigration flux	$2.86\cdot10^{-8}$ days^{-1}
α	Rate of perceived risk of vaccine side effects	1 days^{-1}
θ_0	Minimum perceived risk of infection	0 days^{-1}
θ_1	Rate of perceived risk of infection	450–4000 days^{-1}
N	Total population	$6\cdot10^7$
T	Length of the planning horizon	10 years
u_{min}	Minimum rate of efforts into awareness campaigns	0 days^{-1}
u_{max}	Maximum rate of efforts into awareness campaigns	$0.5\alpha p_c^2-0.7\alpha p_c^2$
K_d	Average unit cost per infected case	307 USD
K_v	Average unit cost of vaccination	21.08 USD
C_d	Total cost of infection	$K_d\beta N$
C_v	Total cost for vaccination	$K_v\mu N$
$C_u^{(o)}$	Cost for implementation of awareness campaigns	$N\mu K_v/(\alpha^2p_c^3)$

Table 3.1: Epidemiological, behavioral and control–related parameters values.

C1 $(\theta_1,\, u_{max}) = (2000 \text{ days}^{-1},\, 0.7\alpha p_c^2)$, corresponding to a large perceived relative risk of infection and a high level of intervention;

C2 $(\theta_1,\, u_{max}) = (450 \text{ days}^{-1},\, 0.5\alpha p_c^2)$, corresponding to intermediate perceived relative risk of infection and level of intervention;

C3 $(\theta_1,\, u_{max}) = (450 \text{ days}^{-1},\, 0.7\alpha p_c^2)$, corresponding to an intermediate perceived relative risk of infection and a high level of intervention;

C4 $(\theta_1,\, u_{max}) = (4000 \text{ days}^{-1},\, 0.5\alpha p_c^2)$, corresponding to a very large perceived relative risk of infection and an intermediate level of intervention;

C5 $(\theta_1,\, u_{max}) = (4000 \text{ days}^{-1},\, 0.7\alpha p_c^2)$, corresponding to a very large perceived relative risk of infection and a high level of intervention.

Remind that in the 'slower' imitation speed model with $u(t) = u = const.$ the threshold $u = \alpha p_c^2$ would ensure elimination [65].

As in [21,61,65], we also include a small immigration/emigration constant flux ε to take into account the immigration of infected individuals during inter–epidemic periods. Precisely, a positive influx $+\varepsilon$ is added to the equation (3.6b), balanced by a negative term $-\varepsilon$ in the equation (3.6a). Clearly, this constant influx term must be taken into account also in (3.12).

As far as the optimal control is concerned, the most specific parameter is C_u, because it defines the weight of the communication strategy cost w.r.t. the other costs. We will use two values: a baseline value $C_u = C_u^{(o)}$ and a larger value $C_u = 5C_u^{(o)}$. The latter is a test case which is employed to assess how the control changes in the case of substantially larger costs for the public health campaigns aimed at increasing the propensity to vaccinate.

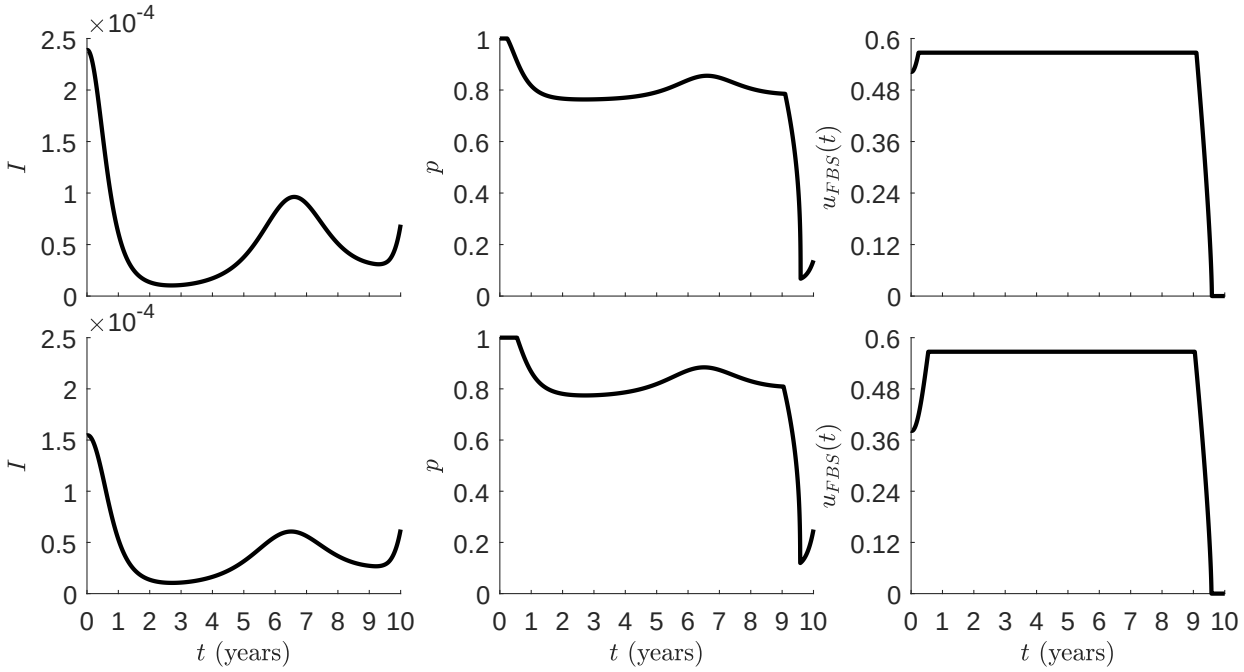

Figure 3.1: OC solutions by FBS method for the simulation scenarios C1 (top row) and C5 (bottom row). Left panels: I; central panels: p; right panels: $u_{FBS}(t)$. Initial data as in [65], that is: $S(0) = 0.0999972$, $I(0) = 2.3878 \cdot 10^{-4}$ for the case C1; the endemic equilibrium of model (3.6) with $u(t) \equiv 0$ for the case C5. Other parameter values are listed in Table 3.1.

3.5 Numerical results

Optimal solutions by indirect methods

In mathematical biology, the two most adopted numerical algorithms for the numerical OC solution are the forward–backward sweep (FBS) method [201] and the gradient descent or steepest descent (Grad) method [13] (which can also be employed for the OC of spatio–temporal models [173]). Their interest lies on the fact that: i) both of them are based on the Pontryagin's Hamiltonian, and – as such – they aim to numerically solve the Pontryagin's differential–algebraic boundary value problems [240]; ii) they are recursive algorithms, thus they are easy to be implemented and do not require the use of special type libraries, at variance with numerical methods to solve boundary value problems such as the multiple *shooting method* [232]. Note that the point (i) implies that both the FBS and the Grad methods fully take advantage of the analytical results of OC theory, which is very appreciable.

As mentioned above, for our control problem one has no guarantee that Pontryagin necessary conditions of optimality are also sufficient. However, the above algorithms can be used as well. Thus, we numerically investigate our OC problem 'as if' the optimality sufficient conditions would hold. As far as the OC problem is concerned, we employ the public domain routines for the FBS and for the gradient method provided, respectively, by [201] and by [13] for the MATLAB environment [216]. As far as the numerical resolution of the differential equations are concerned, we employ the fourth–order Runge–Kutta method with constant step size, as in [201].

We observe that for $C_u = C_u^{(o)} = N\mu K_v/(\alpha^2 p_c^3)$ both the above–mentioned algorithms converge to numerical solutions whose difference is very small. This suggests that – in the

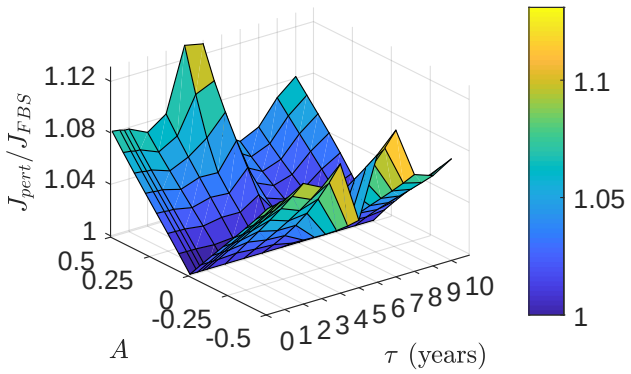

Figure 3.2: J_{pert}/J_{FBS} as function of A and τ for the simulation scenario C4. Initial data: endemic equilibrium of model (3.6) for $u(t) \equiv 0$. Other parameter values are listed in Table 3.1.

numerical cases we analyze – the 'candidate' optimal control is in reality the optimal control. On the contrary, for $C_u = 5C_u^{(o)}$ both algorithms are not able to converge in all the scenarios we considered.

The case $C_u = C_u^{(o)}$ is numerically summarized in Table 3.2, where FBS method is used as reference and the corresponding quantities are labelled with subscript $_{FBS}$. Moreover, panels in Fig. 3.1 show the OC solutions, obtained by means of the FBS algorithm [201], for different combinations of θ_1 and u_{max}, which correspond to the cases C1 (top panels) and C5 (bottom panels) (for the other cases see [97]). The results are quite similar to those of [65], but here the optimal control has an initial increasing behavior, especially in case C5.

Robustness to periodic perturbations As it is well known, the MP does not ensure that the control function obtained by applying it is an actual global minimum. Thus, in order to validate the global optimality of the candidate solution yielded by the Pontryagin principle, we first consider a very simple heuristic approach. The approach consists in assessing the robustness of the candidate optimal control $u_{FBS}(t)$ (numerically obtained by the FBS method) to sinusoidal perturbations of various amplitudes and periods:

$$u_{pert}(t) = \min\left(\max\left(u_{min}, u_{FBS}(t)\left(1 + A\sin\left(\frac{2\pi}{\tau}t\right)\right)\right), u_{max}\right), \tag{3.16}$$

with $A \in [-1/2, 1/2]$ and $\tau \in [0, 10]$ years. Numerical results are displayed in Fig. 3.2 for the case C4 and in [97] for the other cases. We report the values of

$$J_{pert} = J(u_{pert}(\cdot))$$

normalized w.r.t. $J_{FBS} = J(u_{FBS}(\cdot))$, as function of the amplitude A and the period τ. As one can notice, in all cases it is

$$J(u_{pert}(\cdot)) > J(u_{FBS}(t)),$$

suggesting that the algorithm might have found a global optimum.

Optimal solutions by direct methods

As we mentioned in the previous section, in the cases where $C_u = 5C_u^{(o)}$ both FBS and Grad algorithms incur in problems of convergence. The FBS and the gradient descent method

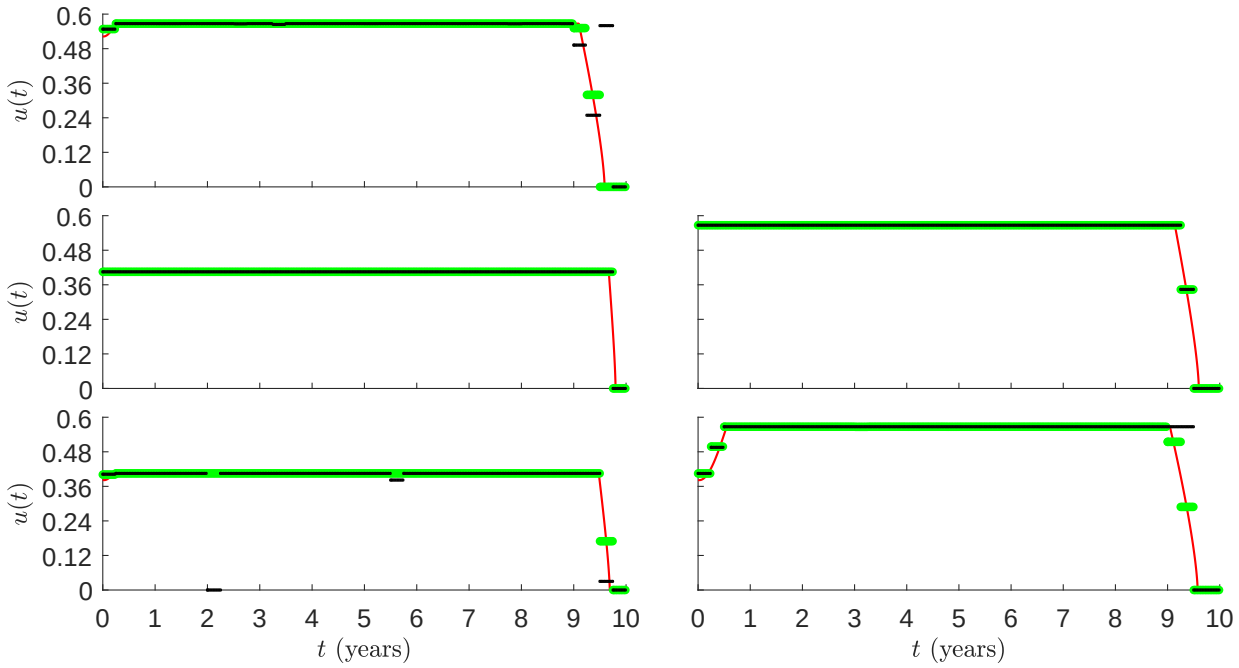

Figure 3.3: Case $C_u = C_u^{(o)}$: OC function $u(t)$ by FBS method (red lines) and one iteration of PSO (green lines) and DE (black lines) algorithms. Left panels, from the top to bottom: cases C1, C3 and C5, respectively. Right panels, from the top to bottom: cases C2 and C4, respectively. Initial data as in [65], that is: $S(0) = 0.0999972$, $I(0) = 2.3878 \cdot 10^{-4}$ for the case C1; the endemic equilibrium of model (3.6) with $u(t) \equiv 0$ for the other cases. Other parameter values are listed in Table 3.1.

belong, similarly to the single and multiple shooting methods [232], to the class of indirect methods. In other words, they are based on the Pontryagin Hamiltonian, i.e. they take advantage of the available variational solution of the OC problem expressed as a boundary value problem for a differential–algebraic system.

In OC theory and applications, however, many deterministic algorithms based on the direct optimization of the OC problem are available [119, 145, 292]. Note that often a relationship between direct methods and the solution of the Pontryagin differential–algebraic system can be shown, as in [133]. However, similarly to FBS and the Grad algorithms, the deterministic direct optimization approach does not guarantee that the found solution actually corresponds to a genuine global minimum.

Thus, in order to solve our OC problem in the cases where $C_u = 5C_u^{(o)}$, we recur to direct optimization by applying two stochastic heuristic optimization algorithms (HOAs). These algorithms are conceived to directly solve general optimization problems and, as such, they are not limited to OC applications.

A major difference between the heuristic optimization algorithms and the OC algorithms is that the first ones are aimed to finite–dimensional problem, the second ones to infinite–dimensional problems. However, the latter any case operate a discretization of the OC problems, i.e. the reduction to a finite dimensional space, although of 'large' dimension due to the small time step usually adopted. Another difference w.r.t. both the FBS and the Grad methods as well as other direct optimization algorithms used in OC is that the heuristic optimization algorithms we have chosen are stochastic. It is the stochasticity that allows to significantly increase the probability that the minimum they find is a global minimum and

not a local one. We will return later on some important implications of the stochasticity of these algorithms. Thus, even for $C_u = C_u^{(o)}$, we apply the HOAs to further validate the results obtained by applying the FBS and the Grad.

When using heuristic approaches one has to transform the initial infinite–dimensional approach in a finite dimensional problem. This, however, is not a heavy constraint for the OC problem to be solved. Indeed: i) even the OC–specific algorithms operate a discretization, i.e. also they are finite dimensional; ii) in the light of the lack of flexibility of PH intervention, this assumption provides OC solutions that are more realistic. In other words, 'real world' campaigns cannot be updated continuously in time, thus a piecewise–constant $u(t)$ is more realistic than a continuous control. Namely, we assume that the communication campaigns enacted by the PHS are updated every three months, i.e. at each new season. This implies, 40 discretization points for the whole control horizon $[0, 10]$ years, and, of course, that the $u(t)$ is a piecewise–constant function.

As far as the global optimization algorithms are concerned, we employ the following two widely diffused algorithms:

- Particle swarm optimization (PSO). This algorithm was originally described in Kennedy and Eberhart [184]. Recent versions include subsequent modifications suggested in [219, 236]. We use the `particleswarm` solver included in the *Global Optimization Toolbox* of MATLAB [216]. We employ the default option values, except for the termination tolerance on the function value (`FunctionTolerance`) and the maximum number of iterations allowed (`MaxIterations`), that we set to 10^{-5} and 200, respectively. The PSO algorithm is based on the concept of swarm intelligence, i.e. the emergent 'pseudo–intelligent' behavior emerging at the collective level in swarms of individuals that follow simple laws of interactions between them and the surrounding environment [184, 219, 236].

- Differential evolution (DE). It was first proposed in [271] and subsequently improved in [272]. We use the algorithm described in [244] and implement the MATLAB code provided by the authors of that book [243]. We employ the default algorithm options, except for the number of population members (I_NP) and the maximum number of generations until optimization stops (I_itermax), that are set to 50 and 800, respectively.

For a description of the above algorithms and further details, please refer to [43]. Our aim here is not to compare their performances, but comparative studies are given in [81, 94, 290]. The choice of PSO and DE algorithms is motivated by their great popularity within the domain of machine intelligence and cybernetic. Both algorithms do not need any gradient information of the function to be optimized, are conceptually very simple and they require minimal parameter tuning [43, 94].

As far as the case $C_u = C_u^{(o)}$ is concerned, for each combination of θ_1 and u_{max} considered, we compare both qualitatively (Fig. 3.3) and quantitatively (Table 3.2) the outputs of the PSO and of the DE algorithms w.r.t. the output of the FBS method. Both DE and PSO algorithms provide optimal controls that are on the whole very close to the ones provided by the FBS method (in turn very close to the ones obtained by the Grad method). However, the output of DE algorithm has sometime large local deviations. This suggests that some degree of flexibility in the implementation of the control does not dramatically change the results. Graphics and data values suggest that, for the specific problem at hand, the PSO algorithm performs slightly better than the DE algorithm.

Case	Method	$\frac{\|\|u(t)-u_{FBS}(t)\|\|_1}{\|\|u_{FBS}(t)\|\|_1}$	J (USD)	$\frac{J-J_{FBS}}{J_{FBS}}$	J_u (USD)	$\frac{J_u-J_{u,FBS}}{J_{u,FBS}}$
C1	FBS	0	$6.51 \cdot 10^8$	0	$1.03 \cdot 10^8$	0
	Grad	$4.28 \cdot 10^{-3}$	$6.51 \cdot 10^8$	$2.27 \cdot 10^{-4}$	$1.03 \cdot 10^8$	$-1.71 \cdot 10^{-3}$
	PSO	$7.36 \cdot 10^{-3}$	$6.51 \cdot 10^8$	$6.16 \cdot 10^{-4}$	$1.04 \cdot 10^8$	$3.28 \cdot 10^{-3}$
	DE	$3.17 \cdot 10^{-2}$	$6.55 \cdot 10^8$	$6.19 \cdot 10^{-3}$	$1.06 \cdot 10^8$	$2.06 \cdot 10^{-2}$
C2	FBS	0	$1.12 \cdot 10^9$	0	$5.53 \cdot 10^7$	0
	Grad	$1.75 \cdot 10^{-7}$	$1.12 \cdot 10^9$	$-2.59 \cdot 10^{-7}$	$5.53 \cdot 10^7$	$3.07 \cdot 10^{-7}$
	PSO	$3.51 \cdot 10^{-3}$	$1.12 \cdot 10^9$	$1.04 \cdot 10^{-4}$	$5.55 \cdot 10^7$	$3.11 \cdot 10^{-3}$
	DE	$3.51 \cdot 10^{-3}$	$1.12 \cdot 10^9$	$1.04 \cdot 10^{-4}$	$5.55 \cdot 10^7$	$3.11 \cdot 10^{-3}$
C3	FBS	0	$7.84 \cdot 10^8$	0	$1.04 \cdot 10^8$	0
	Grad	$1.49 \cdot 10^{-4}$	$7.84 \cdot 10^8$	$2.24 \cdot 10^{-7}$	$1.04 \cdot 10^8$	$-1.19 \cdot 10^{-4}$
	PSO	$6.37 \cdot 10^{-3}$	$7.85 \cdot 10^8$	$3.15 \cdot 10^{-4}$	$1.04 \cdot 10^8$	$2.31 \cdot 10^{-3}$
	DE	$6.37 \cdot 10^{-3}$	$7.85 \cdot 10^8$	$3.15 \cdot 10^{-4}$	$1.04 \cdot 10^8$	$2.34 \cdot 10^{-3}$
C4	FBS	0	$7.00 \cdot 10^8$	0	$5.43 \cdot 10^7$	0
	Grad	$3.69 \cdot 10^{-4}$	$7.00 \cdot 10^8$	$8.76 \cdot 10^{-6}$	$5.44 \cdot 10^7$	$4.11 \cdot 10^{-4}$
	PSO	$7.97 \cdot 10^{-3}$	$7.00 \cdot 10^8$	$4.76 \cdot 10^{-4}$	$5.43 \cdot 10^7$	$-6.44 \cdot 10^{-4}$
	DE	$3.76 \cdot 10^{-2}$	$7.16 \cdot 10^8$	$2.31 \cdot 10^{-2}$	$5.25 \cdot 10^7$	$-3.40 \cdot 10^{-2}$
C5	FBS	0	$5.67 \cdot 10^8$	0	$1.01 \cdot 10^8$	0
	Grad	$1.60 \cdot 10^{-3}$	$5.67 \cdot 10^8$	$7.47 \cdot 10^{-5}$	$1.01 \cdot 10^8$	$-4.20 \cdot 10^{-4}$
	PSO	$9.04 \cdot 10^{-3}$	$5.67 \cdot 10^8$	$1.16 \cdot 10^{-3}$	$1.01 \cdot 10^8$	$3.71 \cdot 10^{-3}$
	DE	$2.09 \cdot 10^{-2}$	$5.69 \cdot 10^8$	$3.33 \cdot 10^{-3}$	$1.04 \cdot 10^8$	$2.89 \cdot 10^{-2}$

Table 3.2: Case $C_u = C_u^{(o)}$: quantities measuring the differences between the OC solutions by deterministic methods (FBS and Grad) and by one iteration of heuristic algorithms (PSO and DE). Outputs by FBS method are used as reference. Parameter values and initial data as in Fig. 3.3.

As far as the representative case $C_u = 5C_u^{(o)}$ is concerned, we obtain a radically different OC solutions compared with the simulations where $C_u = C_u^{(o)}$, as shown in Fig. 3.4 (left panels). Indeed, in all cases the obtained control is strongly non–monotone. For both cases $C_u = C_u^{(o)}$ and $C_u = 5C_u^{(o)}$, PSO performs slightly better and converges in shorter times than DE.

Let us now compare Fig. 3.4 (left panels) with Table 3.3. On the one hand, in Table 3.3 the relative difference of the optimal total costs J obtained with the two algorithms is in all cases very small. On the other hand, in Fig. 3.4 the optimal control obtained by the DE algorithms seems affected by large 'noise' w.r.t. the optimal $u(t)$ obtained by PSO algorithm. On the whole, these results suggest that the system is robust with respect to even large local deviations from the theoretical optimal solution. In other words, the irregular additional oscillations in the optimal control obtained by DE algorithm suggest that a large degree of flexibility is possible when implementing the optimal control.

Alternative schedules of awareness campaigns As we said in the previous sections, actual VACs are not continuous, but they vary in a piecewise–constant fashion. We have seen that, assuming a three months–based update, we obtain, under PSO, a discretized $u(t)$ that is sufficiently close to a continuous control. By adopting DE, we obtain a more noisy solution.

Here, we want to explore the impact of even less flexible policies of intervention to favor vaccination. Namely, we will consider two additional scenarios:

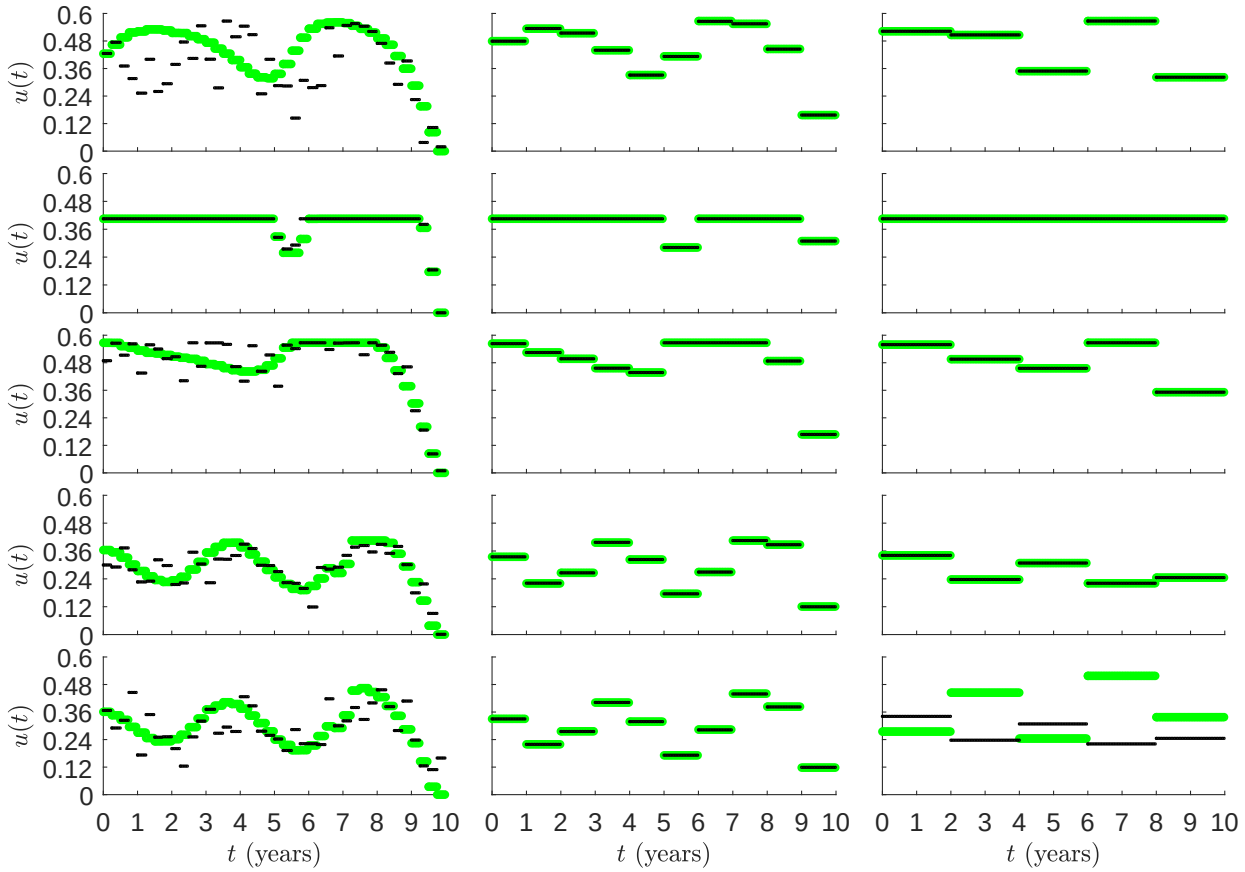

Figure 3.4: Case $C_u = 5C_u^{(o)}$: optimization by one iteration of PSO (green lines) and DE (black lines) algorithms. OC function $u(t)$ with 3 months (left panels), 1 year (central panels) and 2 years (right panels) programming. Rows, from the top to bottom: cases C1, C2, C3, C4 and C5, respectively. Parameter values and initial data as in Fig. 3.3.

Case	**Method**	3 months programming		1 year programming		2 years programming	
		$\boldsymbol{J}$ (USD)	$\boldsymbol{J_u}$ (USD)	$\boldsymbol{J}$ (USD)	$\boldsymbol{J_u}$ (USD)	$\boldsymbol{J}$ (USD)	$\boldsymbol{J_u}$ (USD)
C1	PSO	$1.01 \cdot 10^9$	$3.56 \cdot 10^8$	$1.02 \cdot 10^9$	$3.65 \cdot 10^8$	$1.03 \cdot 10^9$	$3.73 \cdot 10^8$
	DE	$1.07 \cdot 10^9$	$2.68 \cdot 10^8$	$1.02 \cdot 10^9$	$3.65 \cdot 10^8$	$1.03 \cdot 10^9$	$3.74 \cdot 10^8$
C2	PSO	$1.33 \cdot 10^9$	$2.57 \cdot 10^8$	$1.34 \cdot 10^9$	$2.58 \cdot 10^8$	$1.35 \cdot 10^9$	$2.85 \cdot 10^8$
	DE	$1.33 \cdot 10^9$	$2.61 \cdot 10^8$	$1.34 \cdot 10^9$	$2.58 \cdot 10^8$	$1.35 \cdot 10^9$	$2.85 \cdot 10^8$
C3	PSO	$1.17 \cdot 10^9$	$4.25 \cdot 10^8$	$1.17 \cdot 10^9$	$4.28 \cdot 10^8$	$1.19 \cdot 10^9$	$4.20 \cdot 10^8$
	DE	$1.18 \cdot 10^9$	$4.29 \cdot 10^8$	$1.17 \cdot 10^9$	$4.28 \cdot 10^8$	$1.19 \cdot 10^9$	$4.20 \cdot 10^8$
C4	PSO	$8.77 \cdot 10^8$	$1.58 \cdot 10^8$	$8.83 \cdot 10^8$	$1.60 \cdot 10^8$	$9.04 \cdot 10^8$	$1.31 \cdot 10^8$
	DE	$8.84 \cdot 10^8$	$1.50 \cdot 10^8$	$8.83 \cdot 10^8$	$1.61 \cdot 10^8$	$9.04 \cdot 10^8$	$1.31 \cdot 10^8$
C5	PSO	$8.76 \cdot 10^8$	$1.67 \cdot 10^8$	$8.83 \cdot 10^8$	$1.67 \cdot 10^8$	$9.05 \cdot 10^8$	$2.48 \cdot 10^8$
	DE	$8.90 \cdot 10^8$	$1.60 \cdot 10^8$	$8.83 \cdot 10^8$	$1.66 \cdot 10^8$	$9.04 \cdot 10^8$	$1.31 \cdot 10^8$

Table 3.3: Case $C_u = 5C_u^{(o)}$: optimization by one iteration of PSO and DE algorithms. Costs J and J_u for three different temporal control–updates (3 months, 1 year, 2 years). Parameter values and initial data as in Fig. 3.3.

- Yearly programming. We suppose that the PH interventions are updated once per year, for logistic and administrative reasons. For example the PH policies could depend on

the budget law, which is changed on yearly basis;

- Biennial programming. This must not seem an extreme academic case. For example, in Soviet Union, during the leadership of Stalin, key policies actions were regulated by 'quinquennial plans'.

We only simulate the case $C_u = 5C_u^{(o)}$, where the three–months discretized optimal $u(t)$ obtained by heuristic methods is oscillating. We obtain that, if the three–months optimal solutions are oscillating (i.e. scenarios C1, C3, C4 and C5), the same holds for the one–year and two–years scheduling. Of course, the degree of oscillation is smaller for the one–year w.r.t. the three–months scheduling, and smaller for the two–years w.r.t. the one–year scheduling. In the scenario C2, where the optimal control is not oscillating for the three–months scheduling, we get that the two–years scheduling optimal control is predicted to be constant.

As far as the use of PSO versus DE is concerned, we note that, in scenario C5 for the two–years scheduling, the optimal control obtained by the DE method corresponds to a cost that is much smaller than the one found by applying PSO. Moreover, the two controls in such a scenario are very dissimilar. This suggests that PSO does not converge to the actual global minimum, but to a local minimum. This is a rare event but not impossible and confirms that our choice to adopt two different algorithms is appropriate. In all other scenarios the outputs of PSO are very similar to the one obtained by applying DE.

Coming back to FBS and Grad methods

As we have seen, for $C_u = 5C_u^{(o)}$ the FBS and the Grad methods, both deterministic OC–oriented algorithms, have problems of convergence. Thus, we resort to two stochastic *general purpose* algorithms, PSO and DE. As a natural further step, we then employ the piecewise–constant OC solutions obtained by applying these two HOAs as an initial step for both the FBS and Grad methods. Namely, we set as hint values for the OC to be determined the following ones

$$u^{(0)}(t) = u_{PSO}(t)$$

or

$$u^{(0)}(t) = u_{DE}(t),$$

where u_{PSO} and u_{DE} are the optimal solutions by one iteration of PSO and DE, respectively, as given in Fig. 3.4. The rationale in adopting these initial values for the control is that the HOAs find a piecewise–constant OC that ought to be, roughly speaking, quite close (in some suitable normed functional space) to the continuous optimum derived by the Pontryagin theory.

We obtain that, both setting $u^{(0)}(t) = u_{PSO}(t)$ and $u^{(0)}(t) = u_{DE}(t)$, the FBS and Grad algorithms incur in convergence problems. This makes the use of heuristic stochastic optimization methods (the ones we employ or others, such as the simulated annealing) very attractive in all cases where FBS or the Grad or other deterministic algorithms fail to converge. Moreover, even when the deterministic computations converge, the global nature of the resulting optimum can be validated by means of the PSO and DE methods.

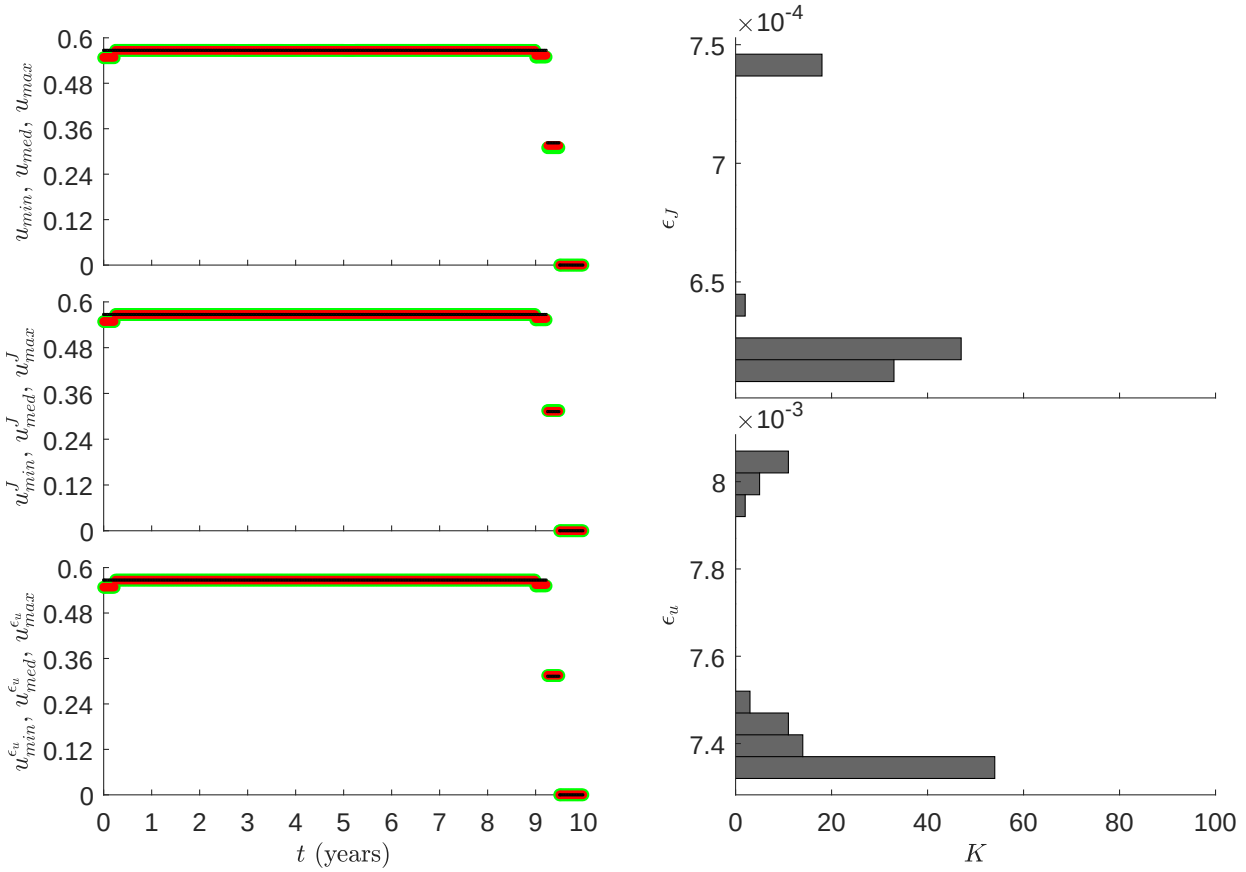

Figure 3.5: Statistical assessment for the case $C_u = C_u^{(o)}$ and simulation scenario C1. Data obtained by applying $K = 100$ times the PSO algorithm. Left top panel: $u_{min}(t)$ (green line), $u_{med}(t)$ (red line) and $u_{max}(t)$ (black line). Left central panel: $u^J_{min}(t)$ (green line), $u^J_{med}(t)$ (red line) and $u^J_{max}(t)$ (black line). Left bottom panel: $u^{\epsilon_u}_{min}(t)$ (green line), $u^{\epsilon_u}_{med}(t)$ (red line) and $u^{\epsilon_u}_{max}(t)$ (black line). Right panels: distribution of ϵ_J (top panel) and of ϵ_u (bottom panel). Parameter values and initial data as in Fig. 3.3.

3.6 Statistical assessment

Since heuristic and evolutionary algorithms are stochastic processes, they produce different outputs at each run. This has interesting implications. Indeed, each output is in principle an estimation of the true minimum, which comes from an unknown multivariate probability distribution. As a consequence, it is important to empirically infer statistical features of this distribution by repeated stochastic optimizations.

The problem is that, since the vectors to be estimated have a dimension that is quite large (40 in the case of three–months scheduling), a fully satisfactory statistical assessment would require very large samples. This would imply computation resources that, unfortunately, are out of our possibilities. Thus, we only propose preliminary statistical assessments made with a relatively small sample, which, however, are of some interest. Namely, for each set of parameters and initial conditions, we perform $K \gg 1$ stochastic optimizations to solve our OC problem ($K = 100$ in the case of three–months scheduling and $K = 200$ in the cases of annual and biennial scheduling). Due to its relatively shorter computational times, we employ the PSO algorithm. Precisely, we perform the following descriptive statistical assessments:

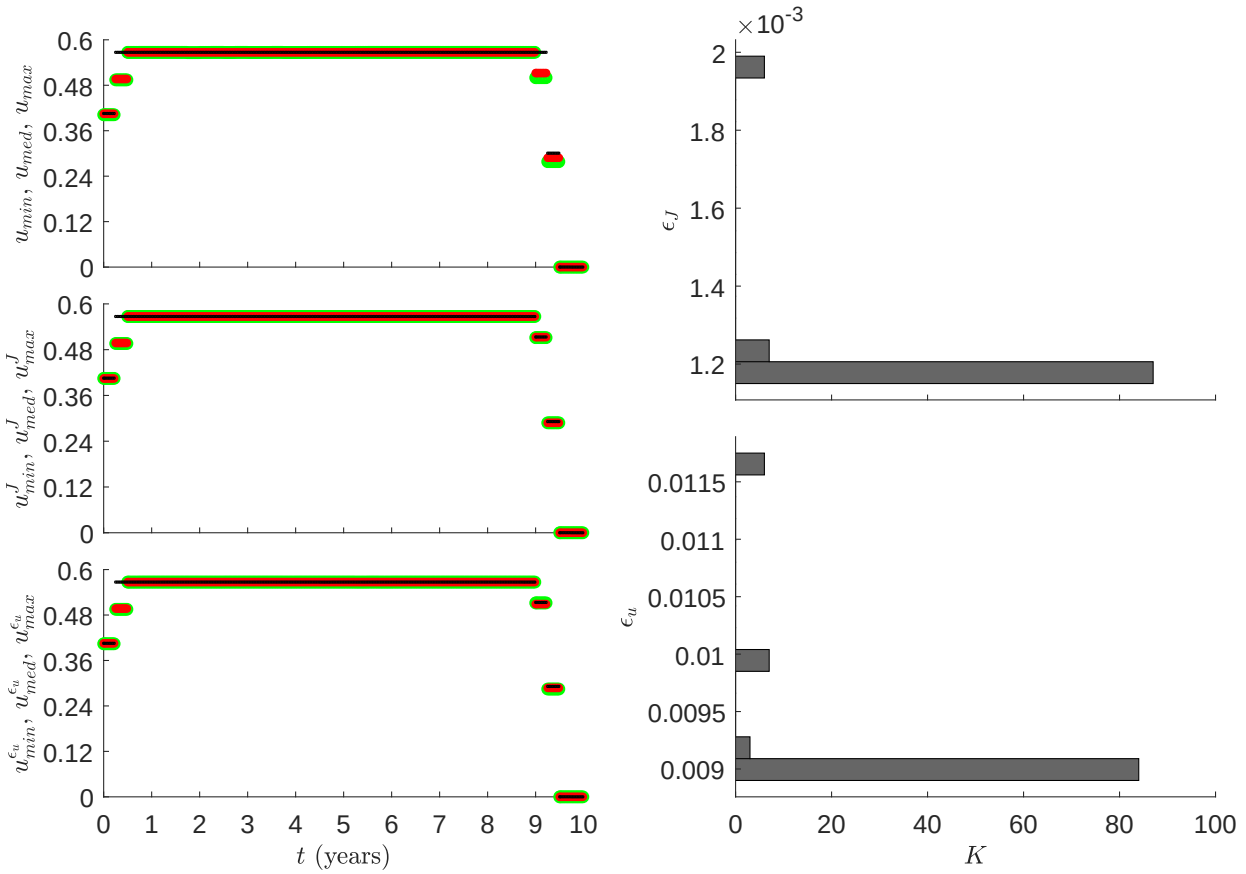

Figure 3.6: Statistical assessment for the case $C_u = C_u^{(o)}$ and simulation scenario C5. Data obtained by applying $K = 100$ times the PSO algorithm. Left top panel: $u_{min}(t)$ (green line), $u_{med}(t)$ (red line) and $u_{max}(t)$ (black line). Left central panel: $u^J_{min}(t)$ (green line), $u^J_{med}(t)$ (red line) and $u^J_{max}(t)$ (black line). Left bottom panel: $u^{\epsilon_u}_{min}(t)$ (green line), $u^{\epsilon_u}_{med}(t)$ (red line) and $u^{\epsilon_u}_{max}(t)$ (black line). Right panels: distribution of ϵ_J (top panel) and of ϵ_u (bottom panel). Parameter values and initial data as in Fig. 3.3.

- Time–wise assessment: basic statistical features of $u(t)$. For each t we compute the median $u(t)$ and the total range over the results obtained in the K optimizations. In other words, let $\Gamma = (u_1(t), \ldots, u_K(t))^T$ be the matrix having as row–vectors the obtained optimal functions at time t, and let us define $\Gamma^{sort} = Sort(\Gamma)$ the sort of Γ by columns. Then $u_{min}(t) = \Gamma_1^{sort}$, $u_{med}(t) = (\Gamma_{K/2}^{sort} + \Gamma_{K/2+1}^{sort})/2$ and $u_{max}(t) = \Gamma_K^{sort}$, where Γ_i^{sort} denotes the i–th row of Γ^{sort}. Note that these three 'pseudo' control functions by construction cannot intersect in isolated points (they can coincide on intervals or in the whole temporal horizon). Of course, since, due to the discretization, $u(t)$ is piecewise–constant, even $u_{min}(t)$, $u_{med}(t)$ and $u_{max}(t)$ are piecewise–constant.

- Global assessment: basic statistical features of J. Namely, let J_{min}, J_{med} and J_{max} be, respectively, the minimum, median and maximum value of J obtained in the K stochastic minimizations, we plot the corresponding three controls (actually, due to the discretization, vectors) $u(t)$, which we denote as $u^J_{min}(t)$, $u^J_{med}(t)$ and $u^J_{max}(t)$. Note that, at variance with the previous case, these three control functions can intersect.

- For the case $C_u = C_u^{(o)}$, where the comparison with the results obtained by FBS method is possible, we perform the following assessments: i) we sort the optimal controls

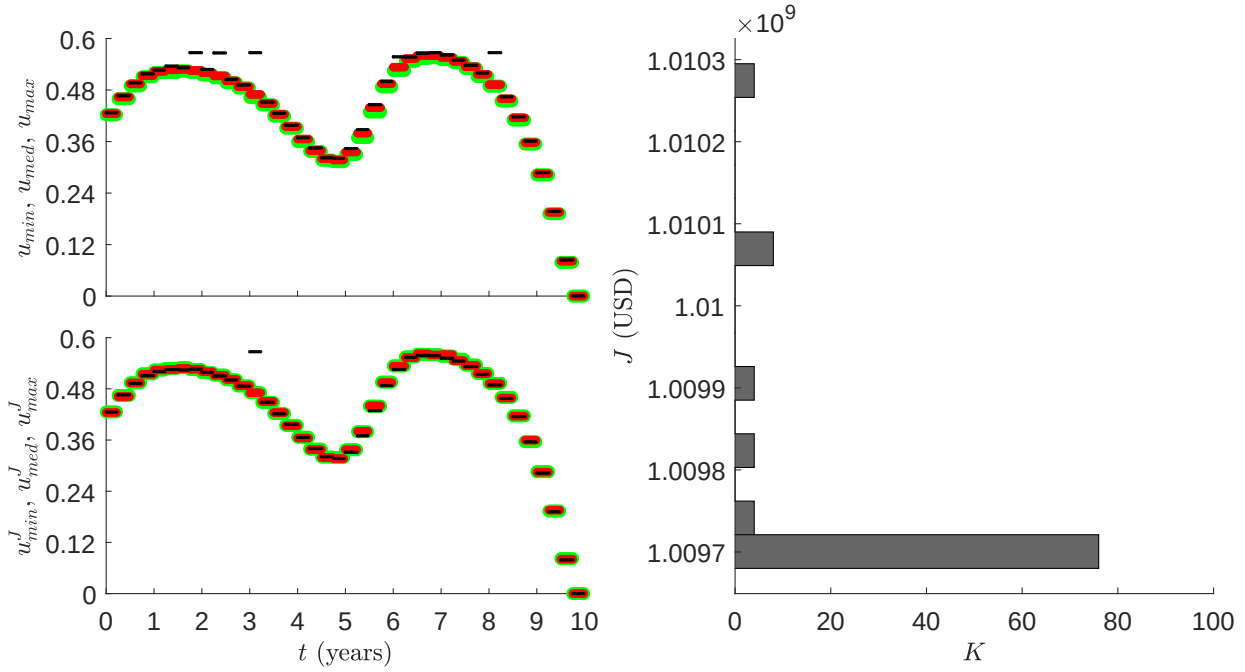

Figure 3.7: Statistical assessment for the case $C_u = 5C_u^{(o)}$ with 3 months programming and simulation scenario C1. Data obtained by applying $K = 100$ times the PSO algorithm. Left top panel: $u_{min}(t)$ (green line), $u_{med}(t)$ (red line) and $u_{max}(t)$ (black line). Left bottom panel: $u^J_{min}(t)$ (green line), $u^J_{med}(t)$ (red line) and $u^J_{max}(t)$ (black line). Right panel: distribution of J. Parameter values and initial data as in Fig. 3.3.

obtained by PSO algorithm by their relative L^1 distance from $u_{FBS}(\cdot)$:

$$\epsilon_u = \frac{||u(t) - u_{FBS}(t)||_1}{||u_{FBS}(t)||_1},$$

and we plot the $u(t)$ with the minimal $(u^{\epsilon_u}_{min}(t))$, median $(u^{\epsilon_u}_{med}(t))$ and maximal $(u^{\epsilon_u}_{max}(t))$ value of ϵ_u; ii) we plot the related histogram of the ϵ_u; iii) we plot the histogram of the relative error of the costs:

$$\epsilon_J = \frac{J - J_{FBS}}{J_{FBS}}.$$

- For the case $C_u = 5C_u^{(o)}$, where no comparison is possible with FBS method due to its lack of convergence, we plot the histogram of the distribution of J over the K stochastic optimizations.

The above described statistical inferences have also another meaning, i.e. to assess how much robust is the numerically inferred optimal control. This is a fundamental information for the practical implementation of the results of the optimal control. Indeed, since in the reality one could appreciably deviate from the theoretical results, it follows that a global optimum that has a large range is far more implementable than another with identical mean and a very small range.

As far as the case $C_u = C_u^{(o)}$ is concerned, numerical results in the most interesting scenarios are displayed in Figs. 3.5–3.6 (for the others see [97]). As far as the case $C_u = 5C_u^{(o)}$ is concerned, numerical results in the most interesting scenarios are displayed in Figs. 3.7–3.9

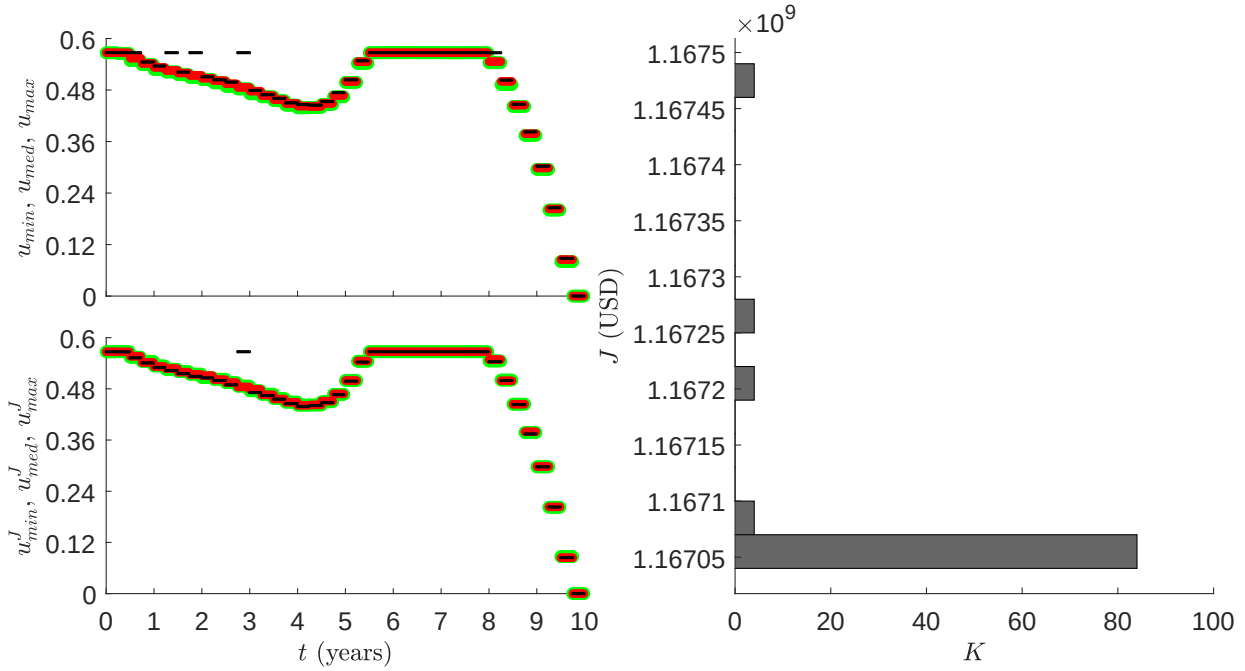

Figure 3.8: Statistical assessment for the case $C_u = 5C_u^{(o)}$ with 3 months programming and simulation scenario C3. Data obtained by applying $K = 100$ times the PSO algorithm. Left top panel: $u_{min}(t)$ (green line), $u_{med}(t)$ (red line) and $u_{max}(t)$ (black line). Left bottom panel: $u^J_{min}(t)$ (green line), $u^J_{med}(t)$ (red line) and $u^J_{max}(t)$ (black line). Right panel: distribution of J. Parameter values and initial data as in Fig. 3.3.

(again, for the others see [97]). Overall, the variance of the distributions both of the errors and of the time courses is very small. In particular, all the found optimal controls are very close to each other in time. At some time points, there are exceptionally outliers. In sum, although the sample is limited because of the above mentioned computational restrictions, the statistical assessment suggests that the PSO algorithm converges to the actual global minimum.

3.7 Discussion and conclusions

In modern society dominated by information and noises coming from Internet, especially through social networks such as Facebook, Twitter, Instagram, etc, the citizens' opinions are extremely volatile. This makes it appropriate to assume that the time–scales of imitation speed [21, 111, 112] are nowadays very short. Hence, we applied a quasi–steady–state approximation (QSSA) to the imitation game dynamics equation modeling the vaccine propensity of the target population. On the one hand, of course, the QSSA implies the loss of some information on the dynamics, but, on the other hand, it allows to better understand the mechanisms underlying the nonlinear system to which it is applied, of course in the scenarios it can be applied.

The application of the QSSA showed that the dynamics of the system is ruled by a particular case of 'open–loop' control, where the control, i.e. $u(t)$, impacts in a nonlinear fashion on the controlled system, i.e. the epidemic system. This in turn allowed us to determine the conditions for disease elimination through VACs. Note that in case of low and medium imitation speed, corresponding to classical societies with far less volatile opinion,

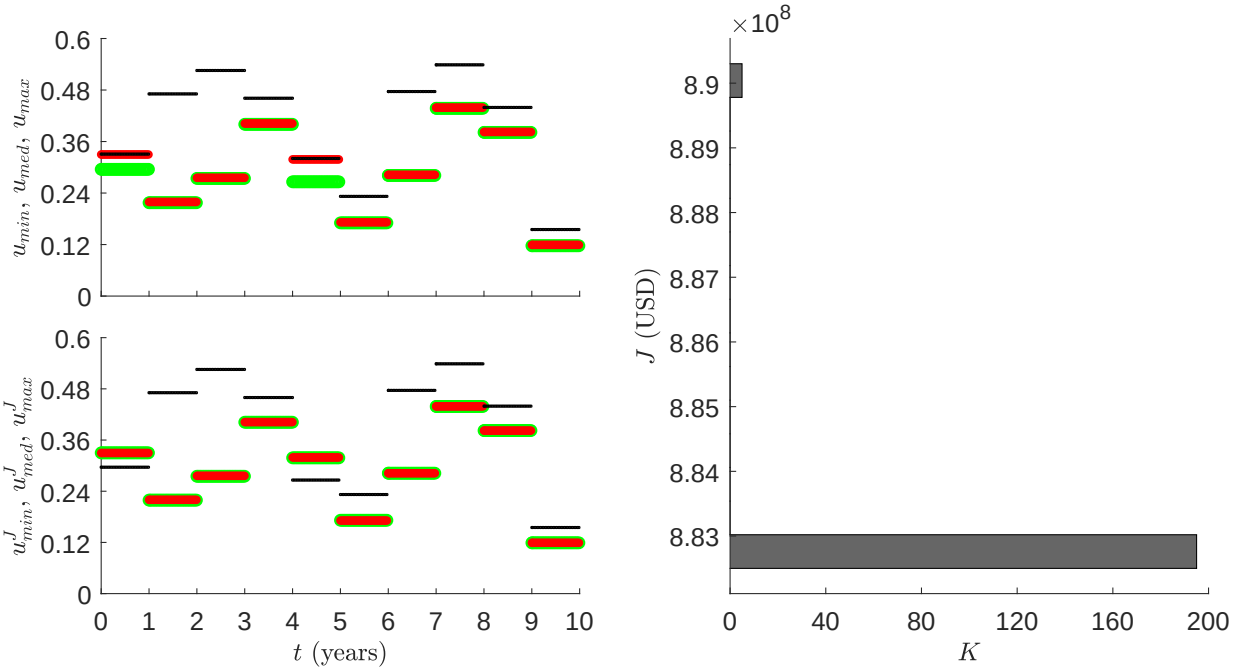

Figure 3.9: Statistical assessment for the case $C_u = 5C_u^{(o)}$ with 1 year programming and simulation scenario C5. Data obtained by applying $K = 200$ times the PSO algorithm. Left top panel: $u_{min}(t)$ (green line), $u_{med}(t)$ (red line) and $u_{max}(t)$ (black line). Left bottom panel: $u^J_{min}(t)$ (green line), $u^J_{med}(t)$ (red line) and $u^J_{max}(t)$ (black line). Right panel: distribution of J. Parameter values and initial data as in Fig. 3.3.

where the QSSA cannot be applied, the elimination condition and the general behavior of the system are far more complex and less conclusive [57]. The QSSA also allowed us to better explain the classical behavioral SIR model with voluntary vaccination introduced in [113]. In particular, the nonzero baseline vaccination rate is related through an increasing function to the actions enacted by the PHS to favor the vaccine uptake.

We then investigated one of most important forms of feedback–based control, of the great relevance in health economy, the optimal control. The resulting optimal control problem presented, w.r.t. the nonlinear 'open–loop' case above commented, a further intriguing feature: the requirements of classical existence theorems are not satisfied. This implies that one has no guarantee that the control $u(t)$ obtained with the Pontryagin procedure is a real minimum. We can only suspect that it is a real minimum. As such it required a double checking.

The two most widespread recursive numerical algorithms to solve the Pontryagin boundary value problem are the FBS and the Grad methods. We applied them to numerically find the optimal control proceeding 'as if' the optimality sufficient conditions hold. The second checking consisted in validating the result by applying a direct global optimization by heuristic optimization algorithms: PSO and DE. Furthermore, the use of HOAs was also and mainly needed since for large values of the specific cost of PHS information campaigns (C_u), the FBS and the Grad algorithms had convergence problems, both by adopting various generic initial hints and by adopting as initial hint the outputs of the HOAs.

We obtained optimal intervention profiles that are strongly oscillating in the scenario where $C_u = 5C_u^{(0)}$, being $C_u^{(0)}$ the baseline value. The obtained optimal controls are

qualitatively similar to those obtained in the case of slow imitation speed and reported in [65]. However, in the fast system the solutions found by the PSO algorithm are more smooth and quantitatively different. We also considered alternative schedules with less frequent update of the strategy: namely we investigated the cases where the strategy is only yearly updated and the extreme case where it is biennially updated. In both cases the non–monotone nature of the control is maintained. In all cases we considered, the solutions obtained by the DE algorithm, which are (roughly speaking) 'quite noisy', showed that the system is robust to multiple local deviations from the theoretical optimum: this robustness is of interest since in real world maintaining a strict scheduling can be difficult.

PSO and DE are stochastic algorithms, i.e. they transform the initial time–continuous dynamical system in a discrete–time stochastic dynamical system. On the one hand, stochasticity is fundamental to find the global optimum and not to be stuck in a local minimum, on the other hand this implies that the output of a single run of an HOA is an instance from a probabilistic distribution, which in our case is multivariate in a large dimension space. For this reason, we proposed in this study to couple the use of HOAs in OC problems with a double statistical assessment: i) of the time profile of the control $u(t)$; ii) of the value of the objective functional J. This will provide the system designers (in our case the PHS officers) an interesting tool to assess the robustness of the optimal control strategy. Namely, in our case, although the sample size was relatively small due to constraints on the available computational resources, the statistical assessment suggested that the PSO algorithm for the problem in study finds the actual global minimum.

Apart the very basic nature of the SIR model, the major limit of our results is that the system to be controlled is deterministic and that the control is purely deterministic as well. However, we note that the heuristic procedures we illustrated here can be applied to stochastic versions of our OC problem. Namely, we plan to investigate a stochastic OC problem based on our model where the following stochastic fluctuations are included: 1) stochastic demographic and epidemic fluctuations modeled by the so called chemical Langevin equation approach [139]; 2) stochastic fluctuations of the contact rate. Another line of research we will soon approach remains, instead, in the deterministic path: application of the investigation we proposed here to the Bauch behavioral epidemic model [21], which has a number of features that makes it quite distinct from the problem we faced here.

Chapter 4

An epidemic model with information–dependent imperfect vaccination

In this chapter, we go on in the line of including behavioral human factors in the modeling of epidemic dynamics, and we investigate a behavioral epidemic model including a partially effective vaccination at all ages. The vaccination is information–dependent, in the sense that the vaccination rate of susceptibles depends on the current and the past information available of the disease prevalence in the population. The weight given to the past history is described by an exponential kernel.

The proposed model presents both the possibility of backward bifurcation and that of oscillations triggered by behavioral memory. Furthermore, a forward hysteresis scenario may take place where multiple endemic states are possible when the basic reproduction number $\mathcal{P}_0$ is greater than one. Finally, a stable endemic state may destabilize via Hopf bifurcation not only when $\mathcal{P}_0 > 1$ but also when $\mathcal{P}_0 < 1$, depending on the interplay between some relevant information–related parameters. The results of this study have been published in [59].

4.1 Background

Immunization plays a driving role among the health interventions against the spread of infectious diseases thanks to its safety and cost–effectiveness [300]. High vaccine uptake levels resulted in drastic declines of many vaccine–preventable diseases or even eradication, as in the very well known case of smallpox. Nonetheless, a critical aspect of vaccination is its degree of protection in terms of effectiveness in preventing the illness as well as the duration of the induced immunity. Some vaccines reduce the infection risk, but do not prevent a vaccinated individual from acquiring and transmitting the disease: they are called *leaky vaccines*. Their use has been much debated, especially for malaria [152,208] (the term *leaky* comes from the literature on malaria vaccines), and for some animal infections, including chickens Marek's disease [195].

In the mathematical epidemiology literature, a large amount of epidemic models including imperfect vaccination can be found (see, just to mention a few papers, [45,110,150,192,268]). A specific outcome often emerging from the analysis of imperfect vaccination models is the coexistence of two stable equilibria as consequence of a *backward* bifurcation occurring when the *basic reproduction number* (say, BRN, denoted by $\mathcal{P}_0$ here) is equal to unity. To be more specific, it happens that a stable disease–free equilibrium (DFE) coexists with two endemic equilibria (one unstable and the other one locally asymptotically stable) for values of $\mathcal{P}_0$ in a certain interval $(P^*, 1)$, with $P^* \in (0, 1)$, whereas, for $\mathcal{P}_0 > 1$, the DFE is unstable and only the stable endemic equilibrium exists (see Figure 4.1). This kind of bifurcation differs from the *forward* bifurcation, which is typical of monostable systems, where for $\mathcal{P}_0 < 1$ the DFE is the unique equilibrium and it is asymptotically stable (possibly globally) and for $\mathcal{P}_0 > 1$ the DFE is unstable and only one asymptotically stable (possibly globally) endemic equilibrium exists.

From the public health viewpoint, the occurrence of a backward bifurcation has negative implications on infection elimination. Indeed, from one hand the BRN must be reduced below a smaller threshold (compared with that of monostable systems) in order to avoid endemic states. From the other hand, since the stable endemic equilibrium remains strictly positive when $\mathcal{P}_0$ passes through unity, the disease burden might undergo a sudden and dramatic jump by switching from zero (if, for $\mathcal{P}_0 < 1$, system is at the DFE) to a positive and relatively high value.

The epidemiological consequences of backward bifurcation have been widely discussed in the literature (see e.g. [150, 234] and references therein). Generally speaking, this type of

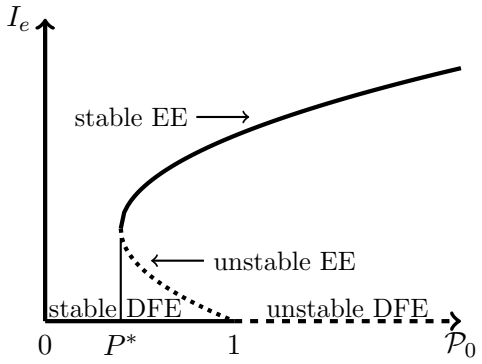

Figure 4.1: Qualitative bifurcation diagram representing a backward bifurcation. The values of the infected fraction at equilibrium I_e are plotted vs the basic reproduction number $\mathcal{P}_0$. The solid lines (–) denote stability; the dashed lines (- -) denote instability.

phenomenon may arise due to epidemiological mechanisms, such as the exogenous re–infection in tuberculosis transmission models and the host disease–induced mortality in models of vector–borne diseases spread. The 'practical' aspects of this particular dynamical phenomenon have been also discussed, for the case of tuberculosis, in [136].

In some specific epidemic models (e.g. [1, 132, 267]) the backward bifurcation can be 'removed' by adopting a mass action incidence (i.e. where the incidence is directly proportional to the product of the susceptibles and infectious compartment sizes) instead of a standard incidence function (which is the mass action incidence normalized by the total population size).

However, even when vaccines confer an adequate protection, the success of mass immunization programs relies on the 'human element', i.e. the degree of social acceptance and adherence [210, 293].

Especially in modern societies, where vaccines are most often voluntary, the propensity to vaccinate may reduce when the prevalence of disease is low, since in this case the perceived risk of vaccine side–effects becomes very large when compared to the perceived current risk of getting infected [64, 113, 114, 293]. This behavior is myopic because it is the vaccination success themselves to encourage people to the exemption, neglecting future resurgence of infection due to coverage decline. As a consequence, a trend towards the decrease of the adherence to immunization campaigns for some vaccines (e.g. seasonal flu and MMR vaccines) has been frequently observed in many countries [303].

The need of introducing the 'human factor' into epidemic models has led since the early 2000s to the development of the *behavioral epidemiology* of infectious diseases, a new branch of mathematical epidemiology [210, 293]. As discussed in Section I.4, several different approaches in modeling vaccinating behavior have been developed, based e.g. on game–theoretic analysis [21, 56, 61, 217] or by means of an *information index* mostly based on the publicly available information concerning the status of the disease in the community [62, 109, 110, 113, 114].

In this last case there is evidence that, compared with the corresponding non–behavioral models, new dynamical phenomena may arise, as the onset of steady oscillations. For SIR–like vaccination models, oscillations may arise when the information function involves the past history of the disease [109, 113, 114], whereas for SEIR–like models oscillations may arise also when the vaccinating behavior depends on current information [64]. Thus, human

behavior might be a critical factor in explaining the presence of oscillations in time–series of some vaccine–preventable infectious diseases.

In the large corpus of scientific research in behavioral vaccination modeling, to the best of our knowledge, the interplay between vaccine imperfection and individuals choices has been investigated only in two recent papers [110, 194]. In [110], an SISV model with partially effective and waning pediatric vaccination has been considered where the parents propensity to vaccinate or not vaccinate their children is modeled by assuming that vaccine uptake of newborns is an increasing function of current infection prevalence. The SIRV model [194] incorporates both information–dependent imperfect vaccination at all ages and saturated treatment; vaccination rate is modeled as a saturating function of the information about the present and the past history of disease prevalence. Both models [110, 194] predict the possibility of backward bifurcation and the coexistence of multiple endemic steady states when the basic reproduction number is greater than one. This last scenario is often referred as *forward hysteresis* [149, 165, 294]. Furthermore, in Kumar *et al.* [194], the saturation in medical resources (vaccination and treatment) may cause the occurrence of Hopf bifurcations.

As it is well known, imperfect vaccines may be addressed not only to infants, since they are mainly linked to emergent or re–emergent diseases (like dengue [305], malaria [304], HIV [306], TB [307]), including constantly evolving viruses (like those of influenza [74]). For example: Dengvaxia®, the first dengue vaccine to be licensed, registered a mean effectiveness of 59.2% [305]; RTS,S/AS01 reduces malaria not more than 39% [304]; flu vaccine effectiveness widely ranges from season to season, but in general does not exceed the $60 - 70\%$ about [25, 74]. Whereas, most of the 'routine' childhood vaccines are able to confer higher rates of protection: 97% for measles and rubella [73], 88% for mumps [73], 88% to 98% for varicella [72]. The two currently used poliovirus vaccines produce immunity in more than 95% of recipients [75].

It is worth to point out again that the dynamics of vaccine–preventable infectious diseases under voluntary vaccination is a complex physical phenomena. As stressed in [293], such a dynamics straight depends on human decisions which, in turn, are based on the balance between the perceived risks of getting infected and the perceived risks of being affected by vaccine–related side effects. The intrinsic difficulty of quantitatively representing human behavior makes the modeling phase complex and the resulting mean–field models show dynamics radically different from those of the basic models with mandatory vaccination. Therefore, the physical phenomenon described here is very different from the impact of media on the disease spread explored in many classical and recent papers (see e.g. [3, 93, 220, 221, 280]). Here, in general, the disease awareness results in a reduced rate of infection transmission due to the avoidance of risky contacts [79, 93, 275, 280] or is treated as an additional *media* variable that represents the cumulative density of awareness in the population and weights the transfer of aware susceptibles in a different class [3, 220, 221].

In this chapter, mainly motivated by the work done in [45, 110, 192], we consider an SISV model with imperfect vaccination at all ages and assume that vaccine uptake levels depend on the current and past information on the disease by following the idea developed in [109,113,114]. We perform a qualitative analysis based on stability theory and bifurcation theory. The analysis shows that the behavioral model reveals a much more complex dynamics compared to the basic classical model, including the possibility of multi–endemicity and information–induced oscillations via Hopf bifurcations, phenomena that can arise both above and under the threshold $\mathcal{P}_0 = 1$. We present also some numerical simulations to support the analytic findings.

The chapter is organized as follows: in Section 4.2 we introduce the model and give some basic properties. Section 4.3 is devoted to equilibria and local stability. In Section 4.4 the bifurcation curve is derived. Central manifold analysis is performed in Section 4.5 to obtain sufficient conditions for backward or forward bifurcation at $\mathcal{P}_0 = 1$. In Section 4.6 numerical simulations are provided for two different formulations of the vaccination coverage function. Concluding remarks are given in Section 4.7.

4.2 The model and its basic properties

In [45] the basic Susceptible–Infected–Susceptible (SIS) model for the transmission of a generic vaccine–preventable infectious disease is enhanced by the inclusion of a partial effective vaccine providing waning immunity. Following the idea of the information–dependent epidemic models in behavioral epidemiology [210, 293], here we assume that the vaccination is fully voluntary and the choice to get vaccinated or not depends on the available information and rumors concerning the spread of the disease in the community. The model is given by the following system of differential equations:

$$\begin{aligned} \dot{S} &= \mu(1-S) - \beta SI - \varphi(M)\, S + \gamma I + \vartheta V \\ \dot{I} &= \beta SI + \sigma\beta VI - (\gamma+\mu)\, I \\ \dot{V} &= \varphi(M)\, S - \sigma\beta VI - (\vartheta+\mu)V. \end{aligned} \tag{4.1}$$

The state variables $S(t)$, $I(t)$ and $V(t)$ denote the fractions of susceptible, infected (and infectious) and vaccinated individuals at time t, respectively. All the parameters are positive constants: μ is the birth rate, which is assumed to be identical to the natural death rate; β is the disease transmission rate, $\sigma\beta$ $(0 < \sigma < 1)$ is the reduced transmission rate for vaccinated subjects, γ is the rate of recovery from the infection and ϑ is the vaccine waning rate.

In (4.1) vaccination is assumed to be voluntary and information–dependent. The information on the status of the disease in the community is described by means of the *information index* $M(t)$ [109, 110, 113, 114]. The vaccination rate is therefore modeled by the information–dependent function:

$$\varphi(M) = \varphi_0 + \varphi_1(M), \;\; 0 < \varphi_0 < 1, \tag{4.2}$$

where the constant φ_0 represents the fraction of the population that chooses to get vaccinate regardless of rumors and information about the status of the disease in the population, while $\varphi_1(M(t))$ represents the fraction of the population whose vaccination choice is influenced by the information. We require that $\varphi_1(0) = 0$ and φ_1 is a continuous, differentiable and increasing function.

Generally speaking, the transmission of information is often preceded by articulated routine procedures (clinical tests, notification of cases, reporting delays to public health authorities, etc) and the consequent awareness of disease presence to the population takes time. Moreover, some people may have memory of past epidemics (especially the most recent ones) or may have acquired it from family history. Therefore, as anticipated in Section I.4, the information index M is described by the distributed delay

$$M(t) = \int_{-\infty}^{t} \tilde{g}\left(S(\tau), I(\tau), V(\tau)\right)\, K(t-\tau)d\tau, \tag{4.3}$$

where the function $\tilde{g}$ describes the information that individuals consider to be relevant for making their choice to vaccinate or not to vaccinate. It is often assumed that the index $M(t)$ summarizes the current and the past history of the disease prevalence [109,113,114], so that $\tilde{g}$ depends only on prevalence:

$$\tilde{g} = \begin{cases} 0 & \text{if } t < 0 \\ g(I) & \text{if } t \geq 0 \end{cases}$$

where g is a continuous, differentiable, increasing function such that $g(0) = 0$. In this sense the choice to vaccinate is influenced by the social alarm caused by the disease, according to the idea of *(pseudo) rational exemption to vaccination* [56,113,114,293].

The delay kernel $K(t)$ in (4.3) represents the weight given to past history of the disease. In the following, we will assume that K is given by the first element $Erl_{1,a}(t)$ of the Erlang family, called *weak kernel* or *exponentially fading memory* (see (I.12) with $n = 1$). With this kernel the maximum weight is assigned to the current information and the delay is centered at the average $1/a$. Therefore, the parameter a takes the meaning of inverse of the average time delay of the collected information on the disease.

With this choice, the dynamics of M is ruled by the equation:

$$\dot{M} = a\,(g(I) - M)\,. \tag{4.4}$$

Denoting $N(t)$ the total population and taking $N(0) = 1$, we may replace $S = 1 - I - V$ in (4.1). Taking into account (4.4), we get the following system:

$$\begin{aligned} \dot{I} &= [\beta(1 - I) - (\mu + \gamma) - (1 - \sigma)\beta V]\, I \\ \dot{V} &= \varphi\,(M)\,(1 - I - V) - (\vartheta + \mu + \sigma\beta I)V \\ \dot{M} &= a\,(g(I) - M)\,. \end{aligned} \tag{4.5}$$

It is not difficult to check that set $\tilde{\mathcal{D}} = \left\{(I, V, M) \in \mathbb{R}^3_+ : I + V \leq 1,\ M \leq g(1)\right\}$ is positively invariant for model (4.5).

Now, let us introduce the quantity

$$\zeta = 1 - \frac{1}{\mathcal{R}_0}, \tag{4.6}$$

where

$$\mathcal{R}_0 = \frac{\beta}{\gamma + \mu}. \tag{4.7}$$

The first equation of system (4.5) can be written:

$$\dot{I} = \beta\,[\zeta - I - (1 - \sigma)V]\, I \leq \beta I\,[\zeta - I]\,, \tag{4.8}$$

i.e. it asymptotically holds $I(t) \in [0, \zeta]$. Therefore, we shall limit the analysis of model (4.5) in the region

$$\mathcal{D} = \left\{(I, V, M) \in \mathbb{R}^3_+ :\ I \leq \zeta,\ I + V \leq 1,\ M \leq g(\zeta)\right\}. \tag{4.9}$$

Remark 4.1. *If we denote by p the fraction of vaccinated newborns, the inequality $p > \zeta$, where ζ is given in (4.6), is the well known threshold condition for the disease elimination in SIR–like models of diseases with mandatory and fully effective vaccination of newborns (i.e. the Herd immunity condition, see [47, 214]).*

4.3 Equilibria and stability properties

Denote the generic equilibrium of (4.5) by

$$E_e = (I_e, V_e, M_e)\,. \tag{4.10}$$

The components will be the solutions of the algebraic system obtained by setting the r.h.s. of (4.5) equal to zero. It immediately follows that model (4.5) admits the disease–free equilibrium

$$E_0 = \left(0, \frac{\varphi_0}{\varphi_0 + \vartheta + \mu}, 0\right). \tag{4.11}$$

Let us introduce

$$\mathcal{P}_0 = \mathcal{R}_0/\rho, \tag{4.12}$$

where $\mathcal{R}_0$ is given in (4.7) and

$$\rho = \frac{\varphi_0 + \vartheta + \mu}{\sigma\varphi_0 + \vartheta + \mu}. \tag{4.13}$$

It is easy to verify that the local stability properties of E_0 are not affected by the function $\varphi_1(M(t))$. Therefore the same results obtained in the case of constant vaccination rate and no information dependence may be established [45]:

Proposition 4.2. *If $\mathcal{P}_0 < 1$ the disease–free equilibrium E_0 is locally asymptotically stable. If $\mathcal{P}_0 > 1$, then E_0 is unstable.*

Remark 4.3. *It is possible to show (see [45]) that if $\mathcal{R}_0 < 1$ (i.e. $\zeta < 0$), than E_0 is also globally asymptotically stable. This property is a consequence of the differential inequality (4.8).*

Denote the generic endemic equilibrium (EE) of (4.5) by (4.10), where now $I_e > 0$. From the equation in (4.8) and the third equation of (4.5) it follows:

$$V_e = \frac{\zeta - I_e}{(1-\sigma)}, \tag{4.14}$$

and

$$M_e = g(I_e). \tag{4.15}$$

Furthermore, $E_e \in \mathcal{D} \setminus \{E_0\}$ implies $0 < I_e \leq \zeta$ and $0 < I_e + V_e \leq 1$, with ζ given in (4.6). Therefore it must be:

$$I_{inf} \leq I_e \leq \zeta, \tag{4.16}$$

where

$$I_{inf} = \max\left(0,\, 1 - \frac{1}{\sigma\mathcal{R}_0}\right), \tag{4.17}$$

and $I_e \neq 0$.

Substituting (4.14) and (4.15) into the second equation of (4.5) we obtain I_e as solutions of

$$\chi(I) = \psi(I), \tag{4.18}$$

where

$$\chi(I) = \varphi\left(g(I)\right)\left(\frac{1}{\mathcal{R}_0} - \sigma\left(1 - I\right)\right) \tag{4.19}$$

and

$$\psi(I) = (\vartheta + \mu + \sigma\beta I)(\zeta - I). \tag{4.20}$$

The next theorem (Theorem 4.5) states that model (4.5) can admit both multiple super–critical (i.e. above the threshold $\mathcal{P}_0 = 1$) and sub–critical (i.e. below the threshold $\mathcal{P}_0 = 1$) endemic equilibria.

Remark 4.4. *In Theorem 4.5 we will estimate the number of endemic equilibria for model (4.5) in the case that they refer to simple solutions of (4.18), i.e. all common points between χ and ψ are intersection points. However, two or more equilibria may collide in a unique equilibrium, which will refer to a solution of (4.18) with multiplicity greater than one. Generally speaking, it is reasonable to expect that this only happens in a finite number of points (bifurcation points), as commonly in literature (e.g. [45, 110, 150, 192, 237, 268]). In the following, we assume that this is the rule, i.e. φ and g are such that for almost all values of $\mathcal{P}_0$ all roots of (4.18) are simple. Therefore, when we will refer to the number of endemic equilibria, we often will omit to specify that it is determined 'except at a bifurcation point'.*

Let us introduce the quantities:

$$\mathcal{P}_1 = \frac{\sigma\beta}{\rho(\sigma\beta - (\vartheta + \mu))}, \tag{4.21}$$

and

$$\mathcal{P}_2 = \frac{(2-\sigma)\beta}{\rho(\sigma\beta + (\vartheta + \mu))}. \tag{4.22}$$

We have the following result:

Theorem 4.5. *For $\sigma\beta - (\vartheta + \mu) \leq 0$, model (4.5) admits no endemic equilibria if $\mathcal{P}_0 \leq 1$, and a unique endemic equilibrium if $\mathcal{P}_0 > 1$.*

For $\sigma\beta - (\vartheta + \mu) > 0$, model (4.5) admits a non–negative even number of endemic equilibria if $\mathcal{P}_0 \leq 1$, and an odd number of endemic equilibria if $\mathcal{P}_0 > 1$. In particular, there could be:

(a) sub–critical endemic equilibria if $\mathcal{P}_1 < \mathcal{P}_0 \leq 1$, with $\mathcal{P}_1 > 0$ given by (4.21);

(b) multiple super–critical endemic equilibria if $1 < \mathcal{P}_0 < 1/(\rho\sigma)$ and $\mathcal{P}_0 > \mathcal{P}_1$, or $1/(\rho\sigma) \leq \mathcal{P}_0 < \mathcal{P}_2$, with $\mathcal{P}_2$ given by (4.22).

Proof. In view of Remark 4.3, we look for EE only in case $\mathcal{R}_0 > 1$.

The endemic infected states I_e are positive solutions of (4.18), where $\chi(I)$ and $\psi(I)$ are given by (4.19) and (4.20), respectively. In view of (4.16), we can limit ourselves to seek equilibria in the interval $[I_{inf}, \zeta]$, with I_{inf} and ζ given in (4.17) and (4.6).

Observe that:

(i) both $\chi(I)$ and $\psi(I)$ are non–negative in $[I_{inf}, \zeta]$;

(ii) $\chi(I)$ is increasing in $[I_{inf}, \zeta]$;

(iii) $\psi(I)$ is a concave quadratic function;

(iv) $\psi(\zeta) = 0$, and $\chi(\zeta) = (1-\sigma)/\mathcal{R}_0 > 0$;

(v) $\psi'(I) = aI + b$, where

$$a = -2\sigma\beta < 0, \;\; b = \sigma\beta\zeta - (\vartheta + \mu)\,;$$

(vi) in view of (4.12),

$$\psi'(0) = \sigma\beta - (\vartheta + \mu) - \frac{\sigma\beta}{\rho\mathcal{P}_0},$$

hence

$$\sigma\beta - (\vartheta + \mu) \leq 0 \Longrightarrow \psi'(I_{inf}) \leq \psi'(0) < 0, \tag{4.23}$$

namely, if $\sigma\beta - (\vartheta + \mu) \leq 0$, ψ is strictly decreasing in $[I_{inf}, \zeta]$.

The two following cases have to be distinguished:

- Case I: $\mathcal{P}_0 < 1/(\sigma\rho)$ (i.e. $1 - 1/(\sigma\mathcal{R}_0) < 0$)

  In this case, from (4.17), it follows $I_{inf} = 0$, and

  $$\psi(0) \lesseqgtr \chi(0) \iff \mathcal{P}_0 \lesseqgtr 1. \tag{4.24}$$

  Properties (i)–(vi) and (4.24) imply that, when $\sigma\beta - (\vartheta + \mu) \leq 0$, $\chi(I)$ and $\psi(I)$ will intersect no time if $\mathcal{P}_0 \leq 1$, and exactly one time if $\mathcal{P}_0 > 1$.

  Whereas, when $\sigma\beta - (\vartheta + \mu) > 0$, the inequality

  $$\psi'(0) \lesseqgtr 0$$

  reads:

  $$\mathcal{P}_0 \lesseqgtr \frac{\sigma\beta}{\rho\,(\sigma\beta - (\theta + \mu))} = \mathcal{P}_1$$

  and from properties (i)–(v) and (4.24) it follows that:

  - for $\mathcal{P}_0 \leq 1$, in $[0, \zeta]$, χ starts above or in correspondence of ψ and ends above it. Therefore, there should be no endemic equilibria, if $\mathcal{P}_0 \leq \mathcal{P}_1$; and a non–negative even number of endemic equilibria, except at a bifurcation point, if $\mathcal{P}_0 > \mathcal{P}_1$ (see Figure 4.2, left panel);
  - for $\mathcal{P}_0 > 1$, in $[0, \zeta]$, χ starts out below and ends up above ψ. Therefore, there should be a unique endemic equilibrium, if $\mathcal{P}_0 \leq \mathcal{P}_1$; and an odd number of endemic equilibria, except at a bifurcation point, if $\mathcal{P}_0 > \mathcal{P}_1$ (see Figure 4.2, right panel).

- Case II: $\mathcal{P}_0 \geq 1/(\sigma\rho)$ (i.e. $1 - 1/(\sigma\mathcal{R}_0) \geq 0$)

  In this case $I_{inf} = 1 - 1/(\sigma\mathcal{R}_0)$ and $\chi(I_{inf}) = 0 < \psi(I_{inf})$, namely, in $[I_{inf}, \zeta]$, χ starts out below and ends up above ψ. Further

  $$\psi'(I_{inf}) \lesseqgtr 0 \iff \mathcal{P}_0 \gtreqless \frac{1}{\rho}\frac{2\beta - \sigma\beta}{\sigma\beta + (\vartheta + \mu)} = \mathcal{P}_2.$$

  From the last equivalence and from properties (i)–(v), we obtain that: if $\mathcal{P}_0 \geq \mathcal{P}_2$ there is a unique endemic equilibrium; if $\mathcal{P}_0 < \mathcal{P}_2$, there should be an odd number of endemic equilibria, except at a bifurcation point.

  Again, property (vi) excludes the possibility of multiple super–critical endemic equilibria when the inequality $\sigma\beta - (\vartheta + \mu) \leq 0$ holds.

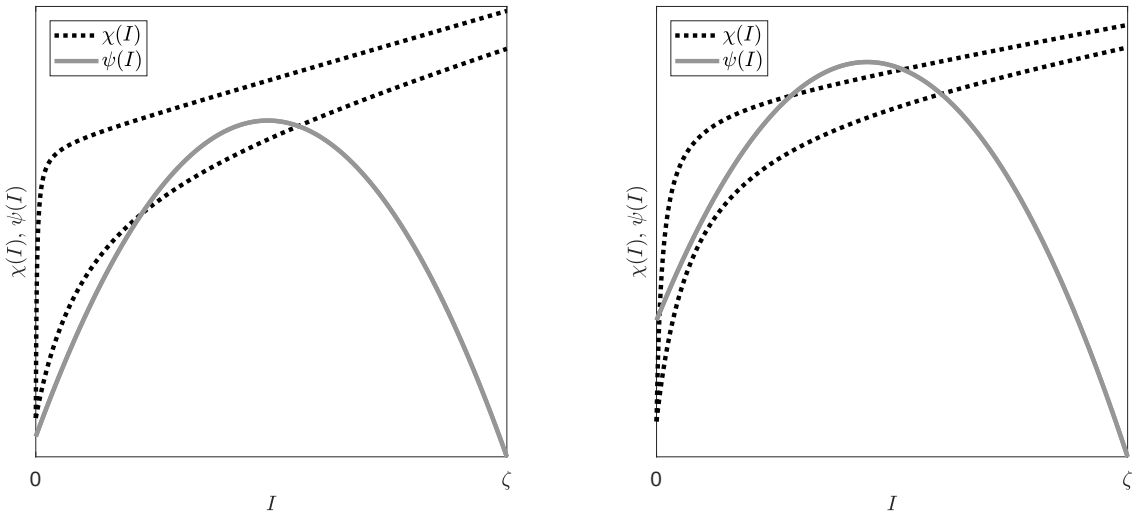

Figure 4.2: Some possible configurations of functions $\chi(I)$ and $\psi(I)$, given in (4.19) and (4.20), for $\sigma\beta - (\vartheta + \mu) > 0$. Left panel: if $\mathcal{P}_0 \leq 1$, there should be a non–negative even number of EE (in figure zero or two). Right panel: if $\mathcal{P}_0 > 1$, there should be an odd number of EE (in figure one or three).

□

In the most general setting, Theorem 4.5 provides only partial information about the existence and the number of endemic equilibria. Some extra assumptions allow us to obtain more specific results. For example, we have:

Proposition 4.6. *Let $\varphi(M)$ and $g(I)$ be the functions introduced in Section 4.2.*

If the function $\varphi(g(I))$ is convex (not necessarily strictly convex) in $[I_{inf}, \zeta]$, with I_{inf} and ζ given by (4.17) and (4.6), then: if $\mathcal{P}_0 \leq 1$, model (4.5) admits no more than two endemic equilibria; if $\mathcal{P}_0 > 1$, model (4.5) admits a unique endemic equilibrium.

Proof. It follows from the assumptions on φ and g that the composite function $\varphi(g(I))$ is positive and increasing in $\mathbb{R}_+$. If $\varphi(g(I))$ is convex in $[I_{inf}, \zeta]$, then also the function $\chi(I)$, given by (4.19), will be convex in $[I_{inf}, \zeta]$ (as product of non–negative, increasing and convex functions).

In view of (4.16) and (4.18), the number of EE is the number of positive intersection points in $[I_{inf}, \zeta]$ of the convex function $\chi(I)$ with the strictly concave function $\psi(I)$, given by (4.20). Thus, it cannot exceed two. The assert follows from Theorem 4.5.

□

Remark 4.7. *Proposition 4.6 applies to the following noteworthy cases: (a): if $\varphi(M)$ and $g(I)$ are convex functions; (b): if there is no information dependence, namely when $\varphi(M) = \varphi_0$ in model (4.5). The latter result coincides with that obtained in [45].*

Let us now perform the local stability analysis of endemic equilibria.

Again, let us denote the generic EE of (4.5) by (4.10) and introduce the quantities:

$$q_0 = \beta\left(1 - \zeta - \sigma(1 - I_e)\right) g'(I_e)\varphi'(g(I_e))I_e > 0 \tag{4.25}$$

$$q_1 = \beta\left(\vartheta + \mu - \sigma\beta\zeta + \sigma\varphi(g(I_e)) + 2\sigma\beta I_e\right) I_e \tag{4.26}$$

$$q_2 = \beta(1 + \sigma)I_e + \vartheta + \mu + \varphi(g(I_e)) > 0. \tag{4.27}$$

Then, the following result can be established:

Theorem 4.8. *Let E_e be an endemic equilibrium of model (4.5).*

If at least one of the inequalities $aq_2 + q_1 \leq 0$, $a(q_1 + q_0) < 0$ holds, then E_e is unstable.

If $aq_2 + q_1 > 0$ and $a(q_1 + q_0) > 0$, then the local stability of E_e depends on the further mutually exclusive conditions:

(i) $q_1 < 0$,

(ii) $q_1 \geq 0$ *and* $q_2^2 - q_0 + 2q_2\sqrt{q_1} < 0$,

where q_0, q_1 and q_2 are given in (4.25), (4.26), (4.27), respectively.

Precisely, if neither (i) nor (ii) is verified, then E_e is locally asymptotically stable (LAS). Otherwise, if (i) or (ii) holds, then there exist two values $\tilde{a}$, a_2, with $0 \leq \tilde{a} < a_2$, such that E_e is unstable for $a \in (\tilde{a}, a_2)$, whereas it is LAS for $a \notin (\tilde{a}, a_2)$. Hopf bifurcations occur at $\tilde{a}$, when $\tilde{a} > 0$, and at a_2.

Proof. The Jacobian matrix of system (4.5) is:

$$J = \begin{pmatrix} \beta(\zeta - 2I - (1-\sigma)V) & -(1-\sigma)\beta I & 0 \\ -\varphi(M) - \sigma\beta V & -\varphi(M) - (\mu+\vartheta) - \sigma\beta I & \varphi_1'(M)(1-I-V) \\ ag'(I) & 0 & -a \end{pmatrix}, \quad (4.28)$$

which evaluated at E_e becomes

$$J(E_e) = \begin{pmatrix} -\beta I_e & -(1-\sigma)\beta I_e & 0 \\ -\varphi(g(I_e)) - \sigma\beta\dfrac{\zeta - I_e}{(1-\sigma)} & -\varphi(g(I_e)) - (\mu+\vartheta) - \sigma\beta I_e & \varphi_1'(g(I_e))\left(\dfrac{1 - \sigma\mathcal{R}_0\,(1-I_e)}{\mathcal{R}_0(1-\sigma)}\right) \\ ag'(I_e) & 0 & -a \end{pmatrix},$$

leading to the characteristic polynomial

$$p(\lambda) = \lambda^3 + d_1(a)\lambda^2 + d_2(a)\lambda + d_3(a),$$

with

$$\begin{aligned} d_1(a) &= a + q_2 > 0 \\ d_2(a) &= aq_2 + q_1 \\ d_3(a) &= a\,(q_1 + q_0)\,, \end{aligned}$$

where q_0, q_1, q_2 are given in (4.25), (4.26), (4.27), respectively.

We choose the inverse of the average information delay, a, as bifurcation parameter because it affects the stability but not the existence of endemic equilibria.

By Descartes' rule it follows that the equilibrium E_e is unstable if $d_2(a) \leq 0$ and/or $d_3(a) < 0$. We exclude the case $d_3(a) = 0$ because it corresponds to a bifurcation point. In Section 4.4, we will observe that the pattern of the bifurcation curve suggests that $d_3(a)$ is negative in correspondence of sub–critical endemic equilibria with odd index, in increasing order of infected fraction, and of super–critical endemic equilibria with even index.

Otherwise, if $d_i(a) > 0$ for all i, then E_e is stable, but can loss stability via Hopf bifurcations. More precisely, according to Routh–Hurwitz theorem, E_e will be LAS if and only if $d_1(a)d_2(a) - d_3(a)$ is positive, equivalently written as

$$f(a) = q_2a^2 + (q_2^2 - q_0)a + q_1q_2. \quad (4.29)$$

Thus, if $q_2^2 - q_0 \geq 0$ and $q_1 \geq 0$, then E_e is LAS independently of the delay, otherwise instability is possible.

Stability continues to prevail if the discriminant Δ of $f(a)$ is negative or null.

Whereas, if $\Delta > 0$, there are two distinct solutions $a_1 < a_2$ for the equation $f(a) = 0$. It is easy to prove that at least one between a_1 and a_2 is positive, i.e. there exist one or two meaningful bifurcation values for the delay parameter a. This circumstance happens if:

- $q_1 < 0$, and in this case only a_2 is positive,

or

- $q_1 \geq 0$, and
$$q_2^2 - q_0 < -2q_2\sqrt{q_1}, \tag{4.30}$$
because
$$\Delta = \left(q_2^2 - q_0 - 2q_2\sqrt{q_1}\right)\left(q_2^2 - q_0 + 2q_2\sqrt{q_1}\right).$$
In this case $0 \leq a_1 < a_2$.

Finally, at a_1 and a_2 the test for non-zero speed is fulfilled [148]

$$f'(a)|_{a=a_i} = \pm\sqrt{\Delta} \neq 0.$$

□

Remark 4.9. *It appears interesting to note that* a priori *the occurrence of Hopf bifurcations is feasible also below the threshold $\mathcal{P}_0 = 1$ in presence of sub–critical endemic equilibria. Such possibility will be confirmed by the numerical simulations provided in Section 4.6.*

4.4 Bifurcation curve

In deriving the expression of the bifurcation curve (the graph of I_e as a function of $\mathcal{P}_0$), we consider β as variable with all the other parameters fixed. As $\mathcal{P}_0$ is a constant multiple of β, we can think of β as the independent variable in the bifurcation equation. Implicit differentiation of the equilibrium condition (4.18) with respect to β gives

$$(q_1 + q_0)\,\partial_\beta I_e = \sigma\beta(1 - I_e)I_e^2 + \frac{(\gamma + \mu)\,(\vartheta + \mu + \varphi_0 + \varphi_1(g(I_e)))}{\beta} I_e,$$

with q_0 and q_1 given by (4.25) and (4.26), respectively.

This implies that the bifurcation curve has positive slopes at equilibrium values with $q_1 + q_0 > 0$ and negative slopes at equilibrium values with $q_1 + q_0 < 0$.

Now, observe that

$$q_1 + q_0 = \beta I_e\left(\chi'(I_e) - \psi'(I_e)\right),$$

hence

$$q_1 + q_0 > 0 \iff \psi'(I_e) < \chi'(I_e)$$

and vice versa, where the functions χ and ψ are given in (4.19) and (4.20), respectively.

According to Theorem 4.5, there could exist an interval preceding the threshold $\mathcal{P}_0 = 1$ in which there is a positive even number of EE: $E_1, ..., E_{2n}$, $n \in \mathbb{N}$, with $E_j = (I_j, V_j, M_j)$.

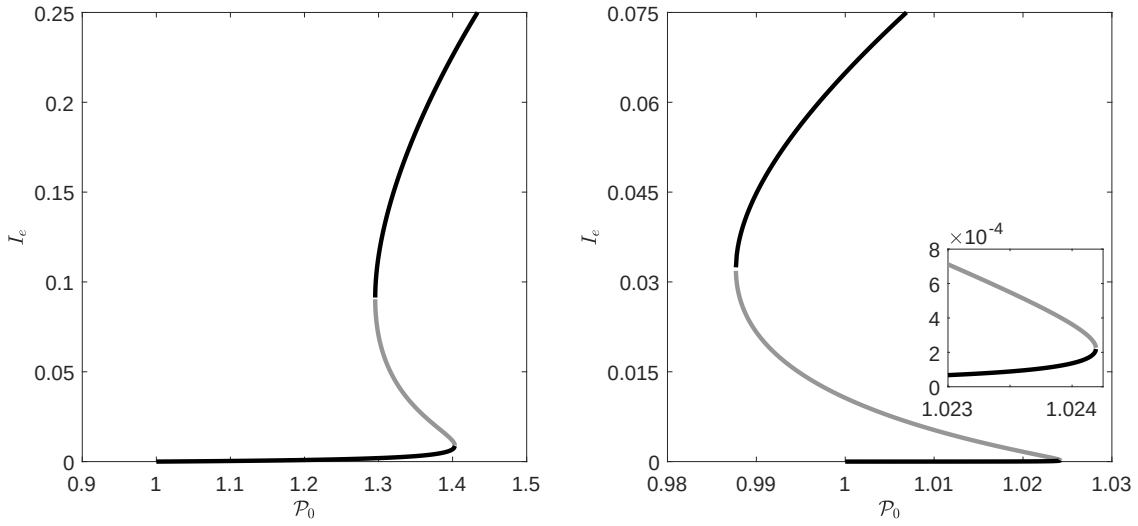

Figure 4.3: Examples of bifurcation curves for model (4.5)–(4.34)–(4.36) in presence of *forward hysteresis* (three super–critical endemic equilibria). Left panel: absence of sub–critical endemic equilibria. Right panel: presence of two sub–critical endemic equilibria. The parameters values are chosen to illustrate the theoretical results and do not refer to specific diseases.

If we order them in increasing size of infected fraction, i.e. $I_j < I_{j+1}$ for all $j = 1, ..., 2n-1$, on the basis of the considerations made in Section 4.3, it is straightforward to realize that $\psi'(I_{2j-1}) > \chi'(I_{2j-1})$ and $\psi'(I_{2j}) < \chi'(I_{2j})$, for $j = 1, ..., n$.

Thus, the bifurcation curve has a negative slope at sub–critical EE with odd index, and a positive slope at those with even index. Instead, for super–critical EE (in increasing order of infected fraction) the situation is reversed: the bifurcation curve has a positive slope at equilibria with odd index (see Figure 4.3, dark lines), and a negative slope at those with even index (see Figure 4.3, gray lines).

4.5 Central manifold analysis

To derive a sufficient condition for the occurrence of a backward or forward bifurcation at $\mathcal{P}_0 = 1$, we can use a bifurcation theory approach. We adopt the approach developed in [69, 116, 287], which is based on the general center manifold theory [148]. In short, it establishes that the normal form representing the dynamics of the system on the central manifold is given by:

$$\dot{u} = b_1 u^2 + b_2 \beta u,$$

where

$$b_1 = \frac{v}{2} \cdot \frac{\partial^2 f}{\partial x^2}(E_0, \beta_c) w^2 = \frac{1}{2} \sum_{k,i,j=1}^{n} v_k w_i w_j \frac{\partial^2 f_k}{\partial x_i \partial x_j}(E_0, \beta_c) \tag{4.31}$$

and

$$b_2 = v \cdot \frac{\partial^2 f}{\partial x \partial \beta}(E_0, \beta_c) w = \sum_{k,i=1}^{n} v_k w_i \frac{\partial^2 f_k}{\partial x_i \partial \beta}(E_0, \beta_c). \tag{4.32}$$

Note that in (4.31) and (4.32) β has been chosen as bifurcation parameter, β_c is the critical value of β, f the right–hand side of system (4.5), $x = (I, V, M)$ the state variables vector,

E_0 the DFE, and v and w denote, respectively, the left and right eigenvectors corresponding to the null eigenvalue of the Jacobian matrix evaluated at critically (at E_0 and $\beta = \beta_c$).

Observe that $\mathcal{P}_0 = 1$ is equivalent to:

$$\beta = \beta_c = (\mu + \gamma)\,\frac{\varphi_0 + \vartheta + \mu}{\sigma\varphi_0 + \vartheta + \mu}$$

so that the disease–free equilibrium is locally stable if $\beta < \beta_c$, and it is unstable when $\beta > \beta_c$.

The direction of the bifurcation occurring at $\beta = \beta_c$ can be derived from the sign of coefficients (4.31) and (4.32). More precisely, if $b_1 > 0$ [resp. $b_1 < 0$] and $b_2 > 0$, then at $\beta = \beta_c$ there is a backward [resp. forward] bifurcation.

For our model, we have the following:

Theorem 4.10. *System (4.5) exhibits a backward [resp. forward] bifurcation at E_0 and $\mathcal{P}_0 = 1$ if*

$$1 - (1-\sigma)\,\frac{\varphi_0^2 + (\vartheta+\mu)\,(\varphi_0 - g'(0)\varphi'(0)) + \varphi_0\sigma\rho(\gamma+\mu)}{(\vartheta+\mu+\varphi_0)^{\,2}} < 0\,[resp. > 0]. \tag{4.33}$$

Proof. The Jacobian matrix (4.28) evaluated at E_0 for $\beta = \beta_c$ becomes:

$$J(E_0,\beta_c) = \begin{pmatrix} 0 & 0 & 0 \\ -\varphi_0 - \dfrac{\sigma\varphi_0(\mu+\gamma)}{(\sigma\varphi_0+\vartheta+\mu)} & -\varphi_0 - (\mu+\vartheta) & \varphi_1'(0)\dfrac{\vartheta+\mu}{(\varphi_0+\vartheta+\mu)} \\ ag'(0) & 0 & -a \end{pmatrix}.$$

Its spectrum is: $\Lambda = \{0, -(\varphi_0+\mu+\vartheta), -a\}$. As expected, it admits a simple zero eigenvalue and the other eigenvalues are real and negative. Hence, when $\beta = \beta_c$ (or, equivalently, when $\mathcal{P}_0 = 1$), the disease–free equilibrium E_0 is a nonhyperbolic equilibrium.

It can be easily checked that a left and a right eigenvector associated with the zero eigenvalue so that $v\cdot w = 1$ are:

$$v = (g'(0), 0, 0)$$
$$w = \left(\frac{1}{g'(0)}, w_2, 1\right)^T,$$

with

$$w_2 = -\frac{\varphi_0^2 + (\vartheta+\mu)\,(\varphi_0 - g'(0)\varphi'(0)) + \varphi_0\sigma\rho(\gamma+\mu)}{g'(0)\,(\vartheta+\mu+\varphi_0)^{\,2}}.$$

The coefficients b_1 and b_2 may be now explicitly computed. Considering only the nonzero components of the eigenvectors and computing the corresponding second derivative of f, it follows that:

$$\begin{aligned} b_1 &= \frac{1}{2}v_1 w_1^2 \frac{\partial^2 f_1}{\partial I^2}(E_0,\beta_c) + v_1 w_1 w_2 \frac{\partial^2 f_1}{\partial I \partial V}(E_0,\beta_c) = \\ &= \frac{1}{2}v_1 w_1^2(-2\beta_c) + v_1 w_1 w_2(-\beta_c\,(1-\sigma)) = -\beta_c\,(w_1 + w_2\,(1-\sigma)) \end{aligned}$$

and

$$b_2 = v_1 w_1 \frac{\partial^2 f_1}{\partial I \partial \beta}(E_0,\beta_c) + v_1 w_2 \frac{\partial^2 f_1}{\partial V \partial \beta}(E_0,\beta_c) = 1 - (1-\sigma)\,\frac{\varphi_0}{\varphi_0+\vartheta+\mu} = \frac{1}{\rho} > 0.$$

Then the local dynamics of the system (4.5) around the equilibrium point E_0 is totally determined by the sign of b_1:

1. if $b_1 > 0$ then, when $\beta < \beta_c$ with $|\beta - \beta_c| \ll 1$, E_0 is locally asymptotically stable, and there exists a positive unstable equilibrium; when $\beta > \beta_c$ with $\beta - \beta_c \ll 1$, E_0 is unstable and there exists a negative and locally asymptotically stable equilibrium.

2. if $b_1 < 0$ then, when $\beta - \beta_c$ changes from negative to positive, E_0 changes its stability from stable to unstable. Correspondingly a negative unstable equilibrium becomes positive and locally asymptotically stable.

More explicitly, system (4.5) exhibits backward [resp. forward] bifurcation at E_0 and $\mathcal{P}_0 = 1$ if

$$w_1 + w_2 (1 - \sigma) < 0 \,[\text{resp.} > 0],$$

which is equivalent to (4.33).

□

4.6 Numerical simulations

In this section we show through numerical simulations that, for suitable values of $\mathcal{P}_0$ smaller than one, model (4.5) may switch from a multistability scenario to long term periodic oscillating dynamics when the bifurcation parameter a varies.

We assume that g depends on prevalence in a linear way:

$$g(I) = kI, \tag{4.34}$$

where k is the *information coverage*. This parameter may be seen as a 'summary' of two opposite phenomena, the disease under–reporting and the level of media coverage of the status of the disease, which tends to amplify the social alarm. The range of variability of k may be restricted to the interval $(0, 1)$ and we take $k = 0.9$. For a detailed discussion on this assumption see [62].

As far as function $\varphi_1(M)$ is concerned, we adopt two different formulations: a saturating Michaelis–Menten function and a linear function.

As regards epidemiological parameter values, we consider a set of parameter values that appear consistent with those of a realistic vaccine–preventable infectious disease. The data are mostly taken from a seasonal influenza scenario [9, 25, 204, 218]. Therefore, it is a purely illustrative choice since model (4.5) may admit, of course, endemic infection and not just single outbreaks as is the case of seasonal influenza.

We take:

$$\begin{aligned} &\beta = 0.999\rho\,(\mu + \gamma) \ \text{days}^{-1},\ \mu = 1/50 \ \text{years}^{-1},\ \varphi_0 = 0.04 \ \text{days}^{-1}, \\ &\gamma \in [1/5, 1/4] \ \text{days}^{-1},\ \vartheta = 1 \ \text{years}^{-1}. \end{aligned} \tag{4.35}$$

We also take $\sigma = 0.15$, namely vaccine administration reduces the transmission rate by 85%. This choice will emphasize one of our main results: a highly (but not totally) effective vaccination is not sufficient by itself to avoid multiple sub–critical endemic equilibria.

In order to investigate the relevant case where the model exhibits a backward bifurcation at E_0 and $\mathcal{P}_0 = 1$ and since in all the ensuing simulations the threshold (let us call it P^*) above which there are sub–critical EE is smaller than 0.999, we finally set β as in (4.35) and hence $\mathcal{P}_0 = 0.999$.

Information dependent vaccination coverage with saturating response

Let $\varphi_1(M)$ be

$$\varphi_1(M) = \frac{CM}{1+DM}, \tag{4.36}$$

with $0 < C \leq D$. As in [113], we set $C = D\,(1-\varphi_0-\varepsilon)$, where $\varepsilon > 0$. This parameterization means an asymptotic overall coverage of $1-\varepsilon$. Here we take $\varepsilon = 0.01$ potentially implying a ceiling of 99% in vaccine uptakes under circumstances of high perceived risk. The ensuing vaccination coverage function is:

$$\varphi_1(M) = (1-\varphi_0-\varepsilon)\,\frac{DM}{1+DM}.$$

By making these choices, equation (4.18) becomes cubic in I and its solutions can be explicitly computed by standard formulas for third–degree equations.

Without going into details, we note that, when a backward bifurcation occurs at $\mathcal{P}_0 = 1$, there are exactly two sub–critical endemic equilibria. As far as super–critical endemic equilibria, the possibility of three EE is not excluded by deriving necessary conditions. Indeed, equation (4.18) can be rewritten as

$$a_0 + a_1 I + a_2 I^2 + a_3 I^3 = 0,$$

with

$$\begin{aligned}
a_0 &= (\vartheta+\mu+\sigma\varphi_0)\left(\frac{1}{\mathcal{P}_0}-1\right)\\
a_1 &= \vartheta+\mu+\sigma\varphi_0 + (Dk(\vartheta+\mu)+\beta\sigma)\left(\frac{1}{\mathcal{R}_0}-1\right) + Dk(1-\varepsilon)\left(\frac{1}{\mathcal{R}_0}-\sigma\right)\\
a_2 &= \beta\sigma + Dk\,(\vartheta+\mu+\sigma(1-\varepsilon)) + Dk\beta\sigma\left(\frac{1}{\mathcal{R}_0}-1\right)\\
a_3 &= Dk\beta\sigma > 0.
\end{aligned}$$

By Descartes' rule of signs it follows that necessary conditions for the existence of three real positive roots are:

$$\begin{aligned}
&a_0 < 0 \iff \mathcal{P}_0 > 1\\
&a_1 > 0 \iff \rho\,(Dk(\vartheta+\mu+\sigma(1-\varepsilon)) + \beta\sigma - (\vartheta+\mu+\sigma\varphi_0))\,\mathcal{P}_0 < Dk(\vartheta+\mu+1-\varepsilon)+\beta\sigma\\
&a_2 < 0 \iff \rho\,(Dk\beta\sigma - \beta\sigma - Dk\,(\vartheta+\mu+\sigma(1-\varepsilon)))\,\mathcal{P}_0 > Dk\beta\sigma,
\end{aligned}$$

and they are satisfiable for appropriate values of $\mathcal{P}_0$.

Two examples of bifurcation curves in the case of forward hysteresis (multiple super–critical endemic equilibria) are depicted in Figure 4.3.

As mentioned above, our main purpose is to numerically derive the dynamics of the disease transmission below the critical threshold $\mathcal{P}_0 = 1$. In particular, we focus on the onset of information–induced oscillations via Hopf bifurcations of an endemic state when system exhibits a backward bifurcation at E_0 and $\mathcal{P}_0 = 1$.

For numerical tests we use the parameters baseline values listed in (4.35), among which we fix $\gamma = 1/4$ days^{-1}. In order to choose an appropriate value for D, we rewrite the backward condition (4.33) as:

$$D < -\frac{(\vartheta+\mu)^2 + \varphi_0\,(\vartheta+\mu+\sigma\,(\vartheta+\mu+\varphi_0-(\gamma+\mu)\rho(1-\sigma)))}{(\vartheta+\mu)(1-\sigma)k\,(1-\varphi_0-\varepsilon)} = D_c.$$

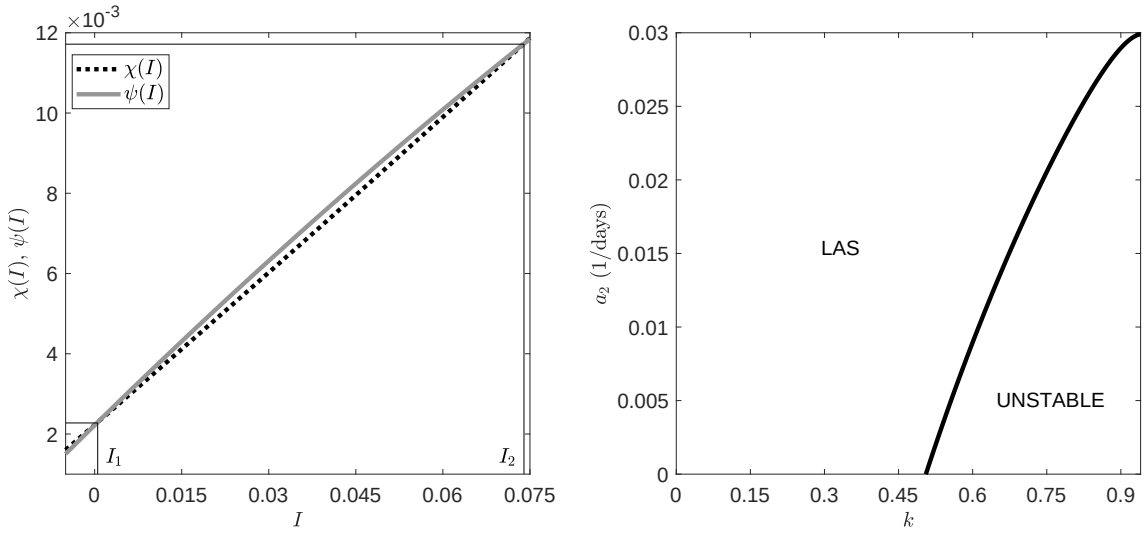

Figure 4.4: Left panel: intersection points of functions $\chi(I)$ and $\psi(I)$, given in (4.19) and (4.20), assuming (4.34) and (4.36). Right panel: the local stability properties of the endemic equilibrium E_2 of model (4.5)–(4.34)–(4.36) in the plane $[a_2, k]$, where a_2 is the positive solution of $f(a) = 0$, with $f(a)$ given in (4.29); Hopf bifurcations occur at the points of the plotted curve. Numerical values for the parameters are indicated in (4.35) or in the text.

We obtain that $D_c \approx 2.870$ and hence finally set $D = 2.5$.

Left panel of Figure 4.4 depicts functions $\chi(I)$ and $\psi(I)$, given in (4.19) and (4.20), whose two intersection points are the two sub–critical endemic infected states: $I_1 < I_2$.

As analytically predicted, the endemic equilibrium E_1 (corresponding to I_1) is unstable. Whereas, stability of endemic equilibrium E_2 (corresponding to I_2) depends on the sign of $f(a)$, with $f(a)$ given in (4.29). Precisely, $f(a) < 0$ for $a \in (0, a_2)$, with $a_2 \approx 2.896 \times 10^{-2}$ days^{-1}, namely a Hopf bifurcation occurs at $a = a_2$, so that E_2 changes its stability from stable to unstable when a drops below a_2. Right panel of Figure 4.4 illustrates the shape of bifurcation locus $[a_2, k]$, where a_2 is the positive solution of $f(a) = 0$. If the circulating information is not sufficiently 'honest' ($k < k_c \approx 0.505$) the delay in communication does not affect the stability of the endemic state. Conversely, when $k \geq k_c$, a_2 decreases until it is null by decreasing k, namely the shorter the time delay $1/a$ the higher the chances of avoiding destabilization.

Now, let use denote with $\tilde{E} = (\tilde{I}, \tilde{V})$ the stable endemic equilibrium of the system:

$$\begin{aligned} \dot{I} &= [\beta(1 - I) - (\mu + \gamma) - (1 - \sigma)\beta V]\, I \\ \dot{V} &= \varphi_0(1 - I - V) - (\vartheta + \mu + \sigma\beta I)V. \end{aligned} \tag{4.37}$$

This system has been studied in [45] and can be obtained from the first two equations of (4.5) when $\varphi(M) = \varphi_0$ in (4.2) (that is, the public is not influenced by information). By using the same parameter values of Figure 4.4, system (4.37) too exhibits a backward bifurcation.

In Figure 4.5 it is shown the oscillatory dynamics as predicted by the behavioral model (4.5)–(4.34)–(4.36) for $a \in (0, a_2)$. Two relevant initial conditions are employed: the first one (pictures on the top row) is set on the limit cycle and the second one (see bottom row) is on the plane $M = 0$ and corresponds to $\tilde{E}$. In the latter case, the limit cycle is approached from outside, after a long transient period. The long term dynamics of infected individuals is given by oscillations between 6.8% and 8% of the total population with a period of about 1.5 years.

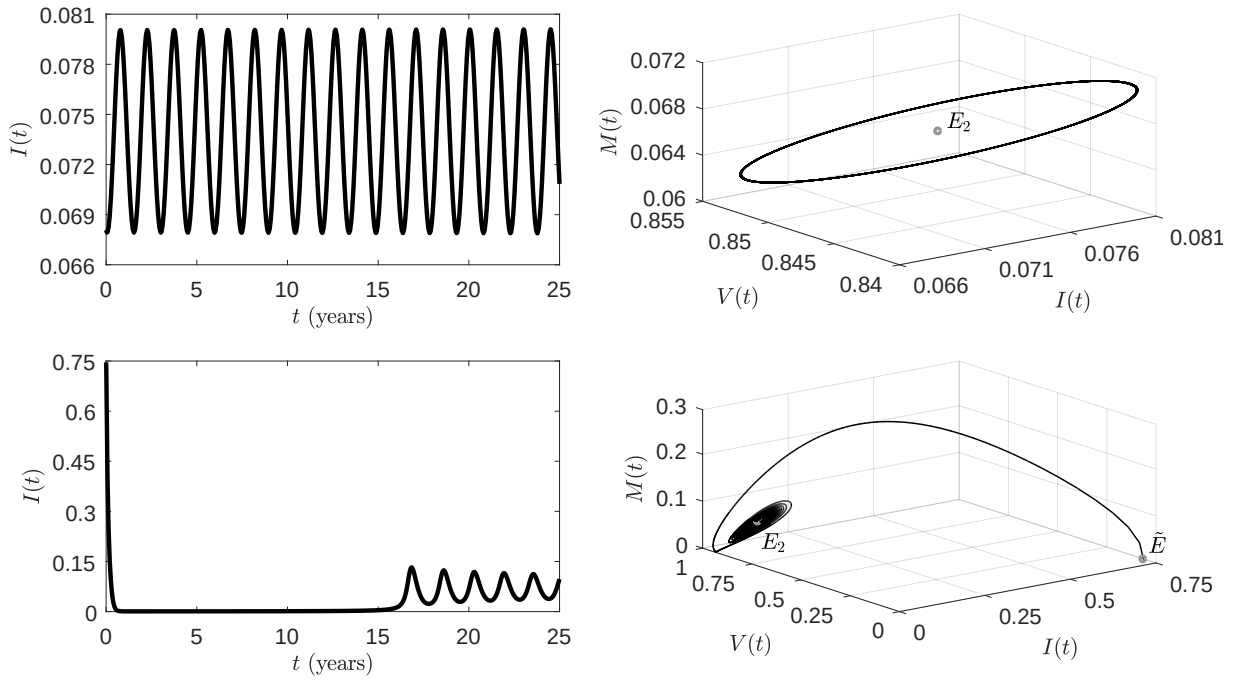

Figure 4.5: Dynamics of the fraction of infected individuals (left panels) and phase portrait (right panels) as predicted by model (4.5)–(4.34)–(4.36), assuming $\gamma = 1/4$ days^{-1}, $D = 2.5$, and $a = 0.994a_2$. Top row: dynamics with initial conditions at a point of the limit cycle. Bottom row: dynamics with initial conditions at the stable endemic equilibrium $\tilde{E}$ of model (4.37) on the plane $M = 0$. The other parameter values are indicated in (4.35) or in the text.

Further attention requires the disease dynamics illustrated in the bottom row of Figure 4.5. Assume that the disease dynamics is following an orbit of system (4.37) approaching the stable endemic equilibrium $\tilde{E}$. At a given time $\tilde{t}$, that for simplicity we assume $\tilde{t} = 0$, the vaccination rate switches from constant value $\varphi = \varphi_0$ to the function $\varphi = \varphi_0 + \varphi_1(M)$, where M is given by (4.3). The ensuing dynamics will be totally different, both qualitatively (oscillatory vs steady) and quantitatively ($I \sim (0.068, 0.080)$ vs $I \equiv 0.746$ about). Namely, due to the higher propensity to vaccinate, much lower prevalence level will be observed, and oscillations will take place.

Information dependent vaccination coverage with linear response

Let $\varphi_1(M)$ be

$$\varphi_1(M) = qM, \tag{4.38}$$

with $0 < q \leq (1 - \varphi_0)/(k\zeta)$, ensuring that $\varphi(M) \leq 1$ (see (4.9)).

Despite less realistic than the previous one (4.36), such a formulation could be a local approximation to more general coverage functions. Further, it allows us to apply Proposition 4.6 (see also Remark 4.7), which ensures that, if a backward bifurcation occurs at E_0 and $\mathcal{P}_0 = 1$, there are exactly two sub–critical endemic equilibria, coincident at $\mathcal{P}_0 = P^*$. Whereas, for $\mathcal{P}_0 > 1$, there is a unique EE.

In performing numerical simulations, we set $q = (0.99 - \varphi_0)/(k\zeta)$, implying a maximum vaccination coverage of 99% at $I = \zeta$, and the other parameter values as listed in (4.35). Among the latter, we fix $\gamma = 1/5$ days^{-1}.

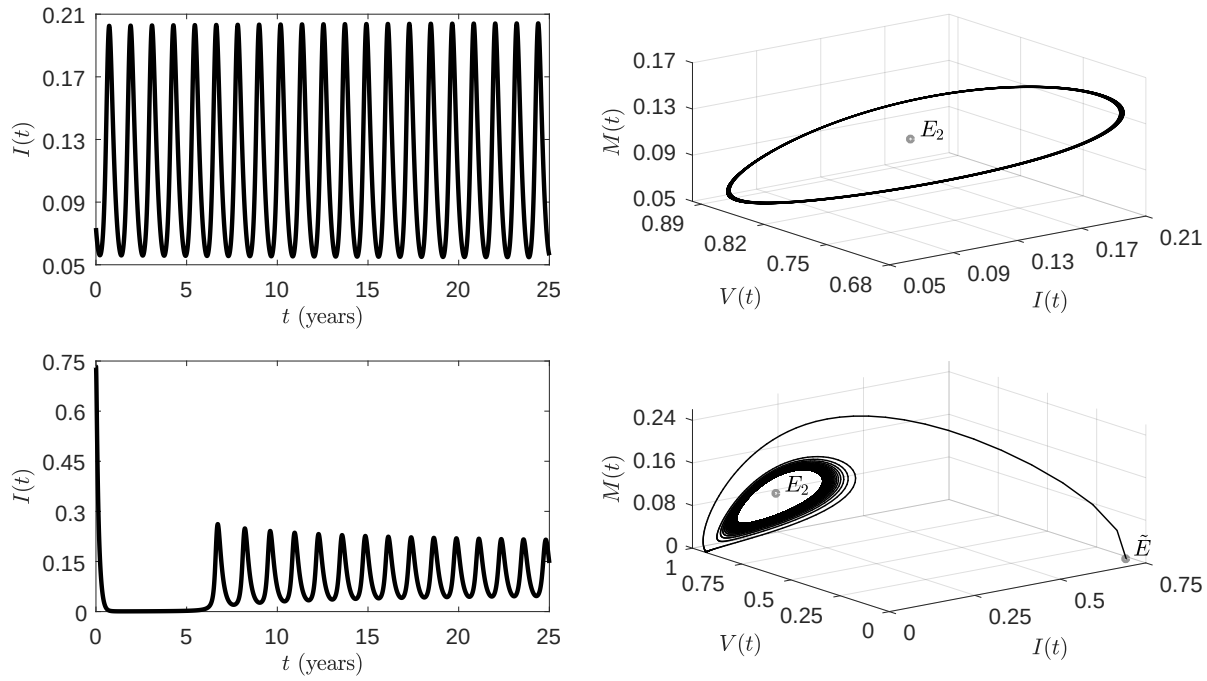

Figure 4.6: Dynamics of the fraction of infected individuals (left panels) and phase portrait (right panels) as predicted by model (4.5)–(4.34)–(4.38), assuming $\gamma = 1/5$ days^{-1} and $a = 0.994a_2$. Top row: dynamics with initial conditions at a point of the limit cycle. Bottom row: dynamics with initial conditions at the stable endemic equilibrium $\tilde{E}$ of model (4.37) on the plane $M = 0$. The other parameter values are indicated in (4.35) or in the text.

As shown in Figure 4.6, the ensuing results are qualitatively similar to those obtained in the previous subsection. Namely, the system admits two sub–critical EE, the greater (in terms of the infected compartment) of them destabilizes via Hopf bifurcation when a significantly decreases (drops below $a_2 \approx 1.856 \times 10^{-2}$ days^{-1}), giving rise to stable oscillations.

4.7 Discussion and conclusions

The aim of this study is to explore the qualitative dynamics of a vaccine–preventable disease, when the healthy individuals in a given community are subject to two coexisting threats: the imperfection of the vaccine and the voluntary (non–)adherence to immunization programs.

In the literature, these two aspects, taken individually, have been widely studied through mathematical models and, generally speaking, the relative studies have enlightened the dangerous implications on the public health: vaccine–induced imperfect and waning immunity is positively associated to the onset of bistability through backward bifurcations [45, 150, 192, 268]. Whereas, individual behavioral vaccinating responses may trigger complicate dynamic patterns, including oscillations [63, 113, 114]. However, only recently attempts to incorporate both the aspects into the same model are arising [110, 194].

In this study, we faced the issue by using a behavioral epidemic model including a partially effective vaccination at all ages. The vaccination rate of susceptibles depends on the current and the past history of the disease prevalence in the population and the weight given to the

past history is described by an exponential kernel.

The model dynamics presents both the possibility of backward bifurcation at $\mathcal{P}_0 = 1$, where $\mathcal{P}_0$ denotes the basic reproduction number, and that of oscillations triggered by behavioral memory. However, two noteworthy aspects arose:

i) multiple but odd endemic states are possible for $\mathcal{P}_0 > 1$ (see Theorem 4.5). This hysteresis scenario is consistent with the dynamics observed for the SISV model of imperfect and prevalence–dependent newborns vaccination studied in [110];

ii) a stable endemic state may destabilize via Hopf bifurcations (see Theorem 4.8). The Hopf bifurcation may occur not only when $\mathcal{P}_0 > 1$ but also when $\mathcal{P}_0 < 1$, depending on the interplay between the inverse of the average information delay a and the information coverage k.

Thus, the spectrum of possible dynamical patterns appears much more diversified compared with that of models including the imperfect vaccine but not behavioral aspects [45] or vice versa [63]. From the empirical point of view, it means new and threatening risks, otherwise neglected: namely, until (and whether) the elimination threshold is ultimately reached, disease prevalence may not only undergo sudden and dramatic jumps due to multistability, but also fall in a cyclic regime, which reflects the realistic alternation of 'races to vaccination', in epochs of social alarm, and of abstention, otherwise.

As a further support to our findings, it must say that they appear in line with those arising by different approaches. More precisely, in [237] an SISV model with imperfect vaccination is formulated on an adaptive network framework. In such a case human response is modeled through a mechanism of rewiring of susceptible nodes to avoid contacts with the infected ones. The ensuing analysis and simulations reveal a bifurcation structure very similar to that of our model, including regions of bistability and of periodic oscillations. Periodicity arising from Hopf bifurcations, but not multiple endemic states, is instead predicted by the time–delayed epidemic model with awareness [3], including waning vaccine–induced immunity. Here, unaware susceptibles become aware thanks to global information campaigns, contacts with aware individuals and reported cases of infection. Destabilization of the unique endemic equilibrium is triggered by the time lag between individuals awareness and consequent responses.

We acknowledge that this is just a further step in shaping the complex problem of the interaction of vaccine effectiveness and human choices. For example, in this direction, real data on vaccinating attitudes could be useful in designing behavior–dependent vaccination uptake functions.

Chapter 5

Modeling social behavior changes during COVID–19 lockdowns

The COVID–19 pandemic that started in China in December 2019 has not only threatened world public health, but severely impacted almost every facet of life, including behavioral and psychological aspects.

In this chapter, we focus on the role played by the 'human element' and propose a detailed mathematical model specific to investigate the effects on the COVID–19 epidemic of social behavioral changes in response to lockdowns. We consider an Susceptible–Exposed–Infected–Recovered–like epidemic model where the contact and quarantine rates depend on the available information and rumors about the disease status in the community.

The model is applied to the case of the first COVID–19 epidemic wave in Italy. We consider the period that stretches between February 24, 2020, when the first bulletin by the Italian Civil Protection was reported and May 18, 2020, when the lockdown restrictions were mostly removed. The role played by the information–related parameters is determined by evaluating how they affect suitable outbreak–severity indicators. We estimate that citizen compliance with mitigation measures played a decisive role in curbing the epidemic curve by preventing a duplication of deaths and about 46% more infections. The results of this study have been published in [60].

5.1 Background

In December 2019, the Municipal Health Commission of Wuhan, China, reported to the World Health Organization a cluster of viral pneumonia of unknown aetiology in Wuhan City, Hubei province. On January 9, 2020, the China CDC reported that the respiratory disease, later named COVID–19, was caused by the novel coronavirus SARS–CoV–2 [288]. The outbreak of COVID–19 rapidly expanded from Hubei province to the rest of China and then to other countries. Finally, it developed in a devastating pandemic affecting almost all the countries of the world [70]. As of November 28, 2020 a total of more than 62 million cases of COVID–19 and 1,453,128 related deaths were reported worldwide [70].

In the absence of a treatment or a vaccine, the mitigation strategies enforced by many countries during the COVID–19 pandemic were based on social distancing. Each government enacted a series of restrictions affecting billions of people, including recommendation of restricted movements for some or all of their citizens, and localized or national lockdown with the partial or full closing–off of non–essential companies and manufacturing plants [50].

Italy was the first European country affected by COVID–19. It was strongly hit by the epidemic which triggered strict restrictions aimed at minimizing the spread of the coronavirus. The actions enacted by the Italian government began at the end of February 2020 with reducing social interactions through quarantine and isolation and rapidly culminated in a *full lockdown* [5, 168]. On May 4, 2020, the *phase two* began, marking a gradual reopening of the economy and limitations easing for residents. This breathing space ended towards the second half of August 2020, when the virus regained strength and progressively grew its prevalence. This marked the arrival of the ongoing* second epidemic wave, characterized by the introduction of both nationwide and community–based restrictive measures [4].

During the period that stretches between January 22, 2020 and November 28, 2020, Italy suffered 1,564,532 official COVID–19 cases and 54,363 deaths [171].

The scientific community promptly reacted to the COVID–19 pandemic. Since the early stage of the pandemic a number of mathematical models and methods was used. Among

*December 2020.

the main concerns were: predicting the evolution of the COVID–19 pandemic worldwide or in specific countries [102, 126, 140]; predicting epidemic peaks and intensive care unit (ICU) accesses [276]; assessing the effects of containment measures [23, 102, 126, 135, 140] and, more generally, assessing the impact on populations in terms of economics, societal needs, employment, health care, death toll, etc [118, 183].

Among the mathematical approaches used, many authors relied on deterministic compartmental models. This approach was successful for reproducing epidemic curves in the past SARS–CoV outbreak in 2002–2003 [151]. Specific studies were focused on the case of the COVID–19 epidemic in Italy: Gatto *et al.* [135] studied the transmission between a network of 107 Italian provinces by using an SEPIA model as a core model. Their SEPIA model discriminates between infectious individuals depending on presence and severity of their symptoms. They examined the effects of the intervention measures in terms of the number of averted cases and hospitalizations in the period February 22 – March 25, 2020. Giordano *et al.* [140] proposed a very detailed model, named SIDARTHE, in which the distinction between diagnosed and non–diagnosed individuals plays an important role. They predicted the course of the epidemic and showed the need to use testing and contact tracing combined with social distancing measures.

The mitigation measures for COVID–19 like social distancing, quarantine and self–isolation were encouraged or mandated [126]. Although the vast majority of people have followed the rules, even in this last case there were many reports of people breaching restrictions [49, 281]. Local authorities needed to continuously verifying compliance with mitigation measures through monitoring by health officials and police actions (checkpoints, use of drones, fine or jail threats, etc). This behavior might be related to costs that individuals affected by epidemic control measures paid in terms of health, including loss of social relationships, psychological pressure, increasing stress and health hazards resulting in a substantial damage to population well–being [51, 118].

Modeling the interplay between human behavior and the spread of infectious diseases is a topic of increasing interest [130, 289] and includes recent models focusing on COVID–19. For example, Acuña–Zegarra *et al.* [2] assumed that sanitary emergency measures are implemented at a given time, after which the population splits in two distinct subpopulations depending on whether they adhere or do not adhere to the measures. Inspired by the behavioral economic model by Chen *et al.* [80], an Susceptible–Exposed–Infectious–Removed (SEIR) model was proposed by Suwanprasert [278] where individuals are allowed to optimally choose their public avoidance actions in response to COVID–19 risk.

In this study, the change in social behavior is described by employing the method of information–dependent models [210, 293] which is based on the introduction of a suitable *information index* (see Section I.4). This method has been applied to vaccine–preventable childhood diseases [113, 293] and is increasingly being used (see [59, 319] for very recent contributions).

The main goal here is to assess the effects on the COVID–19 epidemic of human behavioral changes during the lockdowns. To this aim we build an information–dependent SEIR–like model which is based on the key assumption that the choice to respect the lockdown restrictions, specifically the social distance and the quarantine, is partially determined on a fully voluntary basis and depends on the available rumors and information concerning the spread of the COVID–19 disease in the community.

A second goal of this study is to provide an application of the information index to a specific field–case, where the model is parameterized and the solutions are compared with official data.

We focus on the case of the first COVID–19 epidemic wave in Italy during the period that begins on February 24, 2020, when the first bulletin by the Italian Civil Protection was reported [171], includes the partial and full lockdown restrictions, and ends on May 18, 2020, when the lockdown restrictions were mostly (but just temporally) removed. We stress the role played by circulating information by evaluating the absolute and relative variations of disease–severity indicators as functions of the information–related parameters.

5.2 Model formulation

State variables and balance equations

We assume that the total population N is divided into seven disjoint compartments: susceptible S, exposed E, post–latent I_p, asymptomatic/mildly symptomatic I_m, severely symptomatic (hospitalized) I_s, quarantined Q and recovered R (therefore $N = S + E + I_p + I_m + I_s + Q + R$).

The model is given by the following system of nonlinear ordinary differential equations, where each *balance equation* rules the rate of change of a state variable.

$$\dot{S} = \Lambda - \beta(M)\frac{S}{N-Q}\left(\varepsilon_p I_p + \varepsilon_m I_m + \varepsilon_s I_s\right) - \mu S \tag{5.1a}$$

$$\dot{E} = \beta(M)\frac{S}{N-Q}\left(\varepsilon_p I_p + \varepsilon_m I_m + \varepsilon_s I_s\right) - \rho E - \mu E \tag{5.1b}$$

$$\dot{I}_p = \rho E - \eta I_p - \mu I_p \tag{5.1c}$$

$$\dot{I}_m = p\eta I_p - \chi(M) I_m - \sigma_m I_m - \gamma_m I_m - \mu I_m \tag{5.1d}$$

$$\dot{I}_s = (1-p)\eta I_p + \sigma_m I_m + \sigma_q Q - \gamma_s I_s - \alpha I_s - \mu I_s \tag{5.1e}$$

$$\dot{Q} = \chi(M) I_m - \sigma_q Q - \gamma_q Q - \mu Q \tag{5.1f}$$

$$\dot{R} = \gamma_m I_m + \gamma_s I_s + \gamma_q Q - \mu R. \tag{5.1g}$$

The state variables and the processes included in the model are illustrated in the flow chart in Fig. 5.1. In Tables 5.1 and 5.2, we provide a description for each parameter.

The model formulation is described in detail in the next subsections.

The role of information

We assume that the final choice to adhere or not to adhere to lockdown restrictions is partially determined on a fully voluntary basis and depends on the available information concerning the spread of the disease in the community.

The information is mathematically represented by an *information index* $M(t)$ (see Section I.4 for the general definition), which summarizes the information about the current and past values of the disease [59, 109, 113] and is given by the following distributed delay

$$M(t) = \int_{-\infty}^{t} k\left(Q(\tau) + I_s(\tau)\right) Erl_{1,a}(t-\tau)d\tau.$$

This formulation may be interpreted as follows: the first order Erlang distribution $Erl_{1,a}$ represents an exponentially fading memory[†] (see (I.12) with $n = 1$), where the parameter

[†]Note that the same kernel was adopted in the model of Chapter 4 (Section 4.2).

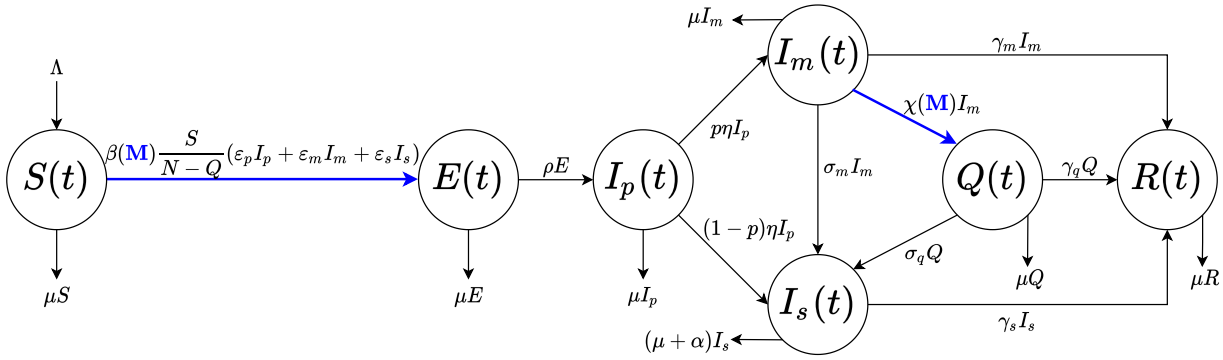

Figure 5.1: Flow chart for the COVID–19 model (5.1)–(5.2). The population $N(t)$ is divided into seven disjoint compartments of individuals: susceptible $S(t)$, exposed $E(t)$, post–latent $I_p(t)$, asymptomatic/mildly symptomatic $I_m(t)$, severely symptomatic (hospitalized) $I_s(t)$, quarantined $Q(t)$ and recovered $R(t)$. Blue color indicates the information–dependent processes in model (see (5.4)–(5.5)–(5.6), with $M(t)$ ruled by (5.2)).

a is the inverse of the average time delay T_a of the collected information, so $T_a = a^{-1}$. We assume that people react in response to information and rumors regarding the daily number of quarantined and hospitalized individuals. The *information coverage* k is assumed to be positive and $k \leq 1$, which mimics the evidence that COVID–19 official data could be under–reported in many cases [126, 198].

With this choice, by applying the linear chain trick [207], we obtain the differential equation ruling the dynamics of M:

$$\dot{M} = a\left(k(Q + I_s) - M\right). \tag{5.2}$$

Formulation of the balance equations

Here we derive in details each balance equation of model (5.1).

Equation (5.1a): Susceptible individuals, $S(t)$
Susceptibles are the individuals who are healthy but can contract the disease. The susceptible population increases by the net inflow Λ, incorporating both new births and immigration, and decreases by natural death – with natural death rate μ – and following infection.

It is believed that COVID–19 is primarily transmitted from symptomatic people (mildly or severely symptomatic). In particular, although severely symptomatic individuals are isolated from the general population by hospitalization, they are still able to infect hospitals and medical personnel [18, 131] and, in turn, give rise to transmission from hospital to the community. The pre–symptomatic transmission (i.e. the transmission from infected people before they develop significant symptoms) is also relevant: specific studies revealed an estimate of 44% of secondary cases during the pre–symptomatic stage from index cases [158]. The importance of the asymptomatic transmission (i.e. the contagion from a person infected with COVID–19 who does not develop symptoms) is a controversial matter [17,308]. However, available evidence suggests that asymptomatic individuals are much less likely to transmit the virus [312]. We also assume that quarantined individuals are fully isolated and therefore unable to transmit the disease.

In summary, the compartments of individuals capable to transmit the disease are I_p, I_s and I_m, which contains not only asymptomatic but also mildly symptomatic individuals.

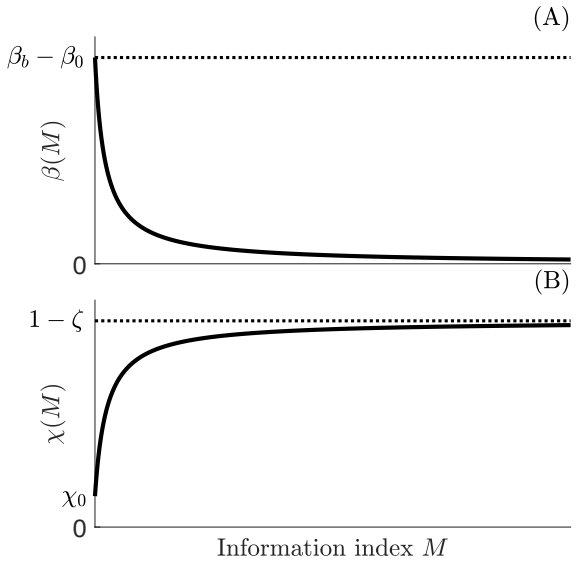

Figure 5.2: Representative shapes of the transmission rate (panel A) and the quarantine rate (panel B) as functions of the information index M.

The routes of transmission from COVID–19 patients as described above are included in the *Force of Infection* (FoI) function, i.e. the per capita rate at which susceptibles contract the infection. Quarantine at home during the lockdown led to the substantial separation of quarantined individuals from the general population. For this reason, we consider the quarantine–adjusted FoI [161], given by:

$$\text{FoI} = \beta(M)\frac{\varepsilon_p I_p + \varepsilon_m I_m + \varepsilon_s I_s}{N - Q}.$$

The transmission coefficients for I_p, I_m and I_s are given by $\varepsilon_p\beta(M)$, $\varepsilon_m\beta(M)$ and $\varepsilon_s\beta(M)$, respectively, with $0 \leq \varepsilon_p, \varepsilon_m, \varepsilon_s < 1$.

The function $\beta(M)$, which models how the information affects the transmission rate, is defined as a piecewise–continuous, differentiable and decreasing function of the information index M, with $\beta(\max(M)) > 0$. We assume that

$$\beta(M) = \pi\left(c_b - c_0 - c_1(M)\right), \tag{5.3}$$

where π is the probability of getting infected during a person–to–person contact and c_b is the baseline contact rate. In (5.3) we represent the reduction in social contacts through the sum of two social distancing contact rates: the constant rate c_0, which represents the choice of social distancing due to the restrictive measures imposed by the government, and an information–dependent voluntary rate $c_1(M)$, with $c_1(\cdot)$ increasing with M and $c_1(0) = 0$. In order to guarantee the positiveness, we assume $c_b > c_0 + \max(c_1(M))$. Following [109], we finally set

$$\beta(M) = \frac{\beta_b - \beta_0}{1 + \delta M}, \tag{5.4}$$

namely $\pi c_b = \beta_b$ (baseline transmission rate), $\pi c_0 = \beta_0$ (mandatory social distancing transmission rate) and $\pi c_1(M) = \delta M(\beta_b - \beta_0)/(1 + \delta M)$, where δ is a positive constant tuning the reactivity factor of voluntary change in contact patterns. For illustrative purposes, see Fig. 5.2.

Equation (5.1b): Exposed individuals, $E(t)$

Exposed (or latent) individuals are COVID–19 infected but are not yet infectious, i.e. capable of transmitting the disease to others. Such individuals arise as the result of new infections of susceptible individuals. The population is diminished by development at the infectious stage (at rate ρ) and natural death.

Equation (5.1c): Post–latent individuals, $I_p(t)$

We assume that after the end of the latency period, the individuals enter in a phase where they are infectious and asymptomatic. We call this phase *post–latency* [66] (other authors call it *pre–symptomatic* phase [135] or *prodromic* phase [102]). Post–latent individuals belong to two groups: a *truly asymptomatic* group $p_a I_p$ (people that have no symptoms throughout the course of the disease) and a *pre–symptomatic* group $(1-p_a)I_p$ (people who develop symptoms at the end of such a phase). The latter, in turn, splits into two subgroups: $p_m(1-p_a)I_p$ will develop mild symptoms, and $(1-p_m)(1-p_a)I_p$ will develop severe symptoms. In our model, we take $p = p_a + p_m(1-p_a)$. Post–latent individuals diminish due to natural death or because they enter the compartment of asymptomatic/mildly symptomatic individuals I_m (at a rate $p\eta$) or that of severely symptomatic individuals I_s (at a rate $(1-p)\eta$).

Equation (5.1d): Asymptomatic/mildly symptomatic individuals, $I_m(t)$

This compartment includes both the asymptomatic individuals, that is infected individuals who do not develop symptoms, and mildly symptomatic individuals [135]. Mildly symptomatic individuals are the only symptomatic individuals that move freely (as far as they can). There is no clear evidence of the relevance of asymptomatic individuals in the COVID–19 transmission. However, asymptomatic individuals test positive in screenings (pharyngeal swabs) and therefore are a part of the count of official diagnoses. Members of this class come from the post–latent stage and get out due to quarantine (at an information–dependent rate $\chi(M)$), worsening symptoms (at rate σ_m), recovery (at rate γ_m) and natural death.

Equation (5.1e): Severely symptomatic individuals (Hospitalized), $I_s(t)$

Severely symptomatic individuals are isolated from the general population by hospitalization. They arise: i) as consequence of the development of severe symptoms by mild illness (the infectious of the class I_m or the quarantined Q); ii) directly from the fraction $1-p$ of post–latent individuals that rapidly develop severe illness. This class diminishes by recovery (at rate γ_s), natural death and disease–induced death (at rate α).

Equation (5.1f): Quarantined individuals, $Q(t)$

Quarantined individuals Q are those who are separated from the general population.

The basic idea is to characterize the quarantined compartment in a way that its temporal evolution can be compared with official data. Therefore we assume that quarantined individuals are asymptomatic/mildly symptomatic individuals. As a matter of fact, the Italian government daily released the number of detected COVID–19 positive cases, which was approximately given by quarantined at home and hospitalized individuals. Self–isolation of susceptible and post–latent individuals is implicitly incorporated in the social distancing term. As for exposed individuals, the permanence in that class is shorter than the infectious classes, hence the potential self–isolation effect of this population on the model dynamics is considered negligible here. We point out that other compartments, like the susceptible or the exposed compartments, could be also split into quarantined and

non–quarantined individuals (see e.g. [228]).

Quarantined individuals diminish by natural death, aggravation of symptoms (at rate σ_q, so that they move to I_s) and recovery (at a rate γ_q).

Quarantine may arise in two different ways. On one hand, individuals may be detected by health authorities and daily checked. Such health active surveillance ensures also that the quarantine is, in some extent, respected. On the other hand, a fraction of quarantined individuals chooses self–isolation since they are confident in the government handling of the crisis or just believe the public health messaging and act in accordance [20].

We assume that the final choice to respect or not respect the self–quarantine depends on the awareness about the status of the disease in the community. Therefore, we define the information–dependent quarantine rate as follows:

$$\chi(M) = \chi_0 + \chi_1(M), \tag{5.5}$$

where the rate χ_0 mimics the fraction of the asymptomatic/mildly symptomatic individuals I_m that has been detected through screening tests and is 'forced' to home isolation. The rate $\chi_1(M)$ represents the undetected fraction of individuals that adopt quarantine by voluntary choice as result of the influence of the circulating information M. The function $\chi_1(\cdot)$ is required to be a piecewise–continuous, differentiable and increasing function w.r.t. M, with $\chi_1(0) = 0$. As in [59, 113], we set

$$\chi_1(M) = (1 - \chi_0 - \zeta)\frac{DM}{1 + DM}, \tag{5.6}$$

where D is a positive constant tuning the reactivity factor of voluntary quarantine, and ζ is a constant such that $0 < \zeta < 1 - \chi_0$. The quantity $1 - \chi_0 - \zeta$ is the value of the quarantine rate by voluntary choices $\chi_1(M)$ that can be reached in the case of a high level of circulating information (i.e. a high level of social alarm, ideally represented by $M \to +\infty$). This means that the total quarantine rate $\chi(M) = \chi_0 + \chi_1(M)$ reaches a ceiling value of $1 - \zeta$ under circumstances of very high perceived risk. A representative trend of $\chi(M)$ is displayed in Fig. 5.2.

Equation (5.1g): Recovered individuals, $R(t)$

After the infectious period, individuals from the compartments I_m, I_s and Q recover at rates γ_m, γ_s and γ_q, respectively. Natural death is also considered. We assume that recovered individuals acquire long lasting immunity against COVID–19, although this is a currently debated question (as of May 22, 2020) and there is still no evidence that COVID–19 antibodies protect from re–infection [311].

5.3 The reproduction numbers

A frequently used indicator for measuring the potential spread of an infectious disease in a community is the basic reproduction number, $\mathcal{R}_0$ (see Section I.1 for the general definition). If the system incorporates control strategies, then the corresponding quantity is named the *control reproduction number* and is usually denoted by $\mathcal{R}_C$ (obviously, $\mathcal{R}_C < \mathcal{R}_0$). In this specific case, if $\beta(M) = \beta_b$ and $\chi(M) = 0$ in (5.1)–(5.2), namely when containment interventions are not enacted, we obtain the expression of $\mathcal{R}_0$; otherwise, the corresponding $\mathcal{R}_C$ can be computed.

Following the procedure and the notations adopted by Diekmann *et al.* [103] and Van den Driessche and Watmough [287], we derive the control reproduction number, $\mathcal{R}_C$. Let us consider the r.h.s. of equations (5.1b)–(5.1c)–(5.1d)–(5.1e)–(5.1f) (the balance equations for the infected compartments), and distinguish the new infections appearance from the other rates of transfer, by defining the vectors

$$\mathcal{F} = \begin{pmatrix} \beta(M)\dfrac{S}{N-Q}(\varepsilon_p I_p + \varepsilon_m I_m + \varepsilon_s I_s) \\ 0 \\ 0 \\ 0 \\ 0 \end{pmatrix}$$

and

$$\mathcal{V} = \begin{pmatrix} (\rho+\mu)E \\ -\rho E + (\eta+\mu)I_p \\ -p\eta I_p + (\chi(M)+\sigma_m+\gamma_m+\mu)I_m \\ -(1-p)\eta I_p - \sigma_m I_m - \sigma_q Q + (\gamma_s+\alpha+\mu)I_s \\ -\chi(M)I_m + (\sigma_q+\gamma_q+\mu)Q \end{pmatrix}.$$

The Jacobian matrices of $\mathcal{F}$ and $\mathcal{V}$ evaluated at model (5.1)–(5.2) disease–free equilibrium

$$DFE = \left(\frac{\Lambda}{\mu}, 0, 0, 0, 0, 0, 0, 0\right)$$

read, respectively,

$$F = \begin{pmatrix} 0 & (\beta_b-\beta_0)\varepsilon_p & (\beta_b-\beta_0)\varepsilon_m & (\beta_b-\beta_0)\varepsilon_s & 0 \\ 0 & 0 & 0 & 0 & 0 \\ 0 & 0 & 0 & 0 & 0 \\ 0 & 0 & 0 & 0 & 0 \\ 0 & 0 & 0 & 0 & 0 \end{pmatrix}$$

and

$$V = \begin{pmatrix} \rho+\mu & 0 & 0 & 0 & 0 \\ -\rho & \eta+\mu & 0 & 0 & 0 \\ 0 & -p\eta & \chi_0+\sigma_m+\gamma_m+\mu & 0 & 0 \\ 0 & -(1-p)\eta & -\sigma_m & \gamma_s+\alpha+\mu & -\sigma_q \\ 0 & 0 & -\chi_0 & 0 & \sigma_q+\gamma_q+\mu \end{pmatrix}.$$

The control reproduction number is given by the spectral radius of the *next generation* matrix FV^{-1} [103, 287]. It is easy to check that FV^{-1} has positive elements on the first row, being the other ones null. Thus, $\mathcal{R}_C = (FV^{-1})_{11}$, yielding

$$\mathcal{R}_C = (\beta_b-\beta_0)\rho\left[\frac{\varepsilon_p}{B_1B_2} + \frac{\varepsilon_m p\eta}{B_1B_2B_4} + \frac{\varepsilon_s(1-p)\eta}{B_1B_2B_6} + \frac{\varepsilon_s p\eta\sigma_m}{B_1B_2B_4B_6} + \frac{\varepsilon_s p\eta\chi_0\sigma_q}{B_1B_2B_4B_5B_6}\right], \quad (5.7)$$

with $B_1 = \rho+\mu$, $B_2 = \eta+\mu$, $B_4 = \chi_0+\sigma_m+\gamma_m+\mu$, $B_5 = \sigma_q+\gamma_q+\mu$, $B_6 = \gamma_s+\alpha+\mu$. Similarly one can prove that the basic reproduction number is given by

$$\mathcal{R}_0 = \beta_b\rho\left[\frac{\varepsilon_p}{B_1B_2} + \frac{\varepsilon_m p\eta}{B_1B_2B_3} + \frac{\varepsilon_s(1-p)\eta}{B_1B_2B_6} + \frac{\varepsilon_s p\eta\sigma_m}{B_1B_2B_3B_6}\right], \quad (5.8)$$

Parameter	Description	Baseline value
t_0	Initial simulation time	February 24, 2020
T	Final simulation time	May 18, 2020
$S(t_0)$	Initial number of susceptible individuals	$60.357 \cdot 10^6$
$E(t_0)$	Initial number of exposed individuals	$1.695 \cdot 10^3$
$I_p(t_0)$	Initial number of post–latent individuals	308.8
$I_m(t_0)$	Initial number of asymptomatic/mildly symptomatic individuals	462.4
$I_s(t_0)$	Initial number of severely symptomatic (hospitalized) individuals	127.4
$Q(t_0)$	Initial number of quarantined individuals	93.7
$R(t_0)$	Initial number of recovered individuals	311.1
$M(t_0)$	Initial value of the information index	101.9
Λ	Net inflow of susceptibles	$1.762 \cdot 10^3$ days^{-1}
μ	Natural death rate	$1.07 \cdot 10^{-2}$ years^{-1}
$\mathcal{R}_0$	Basic reproduction number	3.49
β_b	Baseline transmission rate	2.25 days^{-1}
β_0	Mandatory social distancing transmission rate	$0 - 0.74\beta_b$
ε_p	Modification factor w.r.t. transmission from I_p	1
ε_m	Modification factor w.r.t. transmission from I_m	0.033
ε_s	Modification factor w.r.t. transmission from I_s	0.034
ρ	Latency rate	1/5.25 days^{-1}
η	Post–latency rate	1/1.25 days^{-1}
p	Fraction of post–latent individuals developing no/mild symptoms	0.92
χ_0	Mandatory quarantine rate	0.057 days^{-1}
σ_m	Rate at which members of I_m class hospitalize	0.044 days^{-1}
σ_q	Rate at which quarantined individuals hospitalize	0.001 days^{-1}
α	Disease–induced death rate	0.022 days^{-1}
γ_m	Recovery rate for asymptomatic/mildly symptomatic individuals	0.145 days^{-1}
γ_s	Recovery rate for severely symptomatic (hospitalized) individuals	0.048 days^{-1}
γ_q	Recovery rate for quarantined individuals	0.035 days^{-1}

Table 5.1: Temporal horizon, initial conditions and epidemiological parameters values for model (5.1)–(5.2).

with $B_3 = \sigma_m + \gamma_m + \mu = B_4 - \chi_0$. The first two terms in the r.h.s. of (5.7) describe the contributions of post–latent infectious and asymptomatic/mildly symptomatic infectious, respectively, to the production of new infections close to the disease–free equilibrium. The third, the fourth and the fifth term in (5.7) represent the contribution of infectious with severe symptoms. The severe symptoms can onset soon after the post–latent phase (third term) or after a mildly symptomatic phase (fourth term). In case of quarantine, severe symptoms can onset also during such a stage (fifth term). Note that the last term is missing in the basic reproduction number (5.8), where the possibility for people to be quarantined is excluded. Note also that $\mathcal{R}_C = \mathcal{R}_0$ when $\beta_0 = \chi_0 = 0$.

5.4 Parameterization

Numerical simulations are performed in MATLAB [216]. We use the `ode45` solver for integrating the system and the platform–integrated functions for getting the plots.

The epidemiological parameters of the model as well as their baseline values are reported in Table 5.1. In the same table, simulation time frame and initial conditions are given. A detailed derivation of such quantities is reported in the next subsections.

Epidemiological parameters

As done by Gumel *et al.* [151], we adopt an SEIR–like model with demography and constant net inflow of susceptibles Λ. Including a net inflow of susceptible individuals into the model allows to consider not only new births (which can be assumed to be approximately constant due to the short time span of our analysis), but also immigration, which played a role during the lockdown in Italy. Therefore, the net inflow of susceptibles is given by

$$\Lambda = b\bar{N} + \Lambda_0. \tag{5.9}$$

In (5.9), the parameter Λ_0 is the inflow term due to immigration and $b\bar{N}$ is the inflow term due to births, where b is the birth rate and $\bar{N}$ denotes the total population at the beginning of the epidemic.

The most recent data by the Italian National Institute of Statistics [166] refer to January 1, 2019 and provide a country–level birth rate $b = 7.2/1,000$ years^{-1} and a natural death rate $\mu = 10.7/1,000$ years^{-1}, as well as a resident population of about

$$\bar{N} \approx 60.360 \cdot 10^6 \tag{5.10}$$

inhabitants. Fluctuations in a time window of just over a year are considered negligible. Since global travel restrictions were implemented during the COVID–19 epidemic outbreak [314], we assume that the immigration inflow term Λ_0 accounts only of repatriation of citizens to their countries of origin (Italy in that case) due to the COVID–19 pandemic [121]. In all airports, train stations, ports and land borders travellers' health conditions have been tested via thermal scanners. Although the effectiveness of such screening method is largely debated [248], for the sake of simplicity, we assume that the inflow enters only the susceptible compartment. On the basis of data communicated by the Italian Ministry of Foreign Affairs and International Cooperation [169], a reasonable value for Λ_0 seems to be $\Lambda_0 = 4,000/7$ days^{-1}, namely the average number of repatriated citizens was 4,000 *per* week. Being $\Lambda = b\bar{N} + \Lambda_0$, we finally obtain $\Lambda \approx 1.762 \cdot 10^3$ days^{-1}.

Epidemiological data are based on the current estimates disseminated by national and international health organizations [120, 126, 167, 172, 309, 310] or inferred by modeling studies [102,135,182]. More precisely, the median incubation period is estimated to be from $5 - 6$ days, with a range from $1 - 14$ days, and identification of the virus in respiratory tract specimens occurs $1 - 2$ days before the onset of symptoms [120, 309]. Hence, we set the latency (ρ) and post–latency (η) rates to $1/5.25$ days^{-1} and $1/1.25$ days^{-1}, respectively. From [135], the specific baseline transmission rates for the post–latent ($\varepsilon_p\beta_b$), asymptomatic/mildly symptomatic ($\varepsilon_m\beta_b$) and severely symptomatic ($\varepsilon_s\beta_b$) cases are such that $\varepsilon_m/\varepsilon_p = 0.033$ and $\varepsilon_s/\varepsilon_m = 1.03$. They are in accordance with the observation of high viral load close to symptoms onset (suggesting that SARS–CoV–2 can be easily transmissible at an early stage of infection), and with the absence of reported significant difference in viral load in asymptomatic and symptomatic patients [120]. We set $\beta_b = 2.25$ days^{-1}, which, together with the other parameters, leads to the basic reproduction number $\mathcal{R}_0 \approx 3.49$, a value falling within the ranges estimated in several sources [120, 126, 135, 309].

As made by Kantner and Koprucki [182], we consider that just 8% of infectious individuals shows serious symptoms immediately after the incubation phase, yielding $p = 0.92$. Nonetheless, people with initial mild symptoms may become seriously ill and develop breathing difficulties, requiring hospitalization. It is estimated that about 1 in 5 people with COVID–19 shows a worsening of symptoms [172] within $4 - 5$ days from

onset [167], giving $\sigma_m = 0.2/4.5 \approx 0.044$ days^{-1}. Instead, the possibility that the aggravation happens during the quarantine period is assumed to be more rare: $\sigma_q = 0.001$ days^{-1}.

Governmental efforts in identifying and quarantining positive cases have been implemented since the early stage of epidemics (at February 24, 2020, 94 quarantined people were already registered [171]), hence we consider the daily mandatory quarantine rate of asymptomatic/mildly symptomatic individuals (χ_0) positive for the whole time horizon. From current available data, it seems hard to catch an uniform value for χ_0 because it largely depends on the sampling effort, namely the number of specimen collections (swabs) from persons under investigation, that varied considerably across Italian regions and in the different phases of the outbreak [167, 171]. Since our model does not account for such territorial peculiarities and in order to reduce the number of parameters to be estimated, we assume that $\chi_0 = 1.3\sigma_q$, namely it is 30% higher than the daily rate at which members of the I_m class hospitalize, yielding $\chi_0 \approx 0.057$ days^{-1}.

Following the approach adopted by Gumel *et al.* [151] for a SARS–CoV epidemic model, based on the formula given by Day [95], we estimate the disease–induced death rate as

$$\alpha = (1 - \mu\Theta)\frac{X}{\Theta},$$

where X is the case fatality and Θ is the expected time from hospitalization until death. From [167], we approximate $X = 13\%$ and $\Theta = 6$ days (it is 9 days for patients that were transferred to intensive care and 5 days for those were not), yielding $\alpha \approx 0.022$ days^{-1}. Similarly, the recovery rates γ_j with $j \in \{m, q, s\}$ are estimated as

$$\gamma_j = (1 - \mu\Theta_j)\frac{1 - X}{\Theta_j},$$

where Θ_j is the expected time until recovery or expected time in quarantine/hospitalization. Preliminary data indicate that the virus can persist for up to eight days from the first detection in moderate cases and for longer periods in more severe cases [120], suggesting $\Theta_m = 6$ days is an appropriate value. As far as the time spent in hospitalization or quarantine is concerned, in the lack of exact data we assume $\Theta_s < \Theta_q$ because hospitalized individuals are likely to receive a partly effective, experimental treatment: mainly antibiotics, antivirals and corticosteroids [167]. Moreover, shortages in hospital beds and ICUs led to as prompt as possible discharge [122]. In particular, we set $\Theta_s = 18$ and $\Theta_q = 25$ days, by accounting also for prolonged quarantine time due to delays in test response (if any) and for WHO recommendations of an additional two weeks in home isolation even after symptoms resolve [310].
Crucially, we also estimate the initial exponential rate of case increase (say, g_0), by computing the dominant eigenvalue of the system's Jacobian matrix, evaluated at the disease–free equilibrium. It provides $g_0 \approx 0.247$ days^{-1}, in accordance to that given by Gatto *et al.* [135].

The effects of the lockdown on transmission

We explicitly reproduce in our simulations the effects of the restrictions posed to human mobility and human–to–human contacts in Italy during the first epidemic wave. Their detailed sequence is summarized as follows.

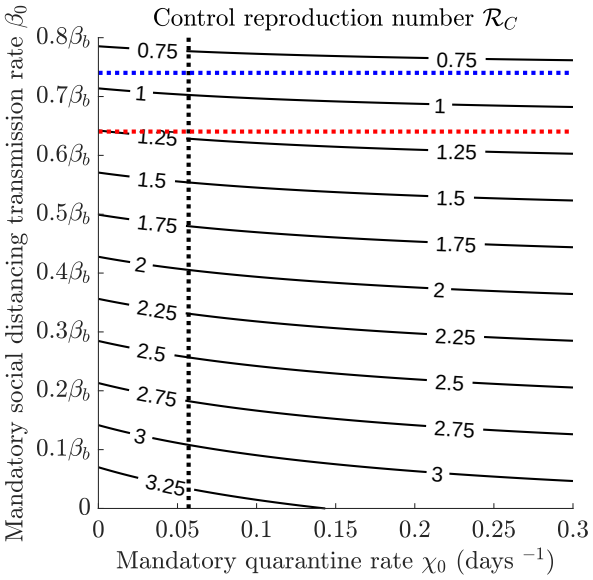

Figure 5.3: Contour plot of the control reproduction number (5.7) versus mandatory quarantine and social distancing transmission rates. Intersection between dotted black and red [resp. blue] lines indicates the value after the first [resp. second] step reduction. Other parameters values are given in Table 5.1.

After the first officially confirmed case (the so–called 'patient one') on February 21, 2020 in the Lodi province, several suspected cases emerged in the south and southwest of the Lombardy region. A 'red zone' encompassing 11 municipalities was instituted on February 22 and put on lockdown to contain the emerging threat. On March 8, the red zone was extended to the entire Lombardy region and 14 more northern Italian provinces, while the rest of Italy implemented social distancing measures. A leak of a draft of this decree prompted a panic reaction with massive movement of people towards Italian regions, especially from the north to the south [282]. The next day, a decree evocatively entitled 'I'm staying at home' was signed: the lockdown was declared for the whole country with severe limitations to mobility and other progressively stricter restrictions.

Soon after, on March 11, 2020, the lockdown was enforced with all commercial and retail businesses – except those providing essential services – closed down [168]. Finally, on March 22, 2020, the *phase one* of restrictions was completed when a *full* lockdown was imposed by closing all non–essential companies and industrial plants [5]. On May 4, Italy entered the *phase two*, representing the starting point of a gradual relaxation of the restriction measures. One week later, shops also reopened and the restrictions on mobility were essentially eliminated, with the only obligation in many regions to use protective masks[‡] [170].

Because data early in an epidemic are inevitably incomplete and inaccurate, our approach has been to try to focus on what we believe to be the essentials in formulating a simple model. Keeping this in mind, we assume that the disease transmission rate incurs in just two step reductions (modeled by the mandatory social distancing transmission rate β_0 in (5.4)), corresponding to

- March 12 (day 17), i.e. after the first rapid succession of lockdown decrees, which cumulatively resulted in a sharp decrease of SARS–CoV–2 transmission;

[‡]This until the emerging of the second epidemic wave.

- March 23 (day 28), that is the starting date of the *full* lockdown that definitely impacted the disease incidence.

In the wake of [126, 140], we account for a first step reduction by 64% (that is $\beta_b - \beta_0|_{17\leq t<28} = 0.36\beta_b$), which drops the control reproduction number (5.7) close to 1 (see Fig. 5.3, dotted black and red lines). It is then strengthened by about an additional 28%, resulting in a global reduction by 74% ($\beta_b - \beta_0|_{t\geq 28} = 0.26\beta_b$) that definitely brings $\mathcal{R}_C$ below 1 (see Fig. 5.3, dotted black and blue lines).

Information–dependent parameters

The information–related parameter values are reported in Table 5.2 together with their baseline values.
Following [59, 113], we set $\zeta = 0.01$ days^{-1} potentially implying an asymptotic quarantine rate of 0.99 days^{-1} if we could let M go to $+\infty$. As mentioned in Section 5.2, the positive constants δ and D tune the information–dependent *reactivity*. In particular, δ is the reactivity factor of voluntary changes in contact pattern by susceptible and infectious individuals; D is the reactivity factor of voluntary quarantine by individuals with no or mild symptoms. Since the variability of contact rate is strongly affected by limitations imposed by government decrees, we assume that the reactivity in choosing self–isolation in response to information is greater than the reactivity in reducing contacts, that is $D > \delta$.

The range of values for the information coverage k and the average time delay of information $T_a = a^{-1}$ are mainly assumed or taken from papers where the information index M is used [55, 59, 109, 113]. The information coverage k may be seen as a 'summary' of two opposite phenomena: the disease under–reporting, and the level of media coverage of the status of the disease, which tends to amplify the social alarm. It is assumed to range from a minimum of 0.2 (i.e. the public awareness is 20%) to 1. The average time delay of information T_a ranges from the case of prompt communication (say, $T_a = 1$ days) to the case of large delay (say, $T_a = 60$ days).

The baseline values of the parameters δ, D, k and a are obtained by comparing the model solutions with the official data regarding the number of hospitalized individuals (I_s), the number of quarantined individuals (Q) and the cumulative deaths as released every day since February 24, 2020 by the Italian Civil Protection Department and archived on GitHub [171].
We get $\delta = 6 \cdot 10^{-7}$ and $D = 9 \cdot 10^{-6}$. With this choice, numerical simulations not displayed here show that the maximum order of magnitude reached by the information index M in the time span considered is equal to 10^5. Moreover, we obtain $k = 0.8$ and $T_a = 3$ days, meaning a level of awareness about the daily number of quarantined and hospitalized individuals of 80%, resulting from the balance between underestimates and media amplification and inevitably affected by rumors and misinformation spreading on the web (the so–called 'infodemic' [254]). Such awareness is not immediate, but information takes on average 3 days to be publicly disseminated, the communication being slowed by a series of articulated procedures: timing for swab tests results, notification of cases, reporting delays between surveillance and public health authorities, and so on.

Of course, parameters setting is influenced by the choice of curves to fit. Available data seem to provide an idea about the number of identified infectious people who have developed mild/moderate symptoms (the fraction that mandatorily stays in Q) or more severe symptoms (the hospitalized, I_s) and the number of deaths, but much less about those asymptomatic or with very mild symptoms who are not always subjected to a screening test.

Parameter	Description	Baseline value
δ	Reactivity factor of voluntary change in contact patterns	$6 \cdot 10^{-7}$
D	Reactivity factor of voluntary quarantine	$9 \cdot 10^{-6}$
ζ	$1-\zeta$ is the ceiling of overall quarantine rate	0.01 days^{-1}
a	Inverse of the average information delay T_a	1/3 days^{-1}
k	Information coverage	0.8

Table 5.2: Information–dependent parameters values for model (5.1)–(5.2).

Initial conditions

In order to provide appropriate initial conditions, we consider the official national data at February 24, 2020 archived on [171]. In particular, we take the number of mandatorily quarantined individuals (at that time, they coincide with Q being the voluntary component negligible) and the hospitalized people (I_s). Then, we use system (5.1)–(5.2) to simulate the temporal evolution of the epidemics prior to February 24, by imposing an initial condition of one exposed case Δt_0 days before in a population of $\bar{N}$ individuals, with $\bar{N}$ given in (5.10). We assume $\beta_0 = 0$ and χ_0 as in Table 5.1 (no social distance restrictions were initially implemented, but quarantine efforts were active since then) and disregard the effect of information on the human social behaviors in this phase ($\delta = D = 0$ in (5.1)–(5.2)). The length of temporal interval Δt_0 is tuned in order to reproduce the official values released for Q and I_s at February 24 and provide estimations for the other state variables, as reported in Table 5.1. We obtain $\Delta t_0 = 31.9$, indicating that the virus circulated since the end of January, as predicted also by Gatto *et al.* [135] and Giordano *et al.* [76].

5.5 Numerical results

Let us consider the time frame $[t_0, t]$, where $t_0 \leq t \leq T$. We consider two relevant quantities, the *cumulative incidence* $\mathrm{CI}(t)$, i.e. the total number of new cases in $[t_0, t]$, and the *cumulative deaths* $\mathrm{CD}(t)$, i.e. the disease–induced deaths in $[t_0, t]$.

For model (5.1)–(5.2) we have, respectively:

$$\mathrm{CI}(t) = \int_{t_0}^{t} \beta(M(\tau)) \frac{S(\tau)}{N(\tau) - Q(\tau)} \left(\varepsilon_p I_p(\tau) + \varepsilon_m I_m(\tau) + \varepsilon_s I_s(\tau)\right) d\tau,$$

where $\beta(M)$ is given in (5.4), and

$$\mathrm{CD}(t) = \int_{t_0}^{t} \alpha I_s(\tau) d\tau.$$

In Fig. 5.4 the time evolution in $[t_0, T]$ of $\mathrm{CI}(t)$ and $\mathrm{CD}(t)$ is shown (panels A and D), along with that of quarantined individuals $Q(t)$ (panel B) and hospitalized individuals $I_s(t)$ (panel C). The role played by information on the public compliance with mitigation measures is stressed by the comparison of the baseline scenario with the *unresponsive* case ($\delta = D = 0$ in (5.1)–(5.2)), that is the case when circulating information does not affect disease dynamics. Corresponding dynamics are labelled by black solid and red dashed lines, respectively.

In the unresponsive case, the cumulative incidence is much less impacted by the lockdown restrictions in comparison with the baseline scenario ($11.45 \cdot 10^5$ vs $7.85 \cdot 10^5$ on May 18). Furthermore, in this case the quarantined individuals given by the model are only those that choose self–isolation when 'forced' by public health authorities after detection. That

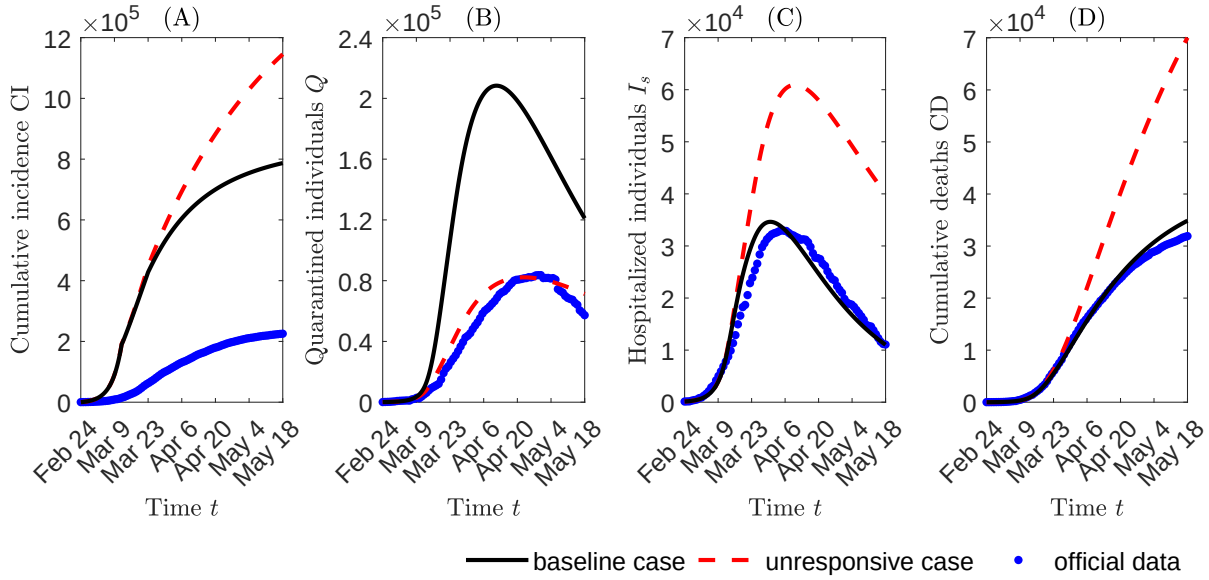

Figure 5.4: Epidemic evolution predicted by model (5.1)–(5.2): Cumulative incidence (panel A), quarantined individuals (panel B), hospitalized individuals (panel C) and cumulative deaths (panel D). The predicted evolution (black solid lines) is compared with the unresponsive case $\delta = D = 0$ (red dashed lines) and with official data (blue dots). Parameter values are given in Tables 5.1 and 5.2.

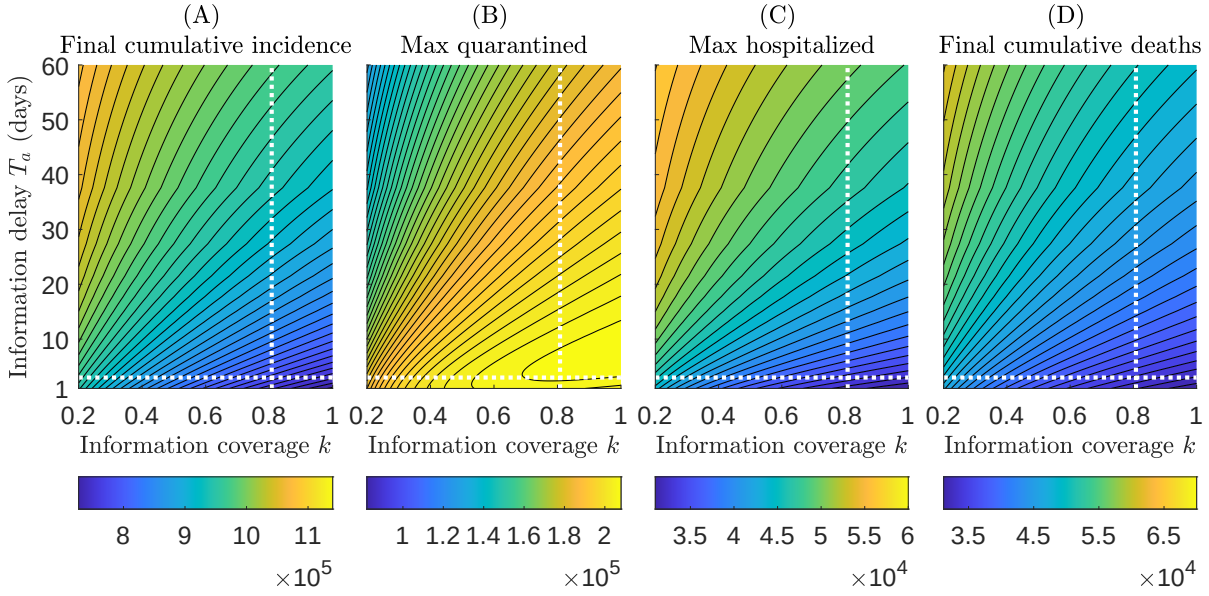

Figure 5.5: Contour plots of relevant quantities versus information coverage k and average delay $T_a = a^{-1}$. Panel A: cumulative incidence CI(T) evaluated at the last day of the considered time frame, i.e. $T = 85$, corresponding to May 18, 2020. Panel B: peak of quarantined individuals max(Q). Panel C: peak of hospitalized individuals max(I_s). Panel D: final cumulative deaths CD(T). The intersection between dotted white lines indicates the values corresponding to the baseline scenario $k = 0.8$, $T_a = 3$ days. Other parameter values are given in Tables 5.1 and 5.2.

is to say, the quarantined individuals predicted by the model reduce to those ones officially detected (i.e. what is counted in the official data). As a consequence, the *peak* of hospitalized

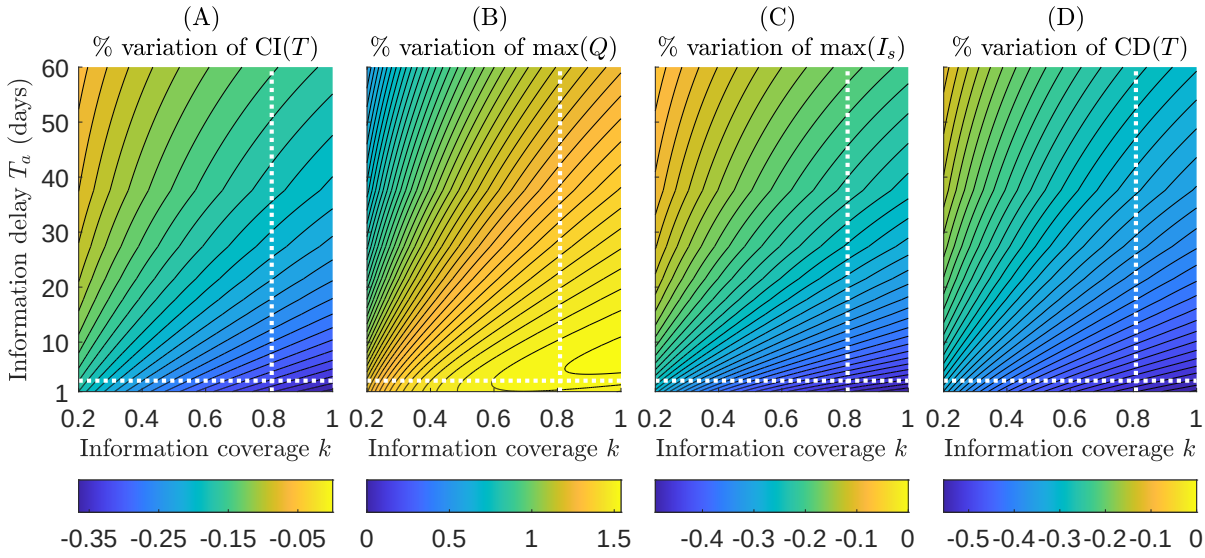

Figure 5.6: Contour plots of the percentage relative change w.r.t the unresponsive case $\delta = D = 0$ versus information coverage k and average delay $T_a = a^{-1}$. Panel A: cumulative incidence CI(T) evaluated at the last day of the considered time frame, i.e. $T = 85$, corresponding to May 18, 2020. Panel B: peak of quarantined individuals max(Q). Panel C: peak of hospitalized individuals max(I_s). Panel D: final cumulative deaths CD(T). The intersection between dotted white lines indicates the values corresponding to the baseline scenario $k = 0.8$, $T_a = 3$ days. Other parameter values are given in Tables 5.1 and 5.2.

patients is about 77% higher and 10 days time–delayed, with a corresponding increase in cumulative death of more than 100%. For all reported dynamics, the deviation between the baseline and the unresponsive case starts to be clearly distinguishable after the first step reduction of 64% in transmission rate (on March 12).
Trends are also compared with officially disseminated data [171] (Fig. 5.4, blue dots), which seem to conform accordingly for most of the time horizon, except for CI, which suffers from an inevitable and probably high underestimation [126, 135, 140, 198]. As of May 18, 2020, we estimate about 785,000 infections, whereas the official count of confirmed infections is 225,886 [171].

We now investigate how the information parameters k and a may affect the epidemic course. More precisely, we assess how changing these parameters affects some relevant quantities: the *peak* of quarantined individuals max(Q) (i.e., the maximum value reached by the quarantined curve in $[t_0, T]$), the peak of hospitalized individuals max(I_s), the cumulative incidence CI(T) evaluated at the last day of the considered time frame, i.e. $T = 85$ (corresponding to May 18, 2020), and the final cumulative deaths CD(T).

The results are shown in the contour plots in Fig. 5.5. As expected, CI(T), max(I_s) and CD(T) decrease proportionally to the information coverage k and inversely to the information delay T_a: they reach the minimum for $k = 1$ and $T_a = 1$ days. Differently, the quantity max(Q) may not monotonically depend on k and T_a as it happens for $k \geq 0.6$ and $T_a \leq 15$ days (see Fig. 5.5B, lower right corner). In such parameter region, for a given value of k [resp. a] there are two different values of a [resp. k] which correspond to the same value of max(Q). The absolute maximum ($\max_{[k,T_a]}(\max(Q))$) is obtained for $k = 1$ and $T_a \approx 7$ days. Note that the pair of values $k = 1$, $T_a = 1$ days corresponds to the less severe outbreak, but not with the highest peak of quarantined individuals.

Case	CI(T)	RCI(T)	max(Q)	Rmax(Q)	max(I_s)	Rmax(I_s)	CD(T)	RCD(T)
$\delta = D = 0$	$11.45 \cdot 10^5$	0	$0.82 \cdot 10^5$	0	$6.09 \cdot 10^4$	0	$7.00 \cdot 10^4$	0
$k = 0.8$ $T_a = 3$ d	$7.85 \cdot 10^5$	-0.31	$2.08 \cdot 10^5$	1.53	$3.45 \cdot 10^4$	-0.43	$3.48 \cdot 10^4$	-0.50
$k = 1$ $T_a = 1$ d	$7.27 \cdot 10^5$	-0.37	$2.05 \cdot 10^5$	1.49	$3.10 \cdot 10^4$	-0.49	$3.12 \cdot 10^4$	-0.55
$k = 0.2$ $T_a = 60$ d	$10.83 \cdot 10^5$	-0.05	$1.30 \cdot 10^5$	0.58	$5.70 \cdot 10^4$	-0.06	$6.21 \cdot 10^4$	-0.11

Table 5.3: Exact and relative values of final cumulative incidence CI(T), the peak of quarantined individuals max(Q), the peak of hospitalized individuals max(I_s), and final cumulative deaths CD(T), for three combinations of information parameters k and T_a (second to fourth row), in comparison with the unresponsive case: $\delta = D = 0$ in (5.1)–(5.2) (first row). Other parameters values are given in Tables 5.1 and 5.2.

In what follows, we compare the relative changes for these quantities w.r.t the unresponsive case. In other words, we introduce the index

$$\mathrm{R}Y = \frac{Y - Y^0}{Y^0},$$

which measures the percentage *relative* change of $Y \in \{\mathrm{CI}(T), \max(Q), \max(I_s), \mathrm{CD}(T)\}$ w.r.t the corresponding quantity Y^0 predicted by model (5.1)–(5.2) with $\delta = D = 0$.

All the possible values arising in the parameter ranges $k \in [0.2, 1]$ and $T_a \in [1, 60]$ days are shown in Fig. 5.6. However, we report in Table 5.3 the results corresponding to the unresponsive case and to three example responsive cases, the baseline and two extremal ones:

(i) the baseline scenario $k = 0.8$, $T_a = 3$ days, which is close to the best possible fitting with official data, given the model and the considered parameter ranges;

(ii) the case of highest information coverage and lowest information delay, $k = 1$, $T_a = 1$ days;

(iii) the case of lowest information coverage and highest information delay, $k = 0.2$, $T_a = 60$ days.

Compared with the baseline scenario, a more accurate and faster communication (case (ii)) would drive to a significant reduction of CI(T), max(I_s) and CD(T) (more precisely, by 37%, 49% and 55%, respectively, see Table 5.3, third row). Moreover, even the worst possible information–based scenario (case (iii)) is significantly better than the unresponsive case (compare first and fourth rows in Table 5.3).

As mentioned above, information and rumors regarding the status of the disease in the community affect the transmission rate $\beta(M)$ (as given in (5.4)) and the quarantine rate $\chi(M)$ (as given in (5.5)).

In our last simulation we want to emphasize the role of the information coverage on the quarantine and transmission rates. In Fig. 5.7 a comparison with the case of low information coverage, $k = 0.2$, is given assuming a fixed information delay $T_a = 3$ days (blue dotted lines). It can be seen that more informed people react and quarantine: an increasing of the maximum quarantine rate from 0.32 to 0.69 days^{-1} (which is also reached a week earlier) can be observed when increasing the value of k to $k = 1$ (Fig. 5.7B).

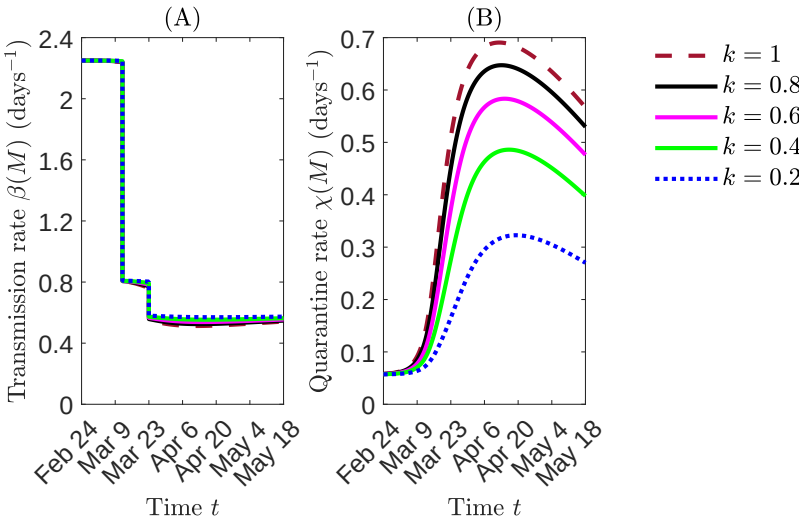

Figure 5.7: Time evolution of the transmission rate (panel A) and the quarantine rate (panel B) of model (5.1)–(5.2), by fixing $T_a = 3$ days. Color meaning is specified in the figure legend and refers to five values of the information coverage k. Other parameter values are given in Tables 5.1 and 5.2.

The effect of social behavioral changes is less evident in the transmission rate where increasing the information coverage produces a slight reduction of the transmission rate mainly during the full lockdown phase (Fig. 5.7A). This reflects the circumstance that the citizens choice of social distancing is not enhanced by the information–induced behavioral changes during the first stages of the epidemic.

5.6 Discussion and conclusions

In this chapter, we have proposed a mathematical approach to investigate the effects on the COVID–19 epidemic of social behavioral changes in response to lockdowns.

Starting from an SEIR–like model, we assumed that the transmission and quarantine rates are partially determined on a voluntary basis and depend on the circulating information and rumors about the disease, modeled by a suitable time–dependent *information index*. We focused on the case of the first COVID–19 epidemic wave in Italy and explicitly incorporated the progressively stricter restrictions enacted by the Italian government, by considering two step reductions in the contact rate (the partial and full lockdowns).

The main results are as follows:

- we estimated two fundamental information–related parameters: the information coverage regarding the daily number of quarantined and hospitalized individuals (i.e. the parameter k) and the information delay (the quantity $T_a = a^{-1}$). The estimate was performed by comparing the model's solutions with official data. We find $k = 0.8$, which means that the public was aware of 80% of real data and $T_a = 3$ days, the time lag that was necessary for information to reach the public;

- social behavioral changes in response to lockdowns played a decisive role in curbing the epidemic curve: the combined action of voluntary compliance with social distance and quarantine resulted in preventing a duplication of deaths and about 46% more

infections (i.e. approximately 360,000 more infections and 35,000 more deaths compared with the *unresponsive* case, as of May 18, 2020);

- even under circumstances of low information coverage and high information delay ($k = 0.2$, $T_a = 60$ days), there would have been a beneficial impact of social behavioral response on disease containment: as of May 18, cumulative incidence would be reduced by about 5% and deaths by about 11%.

Shaping the complex interaction between circulating information, human behavior and epidemic disease is challenging. In this study we have given a contribution in this direction. We provided an application of the information index to a specific field–case, the COVID–19 epidemic in Italy, where the information–dependent model was parameterized and the solutions were compared with official data.

Our study presents limitations that leave the possibility of future developments. In particular: i) the model captures the epidemics at a country level but it does not account for regional or local differences and for internal human mobility (the latter having been crucial in Italy at the early stage of the COVID–19 epidemic); ii) the model does not explicitly account for ICU admissions. The limited number of ICU beds constituted a main issue during the COVID–19 pandemics [122]. This study did not focus on this aspect but ICU admissions could be certainly included in the model; iii) the model could be extended to include age structure. Age was particularly relevant for COVID–19 lethality rate (in Italy the lethality rate for people aged 80 or over was more than double the average value for the whole population [167]).

Further developments may also concern the investigation of optimal intervention strategies during the COVID–19 epidemics and, to this regard, the assessment of the impact of vaccine arrival. In this case, the approach of information–dependent vaccination could be employed [55, 59, 293].

Concluding remarks and perspectives

In this thesis, we formulated and analyzed some control problems relying in the fields of mathematical and behavioral epidemiology of infectious diseases. As the title says, these problems are 'challenging' because they try to formalize real phenomena that are inevitably affected by multiple and complex factors. Despite the simplifications adopted, we obtained interesting and sometimes counter–intuitive results that throw more light on the key mechanisms underlying infectious diseases spread and control. Disparate analytical and numerical techniques (ranging from classical Pontryagin maximum principle to heuristic stochastic optimization algorithms) have been used according to the problem at hand, which acquires also a theoretical value *per se*.

In this context, the planning phase of control activities plays a crucial role. We found that: i) disparate objectives to purse could be conflicting and require qualitatively different control shapes (such as the minimization of epidemic duration and that of epidemic size discussed in Chapter 1); ii) more or less flexible time scheduling should be adopted on the basis of a cost–benefit comparison (as seen for vaccine awareness campaigns in the behavioral change model of Chapter 3); in some cases, the best strategy is to 'do nothing' because the control could even have negative and self–defeating effects (like localized culling activities during wildlife infections investigated in Chapter 2).

Further – when it comes to infections in human populations – the 'perfect plan' should also account for the individuals' (increasingly rapid) response to information about the disease that determines whether or not they will adopt protective tools. The inclusion of behavioral aspects in the model allows, on the one hand, to interpret the trend of past epidemics (such as the first COVID–19 wave in Italy addressed in Chapter 5) and, on the other hand, to alert about the possible risks (like information–induced oscillations of disease prevalence in the model of Chapter 4).

Given the extent and the relevance of the topic, research in these fields is constantly evolving and ever new challenges are launched from the real world (just think of the ongoing COVID–19 pandemic). Also our research is taking further steps. Specifically, in the context of optimal and time–optimal control of SIR model, we intend to make the model more realistic, by assuming that the chance of an individual recovering depends on the time since infection. This can be achieved by adopting the *method of stages* [89], namely assigning to the random variable describing the infectious period an Erlang distribution (rather than an exponential distribution as in the basic SIR).

In view of a COVID–19 vaccine arrival [162, 203], we are also designing and investigating suitable behavioral change models that incorporate the vaccination choice. A first model is the natural modification of the information–dependent epidemic model of Chapter 5, where a (potentially imperfect) vaccine substitute non–pharmaceutical interventions. We intend to compare this approach with that of vaccination models following imitation game dynamics (see Section I.4). To this aim, in the latter the vaccine must address susceptible individuals

at all ages (and not just newborns as assumed so far), thereby not only parents, but all people are subject to the game–theoretic mechanisms between pro and anti–vaccine forces.

Finally, a new line of research we are now undertaking connects mathematical epidemiology with kinetic theory. In particular, on the basis of the non–conservative Boltzmann–type kinetic framework introduced in [205], we want to derive epidemiological compartmental models from a kinetic (mesoscopic) description, in which the microscopic state that characterizes each agent is his/her *viral load*.

Bibliography

[1] H. Abboubakar, J. C. Kamgang, and D. Tieudjo. Backward bifurcation and control in transmission dynamics of arboviral diseases. *Mathematical Biosciences*, 278:100–129, 2016.

[2] M. A. Acuña–Zegarra, M. Santana-Cibrian, and J. X. Velasco-Hernandez. Modeling behavioral change and COVID–19 containment in Mexico: A trade–off between lockdown and compliance. *Mathematical Biosciences*, 325:108370, 2020.

[3] G. Agaba, Y. Kyrychko, and K. Blyuss. Dynamics of vaccination in a time–delayed epidemic model with awareness. *Mathematical Biosciences*, 294:92–99, 2017.

[4] Agenzia Nazionale Stampa Associata. Conte signs new restrictions regime featuring curfew. `https://www.ansa.it/english/news/2020/11/04/conte-approves-new-restrictions-regime-featuring-curfew_1cd48e7a-dac5-4620-9ac9-da99a358aa9f.html`, 2020. (Accessed on November 2020).

[5] Agenzia Nazionale Stampa Associata. Coronavirus: Conte tightens lockdown, closes all non–essential businesses, after almost 800 deaths in 24 hours. `https://www.ansa.it/english/news/2020/03/20/stay-home-or-well-take-other-tough-measures-di-maio_fe91986d-3a31-4dac-8671-44feab0bd506.html`, 2020. (Accessed on May 2020).

[6] A. A. Agrachev and Y. L. Sachkov. *Control Theory from the Geometric Viewpoint*, volume 87 of *Encyclopaedia of Mathematical Sciences*. Springer, Berlin, 2004.

[7] A. I. Alberici and P. Milesi. The influence of the Internet on the psychosocial predictors of collective action. *Journal of Community & Applied Social Psychology*, 23(5):373–388, 2013.

[8] S. A. Alchon. *A pest in the land: new world epidemics in a global perspective*. University of New Mexico Press, Albuquerque, 2003.

[9] M. E. Alexander, C. Bowman, S. M. Moghadas, R. Summers, A. B. Gumel, and B. M. Sahai. A vaccination model for transmission dynamics of influenza. *SIAM Journal on Applied Dynamical Systems*, 3(4):503–524, 2004.

[10] R. M. Anderson, H. C. Jackson, R. M. May, and A. M. Smith. Population dynamics of fox rabies in Europe. *Nature*, 289(5800):765, 1981.

[11] R. M. Anderson and R. M. May. Population biology of infectious diseases: Part I. *Nature*, 280:361–367, 1979.

[12] A. A. Andronov, S. E. Khaikin, and A. A. Vitt. *Theory of Oscillators*. Pergamon Press, Oxford, 1965.

[13] S. Aniţa, V. Capasso, and V. Arnăutu. *An Introduction to Optimal Control Problems in Life Sciences and Economics*. Birkhäuser/Springer, New York, 2011.

[14] E. Asano, L. J. Gross, S. Lenhart, and L. A. Real. Optimal control of vaccine distribution in a rabies metapopulation model. *Mathematical Biosciences and Engineering*, 5(2):219–238, 2008.

[15] V. I. Babitskii. *Theory of Vibroimpact Systems. Approximate Methods.* Nauka, Moscow, 1978.

[16] N. Bacaër. *A Short History of Mathematical Population Dynamics*, chapter Daniel Bernoulli, d'Alembert and the inoculation of smallpox (1760), pages 21–30. Springer, London, 2011.

[17] Y. Bai, L. Yao, T. Wei, F. Tian, D.-Y. Jin, L. Chen, and M. Wang. Presumed asymptomatic carrier transmission of COVID–19. *JAMA*, 323(14):1406–1407, 2020.

[18] M. G. Baker, T. K. Peckham, and N. S. Seixas. Estimating the burden of United States workers exposed to infection or disease: a key factor in containing risk of COVID–19 infection. *PLoS ONE*, 15(4):e0232452, 2020.

[19] R. D. Balicer, S. B. Omer, D. J. Barnett, and G. S. Everly Jr. Local public health workers' perceptions toward responding to an influenza pandemic. *BMC Public Health*, 6:99, 2006.

[20] S. Barari, S. Caria, A. Davola, P. Falco, T. Fetzer, S. Fiorin, L. Hensel, A. Ivchenko, J. Jachimowicz, G. King, G. Kraft-Todd, A. Ledda, M. MacLennan, L. Mutoi, C. Pagani, E. Reutskaja, C. Roth, and F. R. Slepoi. Evaluating COVID–19 public health messaging in Italy: Self–reported compliance and growing mental health concerns. *medRxiv*, 2020.

[21] C. T. Bauch. Imitation dynamics predict vaccinating behaviour. *Proceedings of the Royal Society B*, 272(1573):1669–1675, 2005.

[22] H. Behncke. Optimal control of deterministic epidemics. *Optimal Control Applications and Methods*, 21:269–285, 2000.

[23] Y. Belgaid, M. Helal, and E. Venturino. Analysis of a model for coronavirus spread. *Mathematics*, 8(5):820, 2020.

[24] R. Bellman. *Dynamic Programming*. Princeton University Press, Princeton, 1957.

[25] E. A. Belongia, M. D. Simpson, J. P. King, M. E. Sundaram, N. S. Kelley, M. T. Osterholm, and H. Q. McLean. Variable influenza vaccine effectiveness by subtype: a systematic review and meta–analysis of test–negative design studies. *The Lancet Infectious Diseases*, 16(8):942–951, 2016.

[26] M. Bernardo, C. Budd, A. R. Champneys, and P. Kowalczyk. *Piecewise–smooth Dynamical Systems: Theory and Applications*, volume 163. Springer, London, 2008.

[27] D. Bernoulli. Essai d'une nouvelle analyse de la mortalité causée par la petite vérole et des avantages de l'inoculation pour la prévenir. *Histoire de l'Académie Royale des Sciences Paris*, pages 1–45, 1766.

[28] M. Betta, M. Laurino, A. Pugliese, G. Guzzetta, A. Landi, and P. Manfredi. Perspectives on optimal control of varicella and herpes zoster by mass routine varicella vaccination. *Proceedings of the Royal Society B*, 283(1826):20160054, 2016.

[29] J. Bielby, F. Vial, R. Woodroffe, and C. A. Donnelly. Localised badger culling increases risk of herd breakdown on nearby, not focal, land. *PLoS ONE*, 11(10):1–9, 2016.

[30] G. J. Boender, T. J. Hagenaars, A. Bouma, G. Nodelijk, A. R. W. Elbers, M. C. M. de Jong, and M. van Boven. Risk maps for the spread of highly pathogenic avian influenza in poultry. *PLoS Computational Biology*, 3:e71, 2007.

[31] A. Boklund, T. Halasa, L. E. Christiansen, and C. Enœ. Comparing control strategies against foot–and–mouth disease: Will vaccination be cost–effective in Denmark? *Preventive Veterinary Medicine*, 111:206–219, 2013.

[32] L. Bolzoni, E. Bonacini, R. Della Marca, and M. Groppi. Optimal control of epidemic size and duration with limited resources. *Mathematical Biosciences*, 315:108232, 2019.

[33] L. Bolzoni, E. Bonacini, C. Soresina, and M. Groppi. Time–optimal control strategies in SIR epidemic models. *Mathematical Biosciences*, 292:86–96, 2017.

[34] L. Bolzoni and G. A. De Leo. A cost analysis of alternative culling strategies for the eradication of classical swine fever in wildlife. *Environment and Development Economics*, 12:653–671, 2007.

[35] L. Bolzoni and G. A. De Leo. Unexpected consequences of culling on the eradication of wildlife diseases: the role of virulence evolution. *American Naturalist*, 181:301–313, 2013.

[36] L. Bolzoni, G. A. De Leo, M. Gatto, and A. P. Dobson. Body-size scaling in an SEI model of wildlife diseases. *Theoretical Population Biology*, 73:374–382, 2008.

[37] L. Bolzoni, R. Della Marca, M. Groppi, and A. Gragnani. Dynamics of a metapopulation epidemic model with localized culling. *Discrete & Continuous Dynamical Systems - B*, 25(6):2307–2330, 2020.

[38] L. Bolzoni, L. Real, and G. De Leo. Transmission heterogeneity and control strategies for infectious disease emergence. *PLoS ONE*, 2:e747, 2007.

[39] L. Bolzoni, V. Tessoni, M. Groppi, and G. A. De Leo. React or wait: which optimal culling strategy to control infectious diseases in wildlife. *Journal of Mathematical Biology*, 69:1001–1025, 2014.

[40] M. H. Bond. Host life–history strategy explains pathogen–induced sterility. *American Naturalist*, 168:281–293, 2006.

[41] A. Bouma, A. R. W. Elbers, A. Dekker, A. de Koeijer, C. Bartels, P. Vellema, P. van der Wal, E. M. A. van Rooij, F. H. Pluimers, and M. C. M. de Jong. The foot–and–mouth disease epidemic in The Netherlands in 2001. *Preventive Veterinary Medicine*, 57:155–166, 2003.

[42] M. S. Boyce, A. R. E. Sinclair, and G. C. White. Seasonal compensation of predation and harvesting. *Oikos*, 87(3):419–426, 1999.

[43] O. Bozorg-Haddad, M. Solgi, and H. A. Loaiciga. *Meta–heuristic and evolutionary algorithms for engineering optimization*, volume 294. John Wiley & Sons, Hoboken, 2017.

[44] R. A. Bradhurst, S. E. Roche, I. J. East, P. Kwan, and M. G. Garner. A hybrid modeling approach to simulating foot–and–mouth disease outbreaks in Australian livestock. *Frontiers in Environmental Science*, 3:17, 2015.

[45] F. Brauer. Backward bifurcations in simple vaccination models. *Journal of Mathematical Analysis and Applications*, 298(2):418–431, 2004.

[46] F. Brauer. Mathematical epidemiology: Past, present, and future. *Infectious Disease Modelling*, 2(2):113–127, 2017.

[47] F. Brauer, P. van den Driessche, and J. Wu (eds). *Mathematical Epidemiology*. Springer, Berlin, 2008.

[48] British Broadcasting Corporation. Coronavirus lockdown protest: What's behind the US demonstrations?. `https://www.bbc.com/news/world-us-canada-52359100`. (Accessed on June 2020).

[49] British Broadcasting Corporation. Coronavirus: More than 9,000 fines for lockdown breaches. `https://www.bbc.com/news/uk-52489943`, 2020. (Accessed on May 2020).

[50] British Broadcasting Corporation. Coronavirus: The world in lockdown in maps and charts. `https://www.bbc.com/news/world-52103747`, 2020. (Accessed on May 2020).

[51] A. Brodeur, A. E. Clark, S. Fleche, and N. Powdthavee. Assessing the impact of the coronavirus lockdown on unhappiness, loneliness, and boredom using Google Trends. *arXiv*, 2020.

[52] B. Brogliato. *Nonsmooth Mechanics*. Springer, London, 1999.

[53] D. A. Broniatowski, A. M. Jamison, S. Qi, L. AlKulaib, T. Chen, A. Benton, S. C. Quinn, and M. Dredze. Weaponized health communication: Twitter bots and russian trolls amplify the vaccine debate. *American Journal of Public Health*, 108(10):1378–1384, 2018.

[54] J. Brosig, I. Traulsen, S. Blome, K. Depner, and J. Krieter. Comparison of different control strategies for classical swine fever using emergency vaccination and rapid PCR testing by using a Monte–Carlo simulation model. *Archiv Tierzucht*, 56:988–1004, 2013.

[55] B. Buonomo. Effects of information–dependent vaccination behavior on coronavirus outbreak: insights from a SIRI model. *Ricerche di Matematica*, 2020.

[56] B. Buonomo, G. Carbone, and A. d'Onofrio. Effect of seasonality on the dynamics of an imitation–based vaccination model with public health intervention. *Mathematical Biosciences and Engineering*, 15(1):299–321, 2018.

[57] B. Buonomo, N. Chitnis, and A. d'Onofrio. Time heterogeneous programs of vaccination awareness: modeling and analysis. *Ricerche di Matematica*, 67(1):205–225, 2018.

[58] B. Buonomo and R. Della Marca. Optimal bed net use for a dengue disease model with mosquito seasonal pattern. *Mathematical Methods in the Applied Sciences*, 41(2):573–592, 2018.

[59] B. Buonomo and R. Della Marca. Oscillations and hysteresis in an epidemic model with information–dependent imperfect vaccination. *Mathematics and Computers in Simulation*, 162:97–114, 2019.

[60] B. Buonomo and R. Della Marca. Effects of information–induced behavioural changes during the COVID–19 lockdowns: the case of Italy. *Royal Society Open Science*, 7(10):201635, 2020.

[61] B. Buonomo, R. Della Marca, and A. d'Onofrio. Optimal Public Health intervention in a behavioral vaccination model: the interplay between seasonality, behavior and latency period. *Mathematical Medicine and Biology: A Journal of the IMA*, 36(3):297–324, 2018.

[62] B. Buonomo, A. d'Onofrio, and D. Lacitignola. Global stability of an SIR epidemic model with information dependent vaccination. *Mathematical Biosciences*, 216(1):9–16, 2008.

[63] B. Buonomo, A. d'Onofrio, and D. Lacitignola. The geometric approach to global stability in behavioral epidemiology. In P. Manfredi and A. d'Onofrio, editors, *Modeling the Interplay Between Human Behavior and the Spread of Infectious Diseases*, pages 289–308. Springer, New York, 2013.

[64] B. Buonomo, A. d'Onofrio, and D. Lacitignola. Modeling of pseudo–rational exemption to vaccination for SEIR diseases. *Journal of Mathematical Analysis and Applications*, 404(2):385–398, 2013.

[65] B. Buonomo, P. Manfredi, and A. d'Onofrio. Optimal time–profiles of public health intervention to shape voluntary vaccination for childhood diseases. *Journal of Mathematical Biology*, 78(4):1089–1113, 2019.

[66] V. V. Burmakina, D. V. Pomazkin, and I. D. Prokhorov. Methods for constructing an assessment of the development of the coronavirus pandemic. *Population and Economics*, 4(2):96–102, 2020.

[67] S. P. Carter, R. J. Delahay, G. C. Smith, D. W. Macdonald, P. Riordan, T. R. Etherington, E. R. Pimley, N. J. Walker, and C. L. Cheeseman. Culling–induced social perturbation in Eurasian badgers *Meles meles* and the management of TB in cattle: an analysis of a critical problem in applied ecology. *Proceedings of the Royal Society B*, 274(1626):2769–2777, 2007.

[68] R. Casagrandi and M. Gatto. A persistence criterion for metapopulations. *Theoretical Population Biology*, 61(2):115–125, 2002.

[69] C. Castillo-Chavez and B. Song. Dynamical models of tuberculosis and their applications. *Mathematical Biosciences and Engineering*, 1(2):361–404, 2004.

[70] Center for Systems Science and Engineering at Johns Hopkins University. COVID–19 World Map. `https://coronavirus.jhu.edu/map.html`, 2020. (Accessed on November 2020).

[71] Centers for Disease Control and Prevention. Tiered use of inactivated influenza vaccine in the event of a vaccine shortage. *Morbidity and Mortality Weekly Report*, 54:749–750, 2005.

[72] Centers for Disease Control and Prevention. Varicella vaccine effectiveness and duration of protection. `https://www.cdc.gov/vaccines/vpd-vac/varicella/hcp-effective-duration.htm`, 2012. (Accessed on March 2018).

[73] Centers for Disease Control and Prevention. Measles, mumps, and rubella (MMR) vaccination: What everyone should know. `https://www.cdc.gov/vaccines/vpd/mmr/public/index.html`, 2017. (Accessed on January 2018).

[74] Centers for Disease Control and Prevention. Vaccine effectiveness - How well does the flu vaccine work? `https://www.cdc.gov/flu/about/qa/vaccineeffect.htm`, 2017. (Accessed on March 2018).

[75] Centers for Disease Control and Prevention. Poliomyelitis. `https://www.cdc.gov/vaccines/pubs/pinkbook/polio.html`, 2018. (Accessed on November 2018).

[76] D. Cereda, M. Tirani, F. Rovida, V. Demicheli, M. Ajelli, P. Poletti, F. Trentini, G. Guzzetta, V. Marziano, A. Barone, M. Magoni, S. Deandrea, G. Diurno, M. Lombardo, M. Faccini, A. Pan, R. Bruno, E. Pariani, G. Grasselli, A. Piatti, M. Gramegna, F. Baldanti, A. Melegaro, and S. Merler. The early phase of the COVID–19 outbreak in Lombardy, Italy. *arXiv*, 2020.

[77] B. Chachuat. Nonlinear and dynamic optimization: from theory to practice. Technical report, Automatic Control Laboratory, EPFL, Switzerland, 2007.

[78] M. Chan and K. Kupferschmidt. Q&A. Crisis manager with 194 bosses. *Science*, 350:495, 2015.

[79] C. Chen, N. S. Chong, and R. Smith? A Filippov model describing the effects of media coverage and quarantine on the spread of human influenza. *Mathematical Biosciences*, 296:98–112, 2018.

[80] F. Chen, M. Jiang, S. Rabidoux, and S. Robinson. Public avoidance and epidemics: insights from an economic model. *Journal of Theoretical Biology*, 278(1):107–119, 2011.

[81] S. Chen, J. Montgomery, and A. Bolufé-Röhler. Measuring the curse of dimensionality and its effects on particle swarm optimization and differential evolution. *Applied Intelligence*, 42(3):514–526, 2015.

[82] X. Chen and F. Fu. Imperfect vaccine and hysteresis. *Proceedings of the Royal Society B*, 286(1894):20182406, 2019.

[83] S. Choi and E. Jung. Optimal tuberculosis prevention and control strategy from a mathematical model based on real data. *Bulletin of Mathematical Biology*, 76(7):1566–1589, 2014.

[84] M. Choisy and P. Rohani. Harvesting can increase severity of wildlife disease epidemics. *Proceedings of the Royal Society B*, 273:2025–2034, 2006.

[85] N. S. Chong, B. Dionne, and R. J. Smith. An avian–only Filippov model incorporating culling of both susceptible and infected birds in combating avian influenza. *Journal of Mathematical Biology*, 73:751–784, 2016.

[86] N. S. Chong and R. J. Smith. Modeling avian influenza using Filippov systems to determine culling of infected birds and quarantine. *Nonlinear Analysis: Real World Applications*, 24:196–218, 2015.

[87] S. Cleaveland, K. Laurenson, and T. Mlengeya. Impacts of wildlife infections on human and livestock health with special reference to Tanzania: Implications for protected area management. In S. Osofsky, S. Cleaveland, W. Karesh, M. Kock, P. Nyhus, L. Starr, and A. Yang, editors, *Conservation and Development Interventions at the Wildlife/Livestock Interface: Implications for Wildlife, Livestock and Human Health*, pages 147–151. IUCN, Gland, 2005.

[88] C. Cosentino and D. Bates. *Feedback Control in Systems Biology*. Crc Press, Boca Raton, 2011.

[89] D. R. Cox and H. D. Miller. *The Theory of Stochastic Processes*. Chapman and Hall, London, 1965.

[90] M. J. Coyne, G. Smith, and F. E. McAllister. Mathematic model for the population biology of rabies in raccoons in the mid–Atlantic states. *American Journal of Veterinary Research*, 50(12):2148–2154, 1989.

[91] M. J. Coyne, G. Smith, and F. E. McAllister. FMD vaccine surge capacity for emergency use in the United States. *Veterinary Microbiology and Preventive Medicine Reports*, 8, 2014.

[92] M. G. Crandall and P.-L. Lions. Viscosity solutions of Hamilton–Jacobi equations. *Transactions of the American Mathematical Society*, 277(1):1–42, 1983.

[93] J. Cui, Y. Sun, and H. Zhu. The impact of media on the control of infectious diseases. *Journal of Dynamics and Differential Equations*, 20(1):31–53, 2008.

[94] S. Das, A. Abraham, and A. Konar. Particle swarm optimization and differential evolution algorithms: technical analysis, applications and hybridization perspectives. In Y. Liu, A. Sun, H. T. Loh, W. F. Lu, and E. P. Lim, editors, *Advances of Computational Intelligence in Industrial Systems*, pages 1–38. Springer, Berlin, Heidelberg, 2008.

[95] T. Day. On the evolution of virulence and the relationship between various measures of mortality. *Proceedings of the Royal Society B*, 269(1498):1317–1323, 2002.

[96] M. d. R. de Pinho, H. Maurer, and H. Zidani. Optimal control of normalized SIMR models with vaccination and treatment. *Discrete & Continuous Dynamical Systems - B*, 23(1):79–99, 2018.

[97] R. Della Marca and A. d'Onofrio. Volatile opinions and optimal control of vaccine awareness campaigns: chaotic behaviour of the Forward–Backward Sweep algorithm vs heuristic direct optimization. *Communications in Nonlinear Science and Numerical Simulation*, 2021. (In press).

[98] F. Dercole, A. Gragnani, Y. A. Kuznetsov, and S. Rinaldi. Numerical sliding bifurcation analysis: an application to a relay control system. *IEEE Transactions on Circuits and Systems I: Fundamental Theory and Applications*, 50(8):1058–1063, 2003.

[99] F. Dercole and Y. A. Kuznetsov. Slidecont: An Auto97 driver for sliding bifurcation analysis. *ACM Transactions on Mathematical Software*, 31:95–119, 2005.

[100] R. S. Dhillon and J. D. Kelly. Community trust and the Ebola endgame. *New England Journal of Medicine*, 373(9):787–789, 2015.

[101] M. di Bernardo, M. Feigin, S. Hogan, and M. Homer. Local analysis of C–bifurcations in n–dimensional piecewise–smooth dynamical systems. *Chaos, Solitons & Fractals*, 11(10):1881–1908, 1999.

[102] L. Di Domenico, G. Pullano, C. E. Sabbatini, P.-Y. Boëlle, and V. Colizza. Impact of lockdown on COVID–19 epidemic in Île–de–France and possible exit strategies. *BMC Medicine*, 18(240), 2020.

[103] O. Diekmann, J. A. P. Heesterbeek, and J. A. J. Metz. On the definition and the computation of the basic reproduction ratio R_0 in models for infectious diseases in heterogeneous populations. *Journal of Mathematical Biology*, 28(4):365–382, 1990.

[104] O. Diekmann and M. Kretzschmar. Patterns in the effects of infectious diseases on population growth. *Journal of Mathematical Biology*, 29(6):539–570, 1991.

[105] E. J. Doedel, A. R. Champneys, T. F. Fairgrieve, Y. A. Kuznetsov, B. Sandstede, and X. Wang. *Auto97: Continuation and bifurcation software for ordinary differential equaitions (with HomCont).* Computer Science, Concordia University, Montreal, Canada, 1997.

[106] K. Dong-Hyun. Structural factors of the middle east respiratory syndrome coronavirus outbreak as a public health crisis in Korea and future response strategies. *Journal of Preventive Medicine and Public Health*, 48:265–270, 2015.

[107] C. A. Donnelly, R. Woodroffe, D. R. Cox, F. J. Bourne, C. Cheeseman, R. S. Clifton-Hadley, G. Wei, G. Gettinby, P. Gilks, H. Jenkins, W. T. Johnston, A. M. Le Fevre, J. P. McInerney, and W. I. Morrison. Positive and negative effects of widespread badger culling on tuberculosis in cattle. *Nature*, 439(7078):843, 2006.

[108] C. A. Donnelly, R. Woodroffe, D. R. Cox, J. Bourne, G. Gettinby, A. M. Le Fevre, J. P. McInerney, and W. I. Morrison. Impact of localized badger culling on tuberculosis incidence in British cattle. *Nature*, 426(6968):834, 2003.

[109] A. d'Onofrio and P. Manfredi. Information–related changes in contact patterns may trigger oscillations in the endemic prevalence of infectious diseases. *Journal of Theoretical Biology*, 256(3):473–478, 2009.

[110] A. d'Onofrio and P. Manfredi. Bistable endemic states in a Susceptible–Infectious–Susceptible model with behavior–dependent vaccination. In G. Chowell and J. Hyman, editors, *Mathematical and Statistical Modeling for Emerging and Re–emerging Infectious Diseases*, pages 341–354. Springer, New York, 2016.

[111] A. d'Onofrio, P. Manfredi, and P. Poletti. The impact of vaccine side effects on the natural history of immunization programmes: an imitation–game approach. *Journal of Theoretical Biology*, 273(1):63–71, 2011.

[112] A. d'Onofrio, P. Manfredi, and P. Poletti. The interplay of public intervention and private choices in determining the outcome of vaccination programmes. *PLoS ONE*, 7(10):e45653, 2012.

[113] A. d'Onofrio, P. Manfredi, and E. Salinelli. Vaccinating behaviour, information, and the dynamics of SIR vaccine preventable diseases. *Theoretical Population Biology*, 71(3):301–317, 2007.

[114] A. d'Onofrio, P. Manfredi, and E. Salinelli. Fatal SIR diseases and rational exemption to vaccination. *Mathematical Medicine and Biology: A Journal of the IMA*, 25(4):337–357, 2008.

[115] A. d'Onofrio, P. Manfredi, and E. Salinelli. Vaccinating behaviour and the dynamics of vaccine preventable infections. In P. Manfredi and A. d'Onofrio, editors, *Modeling the Interplay Between Human Behavior and the Spread of Infectious Diseases*, pages 267–287. Springer, New York, 2013.

[116] J. Dushoff, W. Huang, and C. Castillo-Chavez. Backwards bifurcations and catastrophe in simple models of fatal diseases. *Journal of Mathematical Biology*, 36(3):227–248, 1998.

[117] M. Ehrgott. *Multicriteria Optimization*. Springer, Berlin, 2005.

[118] R. Elie, E. Hubert, and G. Turinici. Contact rate epidemic control of COVID–19: an equilibrium view. *Mathematical Modelling of Natural Phenomena*, 15:35, 2020.

[119] G. Elnagar, M. A. Kazemi, and M. Razzaghi. The pseudospectral Legendre method for discretizing optimal control problems. *IEEE transactions on Automatic Control*, 40(10):1793–1796, 1995.

[120] European Centre for Disease Prevention and Control. Disease background of COVID–19. `https://www.ecdc.europa.eu/en/2019-ncov-background-disease`, 2020. (Accessed on May 2020).

[121] European Parliamentary Research Service. Repatriation of EU citizens during the COVID–19 crisis. `https://www1.europarl.europa.eu/RegData/etudes/BRIE/2020/649359/EPRS_BRI(2020)649359_EN.pdf`, 2020. (Accessed on May 2020).

[122] European Society of Anaesthesiology. Dynamics of ICU patients and deaths in Italy and Lombardy due to Covid–19. Analysis updated to 30–March, Day #38 evening. `https://www.esahq.org/esa-news/dynamics-of-icu-patients-and-deaths-in-italy-and-lombardy-due-to-covid-19-analysis-updated-to-30-march-day-38-evening`, 2020. (Accessed on May 2020).

[123] M. I. Feigin. *Forced Oscillations in Systems with Discontinuous Nonlinearities*. Nauka, Moscow, 1994. (In Russian).

[124] J. M. Ferdinands, A. M. Fry, S. Reynolds, J. G. Petrie, B. Flannery, M. L. Jackson, and E. A. Belongia. Intraseason waning of influenza vaccine protection: Evidence from the US influenza vaccine effectiveness network, 2011–2012 through 2014–2015. *Clinical Infectious Diseases*, 64(5):544–550, 2017.

[125] A. F. Filippov. *Differential Equations with Discontinuous Righthand Sides*. Kluwer Academic Publishers, Dordrecht, 1988.

[126] S. Flaxman, S. Mishra, A. Gandy, H. J. T. Unwin, T. A. Mellan, H. Coupland, C. Whittaker, H. Zhu, T. Berah, J. W. Eaton, M. Monod, Imperial College COVID–19 Response Team, A. C. Ghani, C. A. Donnelly, S. M. Riley, M. A. C. Vollmer, N. M. Ferguson, L. C. Okell, and S. Bhatt. Estimating the effects of non–pharmaceutical interventions on COVID–19 in Europe. *Nature*, 584:257–261, 2020.

[127] W. H. Fleming and R. W. Rishel. *Deterministic and Stochastic Optimal Control*, volume 1 of *Applications of Mathematics*. Springer, Berlin, New York, 1975.

[128] Food and Agriculture Organization of the United Nations. Impact of the Ebola virus disease outbreak on market chains and trade of agricultural products in West Africa. Technical report, FAO REOWA (Resilience Team for West Africa/Sahel), Dakar, 2016.

[129] L. G. Frank and R. Woddroffe. Behaviour of carnivores in exploited and controlled populations. In J. L. Gittleman, S. M. Funk, D. W. Macdonald, and R. K. Wayne, editors, *Carnivore Conservation*, pages 419–442. Cambridge University Press, Cambridge, 2001.

[130] S. Funk, M. Salathé, and V. A. A. Jansen. Modelling the influence of human behaviour on the spread of infectious diseases: a review. *Journal of the Royal Society Interface*, 7(50):1247–1256, 2010.

[131] W. H. Gan, J. W. Lim, and D. Koh. Preventing intra–hospital infection and transmission of coronavirus disease 2019 in health–care workers. *Safety and Health at Work*, 2020.

[132] S. Garba, A. Gumel, and M. Abu Bakar. Backward bifurcations in dengue transmission dynamics. *Mathematical Biosciences*, 215(1):11–25, 2008.

[133] D. Garg, M. Patterson, W. W. Hager, A. V. Rao, D. A. Benson, and G. T. Huntington. A unified framework for the numerical solution of optimal control problems using pseudospectral methods. *Automatica*, 46(11):1843–1851, 2010.

[134] M. G. Garner, N. Bombarderi, M. Cozens, M. L. Conway, T. Wright, R. Paskin, and I. J. East. Estimating resource requirements to staff a response to a medium to large outbreak of foot and mouth disease in Australia. *Transboundary and Emerging Diseases*, 63:e109–e121, 2016.

[135] M. Gatto, E. Bertuzzo, L. Mari, S. Miccoli, L. Carraro, R. Casagrandi, and A. Rinaldo. Spread and dynamics of the COVID–19 epidemic in Italy: Effects of emergency containment measures. *Proceedings of the National Academy of Sciences*, 117(19):10484–10491, 2020.

[136] D. J. Gerberry. Practical aspects of backward bifurcation in a mathematical model for tuberculosis. *Journal of Theoretical Biology*, 388:15–36, 2016.

[137] M. Gersovitz and J. S. Hammer. The economical control of infectious diseases. *The Economic Journal*, 114(492):1–27, 2003.

[138] R. Gibbons. *A Primer in Game Theory*. Harvester Wheatsheaf, London, 1992.

[139] D. T. Gillespie. The chemical Langevin equation. *The Journal of Chemical Physics*, 113(1):297–306, 2000.

[140] G. Giordano, F. Blanchini, R. Bruno, P. Colaneri, A. Di Filippo, A. Di Matteo, and M. Colaneri. Modelling the COVID–19 epidemic and implementation of population–wide interventions in Italy. *Nature Medicine*, 26:855–860, 2020.

[141] C. A. Glaser, S. Gilliam, W. W. Thompson, D. E. Dassey, S. H. Waterman, M. Saruwatari, S. Shapiro, and K. Fukuda. Medical care capacity for influenza outbreaks, Los Angeles. *Emerging Infectious Diseases*, 8:569–574, 2002.

[142] R. J. Glauber. Time–dependent statistics of the Ising model. *Journal of Mathematical Physics*, 4(2):294–307, 1963.

[143] P. Glendinning and M. R. Jeffrey. Grazing–sliding bifurcations, border collision maps and the curse of dimensionality for piecewise smooth bifurcation theory. *Nonlinearity*, 28:263, 2015.

[144] L. O. Gostin and E. A. Friedman. A retrospective and prospective analysis of the west African Ebola virus disease epidemic: robust national health systems at the foundation and an empowered WHO at the apex. *The Lancet*, 385:1902–1999, 2015.

[145] N. Goto and H. Kawable. Direct optimization methods applied to a nonlinear optimal control problem. *Mathematics and Computers in Simulation*, 51(6):557–577, 2000.

[146] D. Gromov, I. Bulla, E. O. Romero-Severson, and O. S. Serea. Numerical optimal control for HIV prevention with dynamic budget allocation. *Mathematical Medicine and Biology: A Journal of the IMA*, 35(4):469–491, 2018.

[147] M. Groppi and R. Della Marca. Modelli epidemiologici e vaccinazioni: da Bernoulli a oggi. *Matematica, Cultura e Società. Rivista dell'Unione Matematica Italiana*, 3(1):45–59, 2018.

[148] J. Guckenheimer and P. Holmes. *Nonlinear Oscillations, Dynamical Systems, and Bifurcations of Vector Fields*. Springer, Berlin, 1983.

[149] H. Gulbudak and M. Martcheva. Forward hysteresis and backward bifurcation caused by culling in an avian influenza model. *Mathematical Biosciences*, 246(1):202–212, 2013.

[150] A. Gumel. Causes of backward bifurcations in some epidemiological models. *Journal of Mathematical Analysis and Applications*, 395(1):355–365, 2012.

[151] A. B. Gumel, S. Ruan, T. Day, J. Watmough, F. Brauer, P. Van den Driessche, D. Gabrielson, C. Bowman, M. E. Alexander, S. Ardal, J. Wu, and B. M. Sahai. Modelling strategies for controlling SARS outbreaks. *Proceedings of the Royal Society B*, 271(1554):2223–2232, 2004.

[152] M. Halloran, M. Haber, and I. Longini. Interpretation and estimation of vaccine efficacy under heterogeneity. *American Journal of Epidemiology*, 136(3):328–343, 1992.

[153] W. H. Hamer. Epidemic disease in England – the evidence of variability and of persistence. *The Lancet*, 167:733–738, 1906.

[154] A. Handel, I. Longini, and R. Antia. What is the best control strategy for multiple infectious disease outbreaks? *Proceedings of the Royal Society B*, 274:833–837, 2007.

[155] E. Hansen and T. Day. Optimal control of epidemics with limited resources. *Journal of Mathematical Biology*, 62:423–451, 2011.

[156] D. T. Haydon, M. E. J. Woolhouse, and R. P. Kitching. An analysis of foot–and–mouth–disease epidemics in the UK. *Mathematical Medicine and Biology: A Journal of the IMA*, 14:1–9, 1997.

[157] P. Hayes. When fear becomes panic. *Clinical Nursing Research*, 12:299–303, 2003.

[158] X. He, E. H. Lau, P. Wu, X. Deng, J. Wang, X. Hao, Y. C. Lau, J. Y. Wong, Y. Guan, X. Tan, X. Mo, Y. Chen, B. Liao, W. Chen, F. Hu, Q. Zhang, M. Zhong, Y. Wu, L. Zhao, F. Zhang, B. J. Cowling, F. Li, and G. M. Leung. Temporal dynamics in viral shedding and transmissibility of COVID–19. *Nature Medicine*, 26(5):672–675, 2020.

[159] H. W. Hethcote. The mathematics of infectious diseases. *SIAM Review*, 42:599–653, 2000.

[160] H. W. Hethcote and J. A. Yorke. *Gonorrhea. Transmission Dynamics and Control*. Springer, Berlin, 1984.

[161] H. W. Hethcote, M. Zhien, and L. Shengbing. Effects of quarantine in six endemic models for infectious diseases. *Mathematical Biosciences*, 180(1):141–160, 2002.

[162] S. H. Hodgson, K. Mansatta, G. Mallett, V. Harris, K. R. W. Emary, and A. J. Pollard. What defines an efficacious COVID–19 vaccine? A review of the challenges assessing the clinical efficacy of vaccines against SARS–CoV–2. *The Lancet Infectious Diseases*, 2020.

[163] S. J. Hogan, M. E. Homer, M. R. Jeffrey, and R. Szalai. Piecewise smooth dynamical systems theory: the case of the missing boundary equilibrium bifurcations. *Journal of Nonlinear Science*, 26:1161–1173, 2016.

[164] R. A. Horn and C. R. Johnson. *Matrix Analysis*. Cambridge University Press, Cambridge, 1986.

[165] Z. Hu, W. Ma, and S. Ruan. Analysis of SIR epidemic models with nonlinear incidence rate and treatment. *Mathematical Biosciences*, 238(1):12–20, 2012.

[166] Istituto Nazionale di Statistica. Demography in Figures. `http://www.demo.istat.it/index.html`, 2020. (Accessed on May 2020).

[167] Istituto Superiore di Sanità, EpiCentro. SARS-CoV-2 – Latest available data. `https://www.epicentro.iss.it/en/coronavirus/`, 2020. (Accessed on May 2020).

[168] Italian Civil Protection Department. Chronology of main steps and legal acts taken by the Italian Government for the containment of the COVID–19 epidemiological emergency. `http://www.protezionecivile.gov.it/documents/20182/1227694/Summary+of+measures+taken+against+the+spread+of+C-19/c16459ad-4e52-4e90-90f3-c6a2b30c17eb`, 2020. (Accessed on May 2020).

[169] Italian Ministry of Foreign Affairs and International Cooperation. Foreign Ministry commitment for Italians abroad. `https://www.esteri.it/mae/en/sala_stampa/archivionotizie/approfondimenti/impegno-della-farnesina-per-gli-italiani-all-estero.html`, 2020. (Accessed on May 2020).

[170] Italian Ministry of Health. Covid–19. Phase two: what's opening and what you can do. `http://www.salute.gov.it/portale/nuovocoronavirus/dettaglioNotizieNuovoCoronavirus.jsp?lingua=english&id=4670`, 2020. (Accessed on May 2020).

[171] Italian Ministry of Health. Dati COVID–19 Italia. `https://github.com/pcm-dpc/COVID-19`, 2020. (Accessed on November 2020).

[172] Italian Ministry of Health. FAQ - Covid–19, questions and answers. `http://www.salute.gov.it/portale/nuovocoronavirus/dettaglioFaqNuovoCoronavirus.jsp?lingua=english&id=230#2`, 2020. (Accessed on May 2020).

[173] J. Jang, H.-D. Kwon, and J. Lee. Optimal control problem of an SIR reaction–diffusion model with inequality constraints. *Mathematics and Computers in Simulation*, 171:136–151, 2020.

[174] M. R. Jeffrey and S. J. Hogan. The geometry of generic sliding bifurcations. *SIAM Review*, 53(3):505–525, 2011.

[175] K. E. Jones, N. G. Patel, M. A. Levy, A. Storeygard, D. Balk, J. L. Gittleman, and P. Daszak. Global trends in emerging infectious diseases. *Nature*, 451(7181):990, 2008.

[176] W. H. S. Jones, editor. *Hippocrates Collected Works I*. Cambridge Harvard University Press, Cambridge, 1868.

[177] H. R. Joshi. Optimal control of an HIV immunology model. *Optimal Control Applications and Methods*, 23(4):199–213, 2002.

[178] J. T. Jost, P. Barberá, R. Bonneau, M. Langer, M. Metzger, J. Nagler, J. Sterling, and J. A. Tucker. How social media facilitates political protest: Information, motivation, and social networks. *Advances in Political Psychology*, 39(S1):85–118, 2018.

[179] E. Jung, S. Iwami, Y. Takeuchi, and T.-C. Jo. Optimal control strategy for prevention of avian influenza pandemic. *Journal of Theoretical Biology*, 260(2):220–229, 2009.

[180] E. Jung, S. Lenhart, and Z. Feng. Optimal control of treatments in a two–strain tuberculosis model. *Discrete & Continuous Dynamical Systems - B*, 2(4):473–482, 2002.

[181] D. H. Kamens. Chapter 9 The construction of public opinion. In D. H. Kamens, editor, *Beyond the Nation–State*, pages 257–279. Emerald Group Publishing Limited, Bingley, 2012.

[182] M. Kantner and T. Koprucki. Beyond just "flattening the curve": Optimal control of epidemics with purely non–pharmaceutical interventions. *Journal of Mathematics in Industry*, 10(23), 2020.

[183] S. M. Kassa, J. B. Njagarah, and Y. A. Terefe. Analysis of the mitigation strategies for COVID–19: From mathematical modelling perspective. *Chaos, Solitons & Fractals*, 138:109968, 2020.

[184] J. Kennedy and R. Eberhart. Particle swarm optimization. In *Proceedings of the IEEE International Conference on Neural Networks*, pages 1942–1945, Perth, Australia, 1995.

[185] W. O. Kermack and A. G. McKendrick. A contribution to the mathematical theory of epidemics. *Proceedings of the Royal Society A*, 115(772):700–721, 1927.

[186] W. O. Kermack and A. G. McKendrick. Contributions to the mathematical theory of epidemics, part. II. *Proceedings of the Royal Society A*, 138:55–83, 1932.

[187] W. O. Kermack and A. G. McKendrick. Contributions to the mathematical theory of epidemics, part. III. *Proceedings of the Royal Society A*, 141:94–112, 1933.

[188] W. A. Kerr, L. J. Loppacher, and J. E. Hobbs. International standards for regulating trade when BSE is present: Why are they being ignored? *Current Agriculture, Food and Resource Issues*, 8:1–15, 2007.

[189] D. E. Kirk. *Optimal Control Theory: An Introduction*. Prentice–Hall, New Jersey, 1970.

[190] T. J. D. Knight-Jones and J. Rushton. The economic impacts of foot and mouth disease – What are they, how big are they and where do they occur? *Preventive Veterinary Medicine*, 112:161–173, 2013.

[191] M. Koopmans, B. Wilbrink, M. Conyn, G. Natrop, H. van der Nat, H. Vennema, A. Meijer, J. van Steenbergen, R. Fouchier, A. Osterhaus, and A. Bosman. Transmission of H7N7 avian influenza A virus to human beings during a large outbreak in commercial poultry farms in The Netherlands. *The Lancet*, 363:587–593, 2004.

[192] C. M. Kribs-Zaleta and J. X. Velasco-Hernandez. A simple vaccination model with multiple endemic states. *Mathematical Biosciences*, 164(2):183–201, 2000.

[193] A. J. Kucharski, A. Camacho, S. Flasche, R. E. Glover, W. J. Edmunds, and S. Funk. Measuring the impact of Ebola control measures in Sierra Leone. *Proceedings of the National Academy of Sciences*, 112(46):14366–14371, 2015.

[194] A. Kumar, P. K. Srivastava, and R. Gupta. Nonlinear dynamics of infectious diseases via information–induced vaccination and saturated treatment. *Mathematics and Computers in Simulation*, 157:77–99, 2019.

[195] K. Kupferschmidt. Risk of 'leaky' vaccines debated. *Science*, 349(6247):461–462, 2015.

[196] Y. A. Kuznetsov, S. Rinaldi, and A. Gragnani. One–parameter bifurcations in planar Filippov systems. *International Journal of Bifurcation and Chaos*, 8:2157–2188, 2003.

[197] S. Lachish, H. Mccallum, D. Mann, C. E. Pukk, and M. E. Jones. Evaluation of selective culling of infected individuals to control Tasmanian devil facial tumor disease. *Conservation Biology*, 24(3):841–851, 2010.

[198] A. Lachmann. Correcting under–reported COVID–19 case numbers. *medRxiv*, 2020.

[199] H. J. Larson, L. Z. Cooper, J. Eskola, S. L. Katz, and S. Ratzan. Addressing the vaccine confidence gap. *The Lancet*, 378(9790):526–535, 2011.

[200] A. Lee and J. Choo. The impact of epidemics on labor market: identifying victims of the Middle East Respiratory Syndrome in the Korean labor market. *International Journal for Equity in Health*, 15:196, 2016.

[201] S. Lenhart and J. T. Workman. *Optimal Control Applied to Biological Models*. Crc Press, London, 2007.

[202] C.-C. Lin and L. A. Segel. *Mathematics Applied to Deterministic Problems in the Natural Sciences*. SIAM, Philadelphia, 1988.

[203] M. Lipsitch and N. E. Dean. Understanding COVID–19 vaccine efficacy. *Science*, 370(6518):763–765, 2020.

[204] Y. Liu and J. Cui. The impact of media coverage on the dynamics of infectious disease. *International Journal of Biomathematics*, 1(1):65–74, 2008.

[205] N. Loy and A. Tosin. Non–conservative Boltzmann–type kinetic equations for multi–agent systems with label switching. (Submitted).

[206] G. MacDonald. *The Epidemiology and Control of Malaria*. Oxford University Press, Oxford, 1957.

[207] N. MacDonald. *Biological Delay Systems: Linear Stability Theory*. Cambridge University Press, Cambridge, 1989.

[208] M. Mackinnon, S. Gandon, and A. Read. Virulence evolution in response to vaccination: The case of malaria. *Vaccine*, 26:C42–C52, 2008.

[209] S. Maharaj and A. Kleczkowski. Controlling epidemic spread by social distancing: Do it well or not at all. *BMC Public Health*, 12:679, 2012.

[210] P. Manfredi and A. d'Onofrio, editors. *Modeling the Interplay Between Human Behavior and the Spread of Infectious Diseases*. Springer, New York, 2013.

[211] M.-J. J. Mangen, A. W. Jalvingh, M. Nielen, M. C. M. Mourits, D. Klinkenberg, and A. A. Dijkhuizen. Spatial and stochastic simulation to compare two emergency–vaccination strategies with a marker vaccine in the 1997/1998 Dutch Classical Swine Fever epidemic. *Preventive Veterinary Medicine*, 48:177–200, 2001.

[212] S. Marangon, M. Cecchinato, and I. Capua. Use of vaccination in avian influenza control and eradication. *Zoonoses and Public Health*, 55:65–72, 2008.

[213] H. J. Marquez. *Nonlinear Control Systems: Analysis and Design*. John Wiley & Sons, Hoboken, 2003.

[214] M. Martcheva. *An Introduction to Mathematical Epidemiology*. Springer, New York, 2015.

[215] P. M. Massey, A. Leader, E. Yom-Tov, A. Budenz, K. Fisher, and A. C. Klassen. Applying multiple data collection tools to quantify human papillomavirus vaccine communication on Twitter. *Journal of Medical Internet Research*, 18(12):e318, 2016.

[216] MATLAB. Matlab release 2019b. The MathWorks, Inc., Natick, MA, 2019.

[217] M. L. N. Mbah, J. Liu, C. T. Bauch, Y. I. Tekel, J. Medlock, L. A. Meyers, and A. P. Galvani. The impact of imitation on vaccination behavior in social contact networks. *PLoS Computational Biology*, 8(4):e1002469, 2012.

[218] J. Mereckiene. Seasonal influenza vaccination and antiviral use in EU/EEA Member States. Technical report, European Centre for Disease Prevention and Control, `https://ecdc.europa.eu/en/publications-data/seasonal-influenza-vaccination-antiviral-use-eu-eea-member-states`, 2018.

[219] E. Mezura-Montes and C. A. C. Coello. Constraint–handling in nature-inspired numerical optimization: Past, present and future. *Swarm and Evolutionary Computation*, 1(4):173–194, 2011.

[220] A. Misra, A. Sharma, and J. Shukla. Modeling and analysis of effects of awareness programs by media on the spread of infectious diseases. *Mathematical and Computer Modelling*, 53(5-6):1221–1228, 2011.

[221] A. Misra, A. Sharma, and V. Singh. Effect of awareness programs in controlling the prevalence of an epidemic with time delay. *Journal of Biological Systems*, 19(2):389–402, 2011.

[222] D. M. Morens, G. K. Folkers, and A. S. Fauci. The challenge of emerging and re–emerging infectious diseases. *Nature*, 430(6996):242–249, 2004.

[223] M. K. Morters, O. Restif, K. Hampson, S. Cleaveland, J. L. N. Wood, and A. J. K. Conlan. Evidence–based control of canine rabies: a critical review of population density reduction. *Journal of Animal Ecology*, 82(1):6–14, 2013.

[224] R. Morton and K. Wickwire. On the optimal control of a deterministic epidemic. *Advances in Applied Probability*, 6:622–635, 1974.

[225] G. G. Mwanga, H. Haario, and V. Capasso. Optimal control problems of epidemic systems with parameter uncertainties: application to a malaria two–age–classes transmission model with asymptomatic carriers. *Mathematical Biosciences*, 261:1–12, 2015.

[226] N. Nathan, M. Barry, M. Van Herp, and H. Zeller. Shortage of vaccines during a yellow fever outbreak in Guinea. *The Lancet*, 358:2129–2130, 2001.

[227] R. L. M. Neilan, E. Schaefer, H. Gaff, K. R. Fister, and S. Lenhart. Modeling optimal intervention strategies for cholera. *Bulletin of Mathematical Biology*, 72(8):2004–2018, 2010.

[228] C. N. Ngonghala, E. Iboi, S. Eikenberry, M. Scotch, C. R. MacIntyre, M. H. Bonds, and A. B. Gumel. Mathematical assessment of the impact of non–pharmaceutical interventions on curtailing the 2019 novel Coronavirus. *Mathematical Biosciences*, 325:108364, 2020.

[229] NHS Digital and Public Health England. Childhood vaccination coverage statistics – England 2018–19. `https://digital.nhs.uk/data-and-information/publications/statistical/nhs-immunisation-statistics/england-2018-19`, 2019.

[230] H. Nishiura and R. Omori. An epidemiological analysis of the foot–and–mouth disease epidemic in Miyazaki, Japan, 2010. *Transboundary and Emerging Diseases*, 57:396–403, 2010.

[231] J. On, H.-A. Park, and T.-M. Song. Sentiment analysis of social media on childhood vaccination: Development of an ontology. *Journal of Medical Internet Research*, 21(6):e13456, 2019.

[232] M. R. Osborne. On shooting methods for boundary value problems. *Journal of Mathematical Analysis and Applications*, 27(2):417–433, 1969.

[233] P. L. Paarlberg, A. H. Seitzinger, J. G. Lee, and K. H. Mathews Jr. Economic impacts of foreign animal disease. Technical Report Economic Research 57, USDA, 2008.

[234] S. Pandey and E. Venturino. A TB model: Is disease eradication possible in India? *Mathematical Biosciences and Engineering*, 15(1):233–254, 2018.

[235] D. J. Paton, A.-E. Füssel, W. Vosloo, and K. De Clercq. The use of serosurveys following emergency vaccination, to recover the status of "foot–and–mouth disease free where vaccination is not practised". *Vaccine*, 32:7050–7056, 2014.

[236] M. E. H. Pedersen. Good parameters for particle swarm optimization. Technical Report HL1001, Hvass Laboratories, Copenhagen, Denmark, 2010.

[237] X.-L. Peng, X.-J. Xu, M. Small, X. Fu, and Z. Jin. Prevention of infectious diseases by public vaccination and individual protection. *Journal of Mathematical Biology*, 73(6-7):1561–1594, 2016.

[238] F. Peterka. Part 1: Theoretical analysis of n–multiple (1/n)–impact solutions. *CSAV Acta Technica*, 26(2):462–473, 1974.

[239] P. T. Piiroinen and Y. A. Kuznetsov. An event–driven method to simulate Filippov systems with accurate computing of sliding motions. *ACM Transactions on Mathematical Software*, 34:13, 2008.

[240] L. S. Pontryagin, V. G. Boltyanskii, R. V. Gamkrelidze, and E. F. Mishchenko. *The Mathematical Theory of Optimal Processes*. International Series of Monographs in Pure and Applied Mathematics. Interscience Publishers, Los Angeles, USA, 1962.

[241] L. C. Pope, R. K. Butlin, G. J. Wilson, R. Woodroffe, K. Erven, C. M. Conyers, T. Franklin, R. J. Delahay, C. L. Cheeseman, and T. Burke. Genetic evidence that culling increases badger movement: implications for the spread of bovine tuberculosis. *Molecular Ecology*, 16(23):4919–4929, 2007.

[242] T. Porphyre, K. M. Rich, and H. K. Auty. Assessing the economic impact of vaccine availability when controlling foot and mouth disease outbreaks. *Frontiers in Veterinary Science*, 5:547, 2018.

[243] K. Price and R. M. Storn. Differential evolution (DE) for continuous function optimization. `http://www1.icsi.berkeley.edu/~storn/code.html`. (Accessed on December 2019).

[244] K. Price, R. M. Storn, and J. A. Lampinen. *Differential Evolution: a Practical Approach to Global Optimization*. Springer, Berlin, Heidelberg, 2006.

[245] A. T. Price-Smith. *Contagion and chaos: disease, ecology, and national security in the era of globalization*. The MIT Press, Cambridge, Massachusetts, 2009.

[246] W. J. M. Probert, K. Shea, C. J. Fonnesbeck, M. C. Runge, T. E. Carpenter, S. Dürr, M. G. Garner, N. Harvey, M. A. Stevenson, C. T. Webb, M. Werkman, M. J. Tildesley, and M. J. Ferrari. Decision–making for foot–and–mouth disease control: Objectives matter. *Epidemics*, 15:10–19, 2016.

[247] O. Prosper, N. Ruktanonchai, and M. Martcheva. Optimal vaccination and bednet maintenance for the control of malaria in a region with naturally acquired immunity. *Journal of Theoretical Biology*, 353:142–156, 2014.

[248] B. J. Quilty, S. Clifford, CMMID nCoV working group2, S. Flasche, and R. M. Eggo. Effectiveness of airport screening at detecting travellers infected with novel coronavirus (2019–nCoV). *Eurosurveillance*, 25(5):2000080, 2020.

[249] A. Rachah and D. F. M. Torres. Dynamics and optimal control of Ebola transmission. *Mathematics in Computer Science*, 10(3):331–342, 2016.

[250] K. Rajiah, M. K. Maharajan, P. Y. Yin, Y. W. Yee, W. W. Lin, and C. H. Kean. Zika outbreak emergency preparedness and response of Malaysian private healthcare professionals: are they ready? *Microorganisms*, 7:87, 2019.

[251] A. V. Rao. A survey of numerical methods for optimal control. Technical Report AAS 09–334, Department of Mechanical and Aerospace Engineering, University of Florida, 2009.

[252] D. Rassy and R. D. Smith. The economic impact of H1N1 on Mexico's tourist and pork sectors. *Health Economics*, 22:824–834, 2013.

[253] T. G. Rawdon, M. G. Garner, R. L. Sanson, M. A. Stevenson, C. Cook, C. Birch, S. E. Roche, K. A. Patyk, K. N. Forde-Folle, C. Dubé, T. Smylie, and Z. D. Yu. Evaluating vaccination strategies to control foot–and–mouth disease: a country comparison study. *Epidemiology and Infection*, 146:1138–1150, 2018.

[254] Reuters Institute for the Study of Journalism. Types, sources, and claims of COVID–19 misinformation. Fact sheet April, 2020.

[255] K. Robinson, T. Cohen, and C. Colijn. The dynamics of sexual contact networks: effects on disease spread and control. *Theoretical Population Biology*, 81(2):89–96, 2012.

[256] S. E. Roche, M. G. Garner, R. M. Wicks, I. J. East, and K. de Witte. How do resources influence control measures during a simulated outbreak of foot and mouth disease in Australia? *Preventive Veterinary Medicine*, 113:436–446, 2014.

[257] H. S. Rodrigues, M. T. T. Monteiro, and D. F. M. Torres. *Systems Theory: Perspectives, Applications and Developments*, chapter Optimal control and numerical software: An overview, pages 93–110. Nova Science Publishers, New York, 2014.

[258] P. Rodrigues, C. J. Silva, and D. F. M. Torres. Cost–effectiveness analysis of optimal control measures for tuberculosis. *Bulletin of Mathematical Biology*, 76(10):2627–2645, 2014.

[259] R. Rosatte, D. Donovan, M. Allan, L.-A. Howes, A. Silver, K. Bennett, C. MacInnes, C. Davies, A. Wandeler, and B. Radford. Emergency response to raccoon rabies introduction into Ontario. *Journal of Wildlife Diseases*, 37(2):265–279, 2001.

[260] R. A. Ross. *The Prevention of Malaria (2nd edition, with Addendum)*. John Murray, London, 1911.

[261] G. Rossi, R. L. Smith, S. Pongolini, and L. Bolzoni. Modelling farm–to–farm disease transmission through personnel movements: from visits to contacts, and back. *Scientific Reports*, 7:2375, 2017.

[262] H. Schättler and U. Ledzewicz. *Geometric Optimal Control: Theory, Methods and Examples*, volume 38 of *Interdisciplinary Applied Mathematics*. Springer, New York, 2012.

[263] W. E. Schmitendorf. Pontryagin's principle for problems with isoperimetric constraints and for problems with inequality terminal constraints. *Journal of Optimization Theory and Applications*, 18(4):561–567, 1976.

[264] M. Schrope. Plans to eradicate polio hit by virus outbreak in Bulgaria. *Nature*, 411:405, 2001.

[265] A. A. Scitovsky and D. P. Rice. Estimates of the direct and indirect costs of acquired immunodeficiency syndrome in the United States, 1985, 1986, and 1991. *Journal of Medial Practice Management*, 3:234–241, 1988.

[266] K. J. Sharkey, R. G. Bowers, K. L. Morgan, S. E. Robinson, and R. M. Christley. Epidemiological consequences of an incursion of highly pathogenic H5N1 avian influenza into the British poultry flock. *Proceedings of the Royal Society B*, 275:19–28, 2008.

[267] O. Sharomi, C. Podder, A. Gumel, E. Elbasha, and J. Watmough. Role of incidence function in vaccine–induced backward bifurcation in some HIV models. *Mathematical Biosciences*, 210(2):436–463, 2007.

[268] O. Sharomi, C. Podder, A. Gumel, S. Mahmud, and E. Rubinstein. Modelling the transmission dynamics and control of the novel 2009 swine influenza (H1N1) pandemic. *Bulletin of Mathematical Biology*, 73(3):515–548, 2011.

[269] M. J. Smith, A. White, J. A. Sherratt, S. Telfer, M. Begon, and X. Lambin. Disease effects on reproduction can cause population cycles in seasonal environments. *Journal of Animal Ecology*, 77:378–389, 2008.

[270] A. Stegeman, A. Bouma, A. R. W. Elbers, M. C. M. de Jong, G. Nodelijk, F. de Klerk, G. Koch, and M. van Boven. Avian influenza A virus (H7N7) epidemic in The Netherlands in 2003: Course of the epidemic and effectiveness of control measures. *Journal of Infectious Diseases*, 190:2088–2095, 2004.

[271] R. Storn. On the usage of differential evolution for function optimization. In *Proceedings of North American Fuzzy Information Processing*, pages 519–523. IEEE, 1996.

[272] R. Storn and K. Price. Differential evolution – a simple and efficient heuristic for global optimization over continuous spaces. *Journal of Global Optimization*, 11(4):341–359, 1997.

[273] S. H. Strogatz. *Nonlinear Dynamics and Chaos*. Perseus Books Publishing, Reading, Massachussetts, 1994.

[274] A. I. Subbotin. *Generalized Solutions of First Order PDEs: the Dynamical Optimization Perspective*. Springer, Basel, 1995.

[275] C. Sun, W. Yang, J. Arino, and K. Khan. Effect of media–induced social distancing on disease transmission in a two patch setting. *Mathematical Biosciences*, 230(2):87–95, 2011.

[276] M. Supino, A. d'Onofrio, F. Luongo, G. Occhipinti, and A. Dal Co. The effects of containment measures in the Italian outbreak of COVID–19. *medRxiv*, 2020.

[277] H. J. Sussmann and J. C. Willems. 300 years of optimal control: from the brachystochrone to the maximum principle. *IEEE Control Systems Magazine*, 17(3):32–44, 1997.

[278] W. Suwanprasert. COVID–19 and endogenous public avoidance: insights from an economic model. `https://papers.ssrn.com/sol3/papers.cfm?abstract_id=3565564`, 2020.

[279] S. Takeuchi and Y. Kuroda. Predicting spread of new pandemic swine–origin influenza A(H1N1) in local mid–size city: evaluation of hospital bed shortage and effectiveness of vaccination. *Nippon Eiseigaku Zasshi*, 65:48–52, 2010.

[280] J. M. Tchuenche and C. T. Bauch. Dynamics of an infectious disease where media coverage influences transmission. *ISRN Biomathematics*, Art. ID 581274, 2012.

[281] The Guardian. Italy charges more than 40,000 people with violating lockdown. `https://www.theguardian.com/world/2020/mar/18/italy-charges-more-than-40000-people-violating-lockdown-coronavirus`, 2020. (Accessed on May 2020).

[282] The Guardian. Leaked coronavirus plan to quarantine 16m sparks chaos in Italy. `https://www.theguardian.com/world/2020/mar/08/leaked-coronavirus-plan-to-quarantine-16m-sparks-chaos-in-italy`, 2020. (Accessed on May 2020).

[283] M. J. Tildesley, V. V. Volkova, and M. E. J. Woolhouse. Potential for epidemic take–off from the primary outbreak farm via livestock movements. *BMC Veterinary Research*, 7:76, 2011.

[284] M. I. Tosa, E. M. Schauber, and C. K. Nielsen. Localized removal affects white–tailed deer space use and contacts. *The Journal of Wildlife Management*, 81(1):26–37, 2017.

[285] F. A. M. Tuyttens, D. W. Macdonald, L. M. Rogers, C. L. Cheeseman, and A. W. Roddam. Comparative study on the consequences of culling badgers (*Meles meles*) on biometrics, population dynamics and movement. *Journal of Animal Ecology*, 69(4):567–580, 2000.

[286] V. I. Utkin. *Sliding Modes and Their Application in Variable Structure Systems*. Mir, Moscow, 1978.

[287] P. Van den Driessche and J. Watmough. Reproduction numbers and sub–threshold endemic equilibria for compartmental models of disease transmission. *Mathematical Biosciences*, 180(1):29–48, 2002.

[288] T. P. Velavan and C. G. Meyer. The COVID–19 epidemic. *Tropical Medicine & International Health*, 25(3):278, 2020.

[289] F. Verelst, L. Willem, and P. Beutels. Behavioural change models for infectious disease transmission: a systematic review (2010–2015). *Journal of the Royal Society Interface*, 13(125):20160820, 2016.

[290] J. Vesterstrøm and R. Thomsen. A comparative study of differential evolution, particle swarm optimization, and evolutionary algorithms on numerical benchmark problems. In *Proceedings of the 2004 Congress on Evolutionary Computation (IEEE Cat. No.04TH8753)*, volume 2, pages 1980–1987, 2004.

[291] F. Vial and C. A. Donnelly. Localized reactive badger culling increases risk of bovine tuberculosis in nearby cattle herds. *Biology Letters*, 8(1):50–53, 2012.

[292] O. von Stryk. Numerical solution of optimal control problems by direct collocation. In R. Bulirsch, A. Miele, J. Stoer, and W. K., editors, *Optimal Control*, pages 129–143. Springer, Basel, 1993.

[293] Z. Wang, C. T. Bauch, S. Bhattacharyya, A. d'Onofrio, P. Manfredi, M. Perc, N. Perra, M. Salathé, and D. Zhao. Statistical physics of vaccination. *Physics Reports*, 664:1–113, 2016.

[294] I. M. Wangari and L. Stone. Backward bifurcation and hysteresis in models of recurrent tuberculosis. *PLoS ONE*, 13(3):1–29, 2018.

[295] L. M. Wein, D. L. Creaft, and E. H. Kaplan. Emergency response to an anthrax attack. *Proceedings of the National Academy of Sciences*, 100:4346–4351, 2003.

[296] K. Wickwire. Optimal isolation policies for deterministic and stochastic epidemics. *Mathematical Biosciences*, 26:325–246, 1975.

[297] K. Wickwire. Mathematical models for the control of pests and infectious diseases: A survey. *Theoretical Population Biology*, 11(2):182–238, 1977.

[298] R. Woodroffe, S. Cleaveland, O. Courtenay, M. K. Laurenson, and M. Artois. Infectious disease in the management and conservation of wild canids. In D. W. Macdonald and C. Sillero-Zubiri, editors, *The Biology and Conservation of Wild Canids*, pages 124–142. Oxford University Press, Oxford, 2004.

[299] M. Woolhouse, M. Chase Topping, D. Haydon, J. Friar, L. Matthews, G. Hughes, D. Shaw, J. Wilesmith, A. Donaldson, S. Cornell, M. Keeling, and B. Grenfell. Epidemiology – foot–and–mouth disease under control in the UK. *Nature*, 411:258–259, 2001.

[300] World Health Organization. State of the world's vaccines and immunization. Third edition. `http://www.who.int/immunization/sowvi/en/`, 2010. (Accessed on January 2018).

[301] World Health Organization. Oral cholera vaccine stockpile for cholera emergency response. `https://www.who.int/cholera/vaccines/Briefing_OCV_stockpile.pdf?ua=1`, 2013. (Accessed on January 2019).

[302] World Health Organization. Rapidly growing outbreak of meningococcal disease in Niger. `https://www.who.int/csr/don/15-may-2015-niger/en/`, 2015. (Accessed on January 2019).

[303] World Health Organization. Addressing vaccine hesitancy. `http://www.who.int/immunization/programmes_systems/vaccine_hesitancy/en/`, 2016. (Accessed on March 2018).

[304] World Health Organization. Q&A on the Phase 3 trial results for malaria vaccine RTS,S/AS01. `http://www.who.int/malaria/media/rtss-phase-3-trial-qa/en/`, 2017. (Accessed on February 2018).

[305] World Health Organization. Questions and answers on dengue vaccines. `http://www.who.int/immunization/research/development/dengue_q_and_a/en/`, 2017. (Accessed on February 2018).

[306] World Health Organization. HIV vaccine development. `http://www.who.int/immunization/research/development/hiv_vaccdev/en/`, 2018. (Accessed on February 2018).

[307] World Health Organization. Tuberculosis vaccine development. `http://www.who.int/immunization/research/development/tuberculosis/en/`, 2018. (Accessed on March 2018).

[308] World Health Organization. Coronavirus disease 2019 (COVID-19): Situation Report – 73. `https://www.who.int/docs/default-source/coronaviruse/situation-reports/20200402-sitrep-73-covid-19.pdf?sfvrsn=5ae25bc7_6`, 2020. (Accessed on April 2020).

[309] World Health Organization. Coronavirus disease (COVID–19) Pandemic. `https://www.who.int/emergencies/diseases/novel-coronavirus-2019`, 2020. (Accessed on May 2020).

[310] World Health Organization. Home care for patients with COVID–19 presenting with mild symptoms and management of their contacts. `https://www.who.int/publications-detail/home-care-for-patients-with-suspected-novel-coronavirus-(ncov)-infection-presenting-with-mild-symptoms-and-management-of-contacts`, 2020. (Accessed on May 2020).

[311] World Health Organization. Immunity passports in the context of COVID–19. `https://www.who.int/news-room/commentaries/detail/immunity-passports-in-the-context-of-covid-19`, 2020. (Accessed on May 2020).

[312] World Health Organization. Transmission of SARS–CoV–2: implications for infection prevention precautions. `https://www.who.int/news-room/commentaries/detail/transmission-of-sars-cov-2-implications-for-infection-prevention-precautions`, 2020. (Accessed on July 2020).

[313] World Organisation for Animal Health. OIE policy paper on vaccine banks, October 2018. Technical report, OIE, 2018.

[314] World Tourism Organization. COVID–19 related travel restrictions. A global review for tourism. Second report as of 28 April 2020. `https://webunwto.s3.eu-west-1.amazonaws.com/s3fs-public/2020-04/TravelRestrictions%20-%2028%20April.pdf`, 2020. (Accessed on May 2020).

[315] Y. Xiao, X. Xu, and S. Tang. Sliding mode control of outbreaks of emerging infectious diseases. *Bulletin of Mathematical Biology*, 74:2403–2422, 2012.

[316] Y. Xiao, X. Xu, and S. Tang. A threshold policy to interrupt transmission of West Nile Virus to birds. *Applied Mathematical Modelling*, 40:8794–8809, 2016.

[317] J. Zhang, J. Lou, Z. Ma, and J. Wu. A compartmental model for the analysis of SARS transmission patterns and outbreak control measures in China. *Applied Mathematics and Computation*, 162:909–924, 2005.

[318] S. Zhao, Y. Kuang, C.-H. Wu, D. Ben-Arieh, M. Ramalho-Ortigao, and K. Bi. Zoonotic visceral leishmaniasis transmission: modeling, backward bifurcation, and optimal control. *Journal of Mathematical Biology*, 73(6-7):1525–1560, 2016.

[319] L. Zhu, X. Zhou, Y. Li, and Y. Zhu. Stability and bifurcation analysis on a delayed epidemic model with information–dependent vaccination. *Physica Scripta*, 94(12):125202, 2019.